Inaugural dissertation

for

obtaining the doctoral degree

of the

Combined Faculty of Mathematics, Engineering and Natural Sciences

of the

Ruprecht - Karls - University

Heidelberg

Presented by

M.Sc. Dominik Kiemel

born in Schwäbisch Gmünd, Germany

Oral examination 19.10.2023

Elucidation of the mechanism-of-action of highly potent Dengue virus NS4B inhibitors JNJ-A07 and JNJ-1802

Referees: Prof. Dr. Dr. h.c. Ralf Bartenschlager

Prof. Dr. Walter Nickel

Acknowledgements

The work presented here was carried out between December 2017 and July 2023 under the supervision of Prof. Ralf Bartenschlager in the Molecular Virology Group at the Centre for Integrative Infectious Disease Research at Heidelberg University Hospital.

While a dissertation is defined as an independent scientific work, from my point of view it would be wrong to deduce that doctoral studies would be possible without a network of supporters. During my time as a doctoral student, which I consider an important personal phase in my life, I have experienced valuable help and energetic commitment from many people. Therefore, I would like to take this opportunity to express my deep gratitude and appreciation for this.

First and foremost, I would like to thank my supervisor, Prof. Ralf Bartenschlager, for accepting me as a member of his research group and giving me the opportunity to work on a project tailored to my passion for applied drug discovery. *Ralf, you are an inspiring mentor, your dedication to scientific research is unmatched in my view, and I don't think I can fully comprehend today the value of the lessons I have learned from you.*

My PhD thesis was designed from the beginning as a public-private partnership with Janssen Pharmaceuticals. I find this term entirely appropriate. At no time did I have the feeling of being an outsourced service provider. Instead, I was entrusted with the task of unraveling the mechanism-of-action of novel dengue antiviral drugs in an independent manner and was encouraged to publish my results. I would like to thank everyone involved for their trust and confidence, especially Dr. Marnix van Loock and Dr. Olivia Goethals as project manager. *Thank you, Olivia, for the many constructive meetings and the valuable insights into the pharmaceutical industry. I have always considered it a great privilege to be able to work on an advanced development project for a first-in-class drug against such a burdensome disease as dengue fever.*
In this sense, I would also like to thank the pioneers of the project at KU Leuven, in particular Dr. Suzanne Kaptein and Prof. Johan Neyts. *It has been a great pleasure to collaborate with you.*

External feedback is very important for a successful dissertation. In this sense, I would like to thank Prof. Walter Nickel for his willingness to serve as a second reviewer for this thesis. I would like to thank him as well as Dr. David Will, Prof. Laurent Chatel-Chaix, Prof. Friedrich

Frischknecht and Prof. Volker Lohmann for their participation in my thesis advisory committee and/or my PhD defense committee.

One of my core convictions, which has strengthened during my PhD studies, is that outstanding research is only possible in a laboratory where team spirit and enthusiasm for science are actively practiced. I consider myself lucky to have found myself in such a place. Over the years, many colleagues have become deep friends, and this circle of great people is not limited to the Bartenschlager group, but also includes members of the Lohmann, Ruggieri and Urban groups. Thank you for the many wonderful moments inside and outside the lab. A special thanks goes to the "Nachtschicht-Gang", who made the dark time during the Corona restrictions a lot brighter.

It is in the nature of an academic research group that colleagues come and go. An exception for me was my doctoral colleague Sarah Göllner. We went through the important stages of a doctorate more or less synchronously, which led to a special emotional bond that helped us get through the most challenging phases. *Thank you, Sarah!*
I would like to extend my gratitude to Dr. Mirko Cortese for introducing me to the lab, and to Dr. Solène Denolly and Uta Haselmann for their active participation in my project. I am thankful to Dr. Vibor Laketa for his expert assistance and access to the Infectious Diseases Imaging Facility and to Dr. Charlotta Funaya for her continuous support and access to the Electron Microscopy Core Facility at the University of Heidelberg.

With Annika Rammelt and Ann-Sophie Kröll, I was lucky to supervise two outstanding interns during my time in the lab. *Ann-Sophie and Annika, you both did a great job and I am proud of you!*

It is important to me not to forget the people who keep the lab running in the background, be it through technical assistance, IT or administrative functions. In this sense, a big thank you to Marie Bartenschlager, Micha Fauth, Ulrike Herian, Sabine Scholl, Fredy Huschmand, Dr. Sandra Bühler, Dr. Ilka Rebhan and Pilar Milla!

My greatest thanks go to my family, especially to my parents, who have supported my scientific curiosity from childhood until today and who have always been there for me when I needed them. *Ohne euch wäre ich nicht da, wo ich heute bin. Danke.*

Summary

Dengue virus (DENV) is a highly prevalent pathogen of the *Flaviviridae* family that can be transmitted to humans by the bite of female *Aedes* mosquitoes. Although only a small proportion of infections result in a potentially life-threatening disease characterized by haemorrhagic fever and shock, even the majority of the approximately 100 million annual symptomatic cases, which typically present with a debilitating but self-limiting febrile infection, collectively cause an enormous medical and socioeconomic burden, particularly in tropical countries where most infections occur. Despite the great need, antiviral drugs for prevention or treatment of the disease are not yet available.

As part of my PhD research, I have been working on elucidating the mechanism-of-action of two novel DENV-specific drug candidates named JNJ-A07 and JNJ-1802. JNJ-A07 is the first compound for which nano- to picomolar activity against all available genotypes within the four DENV serotypes has been demonstrated *in vitro*. JNJ-1802 is from the same chemical series of compounds and was selected for the clinical development process based on improved pharmacological properties.

Using expression-based systems, I uncovered that JNJ-A07 blocks the formation of a previously unknown interaction between the viral protease-helicase complex NS2B/NS3 and another viral component, the NS4A-2K-NS4B cleavage intermediate. The same inhibition of interaction was found for JNJ-1802. Electron microscopy studies showed that blocking NS2B/NS3 interaction with NS4A-2K-NS4B by JNJ-A07 is functionally linked to a halt in the assembly of vesicle packets (VPs), which are membrane invaginations on the endoplasmic reticulum. As revealed by pulse-chase analysis in the context of the viral polyprotein, JNJ-A07 does not affect the cleavage kinetics of NS4A-2K-NS4B, suggesting that delayed protein maturation is unlikely to be a mediating effect and that instead JNJ-A07 inhibits the assembly of a multi-protein complex around NS4A-2K-NS4B and NS2B/NS3, which is structurally important for the biogenesis of vesicle packets. In any case, their loss explains the antiviral activity of JNJ-A07 since VPs are essential for viral replication processes. In support, I demonstrated that resistance mutations, which remarkably all accumulated in the sequence of NS4B, rendered both the NS4A-2K-NS4B interaction with NS2B/NS3 and *de novo* formation of VPs less sensitive to JNJ-A07. Furthermore, these mutations caused a reduced level of co-localization between NS4B-containing structures and a photoaffinity derivative of JNJ-A07, implying diminished compound binding as an important component of the resistance mechanism. Surprisingly, I found that some of the mutants had little or no fitness deficits in

mammalian cells. In fact, the strongest resistance mutant, NS4B L94F, showed a pronounced fitness advantage in this system; however, virus mutants containing L94F were unable to replicate in mosquito cells.

In conclusion, the results presented in this dissertation provide important insights into novel DENV-specific inhibitors with unprecedented activity. Moreover, the discovered NS4A-2K-NS4B interaction with NS2B/NS3 delivers new evidence that DENV uses short-lived cleavage intermediates to carry out early steps in the viral replication cycle.

Zusammenfassung

Das Dengue-Virus (DENV) ist ein weit verbreiteter Erreger aus der Familie der *Flaviviridae*, welcher durch den Stich von weiblichen *Aedes*-Mücken auf den Menschen übertragen werden kann. Zwar führt nur ein kleiner Teil der Infektionen zu einer potenziell lebensbedrohlichen Erkrankung, die durch hämorrhagisches Fieber und Schock gekennzeichnet ist, dennoch verursacht auch die Mehrheit der jährlich etwa 100 Millionen symptomatischen Fälle, die typischerweise mit einem schwächenden, aber selbstlimitierenden fiebrigen Infekt einhergehen, in ihrer Gesamtheit eine enorme medizinische und sozioökonomische Belastung, insbesondere in tropischen Ländern, in denen die meisten Infektionen auftreten. Trotz des großen Bedarfs sind antivirale Medikamente zur Prävention oder Behandlung der Erkrankung bisher nicht verfügbar.

Im Rahmen meiner Doktorarbeit habe ich mich mit der Entschlüsselung des Wirkmechanismus zweier neuartiger DENV-spezifischer Wirkstoffkandidaten namens JNJ-A07 und JNJ-1802 beschäftigt. Bei JNJ-A07 handelt es sich um die erste Verbindung, für die *in vitro* nano- bis pikomolare Aktivität gegen alle verfügbaren Genotypen innerhalb der vier DENV Serotypen demonstriert werden konnte. JNJ-1802 stammt aus derselben chemischen Serie an Verbindungen und wurde aufgrund verbesserter pharmakologischer Eigenschaften für den klinischen Entwicklungsprozess ausgewählt.

Mittels Verwendung Expressions-basierter Systeme konnte ich aufdecken, dass JNJ-A07 die Ausbildung einer bisher unbekannten Interaktion zwischen dem viralen Protease-Helikase-Komplex NS2B/NS3 und einer weiteren viralen Komponente, dem NS4A-2K-NS4B Spaltungsintermediat blockiert. Diese Hemmung der Interaktion wurde auch in Bezug auf JNJ-1802 festgestellt. Elektronenmikroskopische Untersuchungen zeigten, dass die Unterbindung der NS2B/NS3-Interaktion mit NS4A-2K-NS4B durch JNJ-A07 funktionell mit einem Stop des Zusammenbaus von Vesikelpaketen (engl. vesicle packets, VPs) verknüpft ist, bei denen es sich um Membraneinstülpungen am endoplasmatischen Retikulum handelt. Wie Pulsmarkierungen im Kontext des viralen Polyproteins offenbarten, wirkt sich JNJ-A07 nicht auf die Spaltungskinetik von NS4A-2K-NS4B aus, sodass eine verzögerte Polyproteinreifung als vermittelnder Effekt unwahrscheinlich erscheint und stattdessen angenommen wird, dass JNJ-A07 den Aufbau eines Multiproteinkomplexes um NS4A-2K-NS4B und NS2B/NS3 inhibiert, welcher von struktureller Bedeutung für die Biogenese der Vesikelpakete ist. In jedem Fall erklärt deren Verlust die antivirale Aktivität von JNJ-A07, da VPs essenziell für virale Replikationsprozesse sind. Unterstützend konnte ich in dieser Arbeit demonstrieren, dass

Resistenzmutationen, die bemerkenswerterweise allesamt in der Sequenz von NS4B akkumulierten, sowohl die NS4A-2K-NS4B Interaktion mit NS2B/NS3, als auch die Neubildung von VPs weniger sensitiv gegenüber JNJ-A07 machten. Zusätzlich bewirkten diese Mutationen ein verringertes Maß an Korrelation zwischen NS4B-haltigen Strukturen und einem Photoaffinitäts-Derivat von JNJ-A07, was auf reduzierte Wirkstoffbindung als eine wichtige Komponente des Resistenzmechanismus hindeutet. Überraschenderweise stellte ich fest, dass einige der Mutanten keine oder nur geringe Fitnesseinbußen in Säugetierzellen zu verzeichnen hatten. Ausgerechnet die stärkste Resistenzmutante NS4B L94F wies in diesem System sogar einen ausgeprägten Fitnessvorteil auf, jedoch waren Virusmutanten, die L94F enthielten, nicht in der Lage, sich in Mückenzellen zu vermehren.

Zusammenfassend gewähren die in dieser Doktorarbeit präsentierten Ergebnisse wichtige Einblicke in neuartige, DENV-spezifische Inhibitoren mit bisher unübertroffener Aktivität. Des Weiteren bietet die entdeckte NS4A-2K-NS4B Interaktion mit NS2B/NS3 einen neuen Beleg dafür, dass DENV kurzlebige Spaltungsintermediate verwendet, um frühe Schritte im viralen Replikationszyklus auszuführen.

Table of contents

List of figures

List of tables

List of abbreviaions

Abbreviation	Meaning
2A	Self-cleaving peptide 2A
7-DMA	7-Deaza-2′-C-methyl-adenosine
AD	anno Domini
ADE	Antibody-dependent enhancement
AMP	*Adenosine* monophosphate
ANOVA	analysis of variance
APC	Antigen-presenting cell
APS	Ammonium persulfate
ARCA	Anti-Reverse Cap Analog
ATP	Adenosine triphosphate
AUP1	Ancient ubiquitous protein 1
BSA	Bovine serum albumin
C	Capsid protein
CAST	castanospermine
CC_{50}	50% cellular cytotoxicity concentration
cGAS	Cyclic GMP-AMP synthase
cHP	Capsid-coding region hairpin element
CHX	Cycloheximide
CIP	Calf Intestinal Phosphatase
CM	Convoluted membrane
CMC	Critical micelle concentration
CPE	Cytopathic effect
CS	Cleavage site
CS	Complementary sequence
Ct	C-terminal
CTP	Cytidine triphosphate
Da	Dalton
DAA	Direct acting antiviral
DALY	Disability-adjusted life years
DAPI	4’,6-diamidino-2-phenylindole
DAXX	Death-associated protein 6
DC	Dendritic cell
DC-SIGN	DC-Specific Intercellular adhesion molecule-3-Grabbing Non-integrin
ddH_2O	Double distilled water
DDM	Dodecyl-β-D-maltoside
DDT	Dichlorodiphenyltrichloroethane
DENV	Dengue virus
DHF	Dengue hemorrhagic fever
DHODH	Dihydroorotate dehydrogenase
DMEM	Dulbecco’s Modified Eagle Medium
DMSO	Dimethyl sulfoxide
DNA	Deoxyribonucleic acid
DNJ	deoxynojirimycin
dsRNA	Double-stranded RNA

Abbreviation	Meaning
DSS	Dengue shock syndrome
DTT	Dithiothreitol
DVPS	Dengue vascular permeability syndrome
E	Envelope protein
E. coli	*Escherichia coli*
EC_{50}	Half maximal effective concentration
ECL	Enhanced chemiluminescence
EDTA	Ethylene diamine tetraacetic acid
EF1α	Human elongation factor-1 alpha
EGTA	ethylene glycol-bis(β-aminoethyl ether)-N,N,N′,N′-tetraacetic acid
eIF	Eukaryotic translation initiation factor
EM	Electron microscopy
EMC	Endoplasmic reticulum membrane protein complex
EMCV	Encephalomyocarditis virus
ER	Endoplasmic reticulum
eRF	Eukaryotic translation termination factor
FAS	Fatty acid synthase
FasL	Fas ligand
Fcγ	fragment crystallizable γ
FcR	fragment crystallizable receptor
GAPDH	Glyceraldehyde 3-phosphate dehydrogenase
GDD	Inactivating mutation in the ZIKV NS5 RdRp domain
GMP	Guanosine monophosphate
GND	Inactivating mutation in the DENV NS5 RdRp domain
Grp78	78 kDa glucose-regulated protein
GTP	Guanosine triphosphate
HA	Hemagglutinin
HBV	Hepatitis B virus
HCV	Hepatitis C virus
HDA	host-directed antiviral
HEPES	4-(2-hydroxyethyl)-1-piperazineethanesulfonic acid
HIV	Human immunodeficiency virus
HPF	Human French Polynesia
HRP	Horseradish peroxidase
Hsp	Heat shock protein
IF	Immunofluorescence
IFN	Interferon
IgE	Immunoglobulin E
IgG	Immunoglobulin G
ImDC	Immature dendritic cell
IMPDH	Inosine monophosphate dehydrogenase
IP	Immunoprecipitation
IRES	Internal ribosome entry site
IRF	Interferon regulatory factor
ISG	Interferon-stimulated gene
IUPAC	International union of pure and applied chemistry

Abbreviation	Meaning
IVT	*In vitro* transcription
JAK	Janus kinase
JEV	Japanese Encephalitis virus
kB	kilobase
KU Leuven	Katholieke Universiteit Leuven
LB	Lysogeny broth
LLOQ	lowest level of quantification
L-SIGN	Liver/lymph node-specific intercellular adhesion molecule-3-grabbing integrin
MAMs	Mitochondria associated membranes
MAVS	Mitochondrial antiviral-signaling protein
MC	Mast cell
MDA5	Melanoma differentiation-associated protein 5
MEM	Minimal Essential Medium
MOA	Mechanism-of-action
mRNA	Messenger RNA
MTase	Methyltransferase
MW	Molecular weight
NaOAc	Sodium acetate
NF-κB	Nuclear factor 'kappa-light-chain-enhancer' of activated B-cells
NI	nucleoside inhibitor
NIAID	National Institute of Allergy and Infectious Diseases
NK cells	Natural killer cells
NLS	Nuclear localization sequence
NMR	Nuclear magnetic resonance
NPL4	Nuclear Protein Localization 4
NS	Nonstructural protein
ns	Not significant
Nt	N-terminal
NTR	Non-translated region
O-PCR	overlap polymerase chain reaction
OE-PCR	overlap extension polymerase chain reaction
OST	Oligosaccharyltransferase
PAA	Polyacrylamide
PABP	poly(A) binding protein
PAL	Photoaffinity labelling
PBS	Phosphate-buffered saline
PBS-T	PBS with Tween 20
PCR	Polymerase chain reaction
PDK (cells)	primary dog kidney (cells)
PFA	Paraformaldehyde
PFU	plaque-forming unit
PhD	Philosophiae doctor/Doctor of Philosophy
PI3K	Phosphoinositide 3-kinase
PIAS-1	Protein inhibitor of activated STAT-1
pIRO-D	plasmid-induced replication organelles of DENV
pIRO-Z	plasmid-induced replication organelles of ZIKV

Abbreviation	Meaning
PRE	paramagnetic relaxation enhancement
prM	Membrane precursor protein
PTB	Polypyrimidine tract-binding protein
pTMS	Putative transmembrane segment
Rab	Rat sarcoma-related in brain
RdRp	RNA-dependent RNA polymerase
RIG-I	Retinoic acid inducible gene I
RLU	Relative light unit
RLuc	Renilla luciferase
RNA	Ribonucleic acid
RNAi	RNA interference
rNTP	Nucleoside triphosphate
rNTPase	Nucleoside-triphosphatase
SAH	S-adenosyl-L-homocysteine
SAM	S-Adenosyl methionine
SARS-CoV-2	Severe acute respiratory syndrome coronavirus 2
SC	Subcloning
SD	Standard deviation
SDM	site-directed mutagenesis
SDS	Sodium dodecyl sulfate
SDS-PAGE	Sodium dodecyl sulfate polyacrylamide gel electrophoresis
SEM	Standard error of the mean
SF2	Helicase superfamily 2
sg	subgenomic
sgDVR2A	Subgenomic DENV-2 with an RLuc reporter
siRNA	Small interfering RNA
SLA	Stem-loop A
SRP	Signal recognition particle
STAT	signal transducer and activator of transcription
STING	Stimulator of interferon genes
TAM	Tyro3/Axl/Mer
TANK	TRAF Family Member Associated NF-κB Activator
TBEV	Tick-borne encephalitis virus
TBK-1	TANK-binding kinase 1
TCR	T-cell receptor
TEM	Transmission electron microscopy
TEMED	Tetramethylethylenediamine
THPTA	Tris(3-hydroxypropyltriazolylmethyl)amine
TIM	T cell immunoglobulin and mucin domain-containing protein
TLR	Toll-like receptor
T_m	Melting temperature
TM	Transmembrane
TMD	Transmembrane domain
TNF	Tumor necrosis factor
TOA	Time-of-addition
TRAF	TNF receptor associated factor
TRIS	tris(hydroxymethyl)aminomethane

Abbreviation	Meaning
UBE2I	Ubiquitin conjugating enzyme E2 I
UPR	Unfolded protein response
VCP	Valosin-containing protein
VP	Vesicle packet
VPE	Vesicle packets element
WHO	World Health Organization
WNV	West Nile virus
WT	Wildtype
YFV	Yellow fever virus
ZIKV	Zika virus

I. Introduction

I.1 Dengue virus as a human pathogen

I.1.1 Origin and evolution of Dengue virus

Dengue fever is a widespread infectious disease in tropical and subtropical regions and poses a major threat to global health.[1]. Today's tremendous prevalence is mainly a result of the sharp increase in human mobility in the post-World War II period on the one hand and the dramatic overall growth in the world's population density on the other hand[2]. However, the course of the disease, which in most cases is characterized by flu-like symptoms, was described as early as 1779 in an outbreak in Batavia, now Jakarta, by the Dutch physician David Bylon[3]. Reports from the same period mention similar occurrences in Tibet, Persia, Egypt, Spain, and Philadelphia, Pennsylvania, suggesting a widespread epidemic or pandemic[4,5]. The term dengue fever is probably a Spanish folk etymology, with the word translating roughly as fastidiousness[6]. However, it is unclear whether the name originally derived from "dandy fever", accounting for the strange attitudes of the infected[7], or from the Swahili phrase "Ka-dinga pepo", meaning "cramp-like seizure"[8]. In the early 20th century, it was recognized that the causative agent of dengue fever is a filterable agent[9] transmitted by mosquitoes of the genus *Aedes*[10,11]. In 1943, Ren Kimura and Susumu Hotta were the first to isolate dengue viruses from patient sera[12]. Albert Sabin and Walter Schlesinger succeeded in this a year later. The latter were also able to show that at least two different serotypes of dengue virus exist by performing cross-immunization and neutralization tests[13], which are now called DENV-1 and DENV-2. In 1953, the serotypes DENV-3 and DENV-4 were identified[14,15]. No further serotypes have been identified to date, but the geographic distribution of the individual ones has changed dramatically in recent decades. Whereas until the 1970s, the occurrence of several serotypes within one region was rather the exception, Figure 1 clearly depicts that the co-circulation of all four serotypes is now the rule in most American and Asian dengue endemic areas[16].

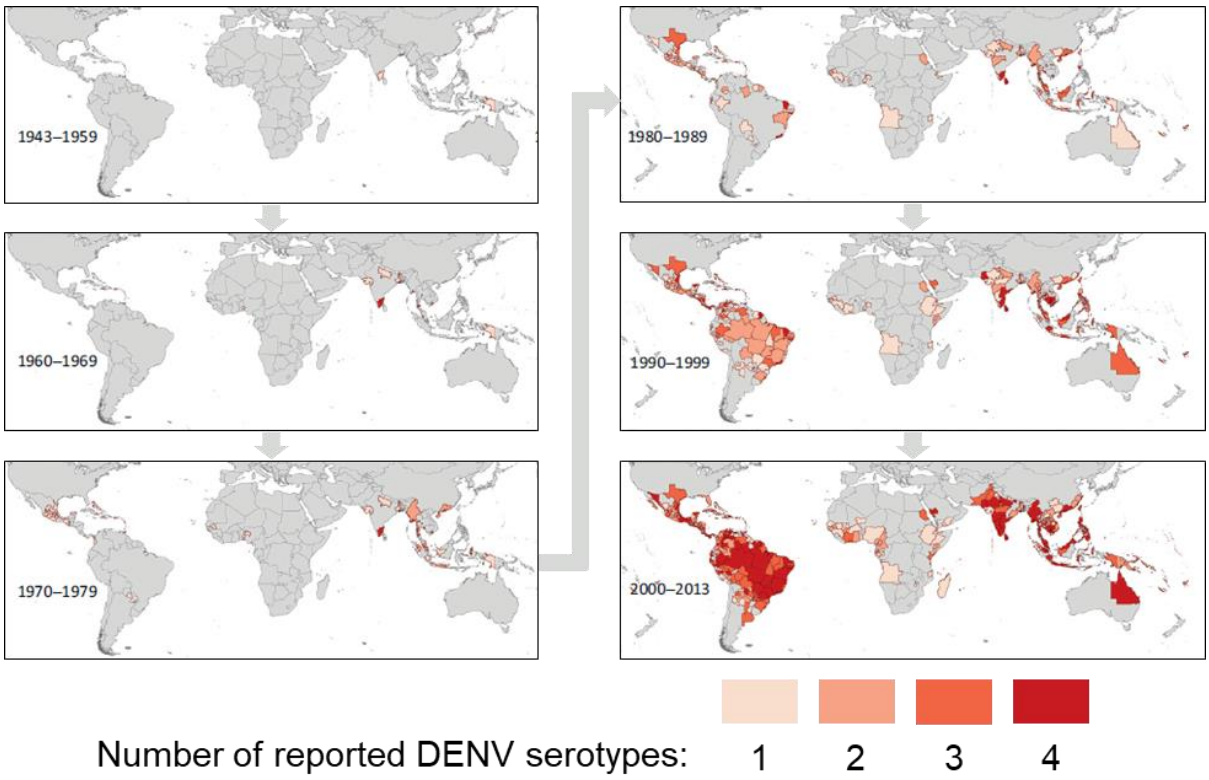

Figure 1. Global DENV co-circulation over time.
A map showing the cumulative number of reported DENV serotypes in different regions of the world, organized by decade. Until the 1980s, most areas reported only one or two serotypes. Today, some regions have reported all four serotypes, despite challenges in data collection. This map highlights the potential increase in co-circulation of the four DENV serotypes, which could be a significant marker of the progression towards hyperendemic transmission. Adapted from Messina et al.[16].

Initially, dengue viruses were taxonomically assigned to togaviruses on the basis of serological analyses, but the advent of improved methods in molecular biology, above all genome sequencing, led to a re-evaluation, so that in 1984 the family Flaviviridae was created within which dengue viruses were grouped into the genus Flaviviruses together with the eponymous yellow fever virus, among others[17].

Today, most flaviviruses are also categorized as arboviruses[18]. That term, which in the long version stands for arthropod-borne viruses, is not of taxonomic nature, but describes the ecological circumstance that the transmission of the virus constantly shuttles back and forth between humans and a bloodsucking (hematophagous) arthropod as vector[19]. There are tick-borne and mosquito-borne flaviviruses, with dengue viruses belonging to the latter. In the vast majority of cases, dengue viruses are transmitted to humans through the bite of an infected adult female mosquito, primarily of the species *Aedes aegypti* and to a lesser extent of the species *Aedes albopictus*[20]. The former live in particular proximity to human settlements and frequently breed in standing water of vessels and containers[21]. The currently circulating

epidemic or endemic variants of dengue virus have adapted to both humans and the *Aedes* species mentioned above, resulting in a transmission cycle referred to as urban. As illustrated in Figure 2, this has now become completely uncoupled from the original sylvatic cycle[22]. Sylvatic dengue viruses circulate in tropical forests between non-human primates as reservoirs and arboreal *Aedes* mosquitoes of different species (including *Aedes luteocephalus*, *Aedes niveus* and *Aedes furcifer*), best described for West Africa and Malaysia[23,24]. Zoonotic transmission of sylvatic dengue viruses to humans has probably occurred frequently in history[25-27], with the first documentation potentially dating back to the third century of the Chin dynasty (265-420 AD)[28]. *Aedes furcifer* plays a special role as a linking vector, since these forest-dwelling mosquitoes occasionally enter peridomestic habitats[29,30]. In turn, people entering tropical forests for occupational reasons (hunting or timber harvesting) are at increased risk of exposure[31]. Zoonotic transmissions usually remain dead-end infections or trigger short-term and locally restricted epidemics[32].

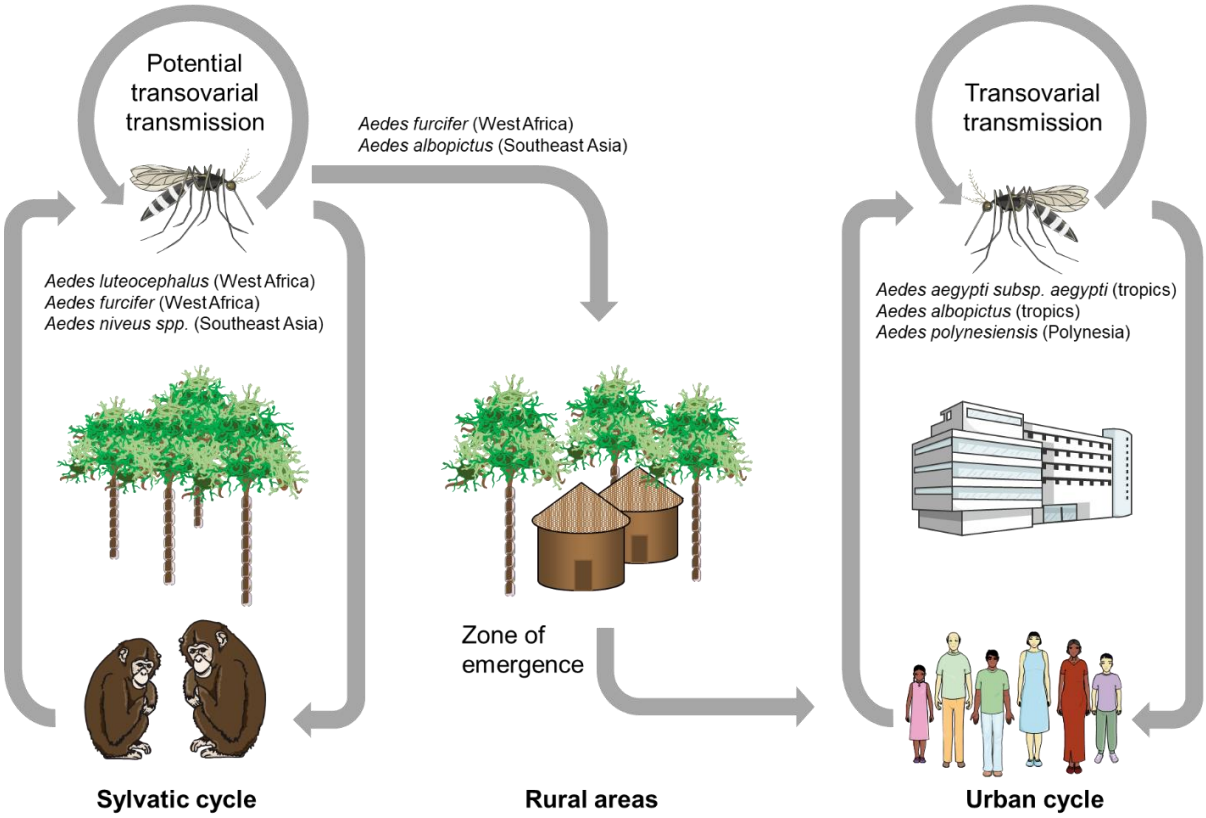

Figure 2. Dengue viruses established a sylvatic and an urban transmission cycle.
Originating from sylvatic habitats, DENVs initially expanded into rural regions in West Africa and Southeast Asia, where human populations and sylvatic cycles overlapped. A vector switch to human-adapted *Aedes aegypti* led to the emergence of a urban transmission cycle. In addition, dengue virus can persist in some *Aedes* species through transovarial transmission, in which infected mosquitoes pass the virus to their eggs. Adapted from Vasilakis et al.[31].

Phylogenetic studies revealed that the urban serotypes DENV-1, DENV-2, and DENV-4 each have at least one sylvatic relative closer to them than the closest urban-related serotype[33]. No sylvatic derivative has yet been isolated for DENV-3; however, anti-DENV-3 antibodies have been detected in Malayan nonhuman canopy dwelling primates, providing indirect evidence for its existence[23,34]. Although the chain of evidence is not yet complete, from today's perspective there is considerable notion that dengue virus segregation into different serotypes has already occurred in primate populations due to geographic (allopatric) or ecological segregation[35]. The emergence of urban DENV-1 to DENV-4 supposedly occurred via four independent evolutionary events and presumably proceeded via a double vector switch first from a canopy-dwelling *Aedes* mosquito (e.g., *Aedes furcifer*) to the peridomestic *Aedes albopictus* and then later to the human-adapted *Aedes aegypti*[33]. Reconstruction of the molecular time scale of DENV evolution is controversial and suffers from the limited availability of sylvatic DENV isolates in some regions of the world, although they most likely exist in large numbers[35]. The most recent common ancestor of all known dengue serotypes probably existed 1000 years or more in the past[33,36]. Since today the greatest biodiversity of sylvatic DENV isolates is found in Malaysia, and significantly exceeds that found in Africa, that common ancestor is thought to have emerged in the former region[22]. However, the time of divergence of the common ancestor into the known serotypes and, more importantly, the time of the zoonotic events that gave rise to today's urban DENV variants cannot be precisely dated. Combining the available studies, for example, the time window for the split of the urban DENV-2 variants from the sylvatic ones ranges from 1400 to 1960 AD[33,36,37]. However, it is considered very likely that the zoonoses occurred in the Asian region at a time when *Aedes aegypti* was still geographically restricted to Africa. This is matched by the fact that contemporary human dengue viruses are significantly better adapted to *Aedes albopictus* than to *Aedes aegypti* in terms of susceptibility, suggesting a longer period of co-evolution[38]. With the advent of intercontinental transport of goods via ocean-going ships in the early modern period, *Aedes aegypti* was probably carried as a stowaway from African to Asian ports[28,39,40]. In the current view, it was the strong adaptation of *Aedes aegypti* to urban habitats that first enabled the occurrence of large epidemic dengue outbreaks and eventually the transition to endemicity[22,41].

I.1.2 Dengue epidemiology

In the last 100 years, the world population has virtually skyrocketed from 2 billion to 8 billion people[42]. One of the reasons for this has been an increase in the global economy's efficiency through international trade in goods, together with the emergence of an industrial and service sector[43]. This has also greatly changed the lives of the general population, and a clear indicator of this is the massive increase in the degree of urbanization. In tropical regions in particular, many cities have barely been able to keep pace with the growing number of inhabitants with the result that they exhibit enormous population densities and often suffer from poor infrastructure[44]. Since *Aedes aegypti* is very well adapted to urban environments, this development represented a tremendous expansion of its habitat[41]. At the same time, the greatly increased mobility of humans has led to rapid spread of both the vector and the four dengue serotypes across large parts of the tropics and subtropics[39,45,46]. Last but not least, especially in recent years, climate change has contributed to the opening up of more and more new living areas for the dengue-transmitting mosquitoes - a development that will continue or even accelerate in the coming decades[47,48]. All of this results in the fact that today half of the world's population lives in regions where dengue virus is endemic, and this proportion could rise to 60% by 2080[49]. Currently, about 400 million dengue infections are estimated to occur annually, of which about 100 million are symptomatic[50]. Although most of these cases cause mild to moderate dengue fever, there are also clinically severe forms whose epidemiology is difficult to quantify. Current studies report rates between 0.3% and 1.2% of all clinically manifested cases, but it is pointed out that the generalizability of the data is insufficient for various reasons[51]. Nevertheless, it can be said with certainty that dengue virus is by far the most prevalent human pathogenic flavivirus. By comparison, the annual average number of cases of the related Zika virus over the past decade is reported to be about 50,000 to 300,000[52]. For yellow fever virus, there are currently about 130,000 cases per year, and for West Nile virus, there are less than 10,000[53]. The cumulative disease burden of dengue infections is immense, estimated at 2.4 million disability-adjusted life years (DALYs)[54].

An overcome dengue infection usually induces lifelong immunity to all strains of the same serotype[55], but heterotypic cross-protection against other serotypes is robustly present for only about two years according to current modeling approaches and then steadily declines[56]. This fits with the observation that dengue fever occurs in cyclic epidemics, usually interspersed by heterotypic herd immunity-induced periods of low incidence lasting about three to five years, with serotypes present in a region often alternating in periodic succession[57].

I.1.3 Pathogenesis and pathophysiology of DENV infections

A dengue infection does not necessarily have to be accompanied by symptoms of disease; in fact, modeling studies suggest that asymptomatic courses are the majority[50]. In those cases that are symptomatic, nonspecific flu-like manifestations such as fever, chills and nausea predominate, occurring approximately 4-7 days after a mosquito bite[58]. More specific manifestations such as retro-orbital headache as well as muscle and joint pain may also occur, but are not yet indicative of a severe course, as these, like those already mentioned, resolve on their own in the vast majority of cases after 6-8 days together with the decreasing viral load as illustrated in Figure 3a[59]. While most patients experience improvement in health at this stage, a small fraction suffers from rapid deterioration caused by vascular leakage and associated dengue hemorrhagic fever (DHF)[60]. In addition, with increasing fluid leakage into surrounding tissues, pulse pressure can drop and the patient may go into shock, which is known as dengue shock syndrome (DSS) and is potentially life-threatening[61]. The term "dengue vascular permeability syndrome" (DVPS) is increasingly used as an umbrella term for the complication forms DHF/DSS; in less formal language, "severe dengue" refers to essentially the same condition[62]. Although it has been shown that any of the four serotypes can cause DVPS upon initial dengue contact[63], there is clear evidence that DVPS is more likely to occur in the setting of secondary heterologous dengue infection when cross-protective immunity from previous dengue infections has waned[64]. The viraemia curve is shortened by about 2 days in this scenario, due to both a faster rise and fall (Figure 3b). In addition, higher peak viremia levels are characteristic[59]. The molecular mechanism underlying this observation is termed antibody-dependent enhancement of disease (ADE) and is illustrated in Figure 4. Antibodies produced in response to dengue infection have sufficient neutralizing potential to provide long-term immunity against homotypic variants only. Cross-reactivity against other serotypes is generally low and it is primarily due to quantitatively high titers in the early post-infection period that there is a short-term cross-protection[65,66]. With time, declining titers lead to an inability of the cross-reactive antibodies to neutralize heterotypic virions, yet weak virus-immune complexes are formed, which are then recognized by FCγ receptors on blood-derived monocytes[67,68]. In some cases, this leads to digestion of the pathogen and presentation of antigens on the surface, inducing immune memory recall leading to massive expansion of plasma cells that start to produce heterotypic antibodies[69]. However, the virus often manages to escape its antibody opsonization after uptake into monocytes. The immune cells become the first host cells, from where the virus can then spread rapidly[70]. Progeny viruses are in turn efficiently opsonized,

amplifying the process described. Subsequently, mast cells recognize both IgG and IgE antibodies via different Fcγ receptor subtypes and the Fcε receptor, which initiates mast cell degranulation, leading to the release of various bioactive constituents including among others the vasoactive mediators chymase and leukotrienes, which then promote pathological vascular leakage[71,72]. When viral antigens on the surface of infected cells are recognized by antibodies, the resulting antigen-antibody conjugate can be detected by cytotoxic natural killer cells (NK cells), which then lyse the infected cell in a process called antibody-dependent cellular cytotoxicity. The simultaneous release of cytokines and cytotoxic granules may contribute to the development of a so-called cytokine storm that inflicts the severe manifestations of DVPS. Moreover, the activated NK cells cause collateral damage to the surrounding tissue, which may further enhance a pro-inflammatory environment[73]. Whether cross-reactive memory T-cells tend to be protective or pathological in secondary heterotypic dengue infections is controversial[74-77]. There is at least indication that rapid reactivation of suboptimal memory T-cells from a previous dengue infection can outcompete naïve T-cells that are more specific for the serotype of the current infection; a concept termed original antigenic sin. Because of the lower specificity, the T-cell response could then lead to excessive cytokine production rather than efficient viral clearance, which could contribute to vascular permeability[76,77].

Another candidate that influences DENV pathogenicity is the highly versatile nonstructural viral protein NS1, which increases vascular permeability by multiple mechanisms, presumably to drive viral dissemination[78,79]. In an immune system-independent manner, secreted NS1 can dock to membrane-bound proteoglycans on the luminal side of endothelial cells to trigger various processes from there. In this way, enzymes are activated in the endothelial cells (including neuraminidases, cathepsin L, and heparanase), which then cleave components of the endothelial glycocalyx layer, leading to hyperpermeability of blood vessels[80]. In addition, NS1 stimulates the phosphorylation of β-catenin in a GSK-3β-dependent manner as well as the clathrin-mediated endocytosis of VE-cadherin, resulting in a dysfunction of intercellular junction complexes[81]. Beyond that, secreted NS1 hexamers can be recognized by IgM and IgG antibodies during the acute phase of infection, giving rise to immunoconjugates that can initiate inflammatory processes. On the one hand, this triggers the complement system, resulting in an intensified pro-inflammatory environment[82,83]. On the other hand, platelets and basophils can bind immunoconjugates via their FC receptor, which stimulates the release of vasoactive amines that enhance the permeability of the endothelium[79]. Last but not least, NS1 is known to induce autoantibodies directed against a wide range of host cells including platelets[84,85]. Opsonization of the latter causes accelerated clearance by phagocytes and complement-

mediated lysis, which ultimately leads to the development of thrombocytopenia[86].
NS1-associated processes, which involve the immune system, are intensified in secondary dengue infections, which is another explanation for the increased probability of a severe course of the disease in this context[79].

Advanced sequencing methods have revealed variations within each of the dengue serotypes and led to classification into genotypes[87]. Most sequenced isolates are from patients with a severe course of dengue, whereas those from mosquitoes or sylvatic hosts are underrepresented, so that the current genetic landscape represents only a snapshot[88]. Several studies have investigated whether individual genotypes correlate with disease severity[22]. There is a high level of evidence that the Asian genotypes of dengue serotype 2 are more virulent than the American genotype[89], which has been supported by the experimental finding that those isolates are particularly efficient at infecting dendritic cells[90]. Also, DENV-2 cosmopolitan genotype is associated with increased probability of epigastric pain and shock syndrome[91]. In general, it can be said that DENV-2 causes clinical complications more frequently than the other serotypes[92]. DENV-3, on the other hand, evokes musculoskeletal symptoms at a higher rate[93,94], with muscle pain being particularly common for genotype I and joint pain being more prevalent for serotype 3[91].

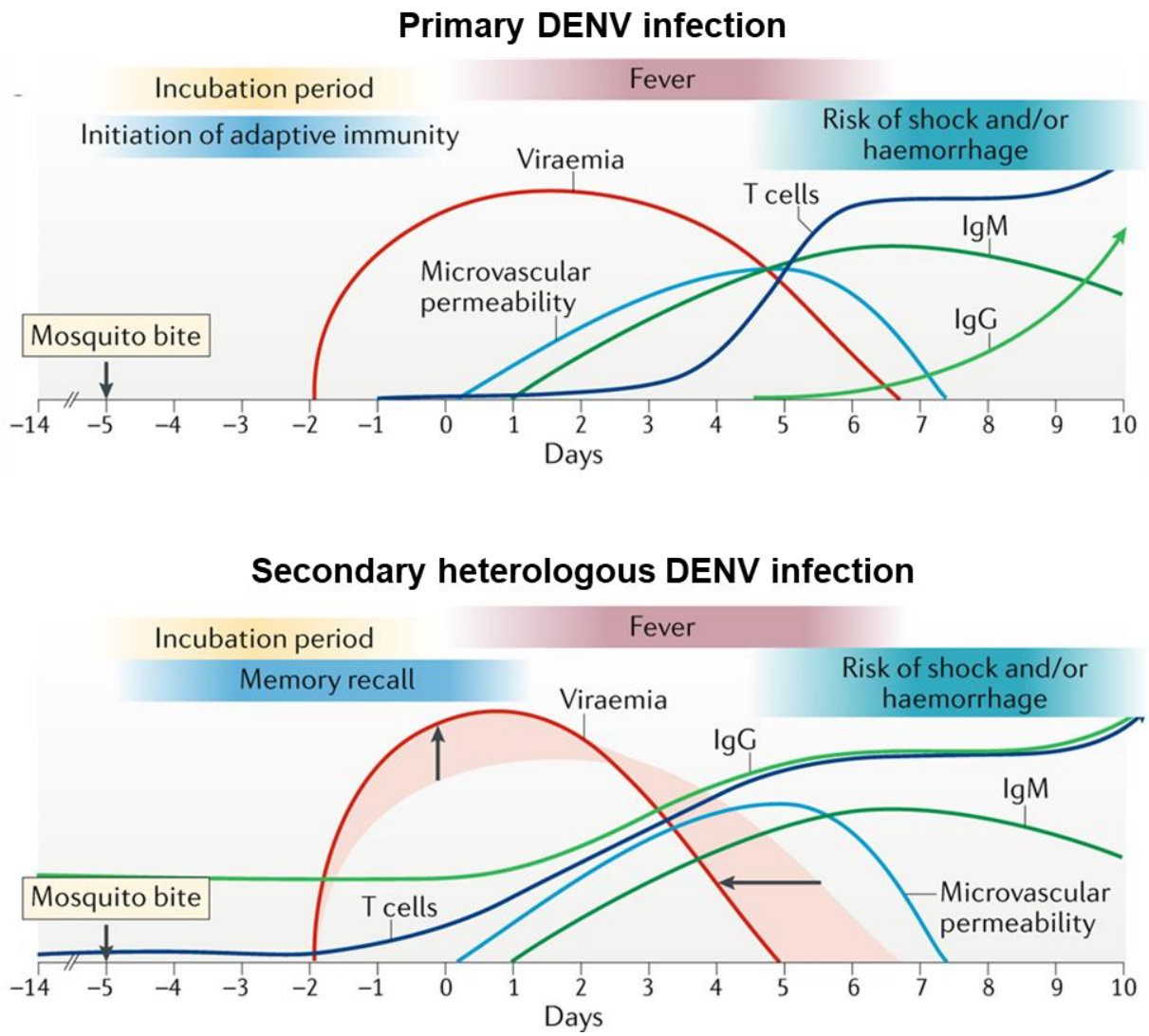

Figure 3. Progression of acute infection and immune responses during symptomatic primary and secondary DENV infection.
Dengue virus infection starts with the bite of a DENV infested mosquito. In case of a primary DENV infection (top panel), an incubation period of 4-6 days follows before the development of fever. The peak of viraemia coincides with high fever and the initiation of IgM and IgG production, which helps clear the infection. Some patients may experience bleeding and/or shock during the resolution of viraemia, which is believed to be immune-mediated. During secondary heterologous DENV infection (bottom panel), the viraemic period is shorter due to cross-reactive immunity, including pre-existing antibodies. Cross-reactive memory T cells trigger an earlier and stronger T cell response compared to the primary infection. The presence of pre-existing immune memory may have a negative impact on immune responses during secondary heterologous DENV infection, increasing the risk of severe dengue. Microvascular permeability, a hallmark of dengue disease, typically becomes clinically apparent during the defervescent stage of the illness. Adapted from St. John & Rathore[59].

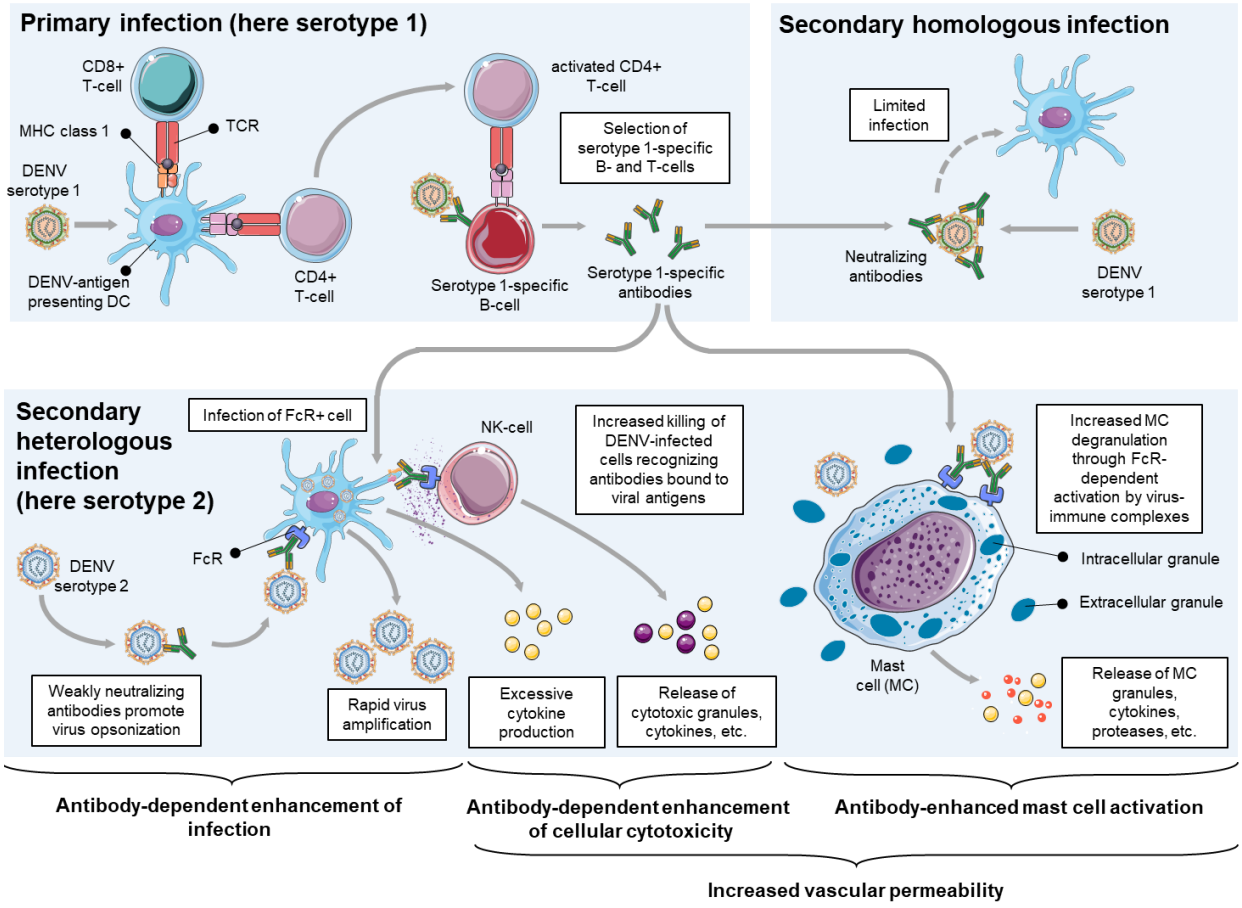

Figure 4. Molecular mechanisms of antibody-dependent enhancement (ADE) of infection and disease severity.
Antibody-dependent pathologies arise during dengue virus infections as a result of pre-existing antibodies against DENV that are interacting with different cell types. There are several theories that describe these interactions and how they can lead to severe disease. After the primary infection, serotype-specific, high-affinity antibodies are generated and can neutralize DENV if present at optimal concentrations. During secondary homologous infection, the levels of pre-existing antibodies may increase, leading to effective neutralization of the virus. On the other hand, during secondary heterologous infection, pre-existing cross-reactive, sub-neutralizing antibodies may trigger opsonization of virus particles and increase their uptake by immune cells, such as monocytes and macrophages, via Fc receptors (FcRs), resulting in antibody-dependent enhancement (ADE). ADE causes an increase in viral replication within infected immune cells and leads to the release of excessive cytokines, resulting in a cytokine storm. Mast cells (MCs) can also recognize virus particles bound by antibodies in an FcR-dependent manner, leading to increased degranulation of pre-stored cytokines and proteases, as well as the synthesis of new cytokines. These cytokines and proteases contribute to increased vascular permeability and leakage during dengue virus infection. Furthermore, antibodies can play a role in the pathology during secondary dengue virus infection through antibody-dependent cellular cytotoxicity, in which antibodies bind to the surface of infected cells, resulting in their direct lysis by natural killer (NK) cells. The release of cytotoxic granules and cytokines by NK cells contributes to the cytokine storm and exacerbates tissue damage during infection clearance. APC stands for antigen-presenting cell, DC stands for dendritic cell, and TCR stands for T cell receptor. Adapted from St. John & Rathore[59].

I.2 Molecular biology of DENV

I.2.1 Genome

The dengue virus genome consists of an approximately 10.7 kb long RNA with positive polarity, which carries a type I cap at the 5' end and, unlike cellular mRNAs, does not possess a poly-A tail at its 3' end[95]. In line with all other flaviviruses, dengue virus lacks access to the host machinery to perform capping[96]. The enzymatic processes are therefore carried out by viral proteins. In a first step, the rNTPase of NS3 removes the γ-phosphate from the 5' nucleotide of nascent viral RNAs[97,98]. Subsequently, NS5 takes over and first attaches a GMP through a 5′-5′ linkage by means of its guanylyltransferase activity, whereupon the attached nucleotide is methylated at the N^7 position by NS5 N^7G methyltransferase activity. At last, NS5 ribose methyl transferase performs a 2' O-methylation at the penultimate nucleotide[99]. The latter modification appears to allow dengue genomic RNA to efficiently evade detection by the early innate immune response[100]. N7-guanine methylation is essential for virus infection and serves several purposes including protection from exonucleases, masking of foreign identity, and stimulation of translation initiation[101-103]. The protein-coding region of the dengue genome contains information for a single polyprotein and is surrounded by highly-structured non-translated regions (NTRs) that extend upstream for about 100 base pairs and downstream for about 450 base pairs[95,104]. Several NTR elements are indispensable for critical steps in the virus life cycle such as translation, replication organelle formation, genome replication or virion assembly[105-109].

I.2.2 Viral proteome

The polyprotein resulting from the single dengue open-reading frame, is processed in an interplay of the viral protease complex (NS2B/NS3) with additional host proteases, ultimately giving rise to three structural proteins (capsid (C), pre-membrane/membrane (prM/M)) and envelope (E)) as well as seven non-structural proteins (NS1, NS2A, NS2B, NS3, NS4A, NS4B and NS5)[110,111]. Since a complete polyprotein has never been detected, it can be assumed that proteolytic processing is initiated in a co-translational manner[104]. There is a body of evidence that the sequence of cleavage events is coordinated. For instance, cleavage of the hydrophobic membrane anchor between capsid and prM first requires viral protease complex-mediated cleavage at its N-terminus on the cytosolic side, in order to enable efficient further processing at the C-terminus by the host signal peptidase complex[112]. Alternation of processing kinetics induced by mutagenesis of cleavage motifs showed immediate effects on nucleocapsid

incorporation into newly forming virus particles[113-115]. Similarly, maturation of the metastable NS4A-2K-NS4B precursor also first requires cleavage of NS4A from 2K-NS4B via the viral protease complex before 2K-NS4B is further metabolized by the host signal peptidase complex to 2K and mature NS4B[116-118]. Figure 5 shows schematically the rough membrane topology of the mature flaviviral proteins, and in subsequent chapters the current state of research with respect to dengue virus is described for each of these.

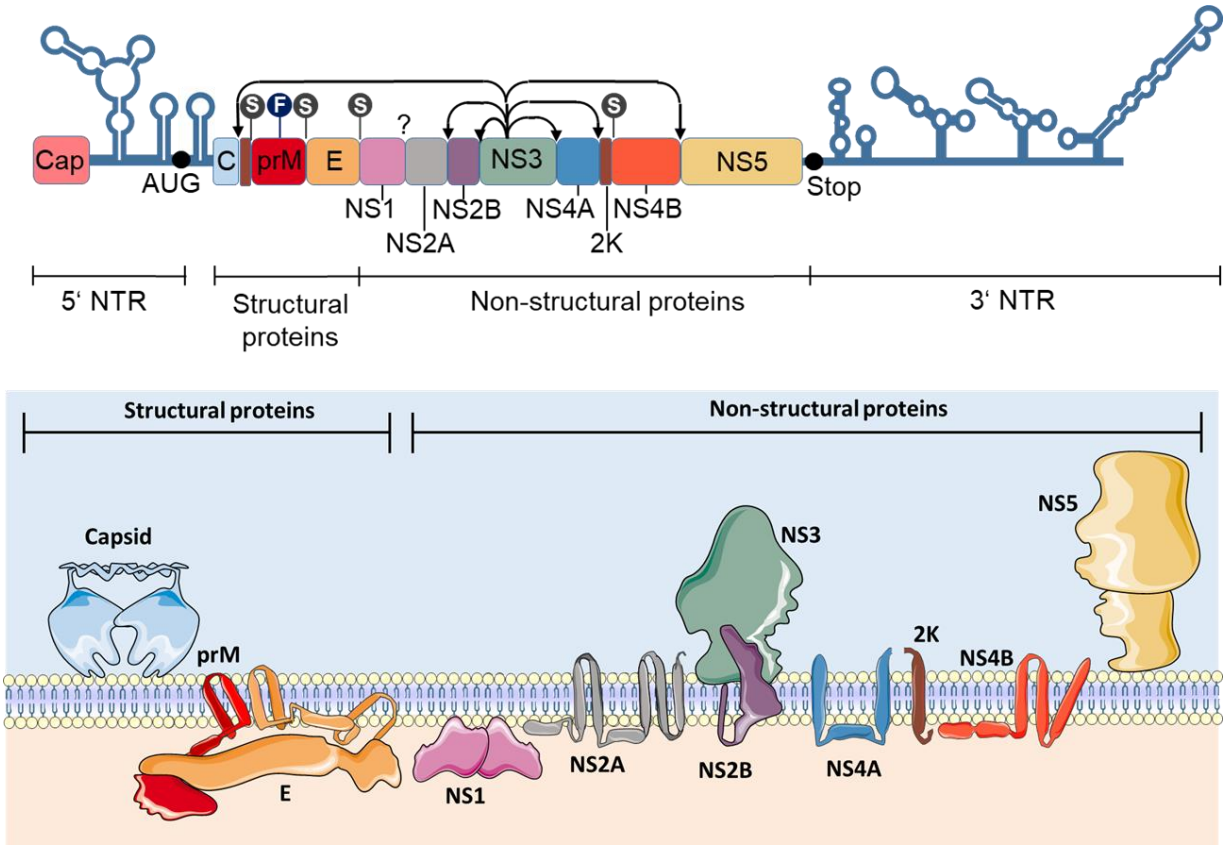

Figure 5. DENV genome organization and membrane topology of mature viral proteins.
The genome of DENV, as depicted in the top panel, consists of a single open reading frame that includes a type 1 cap structure at the 5' end and various secondary RNA structures in both the 5' NTR and 3' NTR regions. The positive strand of DENV encodes for a single polyprotein, not depicted in the panel. Instead, the bottom panel displays all the mature DENV proteins and their locations on the cytoplasmic or luminal side of the ER or within the ER membrane The conversion of the polyprotein into mature proteins is achieved by various proteases, and for ease of understanding, the polyprotein cleavage is depicted in the genome schematic (top panel). Cleavage sites of cellular signal peptidases are represented by grey pinheads marked “S”, while arrows indicate the cleavage steps performed by the viral protease complex NS2B/NS3. The dark blue pinhead marked “F” signifies the cleavage by the Golgi protease furin. A question mark highlights a cleavage site between NS1 and NS2A for which the responsible protease has yet to be identified. While C, prM and E are crucial components of the DENV virion, all non-structural proteins play a role in viral RNA replication. NS1 forms homodimers and contributes to the RNA amplification process and is also an important pathogenicity factor secreted by infected cells. NS2A binds to the 3' NTR to recruit viral RNA genomes for packaging and delivers them to the assembly sites. NS2B, a transmembrane protein, links NS3 to ER membranes and activates its N-terminal serine-type protease. NS4A and NS4B, highly hydrophobic transmembrane proteins, are capable of remodeling intracellular membranes; the 2K peptide between them functions as a signal peptide for co-translational NS4B insertion into the ER membrane. NS5 serves as the RNA-dependent RNA polymerase and also contains a guanylyl-transferase and N-terminal methyl-transferase domain, required for capping and methylation of the viral RNA genome, thus reducing its recognition by cytosolic pattern recognition receptors. Adapted from Neufeldt et al.[119].

Capsid C

The capsid (C) protein of DENV is a strongly basic protein with a molecular weight of 12 kDa that forms homodimers in solution[120]. These dimers display an asymmetric charge distribution, with basic residues clustering on one side of the molecule while a concave apolar surface is present on the opposite side[121]. Although capsid is the viral protein with the lowest degree of conservation within representatives of flaviviruses, the charge distribution is highly conserved as this is essential for interaction with the acidic phosphate backbone of viral RNA[120]. DENV capsid proteins bind RNA with high affinity irrespective of sequence, thus assembling the nucleocapsid and also act as RNA chaperones by resolving unwanted folding patterns[122].

Beyond its structural relevance for nucleocapsid formation, capsid is also known to interact with numerous host proteins. For example, capsid proteins that migrate into the nucleus are thought to bind to histones and thus regulate transcription by disrupting nucleosomes[123]. Furthermore, interaction with Death-associated protein 6 (DAXX) is associated with the initiation of FasL-dependent apoptosis[124]. However, it should be emphasized that capsid exhibits a promiscuous interaction profile, so that many interaction partners could not be assigned any functional role in DENV virus infection[121].

Membrane (precursor) prM/M

Membrane precursor protein (prM) is a ~26 kDa structural protein that, together with the envelope protein (E), is involved in building a lipid-protein envelope that encloses the nucleocapsid[125]. As the name implies, it consists of a glycosylated predomain at the N-terminus and an M-domain anchored to the lipid bilayer via two transmembrane domains at the C-terminus[125]. The main function of prM is to serve the E-protein as a chaperone by controlling its conformational changes during different steps of the secretory pathway[126]. At first, the fusogenic potential of E is suppressed by the formation of prM-E heterotrimers[127]. When passing the Golgi apparatus, prM comes into contact with the resident protease furin. Decreasing pH induces conformational rearrangements in E and prM, so that a furin cleavage site residing between pr and M is getting exposed[128]. After proteolytic processing, pr remains bound to M in a non-covalent manner, thus still preventing premature fusion[129]. The mild pH of the extracellular space triggers the dissociation of the pr fragment from released particles, providing the latter with infectious properties[129].

Envelope E

The envelope (E) protein represents the main surface protein of dengue virus. It has a molecular weight of about 53 kDa and exhibits cell type-dependent glycosylation at several

positions[130,131]. The E-protein encompasses a C-terminal transmembrane anchor domain and a soluble ectodomain, which in turn is composed of three structural domains (D-I, D-II, and D-III)[127]. D-II forms the fusion loop and additionally constitutes the interface through which E-monomers can interact with each other[132]. D-III folds a surface-exposed immunoglobulin-like β-barrel structure containing a pocket putatively involved in host cell receptor recognition[133]. The E-protein undergoes various structural changes during the viral life cycle that support its respective roles in viral assembly, attachment, internalization, and fusion. Thus, in the prefusion state, E proteins form flat homodimers that prevent premature fusion and shield particularly immunogenic epitopes, while the acidification process during endocytosis transforms them into a trimeric configuration that triggers a hemifusion state through which viral RNA enters the cytoplasm[126,134,135].

NS1

NS1 is a very versatile protein, which is found in a cell membrane-associated state at the cell surface, as well as in replication organelles, but can also be secreted as a lipid-containing extracellular species[79]. After processing of the polyprotein, it is initially present in the ER[136,137], where it undergoes various forms of glycosylation that have significant impact on its final molecular weight (that ranges from 46 to 55 kDa) and ultimately determine both its state of oligomerization and its intracellular trafficking route[138]. Dimers associate with the ER membrane and localize predominantly to replication organelles[138,139]. There, they contribute to the proper formation of vesicle packets and establish an interaction with the NS4A-2K-NS4B precursor, which plays a supporting role in viral replication[140]. Another portion of NS1 is directed to the secretory pathway, where the proteins undergo further post-translational modifications in the Golgi apparatus, eventually resulting in NS1 being secreted into the extracellular space as a soluble hexamer[141]. As described in Chapter I.1.3, secreted NS1 contributes to increased vascular permeability through both immune-independent mechanisms and immunogenic paths, which in concert putatively promote viral dissemination and increase the likelihood that dengue viruses are transmitted to mosquitoes upon biting[79,142]. Especially in heterotypic secondary infection with DENV, these NS1-mediated effects are severe, and thus play a major role in the pathogenesis of the potentially life-threatening dengue vascular permeability syndrome (DVPS)[79]. A considerable proportion of the antibodies elicited during a DENV immune response are directed against NS1[143]. Although the mechanism is elusive, anti-NS1 antibodies contribute substantially to immune protection, at least in mice[142].

NS2A

NS2A is a 22 kDa transmembrane protein with so far unresolved structure. It is predicted that NS2A comprises 8 putative transmembrane segments (pTMS), 5 of which are presumed to be true transmembrane domains[144]. A previously unknown host protease cleaves NS2A from NS1 at the N-terminus while, on the opposite side, a cleavage of NS2B is mediated by the viral protease complex NS2B/NS3[137]. Mutagenesis studies have shown that different positions within NS2A are necessary for viral replication, thus the protein is thought to be part of the replicase complex. Yet, in order to fulfill this function, it seems to be necessary that NS2A is expressed in *cis* together with the remaining non-structural proteins[145]. Apart from this, the surface exposed N-terminal part of NS2A is attributed a major role in the virus-induced cytopathic effect[146]. The C-terminus, on the other side, has an essential function in virion assembly. To this end, NS2A recruits both DENV genomes and the viral protease complex NS2B/NS3, brings them together and thus creates the preconditions for virion assembly sites[147]. Finally, for DENV serotypes 1,2 and 4, NS2A has been shown to act in concert with NS4B to inhibit TANK-binding kinase 1 (TBK-1) phosphorylation thus preventing host cells from initiating a RIG-I/MAVS-mediated immune response[148].

NS2B

Non-structural protein 2B is a 15-kDa hydrophobic transmembrane protein whose best-known function is to form a heterodimer with NS3, thereby serving as a co-factor of the viral protease complex[149]. On the one hand, the interaction serves to tether NS3 on the cytosolic side of the ER membrane. However, at least for WNV, NS2B was also shown to shape part of the substrate-binding pocket in the ligand-bound NS2B/NS3 complex[150]. Beyond functions in viral replication, NS2B exerts an antagonistic effect on the host immune response. This is accomplished by targeting cyclic GMP-AMP synthase (cGAS), a cytosolic DNA sensor, for lysosomal degradation. As a result, mitochondrial DNA that enters the cytosol upon DENV-induced damage to mitochondria is no longer recognized there and thus the signaling cascade leading via STING to the production of type I IFN is not triggered[151].

NS3

With a molecular weight of 69 kDa, NS3 is the second largest mature protein resulting from processing of the DENV polyprotein[152]. It comprises two large domains, of which the N-terminal one has the properties of a chymotrypsin-like serine protease and performs both *cis* and *trans* cleavages on the viral polyprotein, while the C-terminal domain represents an NTPase-dependent RNA helicase that on the one hand assists in genome replication, and on

the other hand participates in 5' capping of *de novo* synthesized plus-strand RNA[153]. NS3 requires NS2B first for correct folding, second for membrane tethering and third as an active co-factor of the protease domain[154,155]. The active site of the protease consists of the catalytic triad H51, N75, S135[149] and recognizes substrates that share similarities in an octapeptide sequence in which the actual cleavage site is positioned in the center[156]. As depicted in Figure 6, there is considerable plasticity with respect to the cleavage site mofif, yet it can be generalized that positively charged residues are required at both positions P1 and P2, which are immediately N-terminal to the cleavage site, followed by a small or polar amino acid at position P1', which is the first residue C-terminal to the cleavage site[156].

The helicase domain of the NS3 protein can be classified into three subdomains. The first two show high sequence homology to representatives of helicase superfamily 2 (SF2), contain all helicase-associated enzymatic activities and adopt a folding structure known from the RecA protein[157,158]. The third subdomain forms a kind of tunnel for single-stranded RNA[152]. NS3 helicase is thought to split dsRNA intermediates, which are transiently formed during NS5-mediated strand duplication, as well as to remove RNA secondary structures and RNA-binding proteins to aid in the initiation of a new round of replication[152]. NS3 recognizes viral RNA in a sequence-independent manner and the hydrolysis of ATP provides the driving force for helicase-mediated activities[158]. The underlying rNTPase activity also mediates the removal of the γ-phosphate from newly forming plus strand viral genomes, which is the first step in the construction of the type 1 cap used by DENV[98].

Beyond enzymatic tasks, NS3 excels in numerous interactions with host proteins[159]. Many of these are involved in metabolic pathways related to fatty acid synthesis, autophagy and actin polymerization[160]. Particular attention needs to be paid to an enzyme called fatty acid synthase (FAS). NS3 recruits this host factor to virus-induced replication organelles in a Rab-18 dependent manner, where it stimulates the rate of *de novo* synthesized lipids[161]. In this way, NS3 presumably contributes to membrane remodeling, which is a prerequisite for the structural assembly of vesicle packets, the putative sites of viral replication[160].
Finally, several NS3 mutants were identified that showed a defect in virion assembly but not in replication, so that NS3 probably also plays a role in the former step of the viral life cycle, although the underlying mechanism has not been elucidated[162].

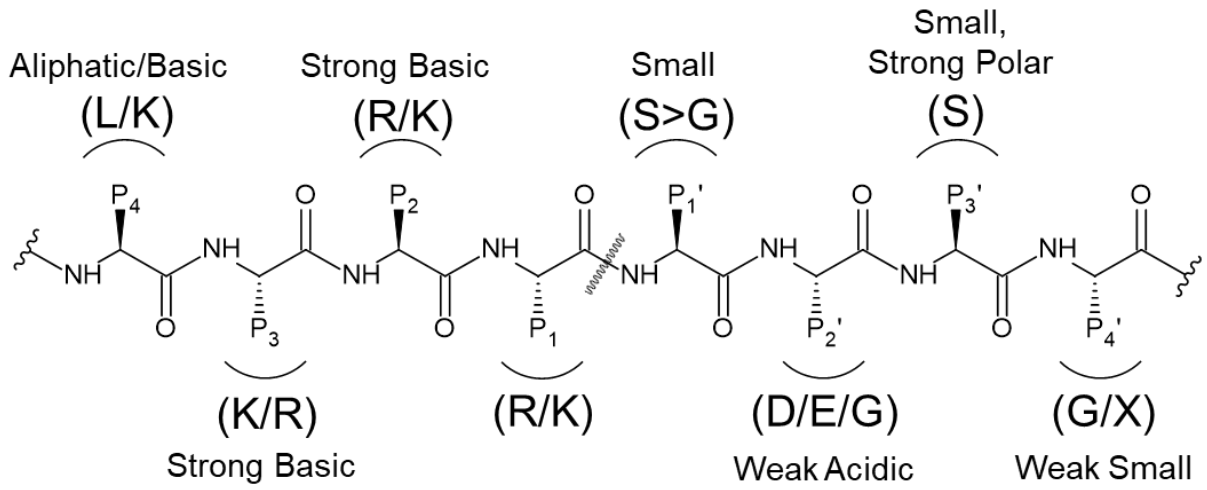

Figure 6. Subsite specificities of DENV NS3 protease.
Adapted from Li et al., 2005. Shown is a DENV NS3 cleavage site consensus motif. The exact position of the proteolytic cleavage is shown by a wavy line in the center of the motif. Amino acid residues upstream of this are denoted P1, P2, P3 and P4 according to their distance, while the downstream counterparts are named P1', P2', P3' and P4' respectively. For each position, the amino acid preference is indicated. A table breaking down the 1-letter amino acid abbreviations can be found in the appendix (Supplementary Table 3).

NS4A

NS4A, like NS4B, is an ER resident transmembrane protein that arises from an NS4 precursor protein termed NS4A-2K-NS4B. The amphipathic N-terminal region of NS4A contains hydrophobic surfaces that interact with the cytoplasmic side of the ER, preferring curved membranes[163]. The C-terminal portion of the protein contains two membrane-spanning transmembrane domains (TMDs) and one in between that is membrane-associated at the ER lumen side[164]. TMD1 is of particular importance since it is essential for NS4A self-oligomerization and presumably also for interaction with the host protein reticulon 3.1A, two processes thought to play driving roles in virus-induced membrane remodeling to form replication organelles[165] although the details are not yet sufficiently understood. In addition, there also seem to be differences among the flaviviruses. For example, in DENV, proteolytic cleavage of the 2K peptide from NS4A is a prerequisite for correct membrane topology as well as for the induction of authentic membrane rearrangements[164]. Conversely, for WNV, the retention of the 2K peptide is still mandatory for these processes[116]. Aside from its involvement in membrane rearrangements, NS4A carries out a whole range of other tasks: Heteromultimeres comprising NS4A and mature NS4B are part of the replicase complex and thus fulfill a role in genome amplification[166]. The interaction of NS4A with vimentin helps to correctly position these complexes within vesicle packets[167]. Moreover, the nuclear ribonucleoprotein polypyrimidine tract-binding protein (PTB) links the DENV genome with NS4A and it has

been shown that this indirect connection is of relevance for the synthesis of negative strand RNA[168]. In addition, DENV NS4A plays an important role in modulating both PI3K-dependent autophagy and AUP1-mediated lipophagy, creating a cellular environment that favors active replication, drives virus production and protects infected cells from death, thereby increasing viral persistence[169,170]. Last but not least, NS4A of DENV serotype 1 is interfering with the host interferon system by inhibiting TBK1, while in serotypes 2 and 4 this mechanism is exclusively executed by NS2A and NS4B[148].

NS4B

Of the four small hydrophobic proteins NS2A, NS2B, NS4A, and NS4B that arise from the DENV polyprotein, the latter is the largest, with a molecular weight of about 27 kDa[171]. Like NS4A, NS4B derives from the NS4A-2K-NS4B precursor through an interplay of the viral protease complex NS2B/NS3 and the host signal peptidase complex[172]. The processing proceeds via an intermediate species called 2K-NS4B. 2K serves as a signal peptide and is required for the correct co-translational membrane insertion and protein folding of NS4B[172]. Mature NS4B is highly conserved among dengue serotypes with sequence homology rates exceeding 85%. The sequence similarity between the different representatives of flaviviruses is lower, but is still at least 50%[171]. Due to its high proportion of hydrophobic amino acids (~40%), NS4B was long thought to be a multi-pass transmembrane protein, however, it was not until 2006 that a precise topology model of NS4B was presented, supported by data from biochemical assays[172]. This model assumes that NS4B has a total of 5 transmembrane domains (TMDs), with TMDs 3 and 5 spanning the membrane from the luminal to the cytosolic side, while TMD 4 crosses the membrane in the opposite direction. TMDs 1 and 2 most likely do not span the membrane but appear to be located in the ER lumen. Prior to cleavage of the NS4B-NS5 junction, the C-terminus of NS4B is located in the cytoplasm, but could possibly migrate across the membrane in small proportions thereafter. It is probably because of the large cytoplasmic loop between TMD3 and TMD4 together with the high flexibility of the N-terminal fragment that previous attempts to elucidate the structure by X-ray crystallography failed[173,174]. However, by NMR spectroscopy, backbone resonance assignments of full-length NS4B in lyso-myristoyl phosphatidylglycerol micelles could be performed, revealing eleven α-helices (α1, α2, α3, α4, α5, α6, α7, α8, α8', α9, α9')[174]. The combination of a paramagnetic relaxation enhancement (PRE) experiment and a hydrogen-deuterium (H-D) exchange assay indicated that α2, α3, α5 and α7 represent transmembrane helices. Similar to the model of Miller and coworkers, helices a9 and a9' together form a 5th transmembrane domain that

behaves differently from the other four and presumably has the potential to change its conformation after proteolytic cleavage at the NS4B-NS5 junction to subsequently interact peripherally with the luminal ER membrane[174]. Recently, available NMR data were combined with a model calculated by the AlphaFold2 algorithm, resulting in a new picture in which NS4B has a total of seven transmembrane domains[171]. Whether this model can be confirmed remains to be seen. A limitation of all models to date is that it cannot be said with certainty that the topology of NS4B expressed alone fully corresponds to the topology of NS4B expressed in the context of the viral polyprotein.

The correct membrane topology of NS4B depends on the host ER membrane protein complex (EMC), whose cellular function is to assist multi-pass transmembrane proteins in inserting TMDs in a chaperone-like manner[175]. Subunit 4 of the EMC complex (EMC4) was proven to physically interact with NS4B and accumulated in puncta that were rich in NS4B[176]. EMC knockout cells displayed both a reduced level of NS4B expression and a dramatic impairment of viral replication[176]. Presumably, the EMC is primarily required for the accurate alignment of the relatively weakly hydrophobic transmembrane domains 1 and 2 at the N-terminus of NS4B, since replacement of all polar and charged amino acid residues in this region resulted in a complete rescue of ectopically expressed NS4B[176]. When NS4B is not expressed as a single entity but is launched via the NS4A-2K-NS4B precursor, the EMC affects the transmembrane domains located in both the NS4A and NS4B parts. Consistent with the results obtained with mature NS4B, a knockout of the EMC impairs NS4A-2K-NS4B expression[177]. Furthermore, the knockout in this case has an additional destabilizing effect on the NS4A-2K-NS4B precursor, as well as on mature NS4B arising from it, suggesting that defects in the proper membrane integration of the NS4A portion of the NS4A-2K-NS4B precursor may transfer to the NS4B portion in a co-translational manner[177].

Both in DENV infected cells and in the context of recombinant NS4B expression, NS4B was shown to be post-translationally modified by N-glycosylation at positions 58 and 62[178]. These modifications are mediated by the oligosaccharyltransferase (OST) complex, with which NS4B physically interacts[179]. They are of critical relevance to RNA replication by presumably ensuring the correct integration of NS4B into the replicase complex. In contrast, a defect in N-glycosylation does not affect the stability of NS4B, nor does it interfere with the assembly, maturation, or secretion of DENV virions[178]. DENV NS4B protein tends to form dimers, which has been documented both in virus-infected cells and by means of recombinantly expressed proteins[180]. Furthermore, it has been achieved to identify the cytosolic loop between TMD 3

and TMD 4 and the C-terminal end of NS4B as the regions that are crucial for this[180]. However, since to date no condition is known by which dimerization can be influenced (either by mutation or by treatment with an active agent), the functional significance of this process for DENV remains unknown.

While NS4B itself is not known for having intrinsic enzymatic activities, it plays an essential role in viral replication by forming interactions with other viral proteins[181]. For instance, the viral non-structural proteins NS4A and NS4B that both derive from the processing of the NS4A-2K-NS4B precursor are able to interact with each other. Heterodimer formation, for which residues 40-76 of NS4A and residues 84-146 of NS4B are particularly relevant, does not strictly require the partners to be expressed in *cis*, but also occurs in *trans* upon recombinant expression of the individual proteins[166]. Within the sequence of NS4A, three sites (L48, T54, and L60) are known to be critical for the establishment of interaction, while such a precise mapping for the NS4B part is not yet available[166]. The targeted introduction of mutations at described sites revealed deficits in viral replication, suggesting a relevance of the NS4A – NS4B interaction for the functionality of the viral replicase complex[166]. A model not yet adequately supported with data is that the early phase of replication organelle formation may be driven by NS4A oligomerization and NS4B dimerization, whereas increased formation of NS4A/NS4B heterodimers subsequently marks the transition towards active replication[155].
Several scientific works investigated the interaction of DENV NS4B with NS3. The fewest of these examined the interaction profile under infection conditions; instead, various surrogate systems were commonly applied. A first indication for a physical interaction between NS3 and NS4B was obtained using a yeast two-hybrid approach[182]. From the results of an *in vitro* unwinding assay, the model derived that NS3 requires the assistance of NS4B to dissociate from single-stranded RNA after completed separation of double-stranded RNA intermediates[182]. These results were experimentally confirmed in another work using similar methods[183]. Subdomains 2 and 3 of the NS3 helicase domain were identified as critical determinants for the interaction with NS4B[173]. Due to topological considerations, the cytosolic loop between NS4B TMD 3 and TMD 4 was carefully investigated for its interaction potential with NS3 using surface plasmon resonance spectroscopy and NMR techniques, whereas the rest of the protein was not further analysed at that time[173]. Indeed, a strong molecular interaction was detected. Alanine-scanning mutagenesis was used to identify several amino acid residues in said cytosolic loop that are essential for the replication fitness of the virus, including NS4B Q134A and M142A[117]. A Co-IP approach in which the NS4A-2K-NS4B

precursor was expressed in the presence of the viral protease complex NS2B/NS3 revealed that said residues are also fundamental for interaction with NS3. By applying a pseudoreversion selection assay, compensatory mutations were identified that mapped predominantly to NS4B but also partially to NS2A, NS3, and NS4A[117]. Recently, another NS4B segment located at its N-terminus (NS4B 51-83) was associated with both NS3 interaction and an effect on NS3 helicase activity[183].

The versatility of NS4B is exemplified by its numerous interactions with host proteins, thus exerting various pro-viral functions beyond viral replication. To this end, an NS4B-mediated antagonism of antiviral defense mechanisms is well studied. For sensing RNA of viral origin, higher eukaryotes express specific pattern recognition receptors (PRRs), mainly endosomal Toll-like receptors 3 and 7 (TLR3, TLR7) as well as the cytoplasmic RNA sensors RIG-I and melanoma differentiation-associated protein 5 (MDA-5)[184,185]. Stimulation of these sensors triggers a signalling cascade that leads transcription factors such as IRF3 and IRF7 as well as NF-kB to migrate into the nucleus where they eventually induce the expression of IFN-α and IFN-β. A signal mediator in this pathway is TBK1, whose activation is prevented by joint action of NS2A with NS4B[148]. Following production, IFN-α and IFN-β are secreted and bind to corresponding receptors in an autocrine or paracrine manner, thus activating JAK-STAT-dependent signal transduction cascades, culminating in the expression of hundreds of so-called IFN-stimulated genes (ISGs), many products of which exhibit antiviral properties[186,187]. Mature NS4B, but not the NS4A-2K-NS4B precursor, has the potential to block STAT-1 phosphorylation[188]. The first 125 amino acids on NS4B have been identified as critical determinants for this, most of which are located on the ER luminal side according to the current topology model[189]. Not least for this reason, it is assumed that NS4B plays a major role in the subversion of the JAK-STAT pathway, but that this possibly occurs in conjunction with other viral proteins like NS5 or host factors such as UBE2I (Ubiquitin conjugating enzyme E2 I) or PIAS-1 (protein inhibitor of activated STAT-1)[181,190].

Moreover, DENV NS4B was shown to block the activating phosphorylation of mitochondrial fission factor DRP1 via an indirect mechanism. This causes on the one hand an elongation of mitochondria, and on the other hand a disruption of the surrounding mitochondria associated membranes (MAMs) by redistribution to convoluted membranes[191]. Consequently, adapter proteins of immune signaling such as STING or 14-3-3ε get into contact with the viral protease complex NS2B/NS3 and are thus inactivated, which as a consequence suppresses RIG-I-dependent activation of interferon responses[70,191,192].

In addition to the interferon response, NS4B also antagonizes the RNAi antiviral defense mechanism, which is active in both DENV host systems - humans and *Aedes* mosquitoes. Here, NS4B does not bind to dsRNA but, via a not fully understood mechanism, impairs the activity of the Dicer protein, which plays a key role in RNAi by cutting dsRNA into short siRNA fragments[193].

The parasitic behavior of viruses causes stress in host cells, and the formation of so-called stress granules is one of several response options available to cells to mitigate the negative effects. NS4B indirectly recruits the cellular ATPase Valosin-Containing Protein (VCP) to DENV replication organelles by physically binding its cofactor named Nuclear Protein Localization 4 (NPL4). This causes the disintegration of stress granules and facilitates the synthesis of proteins that are required for the initiation of viral genome replication[194]. For some members of the flaviviruses, such as WNV, NS4B has also been implicated in hijacking pathways of the unfolded protein response (UPR). However, such evidence has not yet been obtained for DENV NS4B[181,195].

NS5

With a molecular weight of 105 kDa, NS5 is not only the largest of all mature proteins arising from the dengue polyprotein, but also the one with the highest degree of conservation between individual serotypes (67-82%)[196,197]. NS5 is often called the DENV polymerase as it exhibits an RNA-dependent RNA polymerase activity (RdRp)[198]. Both negative-strand and plus-strand RNA can serve as the starting point for genome duplication[199]. This is followed by a process termed *de novo* initiation, meaning that a cyclization of the DENV genome ensures the correct positioning of the polymerase and allows it to commence its activity without the need for a conventional primer [200]. A more detailed description of DENV replication can be found in Chapter I.3.5. Reducing NS5 to its polymerase function is incorrect, as it is a multidomain complex comprising an RdRp domain (AAs 276-900) and a methyltransferase (MTase) domain (AAs 1-265), the latter performing essential steps in the capping of nascent positive-strand RNA genomes[201]. This occurs in concert with the helicase domain of NS3, more specifically with its rNTPase activity, and NS3 and NS5 have also been shown to physically interact with each other for this purpose[202]. The NS5 MTase domain possesses guanylyl transferase activity that can transfer GMP to the 5' nucleotide of the RNA genome under formation of a 5′-5′ linkage after it has been previously modified by NS3[203]. In a sequential order, the MTase then transfers methyl groups first to the N^7 atom of the attached guanine base and then to the 2' O atom of the outermost regular nucleotide[99,204]. The so formed type-1 cap mimics the 5' cap of

eukaryotic mRNA which protects viral genomes from degradation while mediating interaction with the ribosome for translation[205].

Another function of NS5 is to bind to STAT2 in concert with NS4B, thereby directing STAT2 to proteasomal degradation, which in turn blocks the assembly of STAT1/STAT2 complexes and thus prevents the initiation of a type 1 interferon immune response[190].

Finally, it is worth noting that NS5 forms importin a/b1 interactions and thus a large fraction is translocated into the nucleus, although it is as yet unknown how the virus benefits from this[206].

Precursor proteins

As the name suggests, prM is the best studied flaviviral precursor protein, yet it has a special status due to its late maturation in the Golgi apparatus. While at least for YFV and TBEV it has been shown that ER-associated maturation of the structural part of the polyproteins gives rise to C, prM and E so rapidly that intermediates are not detectable in appreciable quantities, metastable precursors from the non-structural portion of the polyprotein are known for several flaviviruses [207,208]. This category includes, for example, the NS1-NS2A precursor, as well as a long intermediate that extends from NS3 to NS5 and from which further products, such as the already mentioned NS4A-2K-NS4B, arise[111,207,209]. Whether these carry out independent functions in the viral life cycle or primarily coordinate the timing of protein maturation is insufficiently understood. The interaction between DENV NS1 and the NS4A-2K-NS4B precursor, which is relevant for efficient replication, represents the only literature-described example of functional involvement of a non-structural intermediate to date[140].

I.2.3 Virion

Dengue particles undergo morphological rearrangements during cell entry and egress and these processes are described in detail in later chapters[210]. At this point, the focus is on the structural characterization of the mature virion, which is about 50 nm in size and carries a spherical lipid envelope in which both E and M proteins are embedded in a repeating pattern of icosahedral symmetry[211]. The E proteins form primarily antiparallel homodimers, which nestle flat against the envelope to form a smooth glycoprotein coat that largely shields the lipid bilayer from the viral exterior[212], but there is a non-negligible plasticity to their structure that is important for immune evasion and virus-receptor interaction[213]. Residing inside the viral envelope is the nucleocapsid, which consists of one copy of a capped single-stranded RNA genome with positive polarity that is enveloped by several hundred copies of C[121]. It exhibits no defined

symmetry and probably has few, if any, contacts with the inner leaflet of the envelope, from which it is separated by a gap about 3 nm in width[211,214].

I.3 Viral life cycle

I.3.1 Tropism and cell binding

After the bite of a human being by an infected mosquito, cells located in the dermal and epidermal layers of the skin are among the first targets of DENV[215]. This category includes for instance Langerhans cells, active dendritic cells, macrophages, mast cells and blood-derived monocytes[216-218]. In these, the virus finds an environment in which it can proliferate. Next, infected immune cells typically enter the lymphatic system, where they further spread the virus[219]. Blood-derived monocytes and myeloid dendritic cells that become infected there eventually carry the infection to several other organs[219,220]. For liver and blood, there is solid evidence that these contribute substantially to virus propagation[221-225]. In addition, the dissemination of the virus to the heart [226,227], brain[228], gastrointestinal tract[229] and bone marrow[230] has been scientifically described, although it is insufficiently investigated whether the results can be generalized to the standard course of disease or represent exceptions[231]. In summary, dengue virus is capable of infecting a variety of different human cell types *in vivo*. Remarkably, even some additional cell lines are permissive *in vitro* due to the lack of an adequate innate immune response resulting from immortalization[232]. Furthermore, DENV also possesses replication competence in various insect tissues and organs[233]. Therefore, it is not surprising that it is not a singular characteristic molecule serving as dengue attachment factor and surface receptor, but that the virus presumably utilizes a wide range of molecules instead[234]. The most prominent candidates as attachment factors are various glycosaminoglycans[235,236]. In addition, neutral glycosphingolipids probably play a major role in both the human and mosquito systems[237,238]. Which receptor molecules are exploited to mediate cell entry depends strongly on the host organism and the particular cell type. In dendritic cells and macrophages, which are among both the earliest and major targets of viral replication in humans, DC-SIGN (dendritic cell-specific intercellular adhesion molecule 3-grabbing nonintegrin), and the mannose receptor, respectively, have been described as relevant structures[239,240]. Together with L-SIGN that is expressed in endothelial cells of liver and lymph nodes they share the characteristic of recognizing mannose-rich N-linked glycans on the surface of DENV E protein[239,241]. Since post-translational modifications are subject to cell type-specific variations, DENV tropism also depends on the cell type in which an individual virus

particle was assembled. As an example, virions that have originated from dendritic cells have very limited ability to infect further cells of that type as they lack DC-SIGN affinity due to a deficiency in mannose-rich N-glycosylation[242]. Other candidates as human DENV receptors include the chaperones Hsp70, Hsp90, and Grp78, which are mainly intracellular proteins but can also reside on the cell surface[243,244]. In addition, ectopic expression of TIM and TAM phosphatidylserine receptors may also contribute to specific DENV binding[245]. In mosquitoes, prohibitin is by far the best described receptor candidate, although more are under investigation[246,247]. In addition to direct cell docking with viral surface structures, DENV actively employs the strategy of ADE, as described previously, whereby cell contacts are mediated via FCγ receptors and immunocomplexes[64]. Also in this entry mechanism, envelope protein E is the primary viral structure in mature virions, exposing most epitopes for antibody binding[248]. However, there are also prematurely secreted virus particles that can hardly infect cells in a direct route, but can contribute to the ADE effect by the binding of antibodies to prM epitopes[249].

I.3.2 Internalization and Fusion

Virus receptor binding on the cell surface triggers an endocytotic uptake process; however, a deeper conceptual generalization is hardly possible for DENV as there is remarkable heterogeneity with respect to the target cell type, the virus origin and the respective dengue genotype. Both the conventional clathrin-dependent endocytic pathway and a non-classical dynamin-dependent variant are reported for DENV, as is micropinocytosis[245,250,251]. In some contexts, fusion takes place early in the endosome, whereas in others, trafficking to a late endosome or to a perinuclear recycling endosome occurs[252]. Following this very diverse step in the viral life cycle, however, there is again great uniformity in the essential role of the E protein in membrane fusion[253]. The latter has a hydrophobic loop with fusogenic potential, which is however concealed in the interface of the E-homodimers in mature virions and at neutral pH. Acidification causes a rearrangement of the homodimers into trimers, which positions the described loop for insertion into the outer leaflet of the endosomal membrane[134,254]. Subsequently, the individual E-trimers fold back in a hairpin-like fashion, driving host and viral membranes into a hemifusion state[134,135]. It is not entirely clear whether the ultimate result is a pore formation through which the viral genome is shuttled into the cytoplasm, or whether the RNA-binding C-protein with its known membrane translocation ability accomplishes this task, bypassing the need for a pore[247,255].

I.3.3 Translation and polyprotein processing

Correctly modified dengue genomes carry a type 1 cap structure at their 5' end, which is used for translation initiation under standard conditions[256]. Typically, this cap structure is recognized by eukaryotic initiation factor 4E (eIF4E) that represents a component of the cap-binding complex eIF4F[257]. On the opposite side, the 3' NTR is able to recruit different host proteins, including the poly-A independent attraction of the poly(A) binding protein (PABP). Presumably, this promotes circularization of viral mRNA, thereby increasing translation efficiency[258]. However, under certain conditions like ER stress that lead to a shutoff of the conventional mechanism of translation initiation, two non-canonical routes are amenable to the dengue virus genome. First, low availability of eIF4A induces structural changes in the 3' NTR, so that the attachment of transcription factors at the 5' end can be achieved in the absence of eIF4A[259]. Second, rearrangements of the 5' NTR presumably lead to the activation of a 5' DENV IRES element[260,261].

A hairpin structure within the sequence coding for C, termed cHP, positions the ribosome at the correct start codon, which is located 14 bp upstream of it[262]. It is not clear whether active translation begins at a free ribosome in the cytosol, which relocalizes to an ER translocon after the signal recognition particle (SRP) has found a binding motif in the nascent C protein, or whether the dengue genome is guided directly to ER-resident ribosomes[104]. The stop codon at the end of the coding sequence initiates the release of the polypeptide chain with the help of the release factors such as eRF1 and eRF3, which completes translation[104,256,263].

I.3.4 Biogenesis and functionality of replication organelles

DENV-induced membrane alterations are evident under the electron microscope. By reorganization of the host endomembrane system, DENV results in two characteristic replication organelles. On the one hand, there are arrays of spherule-like membrane invaginations of rough ER which are about 90 nm in diameter and are called vesicle packets (VPs). On the other hand, there are highly concentrated assemblies of smooth ER known as convoluted membranes (CMs)[264]. Although technology has improved in recent years and we now have high-resolution images of these structures, the precise biological processes that occur within them are only roughly understood.

VPs are thought to house the process of viral replication. For flaviviruses, there are no reports of permissive cell types in which VPs are absent. In addition, double-stranded RNA, as well as viral proteins interacting with RNA, could be detected within these structures[139,264,265]. Meanwhile, we also know elements in the 3' NTR of the DENV genome, which are

indispensable for the formation of vesicle packets, and thus indirectly for viral replication[106]. The VP interior is connected to the cytosol via a pore of about 11 nm in size and it is likely that metabolite exchange and the release of newly formed RNA occurs via this route[106]. Despite sound investigations, convoluted membranes have not been identified in every DENV permissive cell type and are believed to be entirely absent in mosquito cells[266,267] suggesting a cell type-specific function. Thus, they could represent a storage or deposition site for (currently) unneeded viral proteins or lipids[264]. CVs could also contribute to immune shielding, possibly by sequestering pattern recognition receptors or indirectly by participating in the known disruption of mitochondria-associated membranes[119,191]. Moreover, it has been suggested that important steps in polyprotein maturation occur within CVs[268]. However, none of these hypotheses has yet been supported by solid evidence.

Based on experience with other viruses, DENV replication organelle biogenesis is thought to require a complex interplay of host and viral proteins. However, very little is known about the former. Comparatively best characterized is the cytoskeletal protein vimentin, which interacts with NS4A and co-localizes with vesicle packets. However, it is unclear whether it is a direct structural component of the vesicle packets or if it passively stabilizes them[167]. On the viral side, the integral membrane proteins NS4A and NS4B, which also interact with each other, play key roles in membrane remodeling in that their topology favors negative membrane curvature[164,166,172,269]. In the ER lumen, NS1 resides crown-like on the outside of the invaginated vesicles and also contributes to the structure of these organelles[140,270].Furthermore, biogenesis of DENV replication organelles requires intervention in cellular lipid homeostasis. In DENV-infected cells, autophagy-mediated degradation of cytosolic lipid droplets is stimulated to release fatty acids that can be used as the basis for *de novo* synthesis of membrane lipids, and thus for the establishment of new replication organelles[160,271].

I.3.5 RNA replication

A single translation event results in a single copy of each dengue protein and this is certainly not sufficient to form a functional replication vesicle. It can therefore be assumed that a certain local concentration of viral proteins must first be present to form a vesicle together with an RNA strand of positive polarity, which then provides the template for the synthesis of a negative strand[104]. NS5 is thought to compete with components of eIF4F for binding to the 5' cap structure. This first induces refolding of the 5' NTR stem loop A (5' SLA), which increases the binding strength of NS5 to the 5' NTR. In a next step, different elements of the 5' NTR are assumed to interact with counterparts on the 3' NTR so that the genome is deformed in a way

that its structure remotely resembles a pan with a handle[272]. This allows NS5 to be transferred to the 3' end of the (+)RNA strand, marking the start position for replication[273]. As negative strand synthesis proceeds, formation of the genome's panhandle structure is no longer favored, preventing resumption of negative strand RNA synthesis, so that only a single copy of the corresponding negative strand is synthesized from the positive polarity RNA strand that has migrated into the replication vesicle[272]. Models for the synthesis of plus-strand RNA are based on educated guesses rather than on robust evidence. The simplest model is that NS3 helicase activity first slightly splits the ends of the double-stranded RNA, so that on the one hand the 5' SLA can form again on the plus-stranded RNA, but on the other hand the 5' end of the plus-strand and the 3' end of the minus-strand are still in close proximity to each other. As with minus-strand synthesis, the (+)5' SLA would act as the NS5 promoter of plus-strand synthesis and NS5 transfer would then occur to the 3' end of the negative-strand RNA. In principle, multiple plus-strand genomes can be formed simultaneously from a minus-strand template in a wave-like sequence, with NS3 helicase running upstream of each nascent RNA to detach the previous strand from the template. Subsequently, plus-stranded genomes would be released into the cytosol via the pore, while the negative copy would remain in the replication vesicle until the end of its lifetime[272].

I.3.6 Assembly

The assembly of functional virus particles requires a tightly coordinated process. First, C-prM-E precursor proteins accumulate at the later assembly sites which are located at ER membranes adjacent to vesicle packets[104]. In parallel, NS2A concentrates in vicinity to vesicle packets. NS2A can recruit released viral genomes for packaging by binding to the 3' NTR, presumably in competition with factors that promote translation or replication. Subsequently, NS2A traffics the genome to the assembly sites and in addition recruits the viral protease complex NS2B/NS3[147]. The latter then triggers the maturation of the DENV structural proteins, which also involves the host signalase complex. Released C proteins carry a high positive charge and encapsidate the negatively charged RNA genome via electrostatic interactions[274]. The DENV proteins prM and E initiate envelope formation, allowing a copy of the packaged nucleocapsid to integrate before the process is complete[121]. Viral particles then bud into the ER lumen[264,266].

I.3.7 Maturation and release

After budding into the ER, newly synthesized virions are present as immature virus particles characterized by 60 icosahedrically arranged heterotrimeric spikes of prM and E protruding

from the viral envelope, thus increasing the diameter of these noninfectious particles by 10 nm compared to mature virions, which are approximately 50 nm in diameter[127]. This conformation prevents inadvertent fusion with endosomal membranes during egress[104]. For this purpose, dengue virions enter the secretory pathway, thereby passing through the acidic environment of the Golgi and trans-Golgi network, whose pH values of 6.7 and 6, respectively, are significantly lower than that of the ER (pH 7.2)[275]. Consequently, the pH drop causes a rearrangement of the surface structure of E and prM, so that the latter exposes a cleavage site to the cellular protease furin, which then splits the pr peptide off from M[276]. However, at acidic pH, molecular interactions keep pr transiently bound to the viral envelope, which is another strategy to prevent premature virion fusion[129]. In the course of virion secretion into the neutral pH milieu of the extracellular space, the pr peptide detaches thus generating infectious particles, whose structure is described in more detail in chapter I.2.3[277]. The release of mature particles completes the viral life cycle of DENV, which is shown in its entirety in Figure 7. Of note, besides mature particles, DENV infected cells release significant quantities of partially mature (incomplete prM cleavage) and immature particles (no prM cleavage)[278]. The latter are not or only slightly infectious with respect to classical receptor-mediated endocytosis, but stimulate the production of anti-prM antibodies[279]. For unexplained reasons, these have only a very limited neutralizing capacity, but are thus able to promote ADEs in a similar way to heterotypic anti-E antibodies[280].

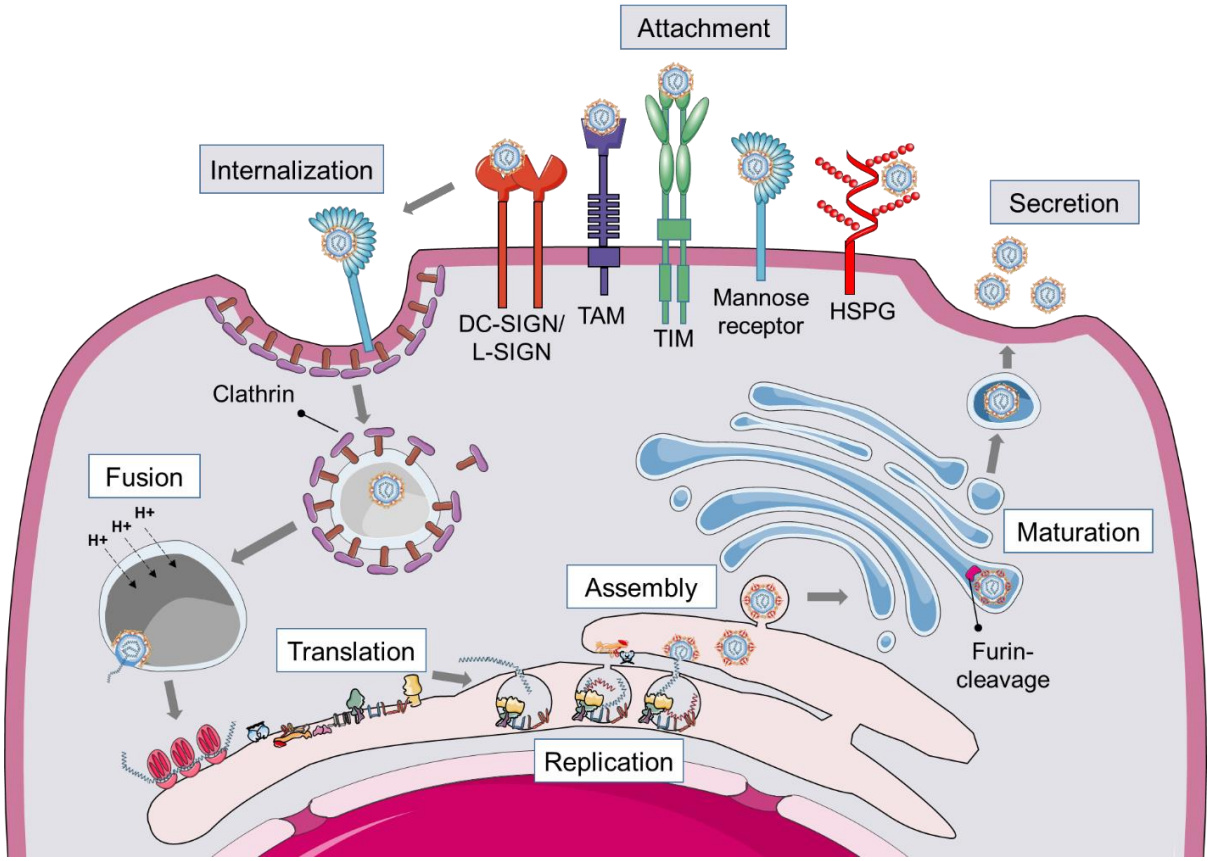

Figure 7. Overview of the infectious life cycle of DENV.
DENV particles can infect a variety of cells in the human body, including Langerhans cells, active dendritic cells, macrophages, mast cells and blood-derived monocytes. The process of infection begins with the binding of viral particles to the surface of susceptible cells through interaction with attachment factors such as glycosaminoglycans or neutral glycosphingolipids. Specific interactions with secondary receptors then initiate the internalization of the virion into the cell. Entry of DENV particles into the cell is predominantly through a clathrin-dependent pathway, whereby they are exposed to an acidic endosomal environment that triggers conformational rearrangements of the envelope glycoproteins, resulting in fusion of the viral and endosomal membranes and release of viral RNA into the cytosol. The released positive-sense RNA is translated by ribosomes at the rough ER to yield a single polyprotein, which is then processed into three structural and seven non-structural proteins. While the structural proteins constitute integral components of the virion, the non-structural proteins are essential for RNA replication, either directly by participating in catalytic processes of genome amplification, or indirectly by orchestrating membrane rearrangements of the ER, including the formation of vesicle packets, the putative organelles in which viral replication takes place. The positive-sense RNA molecules generated by the viral replicase complex can be transported to regions opposite the replication sites where they serve as components for new viral particles in a process that involves RNA encapsidation and budding into the lumen of the ER. Maturation of nascent DENV particles occurs through furin-mediated cleavage of prM along the secretory pathway, ultimately leading to exit from the cell. Adapted from Neufeldt et al.[106].

I.4 Measures against DENV

I.4.1 Vaccines

Despite DENV causing an immense global burden of disease, there is still no widely used DENV vaccine, although vaccines for other flaviviruses (YFV, JEV, TBEV) have been

available for decades[281]. The main reason for this is associated with the phenomenon of ADE. A DENV vaccine that does not confer sufficient immunity against all four serotypes is inadequate not only because of its lack of protective efficacy, but especially because unbalanced immunity, similar to consecutive heterotypic infection events, may increase the risk of a severe course of dengue fever. This ADE effect sometimes occurs years after vaccination, when titers against certain serotypes drop to a critical level. In this context, the tetravalent live attenuated vaccine Dengvaxia®, developed by Sanofi, achieved sad notoriety. Between 2016 and 2018, this vaccine was administered in school-based vaccination campaigns, especially to children and adolescents in Brazil and the Philippines[282]. Already three years after vaccination, the risk of developing DVPS was significantly increased in the vaccinated cohort compared to a placebo control group[283]. The underlying reasons for this are not fully understood; however, concomitant studies showed that Dengvaxia® often did not induce protective immunity against DENV serotype 2 in formerly seronegative subjects[283,284]. In addition to the ADE issue, natural DENV resistance in mice is another hurdle for DENV vaccine development, as the latter organisms represent one of the cheapest and most widely used animal models in pharmaceutical research. Chimeric or immunocompromised mice are only partial substitutes, whereas nonhuman primates show a human-like immune response, but their use is costly and considered ethically problematic in many countries[285]. An additional finding from recent research is that secreted NS1 is a trigger factor for DVPS, yet this issue can be mitigated by NS1-neutralizing antibodies[286]. A dengue vaccine should therefore not only induce an immune response against surface proteins on virions, but also against NS1. In principle, this requirement profile is compatible with all current vaccine types, such as live attenuated vaccine, inactivated vaccine, viral vector vaccine, nucleic acid vaccine and recombinant subunit vaccine, with at least one candidate being investigated for each category[287]. The aforementioned vaccine Dengvaxia® was the first one worldwide to receive market approval. However, due to the post-approval complications, it is currently recommended by the WHO only if individuals can prove a pre-exposure to dengue virus through a point-of-care diagnostic test or if seroprevalence rates in their particular region exceed 80%, but both limitations often pose an unachievable constraint in poorly developed countries due to a lack of testing infrastructure and also preclude the vaccine for most travelers who originate from non-endemic regions[288,289]. Dengvaxia® is a tetravalent live-attenuated vaccine based on the established YFV vaccine strain YF17D, which has been modified by replacing the prM/E region in the YFV genome with corresponding sequences of the respective dengue serotypes. Thus, by design, Dengvaxia® is not able to induce DENV NS1 antibodies.

In 2022, another vaccine developed by Takeda Pharmaceutical, Qdenga® (formerly known as DENVax and TAK-003), received market approval in parts of the world (currently Indonesia and the European Union) and is the only DENV vaccine to date recommended for seronegative individuals[290]. As Dengvaxia®, this is a tetravalent life-attenuated vaccine, but it is based on DENV-2 PDK-53 virus, which was derived by passaging the wild-type DENV-2 16681 virus 53 times in primary dog kidney (PDK) cells[291]. Larger regions of the genetic backbone were exchanged with corresponding sections of the other three serotypes DENV-1, DENV-3, and DENV-4[292]. With TV003/TV005, developed by the US National Institute of Allergy and Infectious Diseases (NIAID), there is another life-attenuated vaccine candidate in an advanced stage of clinical development, while candidates of other vaccine types are still in earlier stages[287,293].

I.4.2 Vector control

Until no vaccine is in widespread use, protective DENV measures primarily rely on avoiding bites by infected vector mosquitoes. One class of measures directly targets these mosquitoes by chemical or biological attack. In addition, many indirect measures aim to prevent contacts between humans and mosquitoes[294]. Some approaches, such as large-scale insecticide spraying, require coordination, trained personnel, and specialized equipment. In contrast, alternative strategies emphasize socially-responsible action and engagement of the affected general population, with organizations supporting this through education and raising awareness[295]. A major hurdle in the fight against DENV is that most studies dealing with the effect of vector control measures have serious deficiencies in their study design, so that reliable statements on the effectiveness can only be made for a few strategies[296]. The installation of fly screens in windows and doors is the measure whose success is best documented[297-299]. This fits with the finding that *Aedes aegypti* mosquitoes prefer to be indoors when foraging for blood meals[300]. In addition, there is at least some evidence for the usefulness of so-called clean-up campaigns that teach social communities how to detect and remove potential breeding sites for mosquito larvae, which often consist of trash (e.g., discarded car tires)[301]. On the other hand, there is insufficient proof for the efficacy of skin repellents, insecticide-treated materials, bed nets, and mosquito traps[296]. For insecticide aerosols and mosquito coils, meta-studies even show a reinforcing effect on infection dynamics, presumably because these low or ineffective measures give people a perceived sense of security and they therefore neglect other, more powerful protective measures[296]. In addition, vector resistances to insecticides (such as DDT or pyrethroids) or larvicides (e.g temefos), are known to develop rapidly and with continued

use of respective agents[302-304].

Due to these problems, major efforts are currently undertaken to establish an innovative vector control method based on the targeted infection of *Aedes* mosquitoes with the endosymbiotic bacterium *Wolbachia pipientis*. Those pathogens infect a wide range of insect species (but not naturally *Aedes aegypti*), transmit vertically via eggs, and manipulate their hosts in a variety of ways[305,306]. One of these mechanisms is the so-called cytoplasmic incompatibility, which means that *Wolbachia*-infected males cannot successfully mate with uninfected females, as this leads to arrested development of early embryos[307]. By means of embryonic microinjections into the developing germ line, it is now possible to stably transfect *Aedes aegypti* with *Wolbachia* bacteria[308]. This technology allows to drastically reduce the vector population by repeated releases of *Wolbachia*-infected males, which are sterile as long as there are no females carrying the same *Wolbachia* strain[309]. In parallel, *Wolbachia* strains could be generated that are capable of conferring specific traits to the *Aedes* vectors that are desired in the fight against dengue such as lower DENV susceptibility or reduced levels of virus in their saliva[310-312]. This approach exploits that infected females gain an indirect reproductive advantage by being able to mate with all types of males, while uninfected females can only mate with uninfected males[313]. Thus, this *Wolbachia* introgression strategy is not aimed at vector elimination, but at containment of the virus by targeted infestation of *Aedes* mosquitoes with *Wolbachia* strains that lower their vector competence[314]. The proposed molecular mechanism for this is that corresponding *Wolbachia* bacteria interfere with the lipid homeostasis of the host cell and engage in active remodeling of ER membranes, thereby competing with flaviviruses, which in turn use similar means to form replication organelles[314-316].

I.4.3 Antivirals

Treatment guidelines for dengue patients currently include recommending rest, adequate intake of water and electrolytes, as well as prescribing analgesics for severe muscle pain and antipyretics for high fever[317,318]. To date, there is no specific antiviral treatment for DENV or for any other flavivirus[319]. In order to understand the underlying reasons, it is important to consider the requirements a DENV antiviral drug needs to meet. Unlike many other viruses for which specific treatment options exist (e.g. HBV, HCV, HIV), DENV induces an acute course of disease[59]. Usually, there are only a few days between the onset of unpleasant symptoms and the peak of the viraemia curve[320,321]. Hence, treatment should be initiated no later than the visit to the physician; there is no window of opportunity for a time-consuming diagnostic test to

clarify which DENV serotype is present in an individual patient. Many of the countries most affected by dengue fever also lack the necessary medical infrastructure for such a procedure. This however implies that a dengue drug must be effective against all dengue serotypes, ideally even against all known genotypes[322]. In addition, efforts should be made to achieve a very favorable side-effect profile so that a drug of this kind can be part of the private medicine cabinet. This saves the trip to the doctor, which can be long and arduous in many poor countries. In addition, this enables prophylactic use, for example in regions with a high epidemic incidence of infection or for travelers who want to protect themselves against dengue fever[323]. Most DENV antiviral candidates described in literature have not fully been optimized with respect to the above listed criteria. The vast majority were examined using *in vitro* assays only, which often did not include all DENV serotypes. Many studies also lack a testing of the respective compounds in a broad panel of cell lines. Such a panel should ideally include human cell types corresponding to the natural DENV tropism[324]. Furthermore, only few projects performed *in vivo* characterizations, e.g., in AG129 mice, thus the pharmacokinetic and safety profile of most DENV compounds is poorly known[325]. For these reasons, most of the reported DENV antiviral compounds have low potential for pharmaceutical use in patients but provide valuable insights into suitable targets. Basically, a distinction can be made between direct-acting antivirals (DAAs), which impair the functionality of viral proteins by binding to them, and host-directed antivirals (HDAs), which target host proteins that are part of cellular signaling pathways hijacked by the virus[324]. Both classes have their specific advantages and disadvantages. Most DAAs are characterized by a large pharmaceutical window, as cellular functions are not or only slightly affected. However, high potency often requires the drug to be strongly adapted to a specific viral protein, which is an obstacle to the development of broad-spectrum antivirals. In addition, the widespread use of DAAs carries the risk of loss of efficacy due to selection of virus variants resistant to the agents[326]. This problem is much less pronounced with HDAs, which also often act against several related viruses, provided they exploit the same addressed pathway[327]. On the downside, the interference of an HDA with host cell homeostasis can lead to undesirable side effects, which is particularly problematic in a prophylactic use case[326].

Host-directed antivirals (HDAs)

The discovery of HDAs is usually preceded by basic research aimed at identifying new host factors. This is typically followed by attempts to repurpose known inhibitors of these structures as antivirals, preferably even drugs in clinical use[328]. The HDAs described below represent a

selection of interesting candidates that highlight the potential, but also the limitations and hurdles of this type of active ingredients. For more in-depth information, several comprehensive reports are available[327,329,330].

Presumably, the most studied cellular targets are the ER-resident enzymes α-glucosidase I and II, which catalyze the sequential trimming of glucose residues on N-glycosylated proteins and thus contribute to their proper folding and maturation[327]. The list of substrates includes the DENV proteins E, prM, NS1 and NS4B[331]. Consequently, *in vitro* experiments showed that inhibition of α-glucosidases by the natural iminosugars deoxynojirimycin (DNJ) and castanospermine (CAST) exhibited impressive antiviral activity against DENV and a number of other flaviviruses[332]. The mechanism-of-action is based in part on reduced stability of prM/E heterodimers formed under inhibition[333]. In addition, misfolding of NS1 was found to be accountable for compound-mediated effects on replication and assembly[334]. An oral prodrug of CAST, called celgosivir, was even studied in a clinical trial but failed to show an alleviating effect on dengue fever there[335]. Follow-up studies identified the dependence of the antiviral effect on virus strain and cell type as the cause for poor *in vivo* efficacy[336].

A good example of the drug repurposing approach is chloroquine. This pharmaceutical agent, originally developed against malaria, interferes with the acidification of endosomes and came into focus when it was additionally discovered that DENV particles require an acidic milieu for productive entry[337]. Although *in vitro* studies did indeed detect a DENV antiviral effect of chloroquine[338,339], with animal studies also supporting the concept[340], human application in two independent clinical trials did not show a positive effect on the course of dengue fever[341,342].

A very intuitive approach to combating viruses in general is to exploit their dependence on host nucleotides by inhibiting host enzymes involved in the *de novo* biosynthesis of such metabolites. A well-characterized target in this sense is inosine-5′-monophosphate dehydrogenase (IMPDH), an enzyme required for guanine nucleotide biosynthesis[343]. Ribavirin acts at least in part via IMPDH blockade resulting in depletion of the intracellular guanine nucleotide (GTP) pool and is approved as a broad-spectrum antiviral[344]. In a similar fashion, brequinar, an antineoplastic agent, inhibits the enzyme dihydroorotate dehydrogenase (DHODH), which is essential for the biosynthesis of pyrimidine bases (cytosine, thymine, uracil)[345]. *In vitro*, both compounds display impressive activity against a wide range of DNA and RNA viruses, including representatives of flaviviruses[346]. *In vivo*, the use is limited to significantly fewer viruses, and there is no efficacy against DENV in this system, probably because blood serves as a buffer for pyrimidines, and the targeted nucleotide depletion in cells is too slow compared to DENV kinetics[251,347,348].

Direct-acting antivirals (DAAs)

As will be briefly outlined in the following section, numerous projects have already been carried out for the identification and development of DENV DAAs. Despite great diversity, it can be generalized that the earliest work focused on viral proteins for which detailed structural information and/or known enzymatic activity was available.

Among components of the DENV structural module, E protein is the best studied DAA target, and depending on the inhibitor, receptor binding, endocytosis, or fusion are affected[324]. In addition, there is an antiviral candidate that has been shown to stabilize capsid self-interaction. As a result, the intracellular distribution of this protein is affected, which impairs entry, assembly and release of virus particles[349].

Of all the non-structural proteins of dengue virus, NS3 is perhaps one of the most intuitive candidates for antiviral drug development. Part of the reason is that it harbors two essential functional domains of known structure that mediate protease activity on the one hand and helicase/ATPase activity on the other[350,351]. In addition, the catalytic sites are highly conserved not only within DENV serotypes but also between representatives of the flaviviruses, which promises potential for the development of pan-flaviviral inhibitors. Furthermore, this is also associated with a large genetic barrier to the emergence of resistance mutations[352]. Another strong argument for investigating DENV protease inhibitors in particular is that for several viruses, including HIV, HCV, and not least SARS-CoV-2, such drugs have already been brought to market and are now indispensable for therapeutic treatment[353,354]. The development of such substances is also favored by the circumstance that approved host protease inhibitors exist for a wide variety of diseases, so that, for example, there is a great deal of expertise in prodrug strategies[355] or in the establishment of robust screening assays[356,357]. Given the numerous studies investigating DENV protease inhibitors and a number of ongoing projects, it is noteworthy that no candidate has yet made it into clinical development. A commonly invoked explanation is that the DENV protease has a strong preference for polybasic substrates, which tends to coincide with poor cell permeability[358]. Another problem with some DENV protease inhibitor candidates is that they have off-targets such as the host proteases thrombin or trypsin, which can lead to significant side effects[359]. The issue of low selectivity is even more pronounced for the NS3 helicase, for which several inhibitors have been described but not pursued[352].

A similar situation exists for the methyltransferase domain of NS5, which, like its host counterparts, uses S-Adenosyl methionine (SAM) as a methyl group donor[99,102]. Thus, although known SAM analogues such as S-adenosyl-L-homocysteine (SAH) or sinefungin show a

pronounced antiviral effect, there is no sufficient therapeutic window due to high cytotoxicity[360].

The RNA-dependent RNA polymerase domain of NS5, on the other hand, seems at first glance to be an ideal target because, although highly conserved, there is no eukaryotic homolog. Approved agents from this class for the treatment of HIV, HCV and SARS-CoV-2 further underscore its potential[353,354]. The category of nucleoside inhibitors (NIs) encompasses all agents that compete with the corresponding endogenous metabolites as substrate analogs. NIs are often designed in such a way that their incorporation into nascent RNA results in direct strand termination; alternatively, they may be designed to pair with different bases, resulting in deleterious mutations in the viral genome[361]. Viral polymerase inhibitors that act allosterically are classified as non-nucleoside inhibitors (NNIs)[328]. With regard to DENV, the latter are just at the beginning of research and the focus is currently clearly on NIs[362]. Several NIs studied for DENV, such as 7-Deaza-2′-C-methyl-adenosine (7-DMA), BCX4430 or NITD008 showed excellent efficacy in cell culture experiments while maintaining a high selectivity index[328,363,364]. However, all these candidates have so far failed *in vivo* or, as in the case of balnapiravir, in a clinical trial due to lack of efficacy and/or high toxicity[352,365,366]. Host kinase-mediated conversion of NIs to biologically active triphosphates varies widely among primary cell types and is generally weaker than in immortalized cells commonly used in *in vitro* experiments, explaining the compromised *in vivo* efficiacy[367,368]. The main reason for observed toxicity is that there are some cell types in the living organism that are very sensitive to off-target inhibition of mitochondrial DNA polymerase γ[369].

NS4B-targetting DAAs

Due in part to setbacks in the development of DENV antiviral agents against known enzymatic targets, there has been an increased focus on so-called phenotypic screening in the recent past to find entirely new pharmaceutical approaches to combat DENV[370]. This is a high-throughput procedure in which cultured cells (mostly Huh7 and Vero E6) are infected with DENV and additionally treated with substances from a library. Depending on whether WT or reporter viruses are used, readout is based on cytopathic effect, fluorescence, or luciferase-mediated luminescence[370].

Hits detected by phenotypic screening can target both viral and host proteins. Especially in the latter case, target identification and elucidation of the mechanism-of-action are extremely challenging[371]. Despite the difficulties, several independent phenotypic screenings revealed

inhibitors that selected for resistance mutations in NS4B, which is remarkable given that NS4B, as described in Chapter I.2.2, has no enzymatic activity but interacts with a wide range of viral and host proteins[371-376]. While there is structural heterogeneity, the substances have in common that they specifically target DENV and have no or only weak activity against other flaviviruses[171]. Some candidates are even serotype-specific and thus lack the characteristic of pan-serotype efficacy that is crucial for a promising DENV drug. This, together with suboptimal physicochemical features, led to the discontinuation of several of these projects[372,374,375]. Fortunately, three pan-dengue inhibitors with favourable pharmacokinetic properties have been identified: JNJ-A07, JNJ-1802, and NITD-688, the latter two of which are now the only DENV drug candidates in clinical development specifically designed for this medical indication[171,377,378].

II. Objectives

In 2009, the KU Leuven launched a project to discover new antiviral agents against dengue virus, combining the virological knowledge of Professor Johan Neyts' group at the Rega Institute with the expertise of the Centre for Drug Design and Discovery, both located in Leuven, Belgium[377]. To this end, a medium-throughput phenotypic screening was performed using a cytopathic effect (CPE) reduction assay against DENV-2, which resulted in the identification of a 3-Acyl-indole derivative (2-((3,4-dimethoxyphenyl)amino)-1-(1H-indol-3-yl)-2-phenylethan-1-one) as a first hit compound[379]. Based on this, the project was developed to lead stage and it was shown that representatives of the new compound class were on the one hand potent in rodents by suppressing DENV replication and at the same time also exhibited favourable properties in terms of physicochemistry and metabolic stability[379]. In 2013, Janssen Pharmaceutica joined the venture. Using their drug development capabilities, over 2000 compound derivatives were synthesized in an iterative process, and subsequently tested against all four DENV serotypes. In this way, a structure-activity relationship could be established and, concomitantly, progress was made in terms of pharmacokinetic properties[377]. JNJ-A07 was the first drug candidate from this program to be characterized in intensive preclinical studies, later followed by JNJ-1802[378]. As these compounds originated from a phenotypic screening approach, the mechanism by which they exert their anti-replicative effect was largely unknown, except for the observation that mutations induced by *in vitro* resistance selection accumulated in the region of the DENV genome encoding the non-structural protein NS4B. Due to profound expertise in molecular virology methods, Professor Ralf Bartenschlager was approached by the aforementioned consortium of KU Leuven and Janssen Pharmaceutica to participate in the venture, in particular to elucidate the mechanism-of-action (MOA) of the new dengue antiviral agents in detail. In December 2017, I was selected by Prof. Ralf Bartenschlager to carry out this task as part of a doctoral research project. Knowledge of the MOA of a drug candidate is relevant for several reasons. One is to find out whether there is an entirely novel mechanism, or whether there are similarities to candidates already investigated in other studies, so that an advantage could be drawn from the insights generated there. Especially in the case of a novel mechanisms-of-action, a deep investigation is necessary to make a solid risk assessment regarding possible side effects and viral resistance formation. Understanding the MOA can help identify biomarkers that can be used to estimate or track the success of a potential therapy. In addition, it may enable the development of improved screening assays for a subsequent generation of antiviral candidates, which could thus be expanded in their spectrum of activity,

for example. Last but not least, an active substance with an unknown mechanism can also be seen as a tool to obtain fundamentally new knowledge about the disease addressed or, in this specific case, about the causative virus. At the beginning of my doctorate, a strategy was developed to identify the mechanism-of-action of the new dengue antiviral candidates. Various milestones were defined for this purpose: A first aim was to confirm that NS4B indeed plays a central role in the mechanism-of-action by demonstrating specific compound association or binding to that protein using a photoaffinity-labelling approach. A further task was to employ transient or stable expression of viral proteins followed by Co-IP experiments to determine whether JNJ-A07 and JNJ-1802 perturb the interaction of NS4B with one or more of its known binding partners. The rationale behind this was that NS4B has no enzymatic activity of its own, thus a compound-mediated restriction of the adapter-like functionality of NS4B was assumed[181]. After successful completion of the previous objective, the follow-up task was set to investigate which of the NS4B-containing species (NS4A-2K-NS4B, 2K-NS4B or mature NS4B) was most important for observed drug-related effects. The deciphering of the resistance mechanism of compound-induced mutations was defined as the next milestone, including the differentiation between driver and passenger mutations, for which it was planned to assess the replication fitness of compound-resistant mutants. Furthermore, answering the open question how JNJ-A07 and JNJ-1802 affect virus replication represented an important research goal, since hitherto performed replication-based approaches suffered from the limitation that the processes of protein synthesis, polyprotein processing, vesicle packets formation and genome amplification are inseparably linked, so that a possible compound interference with one of these steps inevitably affects all others. For a differentiated investigation, it was therefore decided to utilize a newly established expression-based system, designated pIRO-D, an acronym derived from "plasmid-induced replication organelles of DENV"[106]. In this system, cells stably expressing bacteriophage T7 RNA polymerase are transfected with a plasmid from which transcripts are generated in a T7 promoter-dependent manner, carrying the information for the non-structural module of the DENV-2 polyprotein (strain Thailand/16681), flanked by specific parts of the 5' and 3' NTRs. IRES-induced translation leads to the replication-independent formation of authentic DENV replication organelles, which, in combination with transmission electron microscopy, allows the effect of DENV antiviral compounds on these to be studied. A final objective of this dissertation was to find causative links between the individual compound-induced phenotypes in order to establish a conclusive model for the mode-of-action of JNJ-A07 and JNJ-1802.

III. Materials

III.1 Cell lines

Table 1. Cell lines used or generated in this study.
Listed are the cell lines used in this work, each with a reference describing the engineering process. In addition to a brief description, selection markers are listed that were used according to the cell culture protocol in Chapter IV.2.1.

Name	Description	Selection	Source / reference
Huh7	Human hepatoma cell line	-	[380]
Huh7/Lunet	An Huh7 cell-derived clone that was cured of stable HCV replicon expression by selective substance treatment	-	[381]
Huh7/Lunet-T7	Huh7/Lunet cells stably expressing the RNA polymerase of bacteriophage T7	Zeocin	[382]
Huh7/Lunet-T7_DENV-2_NS1_HA	Huh7/Lunet cells stably expressing the RNA polymerase of bacteriophage T7 and DENV NS1 with a C-terminal HA-tag	Puromycin, Zeocin	[269]
Huh7/Lunet-T7_DENV-2_NS2B-NS3	Huh7/Lunet cells stably expressing the RNA polymerase of bacteriophage T7 and the active DENV protease complex NS2B-NS3	Puromycin, Zeocin	[117]
Huh7-T7	Huh7 cells stably expressing the RNA polymerase of bacteriophage T7	Zeocin	[382]
Huh7-T7_DENV-2_NS2B-NS3	Huh7 cells stably expressing the RNA polymerase of bacteriophage T7 and the active DENV protease complex NS2B-NS3	Puromycin, Zeocin	[117]
Huh7-T7_DENV-2_NS2B-NS3_S135A	Huh7 cells stably expressing the RNA polymerase of bacteriophage T7 and the DENV protease complex with a protease-inactivating mutation in NS3 (S135A)	Puromycin, Zeocin	[117]
Huh7-T7_ZIKV-HPF_NS2B-NS3	Huh7 cells stably expressing the RNA polymerase of bacteriophage T7 and the active ZIKV protease complex NS2B-NS3	Puromycin, Zeocin	Płaszczyca et al., unpublished

III.2 Bacteria

Competent bacteria of E. coli strain DH5α (genotype: F^- φ80*lac*ZΔM15 Δ(*lac*ZYA-*arg*F)U169 *rec*A1 *end*A1 *hsd*R17(r_K^-, m_K^+) *pho*A *sup*E44 λ^-*thi*-1 *gyr*A96 *rel*A1) were used for the cloning work described in this work and for amplification of vector plasmids.

III.3 Restriction Enzymes

Table 2. Restriction enzymes used in this study.
All restriction enzymes and buffers were purchased from New England Biolabs, Ipswich, MA, USA. Applied enzymes work optimally at 37°C. For each enzyme, the cutting site motif and activity in the four available commercial buffers are shown. *in case of only one restriction site ** in case of only one restriction site in a 10 kB plasmid

Name	Cutting Site	U per pmol*	U per µg**	NEBuffer ™ 1.1 [%]	NEBuffer ™ 2.1 [%]	NEBuffer ™ 3.1 [%]	CutSmart ™ Buffer [%]
AgeI-Hf	5′... A▼CCGGT...3′ 3′... TGGCC▲A...5′	2.5	0.4	100	50	10	100
AvrII	5′... C▼CTAGG... 3′ 3′... GGATC▲C... 5′	16	2.6	100	50	50	100
BamHI-Hf	5′... G▼GATCC...3′ 3′... CCTAG▲G...5′	6.4	1	100	50	10	100
BglII	5′... A▼GATCT...3′ 3′... TCTAG▲A...5′	5.3	0.9	10	10	100	<10
BsrGI	5′... T▼GTACA...3′ 3′... ACATG▲T...5′	6.4	1	25	100	100	25
BsrGI-Hf	5′... T▼GTACA...3′ 3′... ACATG▲T...5′	6.4	1	10	100	100	100
EcoRI-Hf	5′... G▼AATTC...3′ 3′... CTTAA▲G...5′	6.4	1	10	100	<10	100
KasI	5′... G▼GCGCC...3′ 3′... CCGCG▲G...5′	32	5.2	50	100	50	100
KpnI-Hf	5′... GGTAC▼C...3′ 3′... C▲CATGG...5′	16	2.6	100	25	<10	100
MfeI-Hf	5′... C▼AATTG...3′ 3′... GTTAA▲C...5′	4	0.6	75	25	<10	100
MluI-Hf	5′... A▼CGCGT...3′ 3′... TGCGC▲A...5′	4.6	0.7	25	100	100	100
NcoI-Hf	5′... C▼CATGG...3′ 3′... GGTAC▲C...5′	8	1.3	50	100	10	100
NheI	5′... G▼CTAGC...3′ 3′... CGATC▲G...5′	32	5.2	100	100	10	unspecified
SpeI-Hf	5′... A▼CTAGT...3′ 3′... TGATC▲A...5′	7.4	1.2	25	50	10	100
XbaI	5′... T▼CTAGA...3′ 3′... AGATC▲T...5′	32	5.2	<10	100	75	100
XhoI	5′... C▼TCGAG...3′ 3′... GAGCT▲C...5′	32	5.2	75	100	100	100

III.4 Plasmids and oligonucleotides

A full list of plasmids used in this work can be found in the appendix of this thesis (Supplementary Table 1). There, one can also find information about the cloning method of newly created plasmids. In addition, Supplementary Figure 2 provides the sequence information of employed oligonucleotides that were designed using VectorNTI Advance and were purchased from Sigma-Aldrich (Merck), Darmstadt, Germany.

III.5 Antibodies

Table 3. Primary antibodies used in this study.
Antibodies used are indicated with their respective target structure, a reference number (with indication of the clone in the case of monoclonal antibodies) and their type. In addition, the dilution factor for the respective application is given. IF= Immunofluorescence; WB= Western blot. If nothing is indicated, the antibody was not used for this application. For the source, either the manufacturer is indicated, or a note is added that the antibody is homemade. In the latter case, the antibody was produced according to previously published protocols[172,264].

Target	Description	Type	Dilution WB	Dilution IF	Source
DENV NS1	-	Rabbit polyclonal	1:1000	-	Homemade
DENV NS2B	GTX124246	Rabbit polyclonal	1:1000	-	GeneTex, Irvine, CA, USA
DENV NS3	-	Rabbit polyclonal	1:1000	-	Homemade
DENV NS3	GTX629477, Clone GT2811	Mouse monoclonal	-	1:200	GeneTex, Irvine, CA, USA
DENV NS4B	-	Rabbit polyclonal	1:1000	-	Homemade
DENV NS4B	GTX124250	Rabbit polyclonal		1:200	GeneTex, Irvine, CA, USA
DENV NS5	-	Rabbit polyclonal	1:1000	-	Homemade
ZIKV NS4B	GTX133321	Rabbit polyclonal	1:1000	1:200	GeneTex, Irvine, CA, USA
ZIKV NS3	GTX133320	Rabbit polyclonal	1:1000	-	GeneTex, Irvine, CA, USA
HA	anti-HA.11 epitope tag, clone 16B12	Mouse monoclonal	1:1000	-	BioLegend, San Diego. CA, USA
β-Actin	A5541, clone AC-15	Mouse monoclonal IgG1	1:4000	-	Sigma-Aldrich (Merck), Darmstadt, Germany
GAPDH	G-9 sc-365062	Mouse monoclonal	1:1000	-	Santa Cruz Biotechnology, Dallas, TX, USA

Table 4. Secondary antibodies used in this study.
The secondary antibodies used in this work are indicated with their full name, dilution factor and manufacturer's details.

Antibody	Dilution	Source
Goat anti-Mouse IgG (H+L) Alexa Fluor™ 488, A-11029	1:500 (IF)	Invitrogen, Waltham, MA, USA
Donkey anti-Rabbit IgG (H+L) Alexa Fluor™ 568, A-10042	1:500 (IF)	Invitrogen, Waltham, MA, USA
Goat Anti-mouse HRP A4416	1:12000 (WB)	Sigma-Aldrich (Merck), Darmstadt, Germany
Goat Anti-rabbit HRP A6154	1:5000 (WB)	Sigma-Aldrich (Merck), Darmstadt, Germany
TrueBlot® ULTRA Anti-Mouse IgG HRP clone eB144	1:1000 (WB)	Rockland Immunochemicals, Pottstown, PA, USA
TrueBlot® ULTRA Anti-Rabbit IgG HRP clone eB182	1:1000 (WB)	Rockland Immunochemicals, Pottstown, PA, USA

III.6 Home-made buffers and solutions

Table 5. Composition of buffers and solutions used in this study.
The composition of the buffers and solutions used in this work is listed. Unless otherwise stated, Milli-Q®H_2O served as the basis for the recipes.

Name	Composition
APS solution	10% (w/v) ammonium persulfate
Epon	48 g Glycidyl ether, 19 g DBA hardener, 33 g MNA hardener, 2 g DMP-30
Cytomix	120 mM KCl, 0.15 mM $CaCl_2$, 10 mM KH_2PO_4/K_2HPO_4, 2 mM EGTA, 5 mM $MgCl_2$, 25 mM HEPES [pH 7.6], freshly added 2 mM ATP and 5 mM glutathione
EM fixing buffer	2% glutaraldehyde and 1% PFA in 50 mM cacodylate buffer [pH 7,2] containing 10 mM $MgCl_2$, 10 mM $CaCl_2$, 100 mM KCl and 2% sucrose
Luria-Berthani (LB) medium	10 g Bacto-Trypton, 5 g Yeast Extract, 2.5 g NaCl dissolved in 1 l ddH_2O and sterilized by autoclaving
Luria-Berthani (LB) medium + ampicillin	Sterilized LB medium, supplemented with ampicillin (100 mg/l)
LB-agar medium	20 g Agar in 1 l LB medium, sterilized by autoclaving
LB-agar medium + carbenicillin	LB agar medium, supplemented with cabenicillin (100 mg/l) after melting
Paraformaldehyde (PFA) solution	4% PFA in PBS
PBS-T	0.2% (v/v) Tween-20 in PBS
Phosphate buffered saline (PBS)	8 mM Na_2HPO_4, 2 mM NaH_2PO_4, 140 mM NaCl

Name	Composition
DDM lysis buffer (PBS-based)	0.5% dodecyl-β-D-maltoside (DDM; w/v) in PBS supplemented with one tablet of protease inhibitors (Roche) per 50 ml.
DDM lysis buffer (Tris-based)	150 mM NaCl, 50 mM NaF, 20 mM Tris (pH 7.5), 0.5% dodecyl-β-D-maltoside (DDM; w/v) supplemented with one tablet of protease inhibitors (Roche) per 50 ml.
PAA fixing buffer	10% (v/v) glacial acetic acid, 5% (v/v) methanol
RLuc assay buffer	25 mM Glycine-Glycine [pH 7.8], 15 mM KH_2PO_4/K_2HPO_4 buffer [pH 7.8], 15 mM $MgSO_4$, 4 mM EGTA, 1.43 µM coelenterazine added right before use
RLuc lysis buffer	25 mM Glycine-Glycine [pH 7.8], 15 mM $MgSO_4$; 4 mM EGTA, 10% (v/v) glycerol, 0.1 (v/v) Triton X-100, 1 mM DTT added right before use
rNTP mix for IVT	25 mM ATP, 25 mM UTP, 25 mM CTP, 12.5 mM GTP in ddH_2O
SDS sample buffer (for SDS-PAGE)	120 mM Tris-HCl [pH 6.8], 60 mM SDS, 100 mM DTT, 1.75% glycerol, 0.1% bromophenol blue
SDS-PAGE resolving gel buffer	1.5 M Tris-HCL [pH 8.8], 0.4% (w/v) SDS
SDS-PAGE stacking gel buffer	1 M Tris-HCl [6.8], 0.8% (w/v) SDS
SP6 buffer	400 mM HEPES/KOH [pH 7.5], 80 mM $MgCl_2$, 10 mM Spermidin, 200 mM DTT
T7 buffer	400 mM HEPES/KOH [pH 7.5], 60 mM $MgCl_2$, 10 mM Spermidin, 200 mM DTT
TAE buffer 50x (agarose gel buffer)	2M Tris [pH 8.3], 2M glacial acetic acid, 50 mM EDTA in deionized H_2O
TGS buffer (SDS-PAGE running buffer) 10 x	250 mM Tris, 1.92M glycine, 1% (w/v) SDS in deionized H_2O
Wet blot transfer buffer	25 mM Tris [pH 8.3], 150 mM glycine, 20% (v/v) ethanol in deionized H_2O

III.7 Commercial kits

Table 6. List of commercial kits used in this study.
The commercial kits used in this work are listed with intended use and with manufacturer's details.

Name	Purpose	Source
NucleoBond PC 500	Plasmid isolation (maxiprep)	Macherey-Nagel, Düren, Germany
NucleoSpin Plasmid	Plasmid isolation (miniprep)	Macherey-Nagel, Düren, Germany
NucleoSpin Gel and PCR Clean-up	Purification of DNA fragments from agarose gels or from reaction mixes after PCR or enzymatic digestion	Macherey-Nagel, Düren, Germany
Western Lightning Plus-ECL	Western blot signal visualization	PerkinElmer, Waltham, MA, USA

III.8 Commercial chemicals and consumables

Table 7. Commercial reagents and consumables used in this study.
Chemicals and relevant consumables used in this work are listed with the manufacturer's details.

Name	Source
1,4 Dithiothreitol (DTT)	Roche, Basel, Switzerland
3´-O-Me-7mG(ppp)G RNA Cap Structure Analog (ARCA)	New England Biolabs, Ipswich, MA, USA
Acetone	Sigma-Aldrich (Merck), Darmstadt, Germany
Agarose	ThermoFisher Scientifc, Waltham, MA, USA
Amersham™ Protran® 0.2 µm nitrocellulose membrane	GE Healthcare, Chicago, IL, USA
Ammonium persulfate (APS)	VWR, Radnor, PA, USA
Ampicillin	Roche, Basel, Switzerland
anti-HA agarose beads, clone HA-7	Sigma-Aldrich (Merck), Darmstadt, Germany
Bacto-Trypton	Carl Roth GmbH, Karlsruhe, Germany
Benzonase® Nuclease	Merck Millipore, Burlington, MA, USA
Bovine serum albumin (BSA)	Sigma-Aldrich (Merck), Darmstadt, Germany
Bromophenol blue	Waldeck, Münster, Germany
Calcium chloride	Sigma-Aldrich (Merck), Darmstadt, Germany
Carbenicillin Disodium Salt	Carl Roth GmbH, Karlsruhe, Germany
Cell culture plates	Corning, Corning, NY, USA
Cell scrapers	Sarstedt, Nümbrecht, Germany
Chloroform	Sigma-Aldrich (Merck), Darmstadt, Germany
Coelenterazine h	PJK, Kleinbittersdorf, Germany
Color Prestained Protein Standard P7712	New England Biolabs, Ipswich, MA, USA
Color Prestained Protein Standard P7719	New England Biolabs, Ipswich, MA, USA
cOmplete protease inhibitor	Roche, Basel, Switzerland
Copper(II) sulfate pentahydrate	Sigma-Aldrich (Merck), Darmstadt, Germany
Coverslips	VWR International, Radnor, PA, USA
Cycloheximide	Sigma-Aldrich (Merck), Darmstadt, Germany
DBA hardener	Carl Roth GmbH, Karlsruhe, Germany
Dimethyl sulfoxide (DMSO)	Carl Roth GmbH, Karlsruhe, Germany
Dithiothreitol (DTT)	Sigma-Aldrich (Merck), Darmstadt, Germany
DMP-30	Carl Roth GmbH, Karlsruhe, Germany

Name	Source
DNA loading dye (6x)	New England Biolabs, Ipswich, MA, USA
Dodecyl-β-D-maltosid (DDM)	Carl Roth GmbH, Karlsruhe, Germany
Dulbecco's Modified Eagle Medium (DMEM)	ThermoFisher Scientifc, Waltham, MA, USA
EGTA	Sigma-Aldrich (Merck), Darmstadt, Germany
EM grids	Plano GmbH, Wetzlar, Germany
Ethanol	Honeywell Specialty Chemicals Seelze, Seelze, Germany
Falcon® tubes	Corning, Corning, NY, USA
Fetal calf serum (FCS)	Sigma-Aldrich (Merck), Darmstadt, Germany
Fluoromount G with DAPI	Southern Biotech, Birmingham, AL, USA
GeneRuler 1kb DNA Ladder	ThermoFisher Scientifc, Waltham, MA, USA
Glacial acetic acid	Carl Roth GmbH, Karlsruhe, Germany
Glutaraldehyde	Science Services, Munich, Germany
Glutathione	Sigma-Aldrich (Merck), Darmstadt, Germany
Glycerol	LABOCHEM, Athens, Greece
Glycidyl ether	Carl Roth GmbH, Karlsruhe, Germany
Glycine	ThermoFisher Scientifc, Waltham, MA, USA
Glycine-Glycine	Sigma-Aldrich (Merck), Darmstadt, Germany
Goat Serum	Sigma-Aldrich (Merck), Darmstadt, Germany
HEPES	Carl Roth GmbH, Karlsruhe, Germany
Isopropanol	Honeywell Specialty Chemicals Seelze, Seelze, Germany
L-[S35]Methionine, L-[S35]Cysteine	HARTMANN ANALYTIC, Braunschweig, Germany
L-Ascorbic acid	Applichem, Darmstadt, Germany
Lead citrate	Electron Microscopy Sciences, Hatfield, PA, USA
L-glutamine	ThermoFisher Scientific (Waltham, USA)
Magnesium chloride	Sigma-Aldrich (Merck), Darmstadt, Germany
Methanol	Honeywell Specialty Chemicals Seelze, Seelze, Germany
Microscope slides	Epredia, Portsmouth, NH, USA
MIDORI Green Advance DNA stain	Nippon Genetics Europe, Düren, Germany
Milk powder	Carl Roth GmbH, Karlsruhe, Germany

Name	Source
MNA hardener	Carl Roth GmbH, Karlsruhe, Germany
Multiwell-Plates	Greiner Bio-One, Frickenhausen, Germany
Nonessential amino acids	ThermoFisher Scientifc, Waltham, MA, USA
NTPs (ATP, CTP, GTP, UTP) Lithium Salt	Roche, Basel, Switzerland
Opti-MEM Reduced Serum Medium	ThermoFisher Scientifc, Waltham, MA, USA
Osmium tetroxide	Electron Microscopy Sciences, Hatfield, PA, USA
Parafilm	Bemis, Neenah,, WI, USA
Paraformaldehyde	Science Services, Munich, Germany
Pasteur capillary pipettes	Wilhelm Ulbrich GdbR, Bamberg, Germany
Phenol	Carl Roth GmbH, Karlsruhe, Germany
Phusion High-Fidelity PCR Master Mix with HF Buffer	ThermoFisher Scientifc, Waltham, MA, USA
Picolylazide-Cy5.5	Jena Bioscience, Jena, Germany
Pipet tips	Starlab International, Hamburg, Germany
Polypropylene tubes	Greiner Bio-One, Frickenhausen, Germany
Potassium chloride	Sigma-Aldrich (Merck), Darmstadt, Germany
Potassium hydroxide	Sigma-Aldrich (Merck), Darmstadt, Germany
Potassium phosphate dibasic	Grüssing GmbH, Filsum, Germany
Potassium phosphate monobasic	Sigma-Aldrich (Merck), Darmstadt, Germany
Precision Plus Protein Dual Color Standard	Bio-Rad, Hercules, CA, USA
Protein Assay Dye Reagent Concentrate	Bio-Rad, Hercules, CA, USA
Puromycin	Sigma-Aldrich (Merck), Darmstadt, Germany
Quick CIP (Calf intestine phosphatase)	New England Biolabs, Ipswich, MA, USA
RNasin RNase inhibitor	Promega, Madison, WI, USA
Rothiphorese 40% acrylamide / bisacrylamide mix (29:1)	Carl Roth GmbH, Karlsruhe, Germany
RQ1 RNase free DNase	Promega, Mannheim, Germany
Scalpels	B. Braun, Melsungen, Germany
Serological pipettes	Corning, Corning, NY, USA
Sodium cacodylate trihydrate	Serva, Heidelberg, Germany
Sodium chloride	Bernd Kraft, Maxdorf, Germany
Sodium dodecyl sulfate (SDS)	Applichem, Darmstadt, Germany
Sodium fluoride	Sigma-Aldrich (Merck), Darmstadt, Germany
SP6 RNA polymerase	New England Biolabs, Ipswich, MA, USA

Name	Source
Spermidin	Sigma-Aldrich (Merck), Darmstadt, Germany
Sucrose	Carl Roth GmbH, Karlsruhe, Germany
T4 DNA ligase and ligase buffer	ThermoFisher Scientifc, Waltham, MA, USA
TEMED	Applichem, Darmstadt, Germany
Test tubes/Eppendorf tubes	Sarstedt, Nümbrecht, Germany
TransIT transfection reagent	Mirus Bio, Madison, WI, USA
Tris(3-hydroxypropyltriazolylmethyl)amine (THPTA)	Carl Roth GmbH, Karlsruhe, Germany
Tris-(hydroxymethyl)-aminomethan (TRIS)	Carl Roth GmbH, Karlsruhe, Germany
Tris-HCl	Carl Roth GmbH, Karlsruhe, Germany
Triton X-100	Merck Millipore, Burlington, MA, USA
Trypsin	ThermoFisher Scientifc, Waltham, MA, USA
Tween20	Carl Roth GmbH, Karlsruhe, Germany
UltraPure Agarose	ThermoFisher Scientifc, Waltham, MA, USA
Uranyl acetate	Electron Microscopy Sciences, Hatfield, PA, USA
Whatman® cellulose chromatography papers	GE Healthcare, Chicago, IL, USA
Yeast extract	Carl Roth GmbH, Karlsruhe, Germany
Zeocin	ThermoFisher Scientifc, Waltham, MA, USA
β-Mercaptoethanol	ThermoFisher Scientifc, Waltham, MA, USA

III.9 Equipment

Table 8. List of key laboratory equipment used in this study.
This table lists the laboratory equipment and relevant non-consumables used in this study, indicating the manufacturer.

Name	Manufacturer
5424 R centrifuge	Eppendorf, Hamburg, Germany
Biofuge fresco	Heraeus, Hanau, Germany
BioMax TranScreen LE intensifying screen	Kodak, Rochester, NY, USA
ChemoCam Imager 3.2	Intas Science Imaging Instruments, Göttingen, Germany
Dual Temperature Slab Gel Dryer SE-1125B	Bio-Rad, Hercules, CA, USA
Flex Cycler 2	Analytik Jena, Jena, Germany
Gene Pulser II	Bio-Rad, Hercules, CA, USA

Name	Manufacturer
HERAsafe HS12 cell culture hood	Heraeus, Hanau, Germany
JEM-1400 transmission electron microscope	JEOL, Akishima, Japan
KF-2-60 cold trap	H. Saur, Reutlingen Germany
Labotect C200 Incubator	Labotect, Rosdorf, Germany
Leica DM IRB microscope	Leica, Wetzlar, Germany
Leica EM UC6	Leica, Wetzlar, Germany
Leica SP8 inverted confocal microscope	Leica, Wetzlar, Germany
Mini-PROTEAN Tetra System	Bio-Rad, Hercules, CA, USA
Mithras LB 940 plate luminometer	Berthold Technologies, Bad Wilbad, Germany
MSC-Advantage™ cell culture hood	ThermoFisher Scientifc, Waltham, MA, USA
Multifuge 3 centrifuge	Heraeus, Hanau, Germany
NanoDrop Lite Spectrophotometer	ThermoFisher Scientific
Nikon Ti Eclipse fluorescent miscroscope	Nikon, Tokio, Japan
OmniaTap ultrapure water system	Stakpure GmbH, Niederahr, Germany
Personal Molecular Imager FX	Bio-Rad, Hercules, CA, USA
Screen Eraser-K	Bio-Rad, Hercules, CA, USA
Sorvall Lynx 6000 centrifuge	ThermoFisher Scientifc, Waltham, MA, USA
TC20 Automated Cell Counter	Bio-Rad, Hercules, CA, USA
Thermomixer compact	Eppendorf, Hamburg, Germany
Ultrospec 2100 pro spectrophotometer	Amersham Biosciences, Little Chalfont, UK
UVP Crosslinker CL-1000M	Analytik Jena, Jena, Germany

III.10 Software

Table 9. List of software used in this study.
In this table, the software used in this study is indicated with the respective version number, the purpose of use and vendor information.

Name	Purpose	Source / reference
ChemoStar Imager Version 0.3.29	Digital recording and processing of western blot images	Intas Science Imaging Instruments, Göttingen, Germany
EM-Menu Version 4.0.9.87	Digital recording of EM images	Tietz Video and Image Processing Systems, Gauting, Germany
GraphPad Prism 8.4.3	Statistical analyzes and graph preparation	GraphPad Software, San Diego, CA, USA
ImageJ version 2.1.0/1.53j	Image processing	Wayne Rasband and contributors, National Institutes of Health, USA [383]

Name	Purpose	Source / reference
NIS – Elements Advanced Research Version 5.30.06	Digital recording of immunofluorescence images	Nikon, Minato, Japan
Quantity One 1-D Version 4.5.1	Digital recording and processing of autoradiographs	Bio-Rad, Hercules, CA, USA
VectorNTI Advance Version 11.5.4	Sequence analysis, plasmid maps generation	ThermoFisher Scientific, Waltham, MA, USA

IV. Methods

IV.1 Molecular genetic methods

IV.1.1 Transformation of competent *E. coli* bacteria

Transformation is the process by which plasmid DNA is introduced into bacterial cells[384]. In this work, the transformation was performed employing competent *E. coli* cells of strain DH5α, which had been made chemically competent before use via on ice incubation with $CaCl_2$ during the logarithmic growth phase (long-term storage of competent cells at -80°C is possible). Calcium ions weaken the bacterial cell membrane and neutralize the negative charge of both plasmid DNA and lipopolysaccharides of the bacterial cell wall, thereby promoting the attachment of DNA to the latter[385].

For the purpose of retransformation, 100 to 1000 ng of plasmid DNA in a maximum volume of 1 µl were mixed with 20 µl of DH5α cells, while for cloning procedures, 20 µl of ligation mix were added to 80 µl of DH5α cells. In both cases this was followed by incubation on ice for at least 20 minutes. Thereafter, a so-called heat shock at 42°C was carried out for one minute, whereby the increased Brownian motion assisted plasmids to enter the cell through pores in the cell membrane.

Once incubated again on ice for 5 minutes, 1 ml of LB medium was added and the mixture was shaken at 37°C for 1 h before bacteria were concentrated by centrifugation and 100 µl were transferred to LB-agar plates containing appropriate selective antibiotics (most commonly 100 mg/l carbenicillin, a thermostable ampicillin derivative), which were then cultured either overnight at 37°C or for about 72 h at room temperature.

IV.1.2 Plasmid amplification und preparation

Depending on the required yield of plasmid DNA, preparations were performed on different scales with distinct protocols for the respective purification.

Miniprep

Individual bacterial colonies grown on agar plates were picked with a sterile pipette tip and transferred to polypropylene tubes filled with 5 ml of antibiotic-containing LB medium, which was incubated overnight in a shaker set at 37°C. On the next day, pelleted bacteria were broken up after resuspension using SDS and alkaline lysis. A commercial kit (NucleoSpin Plasmid; Macherey-Nagel, Düren, Germany) was used for these and the following steps. During subsequent neutralisation, denatured plasmid DNA, but not chromosomal DNA, was

completely reconstituted, leaving the former in solution, and precipitating the latter. In the following column chromatography, chaotropic salts supported the adsorption of DNA to the silica column material and the removal of proteins. Elution of DNA was carried out in a 5 mM Tris/HCl buffer (pH 8.5).

Maxiprep

Depending on the expected copy number of the plasmid to be amplified, 400 to 800 ml of LB medium equipped with selective antibiotic were inoculated with 5 ml of overday bacterial culture and incubated overnight at 37°C with shaking. Bacteria were pelleted with a Sorvall Lynx 6000 centrifuge (ThermoFisher Scientifc, Waltham, MA, USA) and further processed using a NucleoBond PC 500 kit(Macherey-Nagel, Düren, Germany) according to the manufacturer's protocol. In contrast to the Miniprep, plasmid DNA purification in the Maxiprep is carried out by ion exchange chromatography, which requires alkaline elution, implying that eluted DNA must first be precipitated with isopropanol before being washed in 70% ethanol and resuspended in 5 mM Tris-HCl buffer.

IV.1.3 Polymerase chain reaction

The polymerase chain reaction (PCR) is a very sensitive method for sequence-specific amplification of DNA[386]. In this work, the technique was applied to obtain substantial amounts of desired DNA fragments for molecular cloning purposes. To this end, a so-called phusion polymerase was employed, which, in contrast to the tac polymerase used in original protocols, has a significantly lower error rate and at the same time exhibits a high reaction rate of about 2000 bp per min. The Phusion Polymerase was delivered with a 2x MasterMix, which contained the polymerase itself as well as nucleotides and buffer components, so that only primers (2.5 μM) and template (~100 ng) dissolved in water had to be added.
In general, the following guidelines were followed in the design of PCR primers:

- Length of 18-24 bases
- 40-60% G/C content
- 1-2 G/C pairs at the 3'end
- Melting temperature (T_m) of 55-65°C and less than 5°C difference between forward and reverse primer
- Avoidance of 4 or more repeats of a mono- or dinucleotide
- Avoidance of complementary regions

- Central positioning of the mismatch in site directed mutagenesis

Complicated PCR reactions (e.g., introduction of a tag or restriction site via an overhang) often did not allow compliance with all of these points. In these cases, individual procedures were followed. The reaction scale chosen was mostly between 50 and 100 µl and a typical thermal cycler program is given in Table 10.

Table 10. PCR cycling conditions.
The temperature and duration for each PCR step are listed. *The annealing temperature given is an average value. If possible, it was adjusted for each PCR to be about 3°C below the melting temperature of the primer with the lower melting temperature.

Step	Temperature	Duration	
Initial denaturation	95°C	3 min	
Denaturation	95°C	30 s	35 x
Annealing	55°C*	30 s	
Elongation	72°C	30 s/kb	
Final elongation	72°C	10 min	
Hold	4°C	∞	

IV.1.4 Restriction digest

Restriction enzymes are endonucleases of bacterial origin that can hydrolytically cleave the phosphodiester bonds of a DNA double-stranded molecule in a site-specific manner[387]. The activity of restriction enzymes is expressed in units (U), with one U being defined as the amount of enzyme required to digest one microgram of reference DNA under optimal reaction conditions within 1 h. By default, the DNA of the bacteriophage lambda (λ) is used for this purpose; in the rare case that the λ-genome does not have a restriction site, the manufacturer must specify which reference DNA was used instead. The molecular weight of a base pair can be approximated with 660 Da, which results in 1 µg λ-DNA being very exactly 1/32 pmol. Depending on the number of restriction sites an enzyme has in the reference genome, a different number of units is needed to cut 1 pmol of a DNA molecule in which a restriction enzyme can only cut once.

For all restriction enzymes used in this work, this amount of units is given in Table 2. Likewise, a unit number can be found for the assumption that this hypothetical plasmid has a length of

10 kB.

For analytical restriction digests, 1 µg of DNA was digested in a reaction volume of 20 µl by default, while 10 µg in 100 µl were used for cloning purposes. Occasionally, the volumes were adjusted, e.g. to ensure that the glycerol content introduced via the enzymes did not exceed 5 % by volume. All digests were performed at 37°C in a suitable buffer for an appropriate time. In double digests for cloning, care was taken to ensure that the reaction did not produce compatible cohesive ends. In addition, half an hour before the end, 5 U of alkaline phosphatase were added to vector digests to remove 5' phosphates, which prevents vector re-ligation.

IV.1.5 Agarose gel electrophoresis

Agarose gel electrophoresis is a technique for separating linear nucleic acid fragments according to their size, taking advantage of the presence of negatively charged phosphate groups in their backbone. When an electric field is applied to a gel matrix of agarose positioned in a chamber filled with TAE buffer (2M Tris [pH 8.3], 2M glacial acetic acid, 50 mM EDTA in deionized H_2O), the DNA/RNA fragments migrate toward the positive electrode. The higher the agarose concentration, the smaller are the gel's pores and the higher is its separation efficiency.

In this work, agarose gel electrophoresis was used for several purposes. First, for quality control of RNA after IVT as described in Chapter IV.1.10, second, for analysis of PCR products or minipreps after test digestion, and third, for preparative purification of DNA after PCR or restriction digestion.

To prepare an agarose gel, 0.7 to 2 g agarose was boiled in 100 ml TAE buffer. After cooling to about 60°C, 3 µl of the nucleic acid dye MIDORI Green Advance was added and the mix was poured into a casting apparatus equipped with appropriate comb. Samples spiked with loading dye were applied to gels along with marker, which were routinely run at a constant 120V. Gels were then analyzed using a blue light transluminator. If required, DNA bands were cut out of the gel with a scalpel and the gel piece was transferred to a test tube.

IV.1.6 Purification of DNA fragments

DNA fragments were purified with a NucleoSpin Gel and PCR Clean-up kit (Macherey-Nagel, Düren, Germany) according to the manufacturer's protocol. DNA entrapped in agarose gel pieces was first released by melting the agarose at 50°C in a sufficient amount of kit buffer NTI.

IV.1.7 DNA Ligation

For DNA ligation, vector and insert were brought together in a suitable buffer containing the enzyme T4-DNA ligase (ThermoFisher Scientifc, Waltham, MA, USA). This enzyme, originally derived from the enterobacterial phage T4, catalyses the formation of phospho-diester bonds between adjacent 5'-phosphate groups and 3'-hydroxyl termini in duplex DNA under ATP hydrolysis.

Where possible, vector and insert were applied in this work in a molar ratio of one to three, with their total mass calculated to be 100 ng. The masses for vector (m_{Vector}) and insert (m_{Insert}) can be obtained from the formulas given, for which only the lengths of vector (l_{Vector}) and insert (l_{Insert}) need to be known.

$$m_{Insert} = \frac{100\ ng}{1+\frac{l_{Vector}}{3 * l_{Insert}}} \qquad m_{Vector} = 100\ ng - m_{Insert}$$

DNA was supplemented with ddH_2O, 2 µl T4 buffer concentrate, and 1 µl T4 polymerase to a total volume of 20 µl and incubated either for 1 h at RT or overnight at 16°C. In addition to ligation of vector and insert, a vector only control was always included, in which the volume of insert DNA was replaced by ddH_2O.

IV.1.8 Cloning strategies

In this work, many new constructs were produced by cloning. These are denoted in Supplementary Table 1, which lists all the plasmids used in this dissertation. Generally, each cloning is individual and requires, for example, customized primers. However, there are basic strategic concepts, which are described below. In Supplementary Table 1, it is indicated for each newly cloned plasmid to which of these strategies the cloning process can be related, and together with the listed restriction enzymes or, if applied, primers (sequences given in Supplementary Table 2), the individual cloning approach can be reconstructed for each individual plasmid.

Ordinary subcloning

Ordinary subcloning represented the simplest case of a cloning strategy in this work, as it does not require PCR. Here, a feature on a donor plasmid was transferred into a recipient plasmid by digesting both with the same pair of restriction enzymes and after purification, the insert of the donor plasmid was recombined with the backbone of the recipient plasmid by ligation as shown in Figure 8.

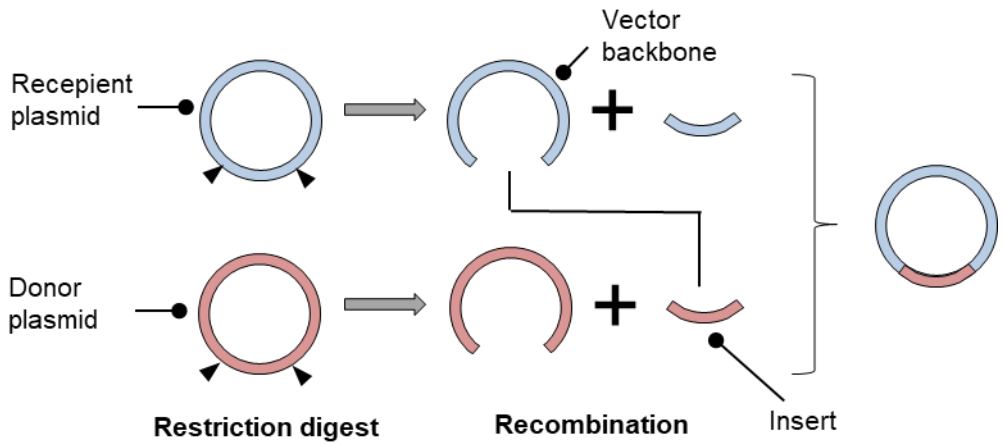

Figure 8. Schematic of ordinary subcloning.
Donor and recipient plasmid were digested with the same pair of restriction enzymes (indicated by black arrowheads) and the backbone of the recipient plasmid as well as the insert of the donor plasmid were purified and added to a ligation mixture to obtain the desired recombined plasmid via transformation and subsequent plasmid preparation.

Overlap PCR/Fusion PCR and site-directed mutagenesis

In many cases, the strategy of ordinary subcloning was not possible, for example, when a feature on a construct A was to be combined with another feature on construct B, but there was no useful restriction site in between. In such a case, a strategy involving overlap PCR, also called fusion PCR, was resorted to. In a first round of PCR, a feature A comprising fragment of construct A, as well as a feature B comprising fragment of construct B were amplified, taking care to create an 18-25 bp overlap region between both fragments. In the overlap or fusion PCR, both previously amplified fragments were then used as templates and thus linked to each other (Figure 9a). A variation of this strategy is the frequently used site-directed mutagenesis, in which short nucleotide substitutions (usually 1 to 3 bases long) were introduced, often with the aim of achieving a desired amino acid exchange. Here, two fragments from the same plasmid were amplified in the first round of PCR, with the forward primer of the C-terminal fragment being reverse complementary to the reverse primer of the N-terminal fragment. In their centers, these primers contained mismatches to the hybridization sequence on the source plasmid, thus introducing mutations (Figure 9b).

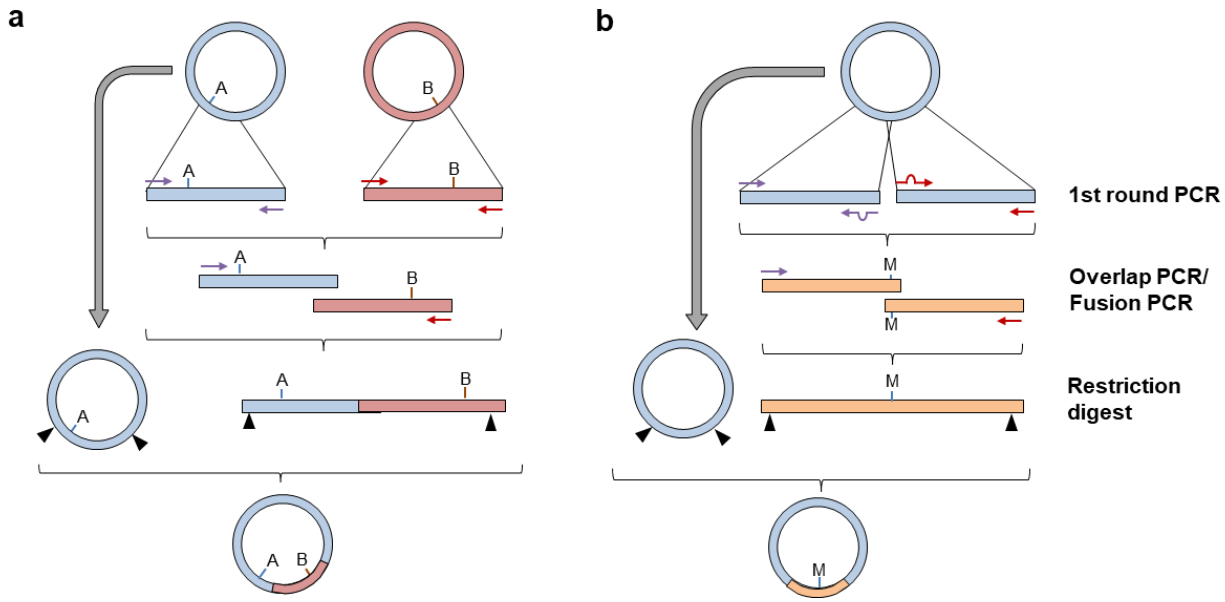

Figure 9. Schematic of overlap/fusion PCR and site-directed mutagenesis.
a, Principle of an overlap extension PCR. Both the donor and recipient plasmids were used as templates for PCR, with the resulting fragments having a complementary region of about 20 bp. This allowed the two fragments to be fused in a downstream PCR where both were used as templates. Like the recipient plasmid, the fused PCR product was digested with a pair of restriction enzymes (black arrowheads) and recombined as an insert with the former. **b**, Principle of site-directed mutagenesis. Using specially designed primers that could not fully hybridize to the template plasmid in their center, a mutation was introduced in the overlapping region of the two fragments generated in the first PCR round. By fusing the two fragments, the mutation site was extended upstream and downstream to reach restriction sites suitable for cloning.

Overlap extension PCR

In general, it is possible to extend primers by about 10-15 terminal bases that do not hybridize with their template. This extension PCR allows the introduction of restriction sites, for example, but is not suitable for larger units such as tags, as the primers would become too long and unspecific in this case. Overlap extension PCR, on the other hand, represents a complex but highly flexible cloning approach. It allows large insertions as well as deletions to be engineered with precision (Figure 10). The basic principle is that in a first round of PCR, fragments to be linked were extended by about 10 base pairs complementary to the terminus of the respective other fragment, resulting in a complementary region comprising a total of about 20 base pairs.

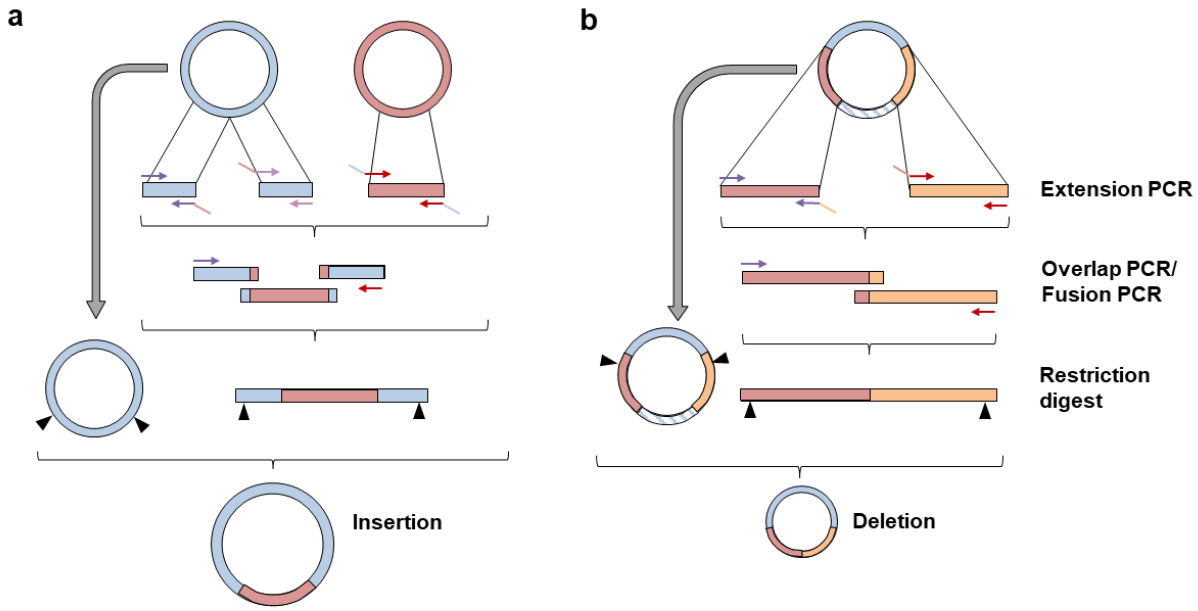

Figure 10. Schematic of cloning procedures with overlap extension PCR.
a, Insertion setup. An insert region was amplified from a donor plasmid using primers extended at their respective 5' ends. Two flanking PCR fragments were generated from the recipient plasmid using overlap extension PCR. The subsequent fusion of the three fragments was either performed in a single step (A+B+C) as depicted or in two consecutive PCR reactions (A+B and AB+C), respectively. **b**, Deletion setup. Using appropriate primers, two mutually overlapping PCR fragments were generated that flanked a plasmid region to be deleted. After fusion, vector and insert were digested (restriction sites illustrated by black arrowheads), ligated and transformed to obtain the desired construct. Not shown in this figure is that insertion and deletion could be combined in one cloning to obtain a custom-fit exchange of a larger region.

IV.1.9 Sequencing

For DNA sequencing, the SupremeRun service of the commercial provider Eurofins Genomics Germany GmbH (Ebersberg, Germany) was used. 20 µl of sample material were adjusted so that the DNA concentration (monitored by NanoDrop spectrophotometer) ranged between 50-100 ng/µl. Primers were provided in test tubes in volumes of 20 µl each, with a concentration of exactly 10 pmol/µl (≙ 10 µM).

IV.1.10 *In vitro* transcription

In vitro transcription is a laboratory technique for producing RNA molecules from a DNA template outside a living cell, for which in this work an established protocol by Fischl and Bartenschlager[388] was followed. Plasmids with a pFK backbone were used as DNA templates, into which a bicistronic gene was inserted that encoded a luciferase enzyme from *Renilla reniformis* (sea pansy) on the one hand and the non-structural module of the DENV-2/16681 polyprotein on the other. An intermediate 2A peptide served to cleave the two protein products. The entire element was flanked by the non-translated regions (NTRs) of the DENV-2 genome

and, upstream of the luciferase, by *cis*-acting RNA elements belonging to a part of the capsid coding region. Based on this design, the constructs were designated as pFK-sgDVR2A (sg = subgenomic; DV = dengue virus; R = *Renilla* luciferase; 2A = 2A peptide). Several constructs were generated to express either the WT polyprotein or variants thereof with JNJ-A07 resistance mutations in NS4B, and for each 10 µg of plasmid DNA was linearized with XbaI (located at the very end of the 3' NTR of the viral genome) and subsequently purified using a NucleoSpin Gel and PCR Clean-up kit (Macherey-Nagel, Düren, Germany). *In vitro* transcription of linearized DNA template was carried out in a total reaction volume of 100 µl SP6 buffer (containing 400 mM HEPES [pH 7.5], 80 mM $MgCl_2$, 10 mM spermidine, and 200 mM dithiothreitol) supplemented by nucleoside triphosphates (3.125 mM ATP, CTP, and UTP and 1.56 mM GTP), 1 mM Ambion® Anti-Reverse Cap Analog (ARCA), 1U/µl RNAsin and 0.8 U/µl SP6 RNA polymerase. After incubation for 2.5 h at 40°C, another 0.4 U/µl SP6 RNA polymerase were added, followed by overnight incubation at 40°C. Finally, template DNA was digested by RNase-free DNAse I treatment for 1 h at 37°C. RNA was purified using acidic phenol-chloroform extraction. First, 60 µl of a 2 M NaOAc solution adjusted to a pH value of 4.5 were added to the reaction mix followed by the addition of 440 µl ddH_2O. Then 400 µl of water-saturated phenol were added, followed by shaking of the mix with a vortexer, incubation on ice for 10 min and separation of the phases by centrifugation. Due to the pH value of below 5, both proteins (e.g. SP6 RNA polymerase) and DNA fragments migrate into the lower phenolic phase, whereas RNA remains in the upper aqueous phase, which was next transferred to a new test tube and mixed with 600 µl of chloroform. By re-mixing the phases followed by centrifugation-assisted separation, phenol was removed from the upper aqueous phase, and the latter was again transferred to a fresh test tube. The subsequent addition of 0.7 volume of isopropanol served to precipitate RNA while keeping nucleotides and salts in solution. After washing of the pellet with 70% ethanol, purified RNA was dissolved in RNase-free water, and molecular weight and integrity were checked by agarose gel electrophoresis.

IV.2 Cell culture

IV.2.1 Cell culture maintenance

Human hepatoma (Huh7) and Huh7/Lunet cells were cultured at 37°C under 5% CO_2 in DMEM complemented with 10% FBS, 2 mM L-glutamine, 100 U/mL penicillin, 100 µg/mL streptomycin and 1% non-essential amino acids (hereafter referred to as $DMEM_{Complete}$). Variants of these cell lines that additionally express a cytosolic form of bacteriophage T7

polymerase along with a zeocin resistance gene have been described previously and were passaged in the above medium supplemented with 5 µg/mL zeocin[117]. Huh7-T7 NS2B-NS3, Huh7/Lunet-T7 NS2B-NS3 and Huh7/Lunet-T7 NS1-HA cells generated by lentiviral transduction as reported elsewhere[117,140] were grown in the additional presence of 1 µg/mL puromycin. As standard, cells were passaged twice a week by first causing them to detach from the cell culture dish via trypsin treatment, resuspending them in fresh medium and then seeding them into new dishes at ratios ranging from 1:6 to 1:8. When experiments required accurate cell numbers, cells were either counted manually in a Neubauer improved hemocytometer or automatically by using the TC20 device (Bio-Rad, Hercules, CA, USA). For long-term storage, cells were harvested by trypsinization, washed with DMEM, and centrifuged. Subsequently, cell pellets were resuspended in FCS with 10% DMSO, temporarily cooled in a -80°C freezer and then transferred to a liquid nitrogen tank. Cell lines were regularly tested for mycoplasma contamination.

IV.2.2 Transient transfection of DNA

Transient transfection of DNA was performed on cells 18 h to 24 h after seeding using the liposomal transfection reagent TransIT-LT1 (Mirus, Madison, WI, USA) following the manufacturer's instructions. Depending on the plate or dish format used for a particular experiment, the amount of DNA required was adjusted to the size of the available surface area (e.g., 0.5 µg in a 24-well format, 2 µg in a 6-well format and 10 µg in a 10 cm plate format, respectively). For each microgram of plasmid DNA, 80 µl of OptiMEM were pipetted into a test tube and the DNA was added and mixed completely by inverting the tube several times. Then, 3 µl of the transfection reagent were added per microgram of DNA and the mixing process described above was repeated. After an incubation period of 15 to 30 minutes, the mix was added to the cells in a dropwise manner. Cell culture medium was changed both before and 4 h after transfection.

IV.2.2 Transient transfection of RNA

Electroporation was used as a technique for transient transfection of RNA molecules. To this end subconfluent Huh7 cells were trypsinized and collected in complete DMEM, requiring 4 x 10^6 cells per sample. Cells were washed once with PBS and resuspended in cytomix buffer (120 mM KCl, 0.15 mM $CaCl_2$, 10 mM potassium phosphate buffer, 25 mM HEPES, 2 mM EGTA, 5 mM $MgCl_2$, pH 7.6, freshly supplemented with 2 mM ATP and 5 mM glutathione) at a density of 1x 10^7 cells/ml. 10 µg of *in vitro*-transcribed RNA was mixed with 400 µl of

cell suspension, transferred to an electroporation cuvette (Bio-Rad; 0.4-cm gap width), and pulsed once with a Gene Pulser II system (Bio-Rad) at 975 µF and 270 V, typically resulting in time constants between 16 and 20 ms. Immediately after pulsing, the cells were transferred to prewarmed complete DMEM and seeded in duplicate into 24-well plates at different densities depending on the planned incubation time (2x 10^5 cells in 1 ml DMEM for 4 h and 24 h; 1x 10^5 cells in 1 ml DMEM for 48 h and 72 h; 0.5x 10^5 cells in 1 ml DMEM for 96 h).

IV.3 *Renilla* luciferase replication assay

In this assay, *Renilla* luciferase activity was determined as a measure of intracellular RNA replication of DENV subgenomic reporter replicons. To this end, replicons were prepared by *in vitro* transcription as described in Chapter IV.1.10 and introduced into cells via electroporation as reported in Chapter IV.2.2. The protocol for the *Renilla* luciferase replication assay is based on the version of Kumar et al.[193], with some adaptations as described below.

At various time points after electroporation (4 h, 24 h, 48 h, 72h and 96 h), cells were harvested by first washing once with PBS and then covering them with 200 µl of luciferase lysis buffer (0.1% Triton X-100, 25 mM glycylglycine, 15 mM $MgSO_4$, 4 mM EGTA, freshly complemented with 1 mM DTT [pH 7.8]). The samples were immediately frozen at -20°C. After collection of all samples, these were thawed simultaneously so that lysis could take place at room temperature. Complete lysis was promoted by cell scraping and careful up and down pipetting. For each well, 25 µl of lysate were transferred in duplicate to a white 96-well plate, which was placed into a luminometer (Mithras LB940, Berthold, Freiburg, Germany). According to a predefined program, 100 µl of assay buffer (25 mM glycylglycine, 15 mM $MgSO_4$, 4 mM EGTA, 1 mM DTT, 2 mM ATP, 15 mM K_2PO_4 [pH 7.8], freshly supplemented with 1.42 µM coelenterazine h) were added to each well and luciferase activity was measured for 10 seconds after shaking and incubation.

IV.4 Immunofluorescence microscopy (IF)

IV.4.1 IF staining

Huh7/Lunet-T7 cells were seeded on coverslips in a 24-well format (35,000 cells/well). Transfection with pIRO-D or pIRO-Z plasmids was performed as described in Chapter IV.2.2. Along with medium exchange 4 h post-transfection, cells were treated with antiviral compounds Compound A, Compound B, JNJ-A07, and NITD-688 or DMSO control (vehicle). Listed compounds were obtained from Janssen Pharmaceuticals, Inc. and stored at -20°C in 100% dimethylsulfoxide (DMSO) as a 5 mM stock. At 18 h after transfection, cells were briefly

washed once with PBS and then fixed for 20 minutes at room temperature (RT) with a 4% paraformaldehyde solution (PFA). Cells were allowed to permeabilize for up to 10 minutes at RT by covering with a PBS solution containing 0.2% Triton X-100 before blocking with 5% goat serum albumin (GSA) in PBS for 1 h. After a brief wash in PBS, the coverslips were placed upside down on 20 µl drops containing primary antibodies in 5% GSA (the corresponding dilutions are given in Chapter III.5. After another round of washing, the samples were treated with Alexa fluorophore-conjugated secondary antibody dilutions (1:500 in 5% GSA; 30 min). Subsequently, the specimens were washed three times with PBS followed by a further three washes with ddH_2O before mounting on slides with Fluoromount G containing DAPI.

IV.4.2 Integration of a photoaffinity-labelling approach

Huh7/Lunet-T7 cells were seeded on coverslips in a 24-well format (35,000 cells/well) and transfected 24 h later with pIRO-D plasmids (WT or compound resistance mutants) or pIRO-Z WT, respectively. Simultaneously with the medium change (4 h post-transfection), cells were treated with either 1 µM Compound A, 1 µM Compound B or DMSO control (vehicle). At 18 h post-transfection, the cells were briefly washed once with PBS whereupon 1 ml of PBS was pipetted into each well. Next, the plates were placed without lids in a UV crosslinker (UVP crosslinker CL-1000M, Analytik Jena) in which the cells were irradiated for 5 min with light at a wavelength of 365 nm, transferring an energy of 200 $\frac{mJ}{cm^2}$. Subsequently, cells were fixed with 4% PFA, permeabilized with and 0.2% Triton X-100 and blocked as described in Chapter IV.4.1. After a short wash in PBS, coverslips were turned upside down and placed on droplets of 20 µl click reaction mixture (aqueous solution containing 1 mM ascorbic acid, 1 mM $CuSO_4 \cdot 5\ H_2O$, 100 µM Tris(3-hydroxypropyltriazolylmethyl)amine (THPTA) and 50 µM Picolyl-Azide-Cy5.5) in a humid, dark chamber. After 1 h incubation at RT, the reaction mixture was removed by washing. Staining with primary and secondary antibodies, as well final washing steps and mounting, were then performed exactly as described in Chapter IV.4.1.

IV.4.3 IF image acquisition and analysis

To determine subcellular colocalization between NS3, NS4B and PAL compounds, 7 cells per sample and experiment were imaged using a Leica SP8 confocal microscope. Pearson correlation coefficients were calculated using the ImageJ plugin Coloc2 (ImageJ version 2.1.0/1.53j; Wayne Rasband and collaborators, National Institutes of Health, USA). Overview

images were taken at 20x magnification on a Nikon Eclipse Ti microscope to classify the morphological pattern of NS4B as well as to quantify NS4B signal intensity.

Sample transfection efficiency was determined by applying a classical IF protocol to stain for NS3. Microscopic imaging was performed on a Nikon Eclipse Ti microscope using a 20x air objective. A minimum of 1000 cells per condition were analyzed using a custom ImageJ macro. Briefly, this macro recognized the outlines of cell nuclei based on the DAPI signal and transferred the contours to the NS3 channel. There, the boundaries were expanded by two pixels in each direction, and the integral of the image signal of each area was read. A mock-transfected control was used to define the background by setting a threshold in such a way that 95% of the cells fell below it. This threshold was then applied to all other samples and the fraction exceeding it was considered transfected.

IV.5 Detection, analysis, and quantification of proteins

IV.5.1 Cell lysis

For detection, analysis, and quantification of proteins as part of a co-immunoprecipitation setup, $2x10^6$ Huh7-T7 or $1x10^6$ Huh7/Lunet-T7 cells (including sublines stably expressing DENV-2 NS2B-NS3 or NS1) were seeded into 10-cm-diameter cell culture dishes 18 to 24 h prior to transfection. Another 18 h later, cells were routinely harvested by scraping 10 cm dishes after PBS washing. For the subsequent lysis, the mild and non-ionic detergent dodecyl-β-D-maltoside (DDM) was used, as it features a very low critical micelle concentration (CMC), resulting in a comparatively small micelle size, which in turn is favourable for the effective solubilisation of transmembrane proteins such as NS4A-2K-NS4B in their native state[389]. Depending on the experimental context, a 0.5% DDM lysis buffer was prepared in PBS or an aqueous solution containing 150 nM NaCl, 50 mM NaF and 20 mM Tris (pH 7.5). In each case, DDM lysis buffer was freshly complemented before each use by dissolving one tablet of protease inhibitors (Roche, Basel, Switzerland) in 50 ml volume. Cells were treated with 500 µl lysis buffer and after 20 min of incubation on ice, lysates were centrifuged for 45 min at 15.000 rpm using a benchtop centrifuge pre-cooled to 4°C, followed by the transfer of supernatants to fresh tubes in order to separate them from cell debris.

In some experimental setups of this dissertation, the interest in protein analysis was solely at the level of total lysates. In these cases, $2x10^5$ Huh7/Lunet-T7 cells were seeded in 6-well plates 18 to 24 h prior to transfection and lysed another 18 h later by adding 100 µl of SDS-sample

buffer (complemented with 1 µl of benzonase) after removal of the medium and a short PBS wash.

IV.5.2 Bradford Assay

Protein concentrations in cleared lysates were determined by performing a Bradford-Assay. To this end, small volumes were mixed with 1 ml of a Bradford working solution that was generated from a commercial concentrate (Protein Assay Dye Reagent Concentrate; Bio-Rad, Hercules, CA, USA). The therein contained Coomassie dye associates with basic amino acids and thus causes comparatively unspecific staining of proteins, shifting the absorption maximum from 470 nm to 595 nm[390]. Consequently, the absorption at the latter wavelength was measured with a Ultrospec 2100 pro spectrophotometer (Amersham Biosciences, Little Chalfont, UK) and the protein concentration could then be calculated by comparison with a standard curve. Protein concentrations of samples from a set were adjusted to the sample of lowest concentration by using lysis buffer for dilution. For each sample, 500 µl of the adjusted lysate were transferred to a fresh tube. 50-100 µl of each sample were saved for later input analysis and the remaining volume was subjected to immunoprecipitation (IP).

IV.5.3 Co-Immunoprecipitation

HA-specific immunoprecipitation was performed with mouse monoclonal anti-HA agarose beads (Sigma-Aldrich/Merck, Darmstadt, Germany) that had been equilibrated to lysis buffer by three consecutive washing steps. Unless explicitly stated otherwise, working operations were executed on ice and centrifugation of the beads, which is part of each washing step, was carried out in a tabletop centrifuge precooled to 4°C at 700 x g.

30 µl of beads were added to each sample, which were then incubated for at least 3 h at 4 °C on a rotating wheel. Following this, two washing steps were conducted with lysis buffer. Thereafter beads of each sample were resuspended in PBS and transferred to fresh test tubes. These were again mounted on a rotating wheel for another 30 min before a final wash in PBS was conducted. Captured proteins were eluted at 37°C in 120 µl of PBS containing 5% SDS followed by an additional elution step in 100 µl of pure PBS. Four sample volumes of acetone were added to the combined eluates to allow overnight precipitation of proteins at -20°C. The samples were subjected to centrifugation at 21,130 x g for 1 h at 4°C. The resulting pellets were air-dried and then reconstituted in SDS sample buffer.

IV.5.4 SDS-PAGE

Tris-glycine SDS-polyacrylamide gel electrophoresis (SDS-PAGE) is a common method used to separate proteins based on their molecular mass[391]. The matrix is a polyacrylamide-based gel, which is composed of two discontinuous parts, the lower one termed resolving gel and the upper one termed stacking gel.

In this work, gels were self-cast according to a recipe as shown in Table 11, with resolving gels having a final PAA content of 10-15% (corresponding to 25-37.5% [v/v] of a 40% acrylamide/ bisacrylamide mix [29:1]).

Table 11. Composition of polyacrylamide gels.
Gels were cast in dedicated equipment by first filling to approximately 80% with resolving gel mix as indicated in the left half of the table. The liquid resolving gel was covered with isopropanol, which was removed after polymerisation. The remaining level was then filled with stacking gel mix, according to the right half of the table. Immediately afterwards, the appropriate combs were inserted.

Resolving gel		Stacking gel	
25% (v/v)	Resolving gel buffer	12.5% (v/v)	Stacking gel buffer
1% (w/v)	APS	1% (w/v)	APS
0.1 % (v/v)	TEMED	0.1 % (v/v)	TEMED
Various % (v/v)	40% AA/BAA mix (29:1)	12.5% (v/v)	40% AA/BAA mix (29:1)
Ad 100%	ddH_2O	Ad 100%	ddH_2O

Connected to electrodes, gels were placed in a chamber filled with a buffer containing Tris, glycine and SDS, whereby anions of the latter attach to proteins and mask their intrinsic charge. Proteins dissolved in SDS sample buffer were boiled at 95°C for 5 minutes and subsequently loaded into pockets of the stacking gel together with a protein marker. The SDS-PAGE was run at constant voltage (30 min at 70 V, afterwards up to 130 V).

The principle behind the method is that the stacking gel's large pores allow proteins to migrate relatively freely. However, on their way to the interface between the stacking and the running gel, they get aligned due to an effect called isotachophoresis. Briefly, when negatively charged glycine molecules from the Tris-Gly buffer enter the stacking gel, they experience a pH drop to 6.8 and thus form zwitterions that move slowly while chloride ions from the stacking gel's Tris-HCl buffer form the leading front. The opposing electric fields created by the differential movement of the ions cause negatively charged proteins to stack in a sharp band.

As the pH rises on entry into the dissolving gel, glycine adopts mainly the anionic form and overtakes the proteins, which then separate by size, more so the narrower the pore structure of the gel.

IV.5.5 Western blot transfer and development

Proteins were transferred from polyacrylamide gels to nitrocellulose membrane using wet electroblotting. To do this, a foam pad was first placed in a gel holder cassette. Next, three layers of Whatman® paper pre-wetted in wet blot transfer buffer (consisting of 25 mM Tris [pH 8.3], 150 mM glycine, 20% (v/v) ethanol in deionized H2O) were placed on top of the foam pad, followed by the gel. Then, a piece of nitrocellulose membrane cut to the size of the gel was placed on top, followed by three more layers of pre-wetted Whatman® paper and a final foam pad. The cassette was then inserted into the electrode unit of a transfer chamber, with the gel facing the cathode and the membrane facing the anode. The chamber was filled with wet blot transfer buffer, and transfer was performed in a cold-room for either 2 h at a constant 400 mA or overnight at a constant 100 mA.

After the transfer, the nitrocellulose membrane was washed quickly in PBS containing 0.2% Tween20. The membrane was then blocked for 1 h in PBS-T containing 10% milk powder. If required, the membrane was cut into pieces and incubated with primary antibodies in PBS-T containing 1% milk powder, either overnight at 4°C or for at least 2 h at room temperature. The membrane was then washed again with PBS-T, before incubation with secondary HRP-antibodies for at least 1 h. The dilutions of primary and secondary antibodies used are stated in Chapter III.5 of the work. Subsequently, the membrane was washed five times consecutively with PBS-T over a period of 30 minutes. Each membrane fragment was then incubated with activated Western Lightning Plus ECL substrate (PerkinElmer, Waltham, MA, USA) for 1 minute before being analyzed on a chemoluminescence imager (ECL ChemoCam Imager, Intas Science Imaging Instruments GmbH, Göttingen, Germany). The quantification of western blot bands was performed using ImageG (Fiji).

IV.5.6 Pulse-chase analysis of protein cleavage kinetics

Pulse-chase labelling with ^{35}S is a technique used to follow the synthesis, processing, and degradation of proteins in cells. The principle of the technique is that cells are briefly exposed to radioactive amino acids, such as ^{35}S-methionine or ^{35}S-cysteine, which are incorporated into the entirety of newly synthesized proteins during a 'pulse' phase. This is followed by a "chase"

phase in which the cells are cultured in a medium without the radioactive amino acids. Collected samples are subjected to immunoprecipitation to purify proteins of interest.

At the start of the experiment, Huh7/Lunet-T7 cells were seeded into the cavities of a 6-well plate ($2x10^5$ cells/well). 24 h post-seeding, cells were transfected with pIRO-D plasmids expressing either the WT non-structural module of the DENV-2 polyprotein or a version thereof harbouring a replication-competent HA-tag in NS4B. 17 h later, the transfection mixture was withdrawn and the cells were cultured for 1 h in starvation medium (DMEM without FCS, cysteine and methionine, but supplemented with 2 mM L-glutamine, 100 U/mL penicillin and 100 µg/mL streptomycin). Following this, the cells were pulse-labelled for 20 minutes using the same starvation medium but supplemented with ^{35}S labelling mix (100 µCi/well). Subsequently, the cells were washed once with $DMEM_{Complete}$ and kept in this medium up to the time of harvest. In case of JNJ-A07 treatment, the compound was present at a concentration of 35 nM throughout the periods of starvation, labelling and incubation. Thereafter, the regular protocol for immunoprecipitation experiments was followed as described in Chapter IV.5.3, with the exceptions that no adjustment of the protein concentration was made, and no control sample of total lysates was taken. Upon immunoprecipitation, 20 µl of each sample was loaded on an SDS-polyacrylamide gel, which after running was fixed in aqueous solution containing 5% methanol and 10% acetic acid. These were then vacuum-dried on filter paper using a combination of a cold trap (KF-2-60, H. Saur, Reutlingen Germany) and a gel dryer (Dual Temperature Slab Gel Dryer SE-1125B; Bio-Rad, Hercules, CA, USA) that was set to a heating temperature of 80°C. On the dried gels, the protein standard was redrawn with radioactive ink (10 µCi/ml). Gels were mounted in a cassette together with a BioMax TranScreen LE intensifying screen (Kodak, Rochester, NY, USA). Using exposure times ranging from 3 to 20 days, the screens were analysed by phosphoimaging and digital images were acquired with a Bio-Rad Personal Molecular Imager FX system. The NS4B-specific bands were quantified using ImageJ and adjusted to the number of cysteine and methionine residues contained in each protein (21 for NS4A-2K-NS4B, 14 for 2K-NS4B, and 13 for NS4B). For each time point, the percentage of NS4A-2K-NS4B precursor in the total amount of NS4B-specific species was calculated and its half-life time was determined by fitting "one phase exponential decay" curves to the data sets via the GraphPad Prism 8.43 software package. Working with ^{35}S-labelled amino acids requires precautions to protect against radiation exposure. One such precaution is working behind a plexiglass shield to reduce the risk of exposure to radioactive particles. In addition, cells were incubated in a container equipped with

a charcoal filter to capture volatile sulphur-containing substances that may be released when the radioactive amino acids are decomposed.

IV.6 Ultrastructural analysis of replication organelles

IV.6.1 Sample preparation for electron microscopy

The workflow employed in this study for assessing the formation of pIRO-D induced vesicle packets closely followed the protocol reported by Goellner et al.[392]. To this end, Huh7/Lunet-T7 cells were seeded in a 24-well format for subsequent electron microscopy analysis (35,000 cells/well). Of note, cells were also seeded in this format for the concomitant determination of transfection efficiency and were seeded in 6-well format to investigate polyprotein cleavage ($2x10^5$ cells/well). The processing of these samples was carried out as described in Chapters IV.4.1 & IV.4.3 and Chapters IV.5.1, IV.5.4 & IV.5.5, respectively. Transfection was performed as detailed in Chapter IV.2.2. The time points of treatment with JNJ-A07, NITD-688, CHX or vehicle as well as the time of sample collection differed in the respective experimental setups, as illustrated by the schematic workflows in the respective figures.

The specimens prepared for TEM analysis were washed shortly with PBS and then exposed to fixative solution (50 mM cacodylic acid sodium trihydrate, 50 mM KCl, 2.6 mM $MgCl_2$, 2.6 mM $CaCl_2$, 1% paraformaldehyde [w/v], 2.5% glutaraldehyde [v/v]; 2% sucrose [w/v], 30 min at RT, then at 4°C). Subsequently, the specimens were contrasted on ice in two consecutive steps, first with 2% osmium tetroxide in 50 mM cacodylate buffer for a minimum of 40 min followed by an incubation with 0.5% aqueous uranyl acetate for up to 16 h. After removal of excess uranyl acetate with water, dehydration was accomplished by serial exchange of the supernatant with ethanol solutions of increasing concentrations (up to pure ethanol). The cells were then embedded in epoxy resin which was allowed to polymerize at 60°C for at least 48 h. From the hardened specimens, thin 70 nm sections were cut, transferred to a formvar-coated TEM grid and post-contrasted with first 3% aqueous uranyl acetate and then saturated aqueous lead citrate for 5 min each.

IV.6.2 Transmission electron microscopy

Air-dried grids were analyzed on a JEOL JEM-1400 transmission electron microscope. In each of two experimental runs, 20 randomly selected cell profiles were scanned for vesicle package elements (VPEs), i.e. vesicles that are part of packages or are located in their vicinity. The number of VPEs quantified was normalised to the respective transfection efficiency of the sample. Vesicle diameters were determined using ImageJ.

IV.6.3 Ribopuromycylation Assay

Ribopuromycylation is a method for assessing the rate of protein synthesis by the labelling of nascent polypeptide chains with puromycin, that is subsequently detected via specific antibodies [393]. In this study, a protocol for the ribopuromycylation method was integrated into the workflow for the determination of vesicle packets formation, as described in Chapters IV.6.1 and IV.6.2. Briefly, cycloheximide (CHX, 200 µg/ml) was added to Huh7/Lunet-T7 cells 15.5 h after transfection to block protein synthesis and thereby prevent the formation of new viral proteins. Another 30 min later, 35 nM JNJ-A07 (or vehicle control) was added. While samples for downstream microscopic analysis (IF, TEM) were processed as normal, samples prepared for ribopuromycylation underwent an additional medium exchange with puromycin-containing $DMEM_{Complete}$ (10 µg/ml) 4 h after JNJ-A07/vehicle treatment. Following incubation at 37°C for 5 minutes, samples were collected and subjected to SDS-PAGE and western blot analysis. While part of the western blot membrane was stained with an NS4B-specific antibody to follow polyprotein processing, the other part was stained with an antibody directed against puromycin.

IV.7 Statistical analysis and data representation

Statistical analysis constituted a major component of the data evaluation performed in this work.

In most cases, statistical hypothesis tests were employed with a significance level set at $p<0.05$. The selection of the test appropriate to an experiment depended on several assumptions about the distribution of the data. In general, a continuous distribution could be assumed for all data sets to be statistically interpreted in this work, so that tests on categorical or discrete variables were not used. As can be seen from Figure 11a, fulfilment of parametric criteria is a major factor in choosing a suitable test. Among those criteria is the normality of the data (which can be checked graphically with a histogram or a Q-Q plot, or with normality tests such as the Kolmogorov-Smirnov test) and the similar variance in different groups being compared (called homoscedasticity, which can be verified with a Brown-Forsythe test). For small sample sizes, the informative power of said tests is low, so that in this case either the fulfilment of the criteria was assumed on the basis of logical considerations or non-parametric tests were used. For the further selection of the test, the number of comparisons within a data set played a role as well as the question whether data were paired or unpaired. In a paired test, each value from one group is directly linked to a corresponding value from the other groups, whereas an unpaired test assumes that the observations in the different groups are independent. The Kruskal-Wallis

test and analysis of variance (ANOVA) were followed by post-hoc tests for multiple testing, with three different options available for the latter, as shown in Figure 11b-d. Of these, Tukey's test is the most general and conservative because it draws all possible pairwise comparisons in a data set. Dunnett's test is specifically designed for situations where a control group is compared to multiple treatment groups and Šidák's test is suitable for a custom subset of pairwise comparisons.
In principle, the more assumptions that can be considered to be met for a test, the greater its statistical power, i.e. its ability to detect even small differences between various groups. With fewer assumptions, a more robust/conservative test must be used, which, however, entails a loss of statistical power.

In a few cases, a confidence interval analysis was performed instead of a statistical hypothesis test. Both are methods of statistical inference based on a restricted sample size. However, while a hypothesis test makes a binary decision about whether a hypothesis is confirmed or rejected, a confidence interval analysis provides an estimate of the true value and a statement about the uncertainty of that estimate[394].

For the generation of graphs as well as for statistical analysis, either an R script or the GraphPad Prism 8.43 software package were used in this work. Specific details of the respective statistical analysis are further described in the legends of the respective figures.

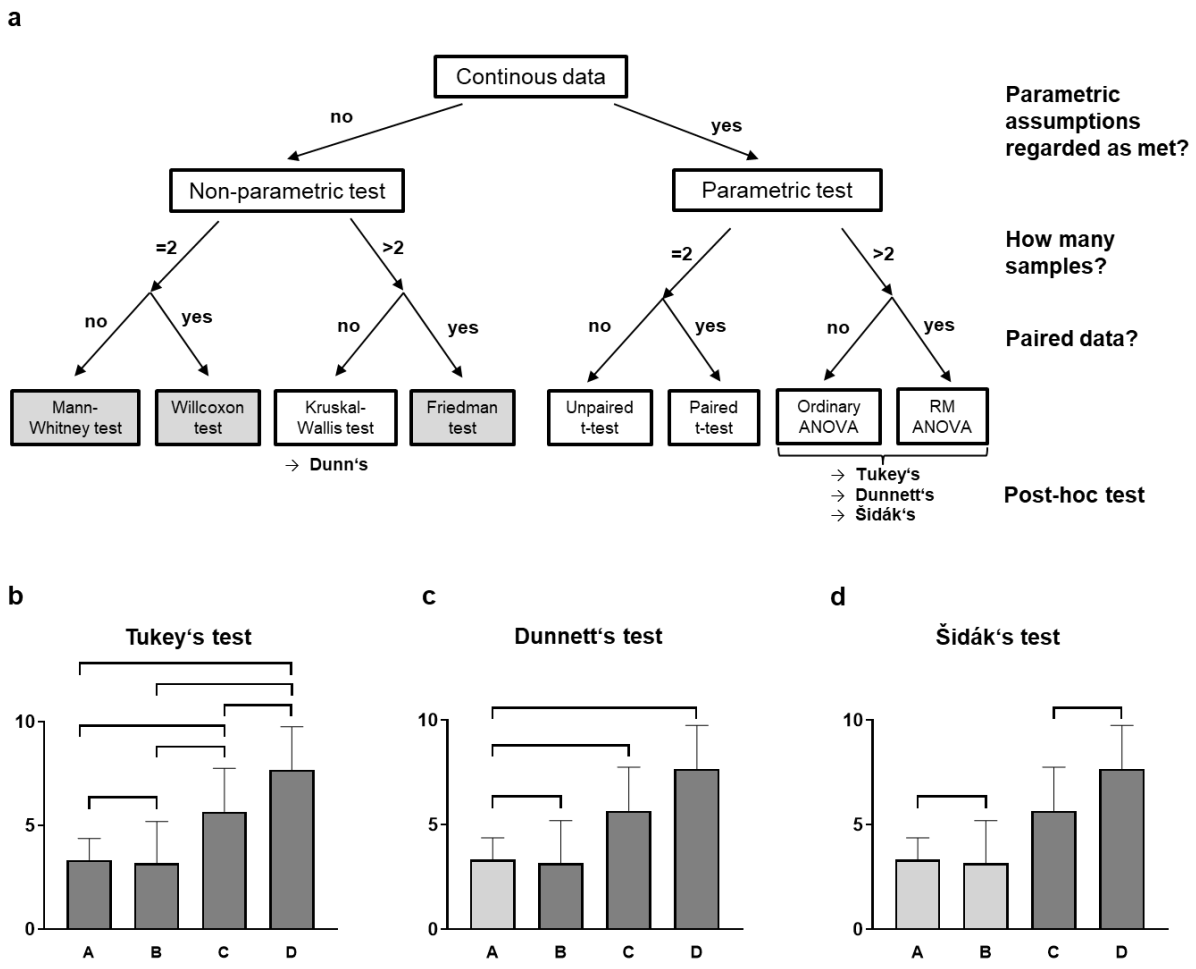

Figure 11. Criteria for the selection of a statistical hypothesis test.
a, Flowchart for selecting statistical hypothesis tests in this dissertation. Shown are statistical tests that stem from the assumption of continuous data structure, which was fulfilled for all experiments conducted. Tests in grey boxes were not used in this work and are only given for completeness. **b-d**, Scenarios for the application of different ANOVA post-hoc tests based on example graphs. Tukey's test (b) is used when performing all pairwise comparisons, Dunnett's test (c) is specialized for comparing samples with a common reference and Šidák's test (d) applies when not all pairwise comparisons are meaningful but only a custom subset of them.

V. Results

As described in previous chapters of this dissertation, the aim of my thesis was to decipher the mechanism-of-action of JNJ-A07 and JNJ-1802. Some of the results built on fundamental data generated with JNJ-A07 that were available at the outset of my research. These data will be briefly covered in the following Chapter V.1.1. All other results presented in subsequent chapters were produced by me or under my direction, unless clearly stated otherwise. Most of the research findings on JNJ-A07 were included in Kaptein et al.[376] or another manuscript (Kiemel et al.) that has been submitted for publication, while data related to JNJ-1802 were published in Goethals et al.[378].

V.1 The pan-serotype dengue virus inhibitor JNJ-A07 targets the interaction of the NS4A-2K-NS4B cleavage intermediate with NS3

V.1.1 Basic results provided by project partners

Starting from a set of 2000 derivatives of a DENV antiviral hit compound, JNJ-A07 was selected for further investigation based on favorable properties. Structurally, it is the (+)-enantiomer of an indoline derivative and significantly more active than its (-)-enantiomer counterpart (Figure 12a). From the latter, JNJ-A07 was isolated via chiral supercritical fluid chromatography[395].

In Vero cells (a cell line derived from African green monkey kidney epithelial cells), the 50% effective concentration (EC_{50}) was in the subnanomolar range with 0.1 nM against DENV strain 2/16681 and 0.2 nM against DENV-2/RL strain. Subnanomolar potency was likewise found in the human hepatoma cell line Huh7 using DENV-2/16681, as well as in human monocytic leukemia THP-1/DC-SIGN cells. The latter result is very interesting because monocytes, together with immature dendritic cells, in which also a strong JNJ-A07 activity was observed (EC_{50} = 2.3 nM), are the putative first target cells for DENV infection in humans. Moreover, it is noteworthy that JNJ-A07, with an EC_{50} of 3.2 nM, has comparable activity in DENV-2/RL-infected *Aedes albopictus* cells of line C6/36, ruling out a human-specific target. Detailed results are listed in Supplementary Table 4. High selectivity indices were observed for all cell lines tested, as cytopathic effects of the molecule on host cells were observed only at concentrations 714- to 130,000-fold higher than the EC_{50} (Supplementary Table 4). Pan-serotype and even pan-serotype activity (at nM to low pM potencies) was detected against a panel of 21 clinical DENV isolates covering the known landscape of genotypes within the four

serotypes (Figure 12b; Supplementary Table 5). JNJ-A07 did not show significant antiviral activity against related flaviviruses (Yellow Fever virus, West Nile virus, Japanese Encephalitis virus, and Zika virus) and also did not show activity/selectivity against a selection of other RNA viruses (e.g., chikungunya virus, hepatitis C virus) and DNA viruses (hepatitis B virus, adenovirus type 5, vaccinia virus) as specified in Supplementary Table 6. Therefore, the molecule is considered highly specific for DENV.

Detailed studies on the effect of the timing of drug treatment on antiviral activity showed that addition of JNJ-A07 to infected cultures could be delayed without loss of antiviral activity as long as intracellular viral RNA synthesis had not yet started to a detectable level, which is approximately 10 h post-infection. When added later, a gradual loss of the inhibitor's antiviral activity was observed (Figure 12c-d). Thus, JNJ-A07 most likely interacts with the viral RNA replication machinery at a very early stage. A similar time dependency was observed with the nucleoside analogue 7-DMA, a nucleosidic inhibitor with broad spectrum activity.

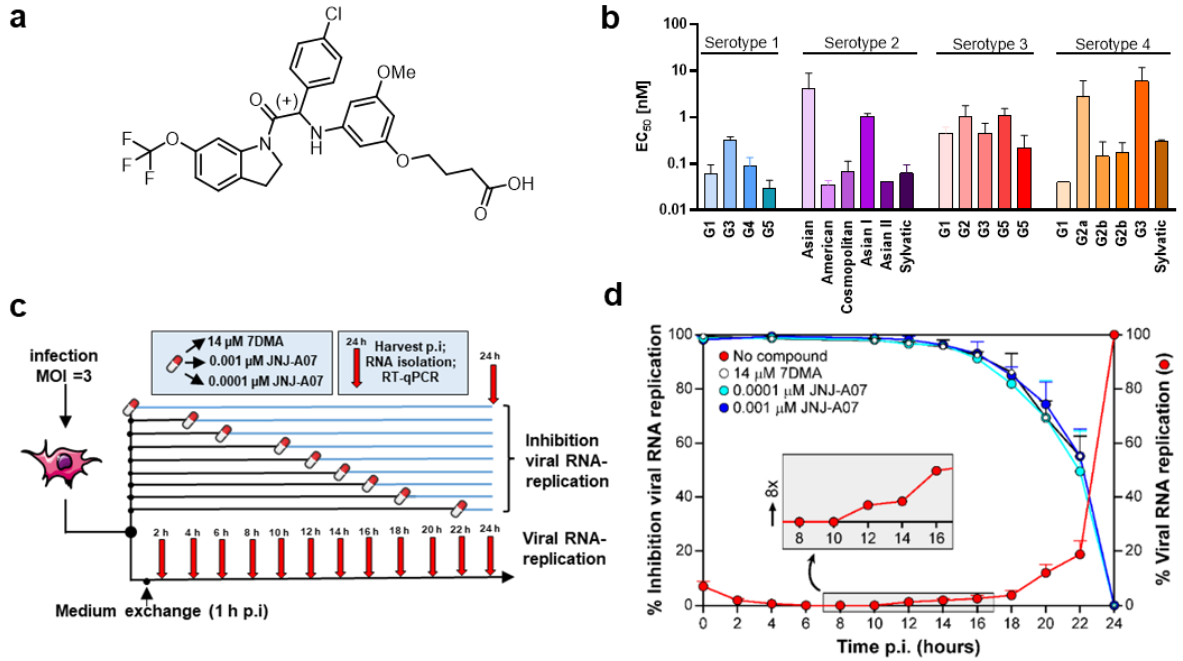

Figure 12. JNJ-A07 exhibits high antiviral potency against all DENV serotypes.
a, Molecular structure of JNJ-A07. **b**, Comparison of the antiviral potency (EC_{50}) of JNJ-A07 with respect to different DENV genotypes. Antiviral assays were carried out using Vero E6 cells and the data represent the mean and standard deviation of at least two independent experiments. The given DENV serotype panel was selected as previously reported[396]. **c**, Experimental setup of the time-of-drug-addition (TOA) assay. **d**, TOA and *in vitro* kinetics of DENV-2 replication. The red curve represents *in vitro* DENV RNA replication in the absence of drug. The onset of intracellular viral replication occurred at 10 h post-infection (p.i.), as depicted in the inset. The time-point dependent inhibitory effect of JNJ-A07 on DENV replication is illustrated by the blue curves (0.0001 µM, light blue; 0.001 µM, dark blue). The broad-spectrum RNA virus inhibitor 7-deaza- 2'-C-methyladenosine (7DMA) was included as a positive control (black curve with white circles). Data (mean ± s.d.) are from at least three independent experiments.

To obtain initial indications for the molecular target of JNJ-A07, resistant variants were selected by passaging DENV-2 in the presence of gradually increasing concentrations of JNJ-A07. In this so-called *in vitro* resistance selection assay, viruses isolated from cell culture supernatant were transferred to freshly seeded cells once per week (Figure 13a). In a total of two independent experiments (denoted A and B sample), this proved to be exceptionally difficult, with completely resistant viruses only being obtained after a protracted experiment lasting more than 40 weeks (A sample: Figure 13b; B sample: Figure 13c). A decrease in sensitivity to JNJ-A07 (32-fold) was first observed during microscopic evaluation of virus-induced CPE at week 15 of the selection process. Over time, fold resistance continued to increase, leading to an almost complete loss of antiviral activity at the end point (week 43). Via genome sequencing, several mutations were identified at the endpoint that were not present in the parallel untreated cultures. All of these accumulated within NS4B (in sample A: L94F, T108I, and T216N; in sample B: F47Y, V91A, L94F, P104S, T108I, and T216P) (Figure 13e). Samples collected during the ongoing *in vitro* resistance selection assay were additionally used to investigate the dynamics of mutation occurrence using whole genome sequencing. In sample A, the first T108I and V91A mutations appeared (in less than 65% of the virus population) at passage 15 and disappeared at passage 20 and passage 25, respectively. After 25 passages, the L94F and T108I mutations were present in 100% of the population, indicating that the mutations coexisted on the same genomes. Finally, at passage 35, the T216N mutation was present in 100% of the population along with the L94F and T108I mutations, and these three mutations persisted until the end of the experiment (passage 43). In sample B, mutations V91A and T108I occurred in less than 60% of the population at passage 15. While T108I disappeared again, V91A was present in 100% of the population at passage 20. T108I finally broke through at passage 25 and the L94F mutation at passage 30. These three mutations (V91A, L94F, and T108I) remained present in 100% of the population. F47Y, P104S, and T216P appeared in later passages (from passage 35) and remained present in 52% (F47Y), 51% (P104S), and 46% (T216P) of the population until the end of the experiment (passage 43).

To determine the inhibitor resistance of the identified mutations, they were inserted separately into a subgenomic DENV-2/16681 Renilla luciferase reporter replicon and the replication rate was thus assessed in a dose-dependent manner to subsequently derive EC_{50} values (Figure 13d). Of note, the L94F mutation that conferred the highest level of resistance (950-fold) is shared by the two virus strains obtained at the end of the independently performed *in vitro* resistance selection assays, and presumably accounts for a significant portion of the more than 50,000-fold reduction in susceptibility of the endpoint virus strains toward JNJ-A07. Most of the

identified resistance mutations did not occur or occurred only at very low frequencies (i.e., ≤0.5% for all 4 serotypes) in clinical DENV isolates (Figure 14) but none of these mutations were found together. Threonine-137 (which appeared and disappeared during the selection experiments in sample A) was present in 3.5% of clinical DENV-2 isolates and in 100% of clinical isolates of the other serotypes. It is considered as a polymorphism as it did not alter antiviral susceptibility to JNJ-A07. The DENV 1/Malaysia, DENV 2/Martinique, DENV 2/Thailand, DENV 3/H87, and DENV 3/Brazil isolates shared 108I or 108A, which may explain the slightly lower susceptibility of some of these viruses to JNJ-A07 compared with the other viruses of the same genotype.

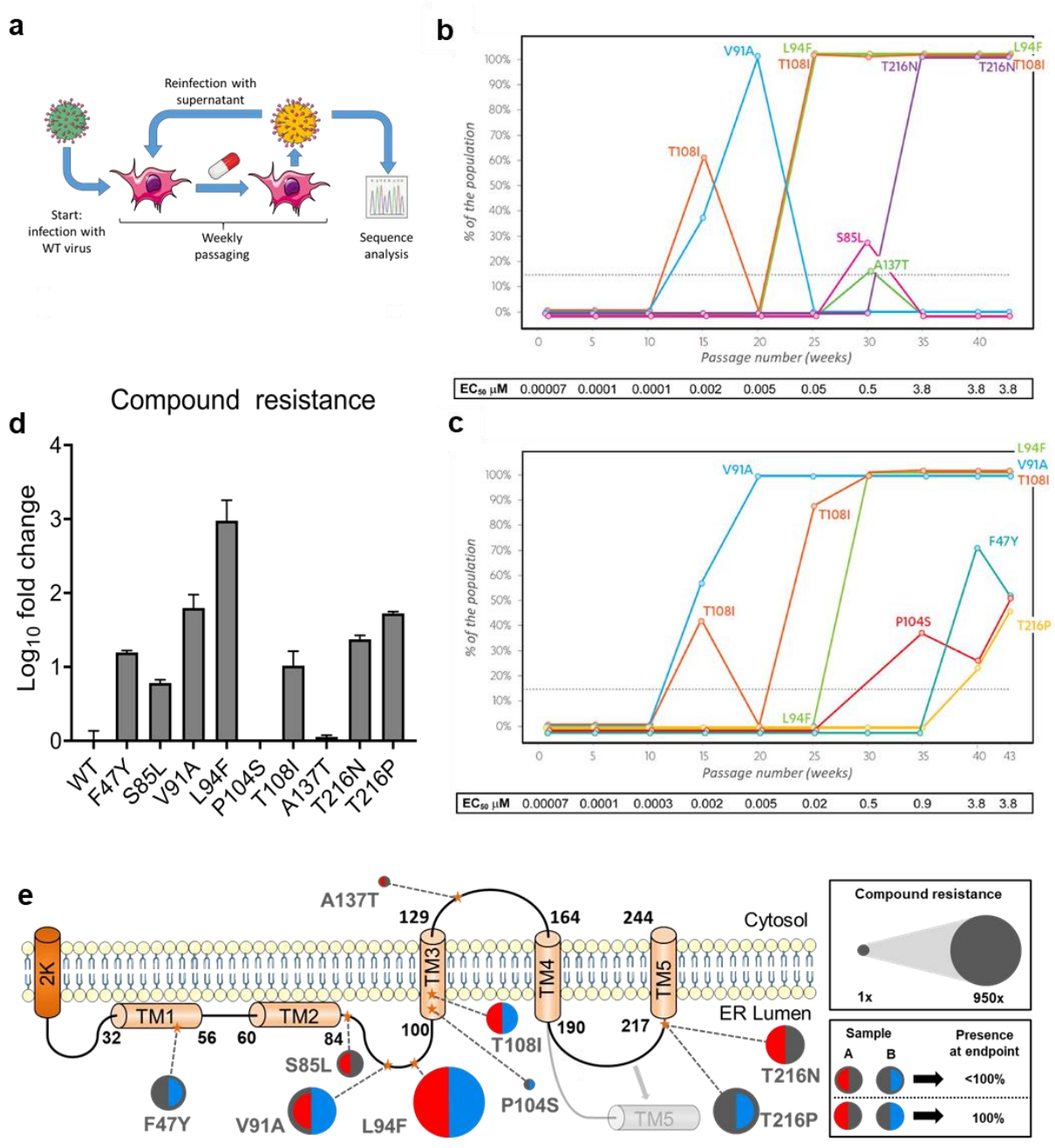

Figure 13. JNJ-A07-induced resistance mutations accumulate in DENV NS4B.
a, Experimental design of the *in vitro* resistance selection assay. DENV-2 was passaged weekly in the presence of gradually increasing concentrations of JNJ-A07. The dynamics of mutation stimulation was studied using whole genome sequencing. **b-c**, The results of the two independent runs of the *in vitro* resistance selection assay, designated sample set A and sample set B, are shown in (b) and (c), respectively. Each coloured line shows the dynamics of the appearance of a particular mutation during passaging of the virus in the presence of JNJ-A07, excluding putative cell culture adaptations observed in parallel controls of infected cells without drug pressure. Whole genome sequencing was performed on DENV variants harvested at every fifth passage (P) and at the end of the experiment (i.e. passage 43). One passage corresponds to one week. The dotted line represents the threshold (15%) for detection of variants compared to WT in the virus population. The increasing EC_{50} values determined by microscopic evaluation of virus-induced CPE are shown below the graphs. **d**, Degree of JNJ-A07 resistance of individual NS4B resistance mutations as determined by subgenomic R2A-replicon assays. **e**, Schematic representation of the membrane topology of DENV NS4B (after Miller et al., 2006). The positions of the resistance mutations selected by JNJ-A07 are highlighted. The amino acid residues assumed to flank the transmembrane segments are from Zmurko et al. (2015)[181].

V.1.2 Analysis of the resistance mechanism of JNJ-A07-induced NS4B mutants

As described in the previous chapter, the mutations identified via *in vitro* resistance selection varied greatly with respect to JNJ-A07 compound resistance when incorporated separately into subgenomic DENV-2 R2A reporter replicons (schematic structure shown in Figure 14a). In principle, this is not an unexpected outcome and can provide valuable insights into the mechanism-of-action of a compound. Behind this is the concept of driver and passenger mutations[397]. Driver mutations confer active resistance to a compound, often by causing reduced binding of a drug to its target, but frequently come at a fitness cost to the virus, as expressed, for example, in reduced replication rates in the absence of the drug when compared directly to WT virus. Passenger mutations, on the other hand, do not directly confer antiviral drug resistance but can compensate for the fitness costs of driver mutations. In some cases, passenger mutations may indirectly contribute to drug resistance by interacting with driver mutations thereby enhancing their effects. As the name of the concept implies, driver mutations usually occur first and then entail passenger mutations. Indeed, JNJ-A07 resistance mutations that individually conferred the highest level of compound resistance (V91A, L94F, and T108I) tended to occur earlier than those that conferred little or no resistance like S85L or P104S (Figure 13). To gain a better understanding of the matter, DENV-2 sg-R2A-reporter replicons harbouring individual resistance mutations were employed once again, this time to determine replication fitness. A replicon with an inactivating mutation in the NS5 RdRp domain (GND) was used as a negative control as it is replication deficient. As can be seen in Figure 14b, several mutations did not affect replication (V91A, T108I, A137T, T216P) while others induced a profound attenuation of replication (F47Y, S85L, P104S, T216N), yet without showing the expected anticorrelation with the level of resistance. On the contrary, L94F, the mutation with the highest resistance (950-fold), was surprisingly the only one that significantly increased replication fitness compared to WT (Figure 14c).

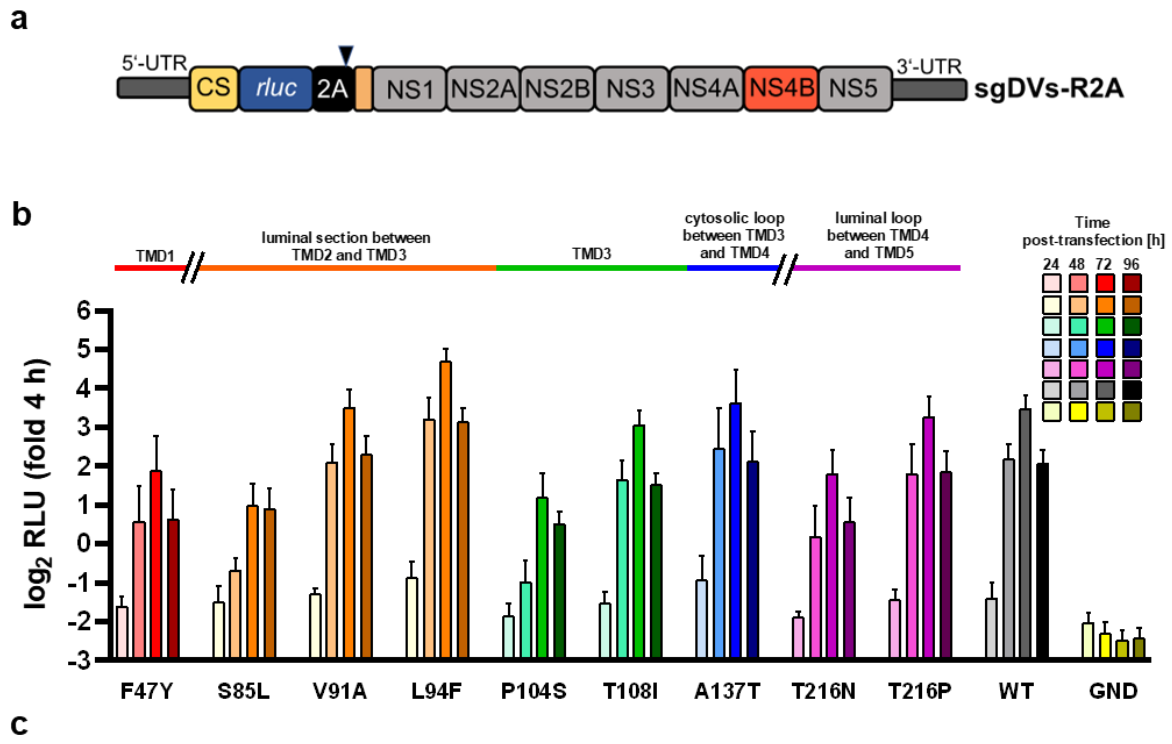

c

NS4B mutation	Replication fitness		Compound resistance		Frequency mutant in clinical isolates†
	Amplification ratio (72h vs. 4h)	Fold change	EC_{50} (μM)	Fold change*	
None (WT)	11.0 ± 3.10	/	0.003 ± 0.002	/	
F47Y	3.70 ± 3.10	0.3	0.035 ± 0.001	16	0%
S85L	1.99 ± 0.90	0.2	0.03 ± 0.003	6	0%
V91A	11.2 ± 4.42	1.0	0.10 ± 0.07	63	1.3% (DENV-2), 0.4% (DENV-3)
L94F	25.8 ± 6.91	2.3	1.1 ± 0.1	950	0%
P104S	2.30 ± 1.26	0.2	0.001 ± 0.0003	1	0%
T108I	8.26 ± 2.48	0.8	0.01 ± 0.02	10	0.1% (DENV-1), 0.9% (DENV-2), 2.6% (DENV-4)
A137T	12.2 ± 10.26	1.1	0.005 ± 0.0001	1	3.5% (DENV-2), 100% in other serotypes
T216N	3.48 ± 1.83	0.3	0.1 ± 0.009	24	0%
T216P	9.68 ± 4.22	0.9	0.1 ± 0.0036	53	0%

Figure 14. Replication fitness of mutants conferring resistance to JNJ-A07.
a, Simplified schematic of the subgenomic DENV reporter replicon (sgDVs-R2A). The Renilla luciferase gene (rluc) is preceded by *cis*-acting RNA elements located in the capsid coding region (CS). Following polyprotein synthesis, a 2A self-cleaving peptide sequence at the C-terminus of rluc provides for correct processing at a cleavage site motif denoted by the black arrowhead. The last transmembrane domain of E (TM E) contains a signal peptide required for proper membrane insertion of the polyprotein. **b**, Effects of NS4B resistance mutations on replication fitness. Resistance mutations identified by two independent *in vitro* resistance selection assays were inserted into the DENV reporter construct. A replication-deficient replicon harboring an inactivating mutation in the NS5 RNA-dependent RNA polymerase domain was included as a negative control. *In vitro* transcribed RNA was transfected into Huh7 cells. At the time points shown in the top right, cells were lysed and Renilla luciferase activity was determined as a marker of replication. Relative light units (RLU) were normalized to the 4 h value to reflect transfection efficiency. Mean and SD are shown from at least three independent experiments, each performed with independent RNA preparations. **c**, Table comparing replication fitness and drug resistance of wild-type and mutant virus. *Fold change in EC_{50} was calculated as the average ratio between the EC_{50} value for the mutant strain compared to EC_{50} value for the WT strain tested within the same experiment. †The natural occurrence of the mutations was retrieved from the Virus Pathogen Resource database (www.viprbrc.org; accessed in May 2020). Prevalence values ≤0.1% are not shown. The effect of resistance mutations in NS4B on replication fitness was determined by a Renilla luciferase subgenomic DENV reporter replicon (sgDVs-R2A). The amplification ratio was determined by normalizing the luciferase signal of the 72 h time point, which marks the peak in signal intensity in all samples, over the 4 h time point, which reflects transfection efficiency. Fold change in the amplification ratio was calculated as the factor between corresponding mutant values over WT. The

effect of resistance mutations in NS4B on the susceptibility of the compound against replication (compound resistance) was determined by a Renilla luciferase subgenomic DENV reporter replicon (sgDVs-R2A). Data represent mean values ± SD from at least three independent experiments. EC_{50}, 50% effective concentration; WT, wild-type replicon virus DENV 2/16681.

To gain a deeper understanding of how JNJ-A07 affects viral replication and by what mechanism identified mutants mediate resistance, I investigated the possible effects of the compound on the NS3 – NS4B interaction. The rationale behind this was that previous work had already revealed the NS4B interaction with the NS2B/NS3 protease/helicase complex plays a critical role in viral replication[117,166]. For example, a Q134A substitution in NS4B that abrogates the NS3 – NS4B interaction is detrimental to DENV replication. To be able to detect effects of JNJ-A07 on the NS3 – NS4B interaction, it was important to uncouple the production of said proteins from viral replication. For this purpose, an expression system was used in which NS4B was expressed as part of the NS4A-2K-NS4B precursor together with the NS2B/NS3 protease-helicase complex (Figure 15a). To facilitate NS4B-specific pull-down, a C-terminal hemagglutinin affinity tag (HA^{Ct}) was appended to NS4B. Cells were transfected with modified NS4A-2K-NS4B-HA constructs, harboring resistance mutations identified in the A sample of the *in vitro* resistance selection assay or the natural polymorphism A137T. In addition, WT NS4B and the Q134A mutant were used as positive and negative controls, respectively, whereas NS4B without HA tag served as a technical control. Cells were treated with either 35 nM JNJ-A07 (~45× EC_{50} in Huh7 cells) or an appropriate amount of solvent control (DMSO) and the experiment was conducted according to the methods description in Chapters IV.5.1 to IV.5.5 (also schematically illustrated in Figure 15b). Western blot images exhibited a striking loss of NS3 co-precipitation upon treatment of the WT transfected sample with 35 nM JNJ-A07 and a more differentiated picture for the mutants (Figure 15c). Ratios of NS4B-HA-containing species and co-precipitated NS3 were measured by quantitative western blot (Figure 15d). For WT NS4B, JNJ-A07 decreased the amount of co-precipitated NS3 by 95% (95% CI: -130% to -60%), corroborating that the compound indeed prevents NS3 – NS4B interaction. Consistently, an almost complete drug-induced loss of the NS3 – NS4B interaction was observed in the S85L and A137T mutants, which confer rather low and no drug resistance, respectively. In contrast, the NS3 – NS4B interaction was barely affected by JNJ-A07 in mutants V91A, L94F, T108I, and T216N, which confer higher drug resistance.

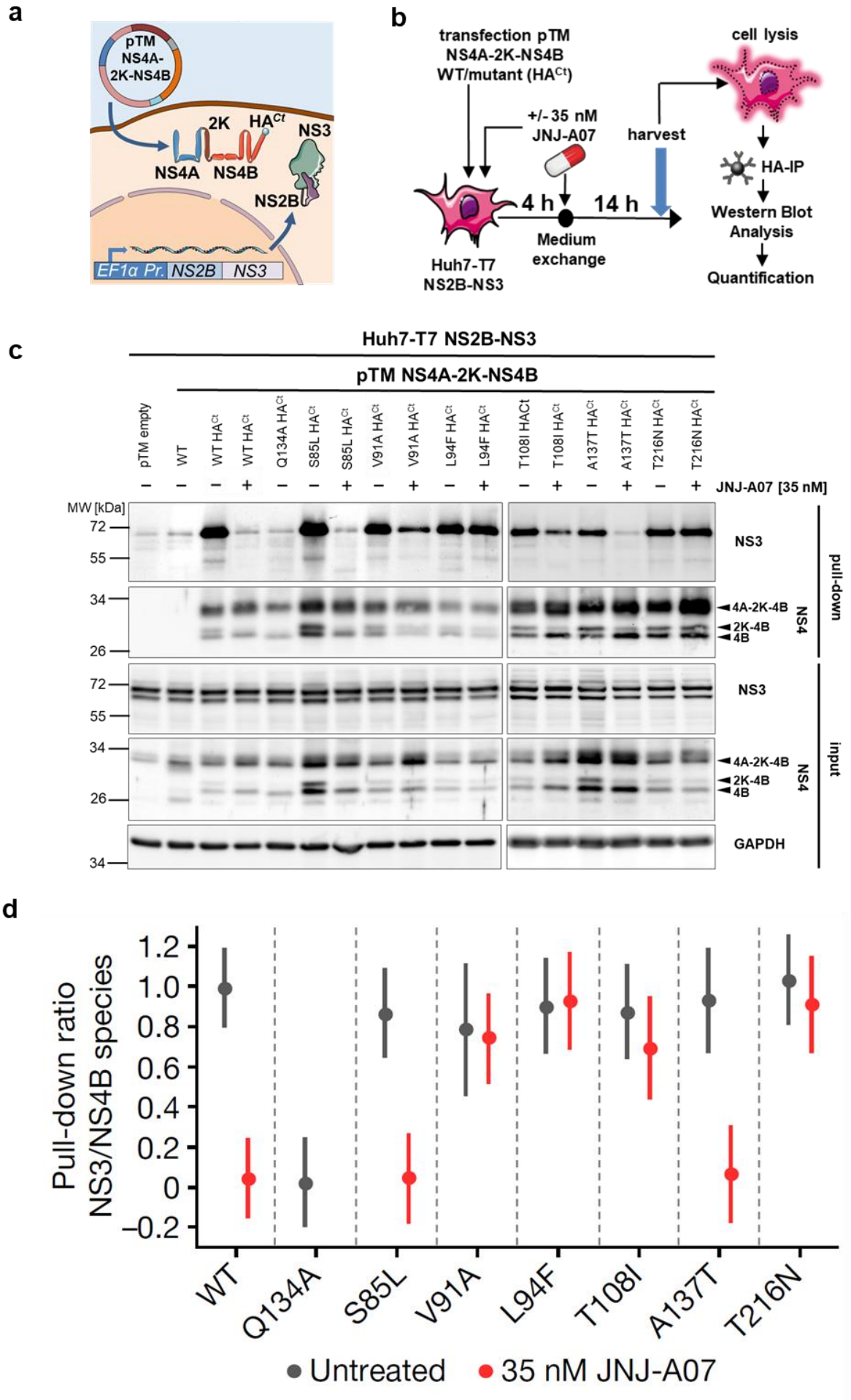
a
pTM NS4A-2K-NS4B
2K
HACt
NS3
NS4A
NS4B
NS2B
EF1α Pr.
NS2B
NS3
b
transfection pTM NS4A-2K-NS4B WT/mutant (HACt)
+/- 35 nM JNJ-A07
harvest
cell lysis
HA-IP
Western Blot Analysis
Quantification
4 h
14 h
Medium exchange
Huh7-T7 NS2B-NS3
c
Huh7-T7 NS2B-NS3
pTM NS4A-2K-NS4B
pTM empty
WT
WT HACt
WT HACt
Q134A HACt
S85L HACt
S85L HACt
V91A HACt
V91A HACt
L94F HACt
L94F HACt
T108I HACt
T108I HACt
A137T HACt
A137T HACt
T216N HACt
T216N HACt
JNJ-A07 [35 nM]
MW [kDa]
72
55
34
26
NS3
4A-2K-4B
2K-4B
4B
NS4
pull-down
input
GAPDH
d
Pull-down ratio NS3/NS4B species
1.2
1.0
0.8
0.6
0.4
0.2
0
–0.2
WT
Q134A
S85L
V91A
L94F
T108I
A137T
T216N
Untreated
35 nM JNJ-A07

Figure 15. Mutations conferring solid compound resistance keep the NS3 – NS4B interaction in presence of JNJ-A07.
a, Cartoon-like depiction of the trans-cleavage system. Huh7 cells stably express on the one hand the T7 polymerase of the bacteriophage T7 (not shown) and on the other hand the viral protease complex NS2B-NS3 under control of the EF1α promoter. Via pTM plasmids that carry a T7 promoter, further proteins, such as NS4A-2K-NS4B here, can be transiently expressed in the cytosol. **b**, Experimental setup to study the effects of JNJ-A07 on the interaction between NS2B/NS3 and WT or mutant NS4B. Huh7-T7 NS2B-NS3 cells, were transfected with pTM plasmids encoding NS4A-2K-NS4B(-HACt), where NS4B corresponds to wild-type (WT) or contains a JNJ-A07 resistance mutation. 4 h post-transfection, cells were treated with JNJ-A07 or DMSO, harvested 14 h later and the lysates were used for HA-specific pull-down. **c**, Captured protein complexes were analysed by western blot. A representative western blot is presented. **d**, For each sample, the ratio of NS3 to all NS4B species (NS4A-2K-NS4B, 2K-NS4B and NS4B) was calculated from at least four independent experiments and normalized to the average untreated WT ratio. Depicted are the estimated marginal means per mutation and treatment together with the corresponding 95% confidence intervals.

V.1.3 JNJ-A07 prevents the formation of complexes between NS4B-containing species and NS2B-NS3 in a dose-dependent manner

According to the workflow shown in Figure 16a, dose-response tests were performed, using WT as well as T108I and V91A as examples of moderate and strong JNJ-A07 resistance mutations (Figure 16b-c). Quantification of the ratio of co-precipitated NS3 to directly precipitated NS4B species showed, on the one hand, that for both WT and mutants, it is possible to block the NS3 – NS4B interaction, but on the other hand, that for the mutants, significantly more compound had to be used than for WT to achieve a comparable effect (Figure 16d). In addition, a dose-dependent decline in the ratio of the 2K-NS4B intermediate to the NS4A-2K-NS4B precursor was observed, with the degree of reduction in the IP samples inversely related to the degree of resistance (Figure 16e). To a lesser extent, this effect was also observed for mature NS4B (Figure 16f). In direct comparison with WT, V91A and T108I increased the EC_{50} of the NS3 – NS4B interaction by a factor of 41 and 9, respectively, consistent with their impact on resistance in viral assays (Figure 17a). Due to a non-specific band of the NS4B antibody at the height of the NS4A-2K-NS4B precursor in the input samples, a reliable quantification of NS4B species proportions could only be performed after pulldown (Figure 17b-d). However, the JNJ-A07-induced reduction in 2K-NS4B was still evident on the blots, indicating that JNJ-A07 affects the processing of the NS4A-2K-NS4B precursor in this assay system, presumably by slowing down the dynamics of NS2B/NS3-mediated cleavage (Figure 17e).

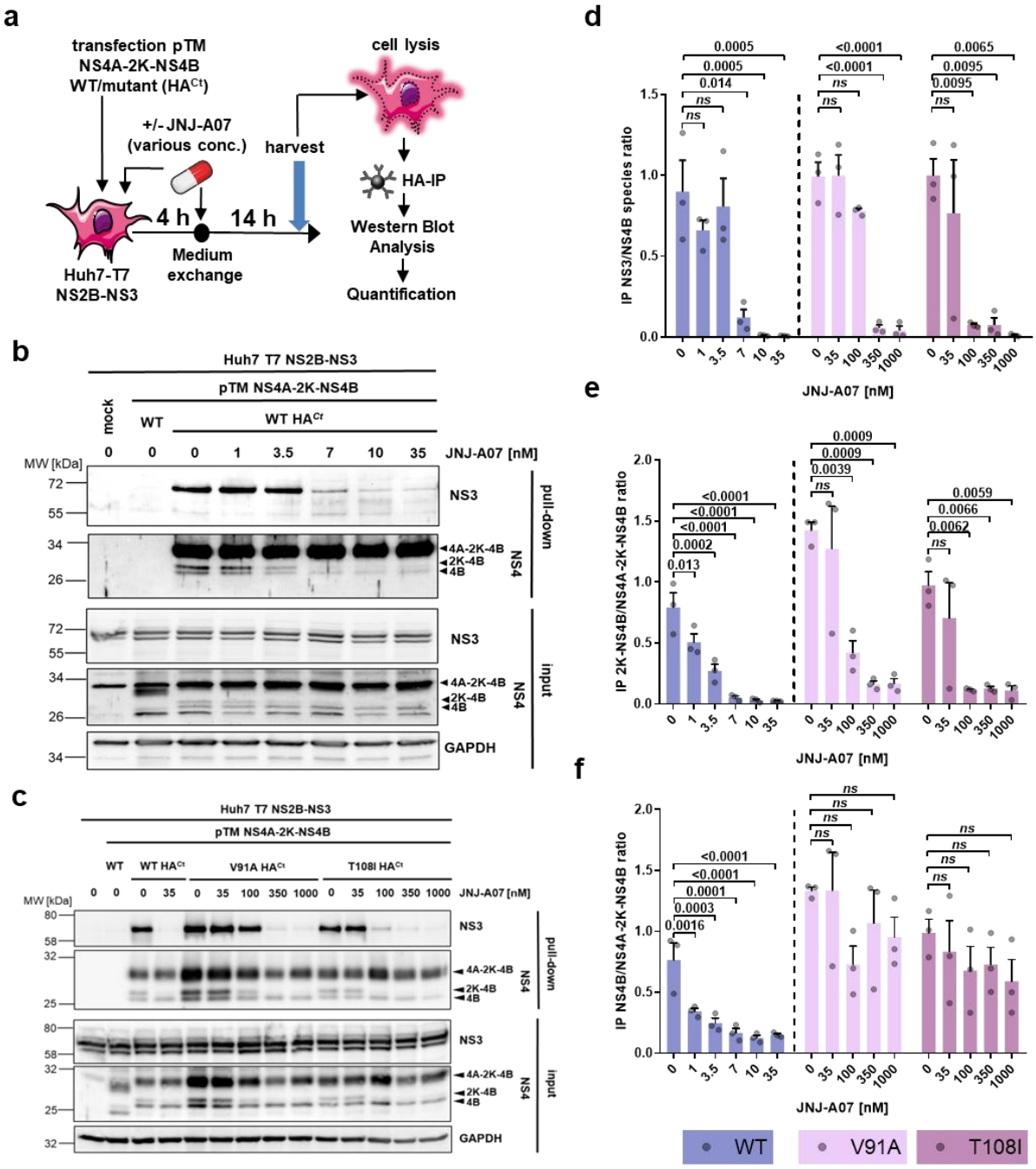

Figure 16. Impact of JNJ-A07 on the interaction between NS3 and various NS4B species.
a, Study design of dose-response experiments to investigate the effect of JNJ-A07 on the interaction between NS3 and either WT or mutant NS4B. **b-c**, Captured protein complexes were analyzed by western blot. A representative outcome for WT is presented in (b), whereas a typical result for mutants V91A and T108I is depicted in (c). Numbers on the left refer to molecular weights (kDa). GAPDH was used as a loading control for cell lysates (input). d-f, Signal intensity levels of NS3, NS4A-2K-NS4B, 2K-NS4B and NS4B obtained from three independent blots were normalized to WT NS4A-2K-NS4B-HA^{Ct} in vehicle-treated control cells. Indicated protein ratios (mean and SEM) were calculated for each sample. The term "NS4B species" refers to the combined signal intensities of NS4A-2K-NS4B, 2K-4B and NS4B. Repeated measures one-way ANOVA with subsequent Dunnett's multiple comparisons test was employed for statistical analysis and p-values are presented in the graphs; *ns*, not significant.

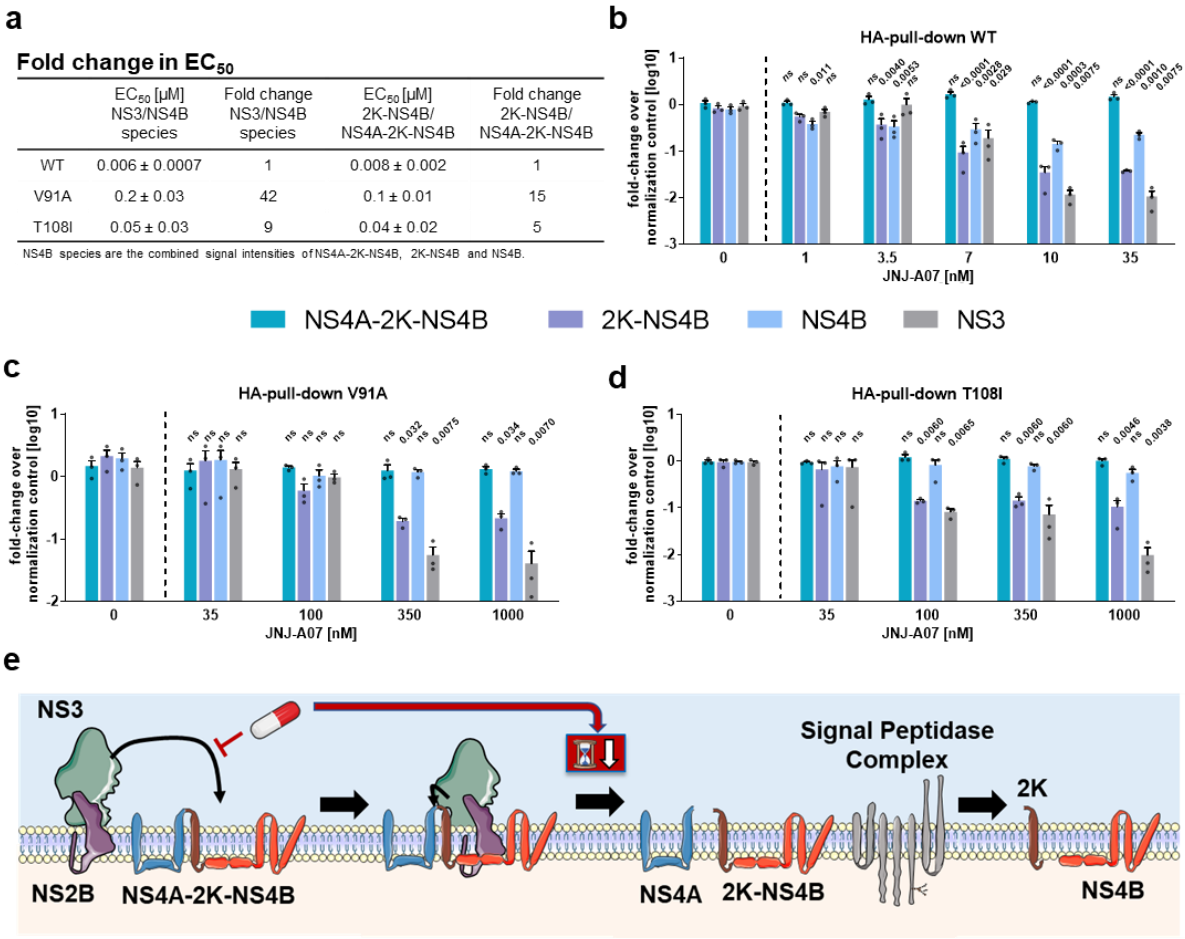

Figure 17. In the trans-cleavage system, JNJ-A07 significantly affects NS4A-2K-NS4B precursor processing.
a-c, The western blots of the experiment outlined in Figure 16a were analyzed for total protein intensities. To this end, respective protein species were quantified for both WT (a) and compound resistant NS4B mutants V91A (b) and T108I (a), normalized to a WT control. The statistical analysis was performed by comparing JNJ-A07-treated samples with the corresponding control to the left of the dashed line by means of ordinary one-way ANOVA followed by Dunnett's multiple comparison test. **d**, EC_{50} values (mean ± SEM) for protein ratios in Figure 16d-e obtained by fitting four-parameter dose-response curves to the results of every individual experiment. The fold change in EC_{50} is the quotient of the mean EC_{50} for WT and corresponding mutant constructs. **e**, Schematic model: In the trans-cleavage system, JNJ-A07 appears to slow down the processing dynamics of the NS4A-2K-NS4B precursor (indicated by the hourglass icon), which is first cleaved by the NS2B/NS3 protease complex at the NS4A-2K cleavage site. Subsequently, 2K-NS4B is processed by the host signal peptidase complex yielding mature NS4B and 2K.

V.1.4 JNJ-A07 blocks *de novo* formation of NS4B/NS3 complexes but does not disrupt existing ones

Since a steady decrease in antiviral activity was observed when the drug was administered after the onset of viral RNA replication (Figure 12d**)**, the kinetics of the JNJ-A07-induced loss of NS3 – NS4B interaction was investigated according to the schematic in Figure 18a. When the inhibitor was added 4 h after transfection, significantly reduced levels of NS3 – NS4B complexes were observed at both the 8 h and 24 h harvest time points (Figure 18b-c). The 1 h

harvest time point was not yet quantifiable due to insufficient protein levels. A different picture was observed with JNJ-A07 treatment 24 h after transfection. At the harvest time points 1 h and 8 h after addition of the compound, at which it can be assumed that the majority of NS3 – NS4B complexes were formed in the absence of JNJ-A07, no significant decrease in the NS3 co-precipitation rate could be detected. Only after 24 h of JNJ-A07 presence, a marked reduction was recorded again. In summary, these results suggest that JNJ-A07 exerts its antiviral effect by blocking *de novo* formation of the NS3 – NS4B complex but does not disrupt them when they are already formed (Figure 18d).

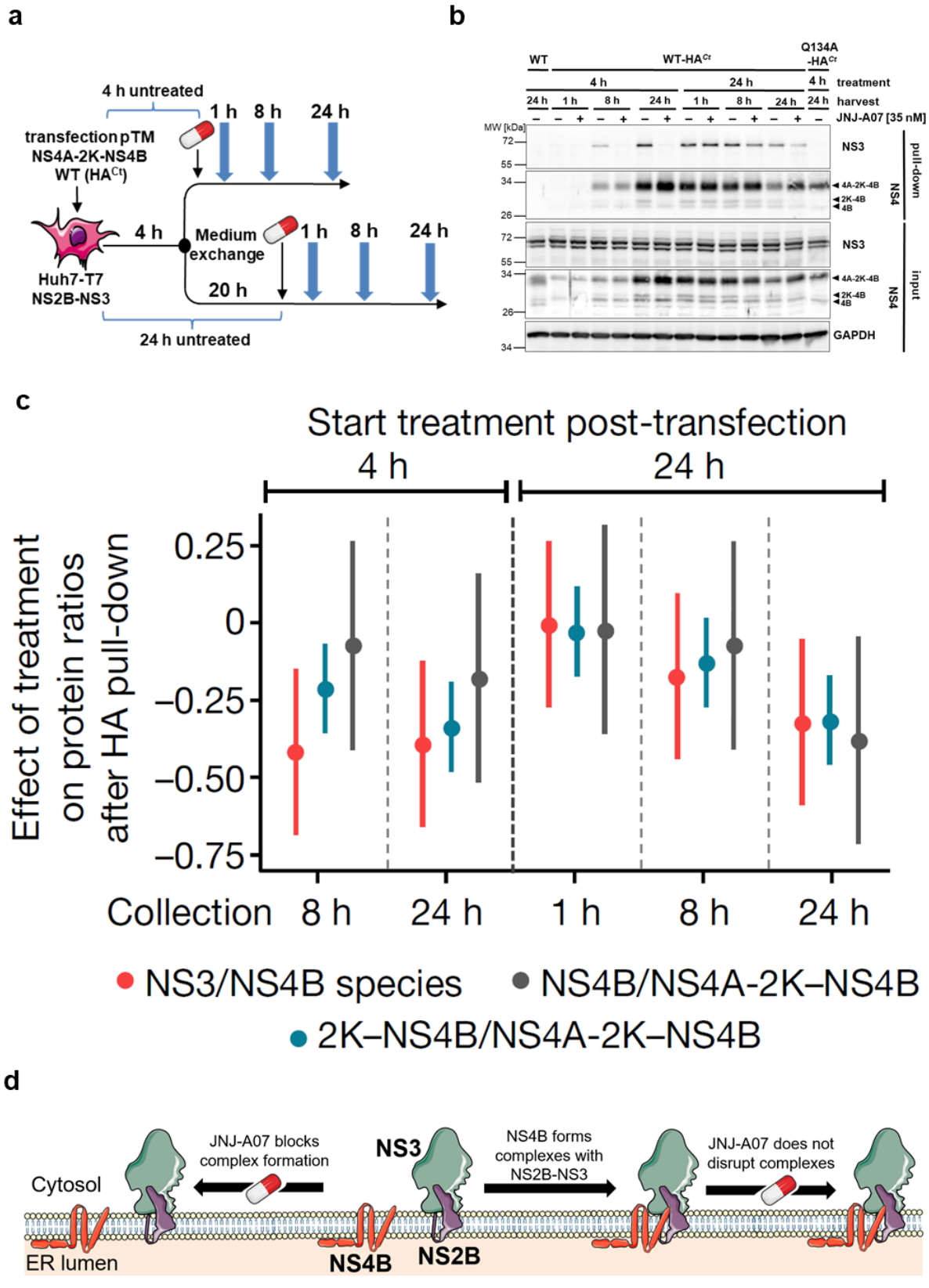

Figure 18. JNJ-A07 blocks the formation of new NS4B/NS3 complexes, but does not affect those that have already formed.

a, Experimental setup to study the kinetics of the JNJ-A07-induced perturbation of the interaction between the viral protease complex NS2B/NS3 and NS4B-containing species. Time points of cell harvest are denoted by blue vertical arrows. **b,** Effect of JNJ-A07 on forming or pre-formed NS3/NS4B complexes. Huh7-T7 NS2B-NS3 cells were treated as described in (a) with 35 nM JNJ-A07 or equal amounts of DMSO. After harvest, lysates were

subjected to HA-specific pull-down and analysed by western blot, together with 20% of the input. A representative western blot is depicted. **c**, Signal intensities of the proteins studied after HA pull-down were quantified from three independent experiments. The JNJ-A07-mediated treatment effect on the indicated ratios was evaluated using linear mixed effects models. Additionally, a random effect was included for each replicate. Please note that the models were fitted separately for the three ratios. Šidák's multiplicity correction was applied to the intervals to account for multiple testing. **d**, Mechanism-of-action model for JNJ-A07. Here, NS4B is representative of all NS4B-containing species (NS4A-2K-NS4B, 2K-NS4B and mature NS4B), both visually and textually, as no differentiation was made in this assay setup. Our results suggest that JNJ-A07 blocks de novo formation of NS4B/NS3 complexes but does not disrupt existing ones. This is in agreement with the TOA experiments showing that JNJ-A07 blocks DENV replication only at early time points after infection.

V.1.5 JNJ-A07 specifically affects the interaction of NS2B/NS3 with the NS4A-2K-NS4B precursor

Given the complexity of NS4B-containing species (NS4A-2K-NS4B, 2K-NS4B and NS4B), the question arose as to whether NS2B/NS3 interacts with all of these proteins and, if so, which of these interactions would be affected by JNJ-A07. To this end, the trans-cleavage system was applied again using Huh7-T7 NS2B-NS3 cells, this time transfected with constructs encoding either the C-terminal HA-tagged NS4A-2K-NS4B precursor or the 2K-NS4B-HA intermediate (Figure 19a). A construct coding solely for NS4B was not considered in this experimental setup because NS4B would not be properly incorporated into membranes in the absence of the 2K peptide. In parallel to the Huh7-T7 NS2B-NS3 cells, an equivalent based on the Huh7 subclone Lunet was also examined here, as these cells were required for later experiments with the pIRO system, and it therefore seemed reasonable to analyze by means of a very fundamental experiment whether there are cell line-specific differences with respect to the NS3 – NS4B interaction.

Regarding transfection, analogous constructs with the Q134A mutation in NS4B, which abolishes the NS2B/NS3 interaction with NS4B, were used as controls. 4 h after transfection, cells were treated with 35 nM JNJ-A07 or vehicle. After a further 14 h, cell lysates were prepared, subjected to HA-specific immunoprecipitation and the levels of captured NS4B proteins together with the also captured NS3 were determined by quantitative western blotting (Figure 19b). Although expression levels were higher in Huh7/Lunet-T7 cells, the expected triad of NS4B, 2K-NS4B and NS4A-2K-NS4B was detected in the input in both cell lines, with the latter being the most abundant (Figure 19b lanes 2 and 9, Figure 19c). The coprecipitation of NS3 was dramatically reduced by treatment with JNJ-A07 (Figure 19b lanes 3 and 10, Figure 19c) or in the case of the non-binding mutant Q134A (Figure 19b lanes 4 and 11, Figure 19). In cells expressing 2K-NS4B, mature NS4B was detected in the input along with a ladder of high molecular weight bands, possibly representing oligomers, whereas uncleaved 2K-NS4B was virtually absent (Figure 19b lanes 5 and 12, Figure 19c). Importantly, no co-precipitation

of NS3 with 2K-NS4B or NS4B was detected. These results suggest that JNJ-A07 blocks the interaction of NS2B/ NS3 with the NS4A-2K-NS4B precursor and not, or to a much lesser extent, with mature NS4B.

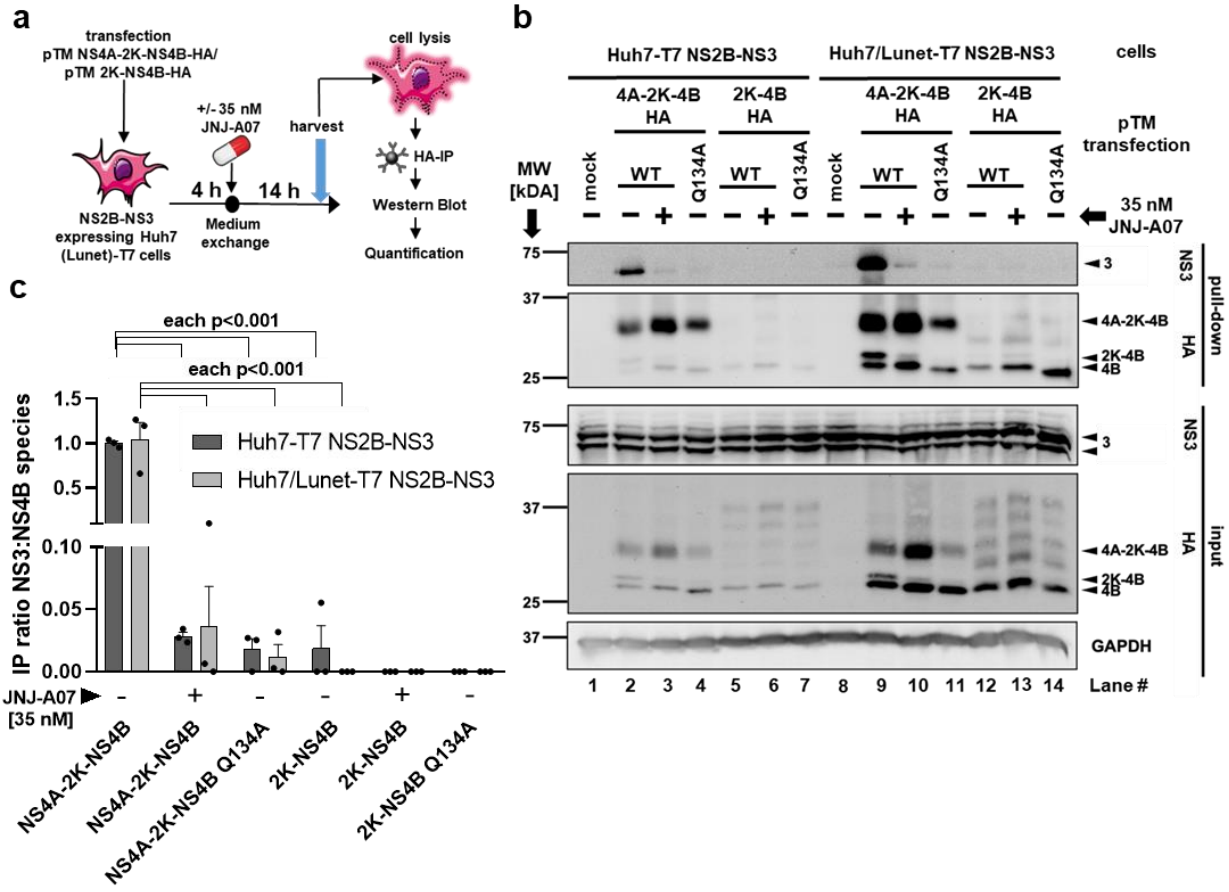

Figure 19. NS2B/NS3 forms a JNJ-A07-sensitive interaction with a mix of all NS4B-containing species, but no interaction with 2K-NS4B and mature NS4B alone.

a, Experimental design: Huh7 or Huh7-Lunet cells stably expressing T7 RNA polymerase and DENV NS2B-NS3 were transfected with T7-based expression constructs coding for either NS4A-2K-NS4B-HA or 2K-NS4B-HA with NS4B corresponding to wild-type (WT) or the NS3 non-binder mutation Q134A. 4 h post-transfection, cells were treated with JNJ-A07 or vehicle, harvested 14 h later and the lysates were subjected to HA-specific pull-down. **b**, Side-by-side comparison of NS3 co-precipitation in both Huh7-T7 cells and Huh7/Lunet-T7 cells expressing either NS4A-2K-NS4B-HA precursor or 2K-NS4B-HA. The eluate after HA precipitation was evaluated by western blot together with 25% of the input. A representative experimental result is presented. **c**, The ratio of NS3 to NS4B species (NS4A-2K-NS4B, 2K-NS4B and NS4B) was determined by quantification of three independent western blots. The p-values shown were calculated by means of two-way ANOVA followed by Dunnett's test.

To support this reasoning, two approaches were developed in which the NS4A-2K-NS4B precursor is not cleaved, while interaction with the NS2B/NS3 complex can still occur (Figure 20a). First, we constructed an NS4A-2K-NS4B mutant in which the protease cleavage site (CS) at the NS4A-2K junction was blocked by an isoleucine substitution at the P1' position (mutant CS P1'Ile). Second, WT NS4A-2K-NS4B was co-expressed with a protease-insensitive

NS2B/NS3 mutant (the serine residue S135 in the protease active site was replaced by alanine). Under both conditions, a stable NS4A-2K-NS4B precursor was detectable, but very little or no 2K-NS4B and NS4B (Figure 20b-c). As shown in the graph in Figure 20d, JNJ-A07 reduced the interaction between NS4A-2K-NS4B and NS2B/NS3 in a dose-dependent manner with EC_{50} values in the single-digit nanomolar range (3.3 nM in the case of CS P1'Ile and 4.1 nM for the protease-active NS2B/NS3 mutant). This value is very close to the EC_{50} concentration of 6.0 nM reported in the experiment presented in Chapter V.1.3 using cells with active NS2B/NS3 protease complex transiently expressing NS4A-2K-NS4B (Figure 17a). Taken together, these observations reinforced the conclusion that JNJ-A07 primarily affects the interaction between NS4A-2K-NS4B precursor and NS2B/NS3.

This finding was followed by the question of whether the observed JNJ-A07-sensitive interaction is an intrinsic property of the NS4A-2K-NS4B precursor or mediated by the NS4A component. To answer this, constructs encoding N-terminal, HA-tagged NS4A were generated (Figure 21a). No NS3 co-precipitation was detected in cells expressing HA-NS4A, regardless of whether JNJ-A07 was added or not (Figure 21b lanes 4 and 5, Figure 21c). In contrast, the drug-sensitive NS4A-2K-NS4B – NS2B/NS3 interaction was reproduced when the N-terminal HA-tagged NS4A-2K-NS4B precursor was co-expressed with NS2B/NS3 (Figure 21b lanes 6 and 7, Figure 21c). Moreover, JNJ-A07 did not induce cleavage between 2K and NS4B, as there was no detection of NS4A-2K in samples isolated from compound-treated cells, whereas a consistent accumulation of uncleaved precursor was detected together with reduced amounts of HA-NS4A, best seen in the IP samples (Figure 21d lanes 3 and 4).

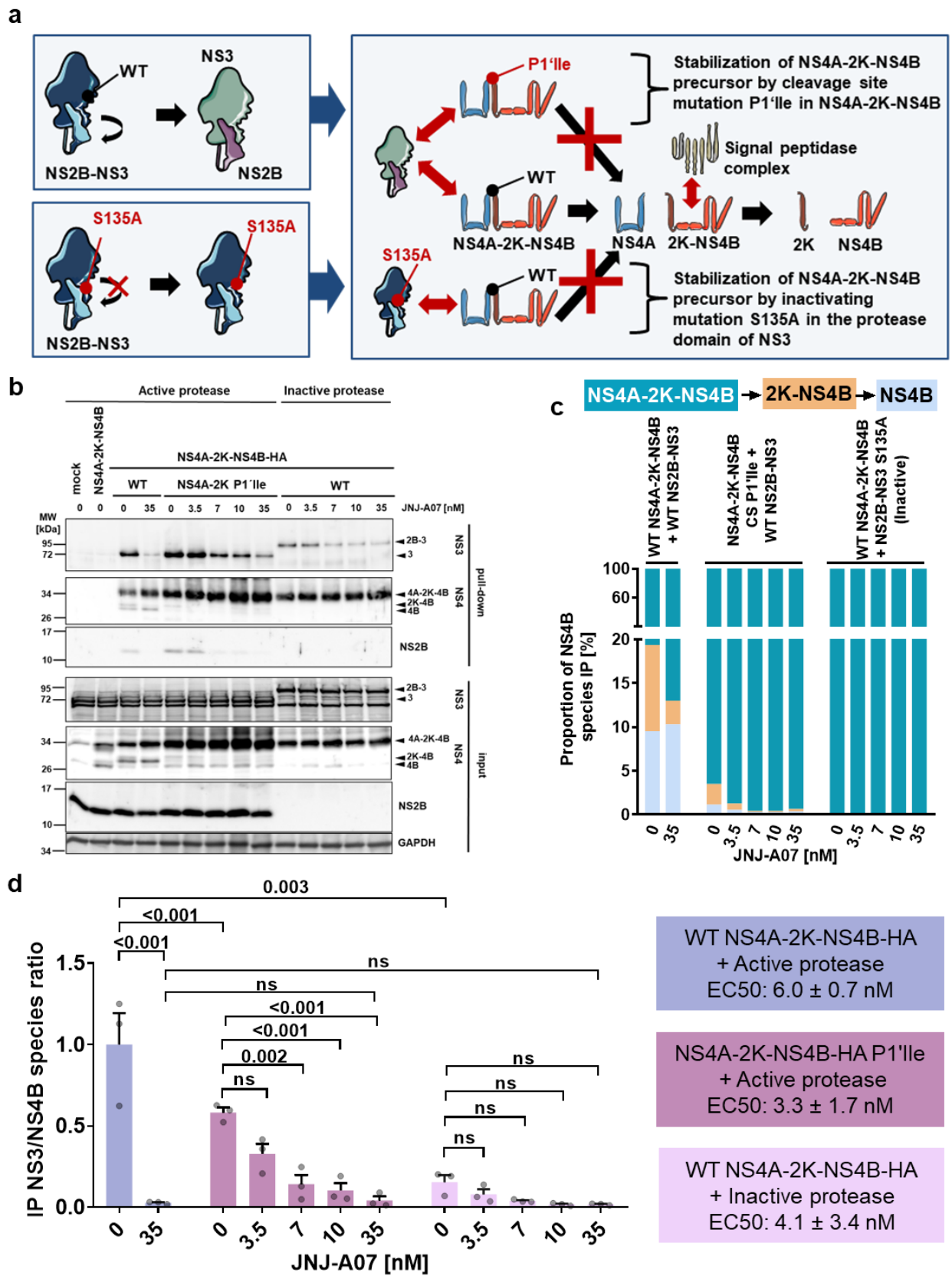

Figure 20. NS2B/NS3 interacts with NS4A-2K-NS4B and this interaction is prevented by JNJ-A07.
a, Schematic depiction of the two approaches pursued to stabilize the NS4A-2K-NS4B precursor intermediate. Modified Huh7-T7 cells were used that stably express an NS2B-NS3 WT polyprotein which is cleaved in *cis* by the NS3 protease domain, releasing NS2B and NS3 that subsequently constitute the viral protease complex

NS2B/NS3 (top left panel). This active complex can cleave the transiently expressed NS4A-2K-NS4B WT precursor at the 2K-NS4B cleavage junction, yielding both mature NS4A and the 2K-NS4B intermediate. The host signal peptidase complex splits off the 2K peptide from the 2K-NS4B intermediate but is incapable of executing this catalytic step on the NS4A-2K-NS4B precursor (right panel, middle lane). Stabilization method 1: Incorporation of a cleavage site mutation called P1'Ile at the 2K-NS4B junction of the NS4A-2K-NS4B precursor induces a structural alteration that renders it unsuitable as a substrate for the viral protease complex (right panel, top lane). Stabilization method 2: Expression of an NS2B-NS3 polyprotein with a protease-inactive mutation (S135A) within the NS3 protease domain intrinsically abolishes the autocatalytic cleavage into NS2B and NS3 (lower left panel). This prevents the processing of all substrates of the viral protease complex, including NS4A-2K-NS4B (right panel, bottom lane). **b**, One of three independent western blots generated to assess dose-dependent effects of JNJ-A07 on the interaction between NS2B/NS3 and stabilized NS4A-2K-NS4B precursor. **c**, Western blot quantification of individual NS4B-containing species in the IP samples (N=3). As expected, no downstream products of the NS4A-2K-NS4B precursor were detected when WT NS4A-2K-NS4B was assayed alongside the inactive protease complex, and only very minor quantities were observed when the NS4A-2K cleavage site mutant P1'Ile was assayed in the presence of the active protease complex. **d**, IP ratios of HA-precipitated NS4A-2K-NS4B and co-captured NS3 were derived from three independent western blot experiments and normalized to vehicle-treated WT NS4A-2K-NS4B in conjunction with active protease. Results are presented as mean and SEM. The indicated p-values were calculated by Šidák's multiple comparison test after one-way ANOVA (ns = non-significant). The EC_{50} values given below for "NS4A-2K-NS4B-HA P1'Ile + Active protease" and "WT NS4A-2K-NS4B-HA + Inactive protease" were calculated by fitting dose-response curves. An EC50 value for "WT NS4A-2K-NS4B-HA + active protease" was taken from Kaptein et al.[376] and is provided here for referential purpose.

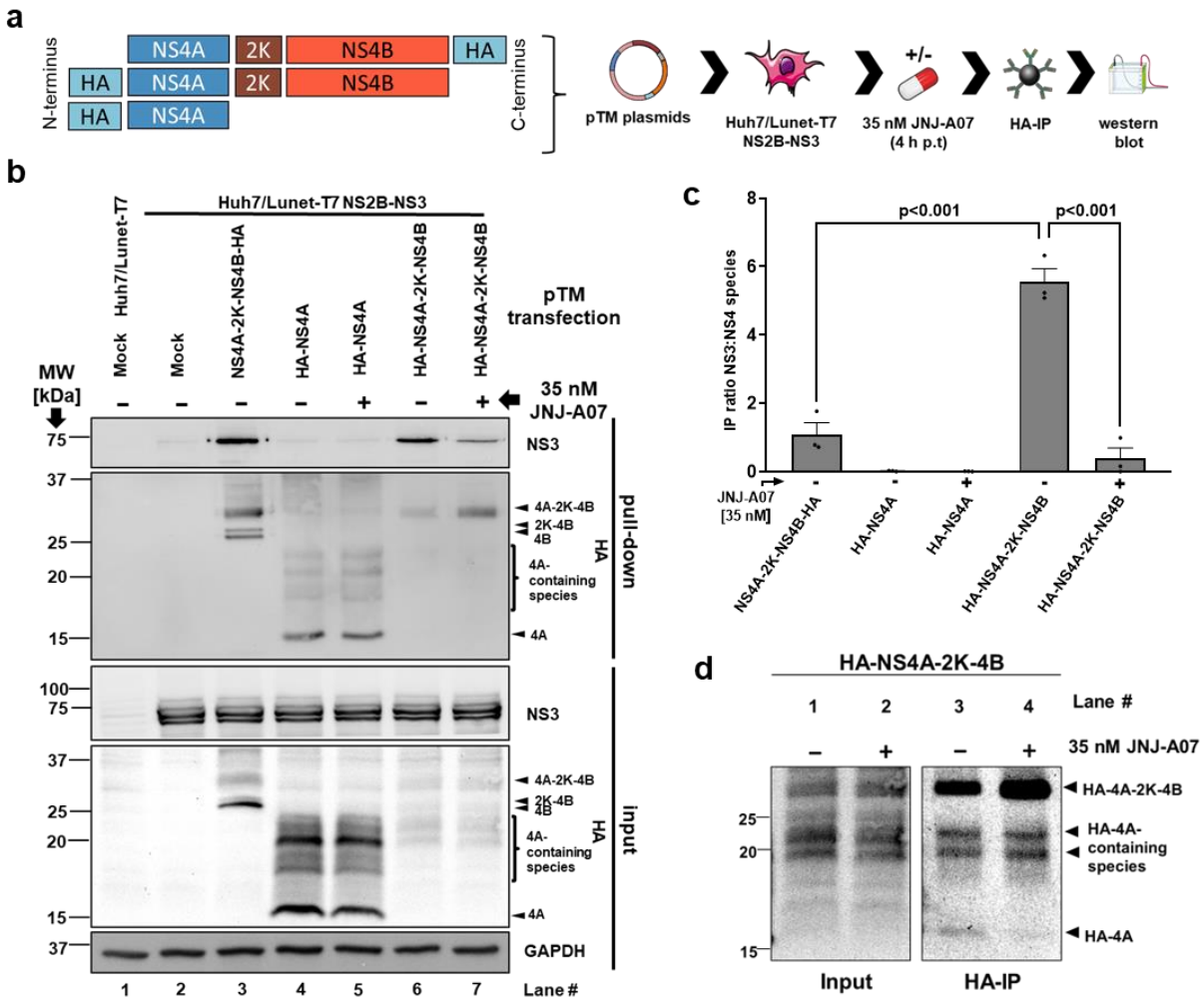

Figure 21. JNJ-A07 does not affect the cleavage order of NS4A-2K-NS4B.
a, Workflow overview. Displayed constructs were transfected into Huh7/Lunet-T7 cells stably expressing NS2B-NS3. 4 h post-transfection, cells were treated with either 35 nM JNJ-A07 or vehicle. After a further 14 h, samples

were collected and used for HA-specific pull-down. Captured proteins were analyzed by western blot. The C-terminally HA-tagged NS4A-2K-NS4B precursor served as a reference. **b**, Representative western blot showing HA pull-down samples and total lysates (25% of input). GAPDH was used as a loading control for cell lysates. **c**, Bar graph representing the ratio of NS3 to NS4B species as assessed by quantification of western blots (n=3); one example is depicted in (b). The indicated p-values were calculated by means of one-way ANOVA followed by Šidák's multiple comparison test. **d**, Cutout of the western blot shown in (b), adjusted for brightness and contrast to highlight NS4A species in pTM HA-NS4B-2K-NS4B transfected samples.

V.1.6 JNJ-A07 does not impair the interaction between NS1 and the NS4A-2K-NS4B precursor

From the existing literature, it is known that the NS4A-2K-NS4B precursor interacts with NS1[140]. Therefore, it seemed plausible that JNJ-A07 could also block this interaction. To test this possibility, plasmids encoding NS4A-2K-NS4B were transiently introduced into Huh7/Lunet-T7 cells stably expressing NS1-HA (Figure 22a). This NS1 variant was fully functional, being able to rescue replication of a DENV-NS1 deletion mutant otherwise incapable of self-replication[140]. Lysates from cells cultured for 14 h in the presence of different concentrations of JNJ-A07 were either evaluated directly or used for HA-specific pull-down, and proteins were analyzed by quantitative western blot (Figure 22b). Within the physiologically relevant range up to 100 nM, a dose-dependent increase in the ratio of NS4A-2K-NS4B to NS1 was observed in the lysates (Figure 22c), presumably due to stabilisation of the precursor in this system. An analogous increase was quantified in the pull-down samples (Figure 22d). Importantly, JNJ-A07 did not reduce the NS1 interaction with NS4A-2K-NS4B. The data demonstrate that JNJ-A07 has no effect on the association of NS4A-2K-NS4B with NS1. Furthermore, the preserved interaction with NS1 suggests that this compound does not elicit a global misfolding of NS4A-2K-NS4B, arguing for a rather selective blocking of the precursor association with NS2B/NS3.

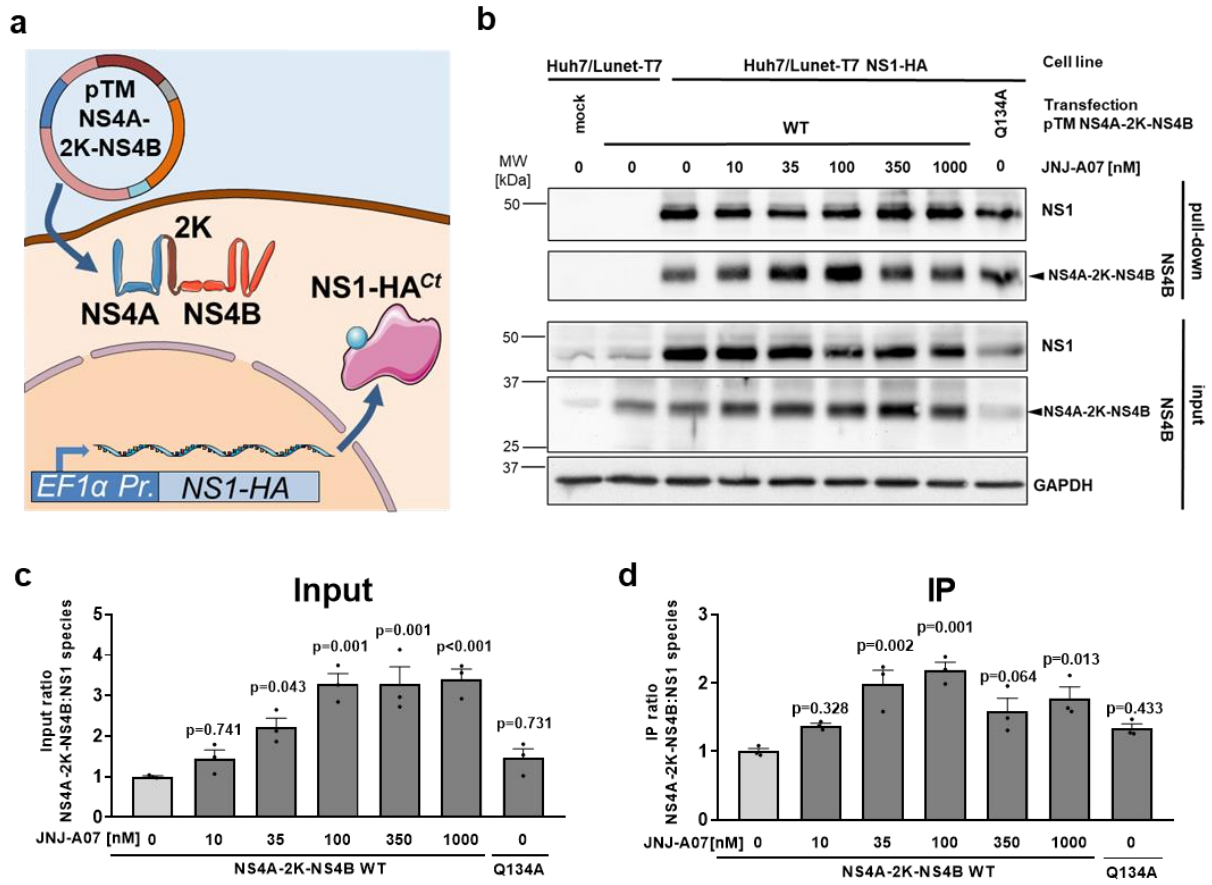

Figure 22. No JNJ-A07-mediated blockade of the NS4A-2K-NS4B precursor-specific interaction with NS1. **a**, Schematic illustration: Huh7/Lunet-T7 cells stably expressing NS1-HA were transfected with constructs coding for NS4A-2K-NS4B. **b**, At 4 h post-transfection, cells were treated with specified concentrations of JNJ-A07 or vehicle, harvested 14 h later, and lysates were subjected to HA-specific pull-down. Captured protein complexes were analyzed by western blot. A representative image is presented (n=3). Numbers on the left indicate molecular weight references. GAPDH was used as a loading control for cell lysates (input). **c-d**, Ratios of NS1 to NS4A-2K-NS4B in input samples (c) and corresponding pull-down samples (d) were calculated with mean and SEM by measuring signal intensities in the three independent experiments. Statistical analysis was performed using one-way ANOVA plus post-hoc test with Dunnett's correction to adjust for multiple testing.

V.1.7 Interspecies variations in the amino acid sequence of NS4B represent a possible explanation for the insensitivity of other flaviviruses to JNJ-A07

As mentioned in Chapter V.1.1, JNJ-A07 is DENV-specific and does not exhibit significant antiviral activity even against close relatives such as ZIKV or YFV. At least for ZIKV, an NS3 – NS4B interaction was detected, so it is not exclusivity of the interaction that could explain the narrow spectrum of activity. In addition to structural differences in the JNJ-A07 binding site (which has not yet been precisely characterized), consideration has been given to the possibility that related flaviviruses may be compound insensitive, since they might naturally feature an NS4B sequence containing amino acids associated with resistance at corresponding positions in DENV NS4B. To this end, a multiple sequence alignment was performed between

DENV-2/16681 and those strains of related flaviviruses that were also used to assess JNJ-A07 for antiviral activity (Figure 23). Indeed, apart from JEV, all the flaviviruses used for the comparison harbored at least one such position in the NS4B sequence, which was identified as resistance-forming in DENV (Figure 24a). Furthermore, it should be noted that the related flaviviruses also displayed variations at positions critical for resistance in DENV, which did not exactly match the DENV amino acid exchange but may potentially impart intrinsic resistance due to similar chemical properties. Using ZIKV as an example, this aspect was analyzed in more detail by replacing the three potentially resistance-mediating residues with the non-resistance-mediating original residues of DENV. This was carried out in sgZIKV-R2A replicons on the one hand and in pTM ZIKV NS4A-2K-NS4B plasmids on the other hand. Assessment of replication fitness revealed that mutants I110T and S218T were replicating similarly to WT, whereas Y87S was showing a severely attenuated phenotype (Figure 24b). Analysis of the NS3 – NS4B interaction revealed that none of the reverted resistance mutations introduced into ZIKV NS4B made the interaction with NS3 sensitive to JNJ-A07 (Figure 24c-d). However, the control mutant Q134A, which was included as a counterpart to DENV NS4B Q134A, showed a drastic loss of NS3 – NS4B coprecipitation in the case of ZIKA, underscoring the importance of the cytosolic loop between NS4B TMD3 and TMD4 for the interaction with NS3.

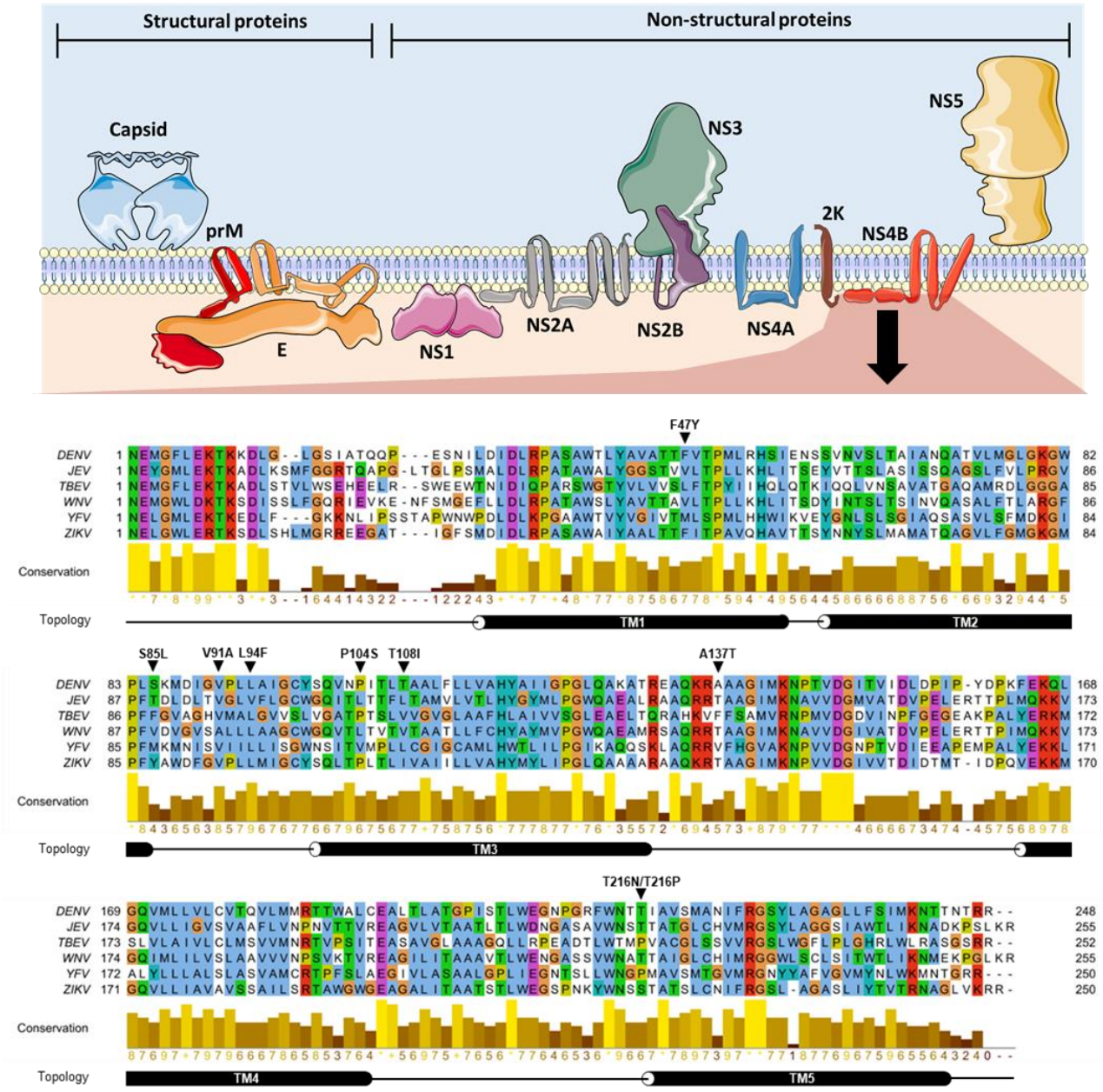

Figure 23. NS4B sequence alignment of related flaviviruses.
The protein sequence of DENV-2/16681 was aligned with corresponding sequences from Japanese encephalitis virus strain JEV CNS769 Laos 2009 (GenBank KC196115), Tick-borne encephalitis virus strain Oshima 5.10 polyprotein gene (MF374487), West Nile virus isolate R94224 CDC polyprotein gene (GenBank MF004388), Yellow fever virus isolate Bolivia 88 1999 polyprotein gene (GenBank MF004382) and Zika virus strain HPF 2013 (GenBank KJ776791) using Clustal Omega Version 2.1. Post-processing was conducted with Jalview 2.11.1.3. The DENV topology model was added manually based on Miller et al.[172]. Black arrowheads are pointing at locations associated with compound-resistance in DENV.

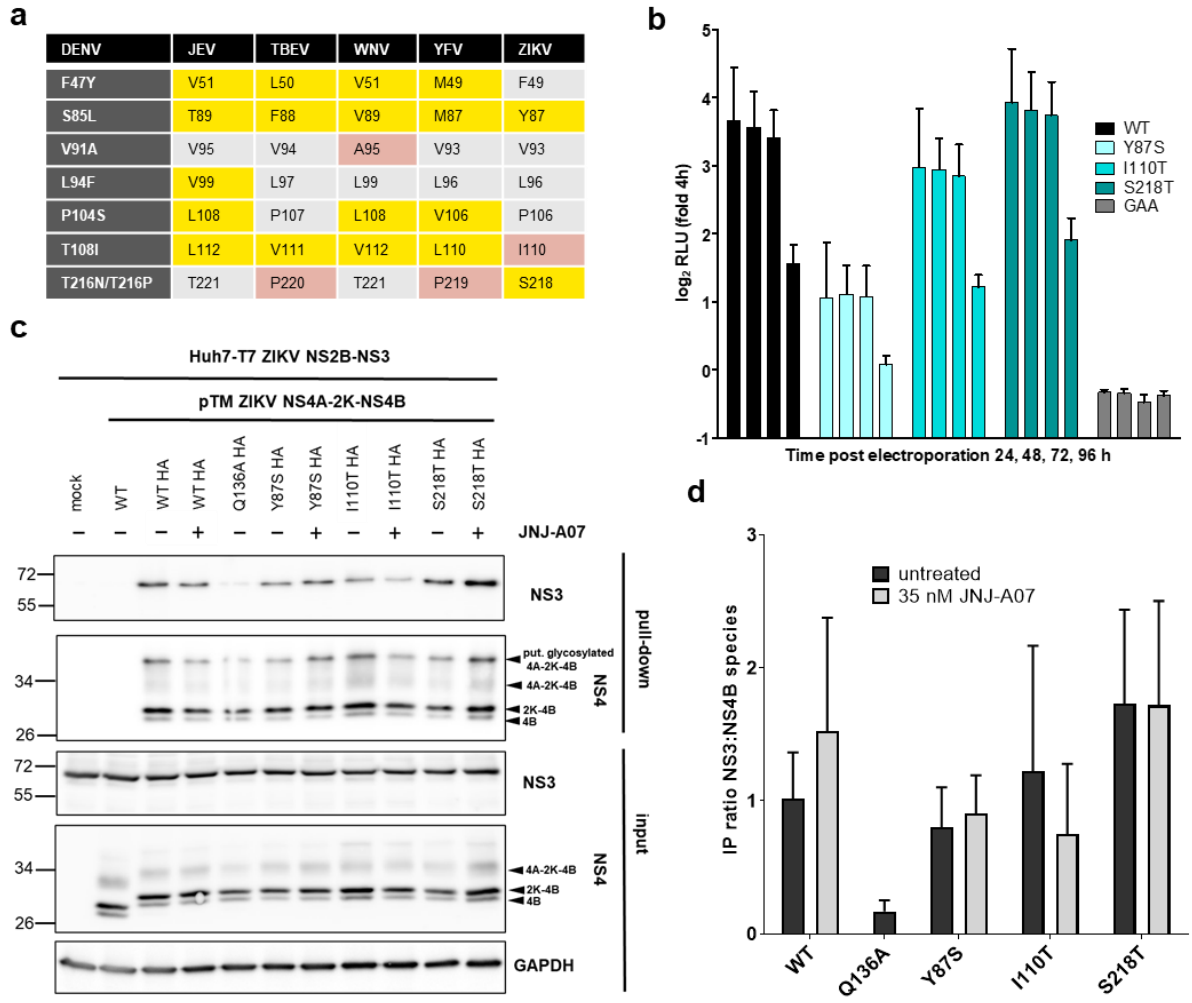

Figure 24. Reverse-resistance mutations in ZIKV NS4B do not render the interaction with NS3 sensitive to JNJ-A07

a, Table, presenting the specific amino acids of interest across the above mentioned flaviviruses. Amino acid variations matching with resistance mutations in DENV are highlighted in red, while variations that differ from WT DENV but do not match with resistance mutations are highlighted in yellow. For instance, ZIKV NS4B (strain HPF 2013) harbors two variations of the latter category (Y87, S218) and one variation (I110) that could potentially contribute to natural compound resistance as it aligns with the DENV mutation site T108I. **b,** Effects of reverse mutations in NS4B on replication fitness. Mutations Y87S, I110T and S218T were into a ZIKV sgR2A replicon system. A replication-deficient replicon containing an inactivating mutation in the NS5 RNA-dependent RNA polymerase domain (GAA) was included as negative control. *In vitro* transcribed RNA was transfected into Huh7 cells. Cells were lysed at 24 h, 48 h, 78 h and 96 h and Renilla luciferase activity was measured as marker of replication. Relative light units (RLU) were normalized to the 4 h value, reflecting transfection efficiency. Plotted are the mean and SD from three independent experiments, each carried out with independent RNA preparations. **c,** Huh7 cells stably expressing the T7 RNA polymerase and ZIKV NS2B-NS3 were transfected with T7-based expression plasmids encoding ZIKV NS4A-2K-NS4B(-HA^{Ct}) with NS4B corresponding to the wild-type (WT), the NS3-non-binder mutant Q136A or containing a reverse DENV mutation. 4 h after transfection, cells were treated with 35 nM JNJ-A07 or DMSO, collected 14 h thereafter and lysates were used for HA-specific pull-down. Protein complexes isolated by HA-specific pull-down were analyzed by western blot (N=2). NS3/NS4B species ratio for each sample was calculated and normalized to the non-drug treated sample.

V.2 JNJ-A07 mediates its antiviral effect by blocking the *de novo* formation of DENV replication organelles

The previous Chapter V.1 demonstrated the outstanding importance of the interaction between the NS4A-2K-NS4B precursor and the viral protease/helicase complex NS2B/NS3 for the mechanism-of-action of JNJ-A07. This chapter presents the results of various approaches to further determine the mechanism-of-action using the so-called pIRO system. When elucidating the mechanism-of-action of antiviral compounds that block replication, such as JNJ-A07, a fundamental limitation of replication-based assays is that all phases of the viral replication cycle, such as protein synthesis, polyprotein processing, vesicle packets formation and genome amplification, are inextricably linked, making it challenging to identify the precise step that is affected by the compound. In the pIRO-D system, an acronym derived from *plasmid-induced replication organelles of DENV*, cells stably expressing bacteriophage T7 RNA polymerase are transfected with a plasmid encoding the non-structural module of the DENV-2 polyprotein (strain Thailand/16681) under control of the T7 promoter. The coding region is flanked by fragments of the DENV-2 capsid sequence and the 3' NTR, with the viral proteins supporting the formation of true vesicle packets in transfected cells (Figure 25a).

V.2.1 PAL-derivatives of JNJ-A07 concentrate intracellularly at locations enriched in DENV but not ZIKV proteins

To characterize the spatial association of investigated antiviral compounds with DENV NS4B, imaging studies were performed. For this purpose, a photoaffinity labelling (PAL) approach was taken involving Compound A and Compound B, having high structural similarity with JNJ-A07 and being enantiomers of each other (Figure 25b-c). Compound A is the (R)-enantiomer and is about 70-fold more active than the (S)-enantiomer Compound B. These PAL compounds featured a diazerine group for covalent cross-linking with target structures in close proximity by UV irradiation (365 nm) as well as a terminal alkyne facilitating conjugation with an adapter molecule in a click chemistry reaction. Huh7/Lunet-T7 cells were used for this and subsequent assays as they allow high transfection efficiency and are suitable for imaging analyses[106]. Cells were transfected with the plasmid encoding the wild-type (WT) NS1-5 polyprotein (pIRO-D), treated with PAL compounds or a vehicle control 4 h later, irradiated with UV and fixed after a further 14 h. The bound compound was visualized after a click reaction with picolylazide-Cy5.5 (Jena Bioscience). NS4B, as well as NS3 as reference, were detected by immunofluorescence. Both viral proteins exhibited a high degree of colocalization

with the labelled Compound A in large puncta possibly corresponding to convoluted membranes and/or vesicle packets, whilst vehicle-treated control cells as well as mock-transfected cells displayed only a diffuse background pattern (Figure 25d). Pearson correlation coefficients between NS4B and the PAL compounds revealed that the less active (S)-enantiomer Compound B gave significantly less colocalization than the more active enantiomer Compound A, but for both compounds the colocalisation was substantially above baseline (Figure 25e). To confirm the specificity of the labelling approach, the same assay was performed but using the ZIKV NS1-5 polyprotein (pIRO-Z). In agreement with the lack of antiviral activity of JNJ-A07 against ZIKV[376], no meaningful colocalization of the compound with ZIKV NS4B was detected (Figure 25f-g). These results support specific binding of the compound to DENV-induced intracellular structures enriched for NS4B and NS3.

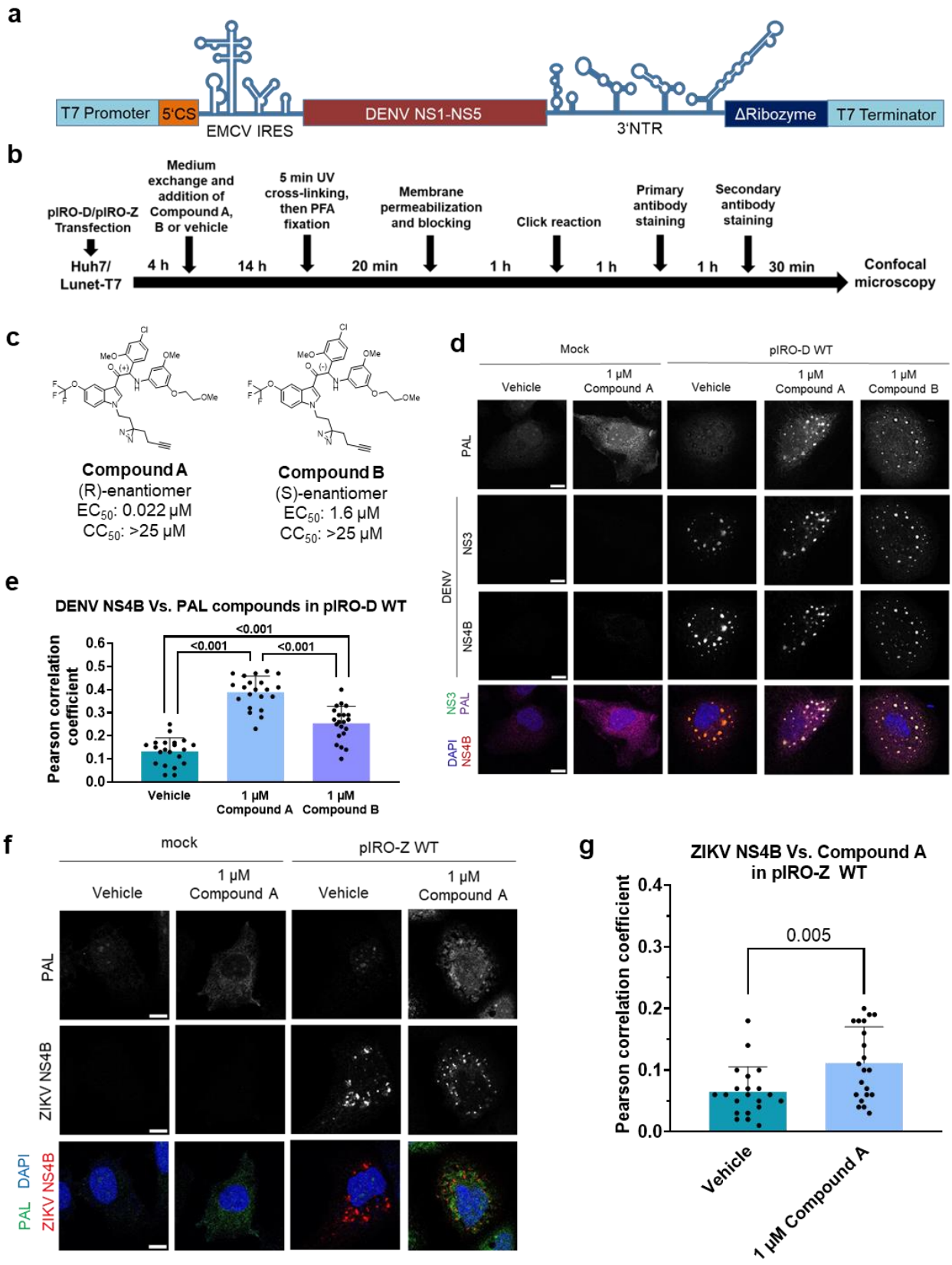

Figure 25. Compound A specifically localizes to intracellular sites enriched for DENV NS4B and NS3.
a, Schematic illustration of the pIRO-D system. Upon transfection of T7-expressing cells with pIRO-D plasmids, the non-structural module of the DENV proteins (NS1-NS5) is expressed independently of viral replication. The coding part is preceded by the T7 RNA polymerase promoter, a short portion of the capsid region containing the

5′ cyclization sequence (CS) and an encephalomyocarditis virus (EMCV) internal ribosome entry site (IRES) to allow high levels of RNA translation. The 3' NTR, which plays an essential non-replicative role in the formation of DENV replication organelles, is located downstream of the coding region. The WT version of pIRO-D is capable of inducing authentic replication organelles including vesicle packets. The pIRO-Z system works in an equivalent manner for ZIKV. **b**, Workflow for performing click labelling and immunofluorescence staining on fixed cells treated with one of the PAL enantiomers or DMSO control (vehicle). It should be noted that a click reaction with picolyl azide-Cy5.5 was performed irrespective of the treatment condition. **c**, Comparison of antiviral activity and cellular cytotoxicity (CC) of Compound A and Compound B. Compound A represents the (R)-enantiomer and is approximately 70-fold more active than the (S)-enantiomer Compound B. **d**, Exemplary confocal microscopic images (60x). Cells were either transfected with the pIRO-D WT construct that encodes the NS1-5 polyprotein or mock transfected. 4 h after transfection, specimens were treated with either 1 µM Compound A, 1 µM Compound B or vehicle. The signals of PAL fluorescence as well as immunofluorescence staining for NS3 and NS4B are shown in the panel along with a merge that includes nuclear DNA staining with DAPI. Scale bar = 10 µm. **e**, Pearson correlation coefficients between PAL and NS4B signals were analyzed for 21 cell profiles (7 from each of the three independent experiments) per pIRO-D WT transfected sample. The mean with standard deviation is shown. One-way ANOVA followed by Tukey's multiple comparison test was performed to obtain statistical parameters. **f**, Colocalization of Compound A with ZIKV NS4B was determined using cells transfected with a ZIKV polyprotein-encoding construct (pIRO-Z). Representative images obtained as described for (d) are shown. Scale bar = 10 µm. **g**, Quantification of PAL and ZIKV NS4B signal-overlap following the procedure described in (e). The displayed p-value was calculated from an unpaired two-tailed t-test.

V.2.2 Resistance mutations significantly affect intracellular accumulation of Compound A at sites highly abundant in DENV proteins

To determine whether JNJ-A07 resistance was due to loss of binding ability of the compound or to some other mechanism, those resistance mutations identified in the A sample of the in vitro resistance selection assay were integrated into the basic pIRO-D construct. NS4B mutants were analysed by means of the colocalisation assay described in the previous chapter. As with WT, all NS4B mutants showed a punctate pattern colocalizing with Compound A (Figure 26a). While the subcellular distribution of NS3 and NS4B was unaffected in DMSO-treated control cells (vehicle), only a very low background signal was detected when these cells were analyzed in the Cy5.5 channel used to visualise dye-coupled Compound A, confirming the specificity of the method applied. Reduced NS4B signal observed for mutants A137T and T216N compared to WT was presumably caused by impaired binding of the primary antibody, as the mutations are located in its epitope. Careful inspection of the Pearson correlation coefficients unveiled a consistently high level of colocalization between Compound A and each of the viral proteins (Figure 26b-c) as well as between NS3 and the various configurations of NS4B (Figure 27a). Despite the fact that colocalization between the compound and the viral proteins was significantly decreased in NS4B mutants compared to WT, the strength of the reduction did not correlate with the degree of resistance imparted by a particular mutation (Figure 26b and Figure 14c). Nevertheless, the parallel reduction in colocalization of NS3 and NS4B with Compound A observed in the different mutants is further evidence of the association between

these two proteins, which are in the focus of JNJ-A07's mechanism-of-action. Collectively, these results imply that diminished compound binding may account for resistance to NS4B inhibitors. However, since the lowest level of colocalization was recorded for T108I and not for the mutations with the highest resistance, V91A and L94F, additional mechanisms might contribute to resistance to this class of antivirals.

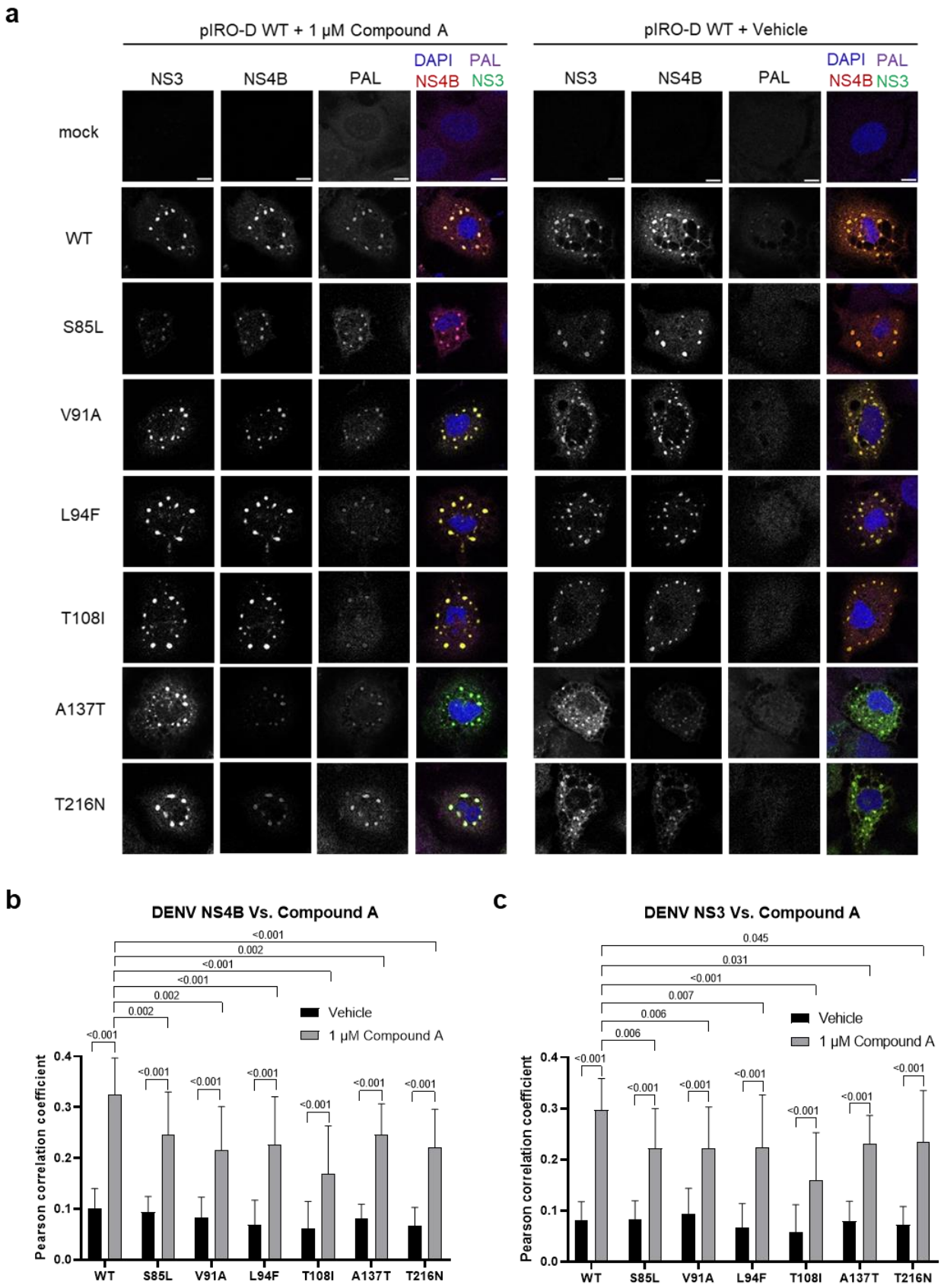
a
pIRO-D WT + 1 μM Compound A
pIRO-D WT + Vehicle
NS3
NS4B
PAL
DAPI PAL
NS4B NS3
mock
WT
S85L
V91A
L94F
T108I
A137T
T216N
b
DENV NS4B Vs. Compound A
Pearson correlation coefficient
Vehicle
1 μM Compound A
<0.001
0.002
<0.001
<0.001
0.002
0.002
<0.001
<0.001
<0.001
<0.001
<0.001
<0.001
<0.001
WT
S85L
V91A
L94F
T108I
A137T
T216N
c
DENV NS3 Vs. Compound A
Pearson correlation coefficient
Vehicle
1 μM Compound A
0.045
0.031
<0.001
0.007
0.006
0.006
<0.001
<0.001
<0.001
<0.001
<0.001
<0.001
<0.001
WT
S85L
V91A
L94F
T108I
A137T
T216N

Figure 26. The accumulation of Compound A at sites rich in DENV proteins is significantly impacted by resistance mutations.
a, IF panel of Huh7/Lunet-T7 cells transfected with pIRO-D WT plasmid or analogues carrying the specified resistance mutations in NS4B. Experimental workflow as illustrated in Figure 25b. Images were acquired by confocal microscopy at 60x magnification. Scale bar = 10 µm. **b-c**, NS4B mutations conferring different levels of resistance to JNJ-A07 were investigated for their effect on the colocalization between the PAL signals and either NS4B (b) or NS3 (c). The corresponding IF panel is presented in (a). Pearson correlation coefficients are plotted with mean and standard deviation calculated from 7 cell profiles for each of 3 independent experiments. Statistical significance was determined by a two-way ANOVA test followed by Šidák's multiple comparisons test.

V.2.3 Compound A increases the clustering of NS3 and NS4B in large puncta

When cells stained for NS3 and NS4B were imaged, it was found that a significant fraction of them showed clustering of the two proteins in puncta that were primarily found in the perinuclear region. It is important to emphasize that this pattern was an almost continuous spectrum, ranging from cells having numerous small dots that resulted in a quasi-diffuse staining, to cells with several very large dots at the other end of the scale. In order to minimize the impact of this spectrum on the determination of Pearson correlation coefficients, cells were selectively chosen that had primarily large, but not excessively large puncta in the NS4B channel. To assess whether Compound A treatment or resistance mutations had an influence on the puncta spectrum, a total of 60 cells per specimen were analyzed with regard to the morphology of their staining pattern, whereby these were semi-quantitatively assigned to one of the three categories "diffuse cytosolic pattern/small puncta," "medium puncta," and "large puncta" (Figure 27b). Compared to the WT, the mutants V91A, L94F and T108I showed a tendency towards smaller puncta in the absence of JNJ-A07 (Figure 27c). Interestingly, both WT and all mutants showed a clear Compound A-induced coalescence of NS3- and NS4B-rich puncta. The underlying reason why mutants V91A, L94F and T108I retained the trend towards smaller puncta after the addition of Compound A was probably due to the different starting levels, rather than to a reduced increase. Next, the question was addressed whether the compound-induced enlargement of NS3- and NS4B-rich puncta was due to a redistribution of intracellular proteins or whether there was a stabilizing effect on NS3- and/or NS4B protein levels. By examining the intensity values for WT NS3 and NS4B both in the presence and absence of Compound A in more than 2000 cells per sample, it was shown that the observation was predominantly due to a concentration of these proteins in puncta-like structures, whereas a compound-induced increase in protein levels was weak and did not reach statistical significance (Figure 27d).

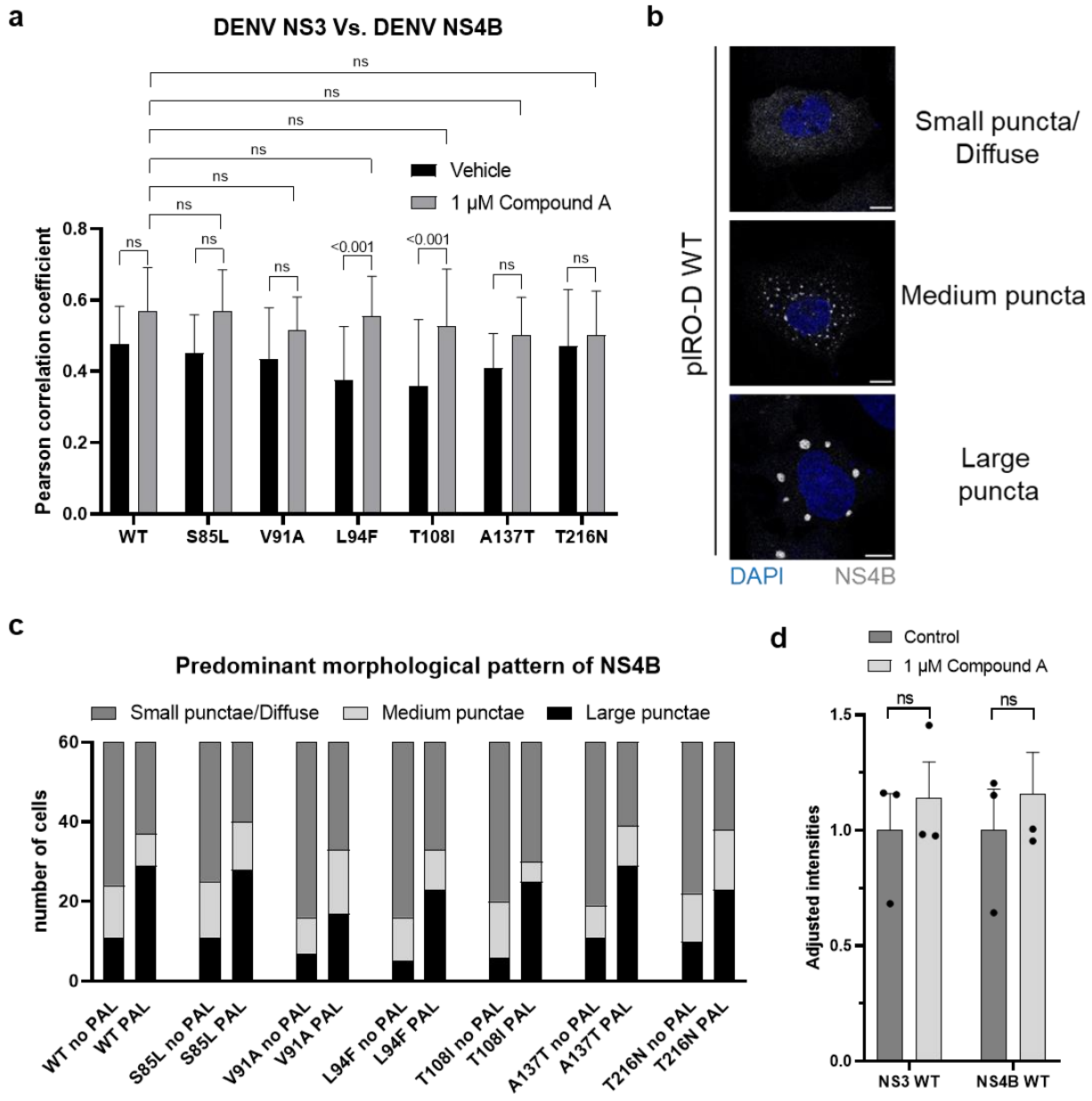

Figure 27. Compound A triggers fusion of NS4B-rich puncta in pIRO-D transfected cells.
a, The data set for which colocalization between Compound A and viral proteins was assessed as shown in Figure 26b-c was analyzed analogously to determine the colocalization between NS3 and NS4B. **b,** The NS4B pattern in pIRO-D transfected cells varies morphologically and can be broadly classified into three groups "large puncta", "medium puncta" and "small puncta/diffuse cytosolic signal". Example images of pIRO-D WT transfected cells are shown. Scalebar = 10 µm. **c,** From three independent experimental runs, 20 transfected cells per sample condition were randomly selected, and assigned to one of the groups presented in (b). The absolute numbers are plotted in the stacked bar graph. **d,** Investigation whether Compound A leads to a cellular increase in viral proteins levels or merely affects their distribution. For this purpose, the mean intensity of the IF signal of WT NS3 and WT NS4B was determined in each of the three experimental runs by automated evaluation of at least 500 transfected cells. The data were normalized by the average of the respective mean intensities of untreated samples. Results support the redistribution model, as no statistically significant intensity differences were detected for both NS3 and NS4B. Statistical analysis was performed by a two-way ANOVA test along with Šidák's multiple comparisons post-hoc test. ns = non-significant.

V.2.4 No discernible impact of JNJ-A07 on NS4A-2K-NS4B cleavage kinetics in the polyprotein setting

In Chapter V.1.3, it was observed by means of the trans-cleavage system that JNJ-A07 alters the steady state cleavage kinetics of the NS4A-2K-NS4B precursor, as inferred from a dose-dependent decline in the 2K-NS4B cleavage intermediate. Knowing that the *trans*-cleavage system is not an ideal setup for authentic determination of cleavage kinetics due to the lack of *cis*-cleavage as well as the non-equimolar ratios of NS2B and NS3 to NS4A-2K-NS4B, pulse-chase experiments were performed in a polyprotein context. This allowed temporal tracking of the exact cleavage kinetics of the NS4A-2K-NS4B precursor. To this end, Huh7/Lunet-T7 cells transfected with a pIRO-D construct encoding the NS1-5 polyprotein bearing a replication-competent HA-tagged NS4B (NS4B-HA*) were used (Figure 28a). Cultures were treated with 35 nM JNJ-A07 or vehicle and, after a starvation period, first radioactively incubated with [^{35}S]-cysteine and methionine for 20 minutes to label *de novo* produced proteins and then further incubated in non-radioactive medium for various periods of time. Fully matured NS4B-HA* and corresponding cleavage intermediates were enriched by pulldown, and proteins were assayed by SDS-PAGE and autoradiography. Rapid and complete conversion of the NS4A-2K-NS4B precursor first into the 2K-NS4B intermediate and then into mature NS4B was noted in both JNJ-A07 and vehicle-treated control cells (Figure 28b). Quantitative analysis of autoradiographs yielded highly comparable NS4A-2K-NS4B cleavage kinetics in JNJ-A07-treated and control cells (Figure 28c), with NS4A-2K-NS4B precursor half-lives of 13.6 ± 2.0 min and 15.4 ± 2.6 min, respectively (Figure 28d). This outcome suggests that the NS4B inhibitor JNJ-A07 has no significant effect on the processing of NS4B-containing polyprotein species.

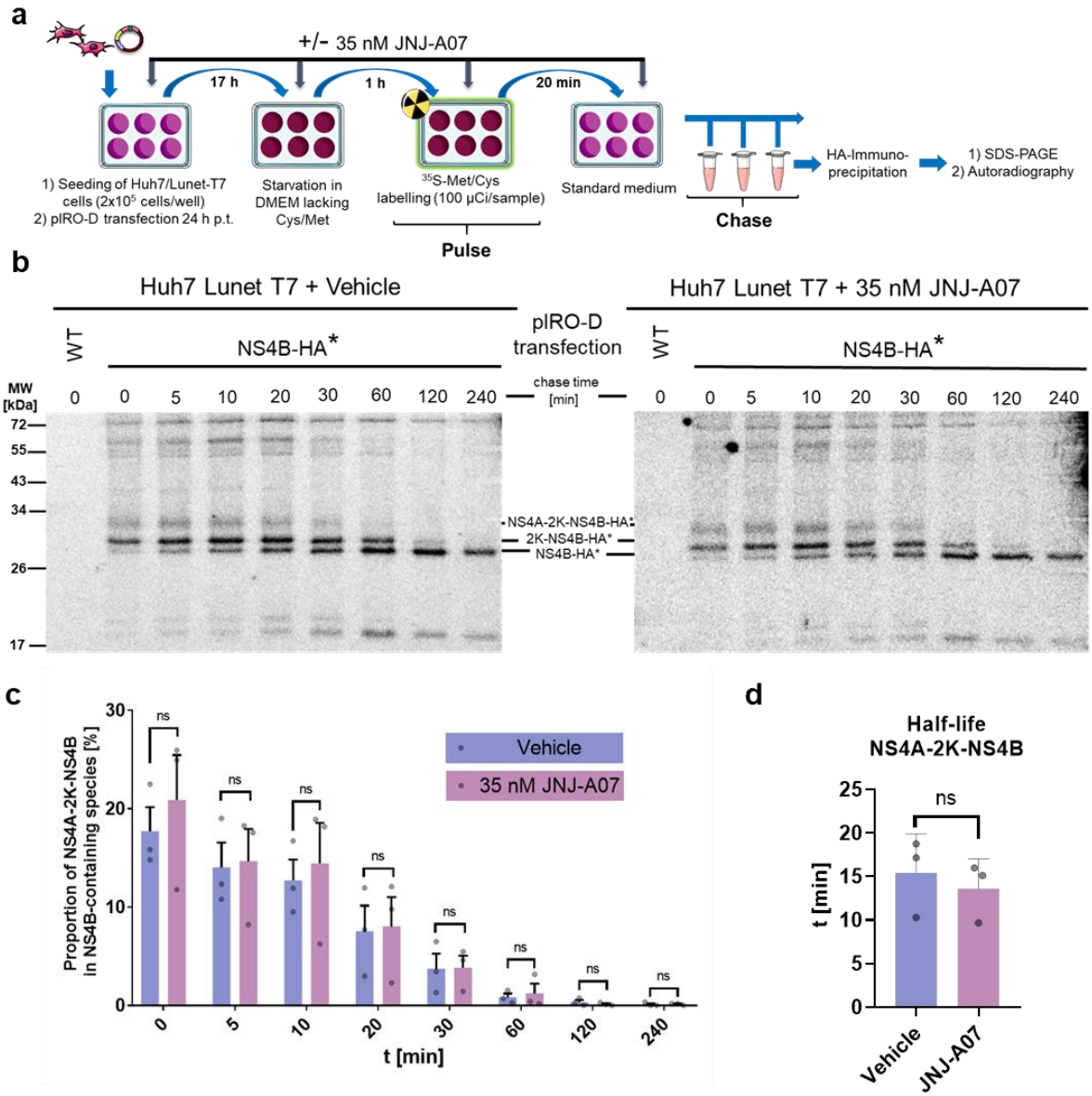

Figure 28. JNJ-A07 does not markedly affect the cleavage rate of NS4A-2K-NS4B in the polyprotein context.

a, Procedure: Huh7/Lunet-T7 cells were transfected with a pIRO-D construct expressing the NS1-5 polyprotein with or without an HA affinity tag inserted into the NS4B N-terminal region downstream of the 2K peptide[191]. After a 30-minute starvation period in methionine- and cysteine-free medium, the cells were incubated in radioactive medium for 20 minutes. At different time points, cells were lysed, subjected to HA-IP and analyzed by autoradiography after SDS-PAGE. **b**, Autoradiogram of protein complexes captured by HA-specific pull-down. The results shown are representative of three independent runs. The numbers above the lanes denote the chase time in minutes. **c**, Signal intensity of NS4B-specific bands was quantified and adjusted for cysteine and methionine residues. The proportion of NS4A-2K-NS4B among all NS4B-containing species is plotted. Šidák's multiple comparison test following a two-way ANOVA revealed no statistically significant differences between JNJ-A07 and vehicle control treated samples at any time point. **d**, One-phase exponential decay curves were fitted to the results of each experiment to obtain three NS4A-2K-NS4B half-life values for both the JNJ-A07 and vehicle control treated groups. The results are presented here with mean and SEM.

V.2.5 In the polyprotein context, Co-IP observations show complex and divergent behaviour to the trans-cleavage system

The Co-IP results obtained so far were generated using the *trans*-cleavage system. However, in infected cells, the viral protease is part of the polyprotein substrate, and therefore the effects of JNJ-A07 on the precursor-protease interaction were comparatively studied in the polyprotein system (pIRO-D). For this purpose, pull-down experiments were performed with lysates of Huh7/Lunet-T7 cells that were expressing a polyprotein with a replication-competent HA-tag in NS4B and had been treated with JNJ-A07 for 18 h. The two systems shared the characteristic that a specific interaction between NS2B/NS3 and NS4B-containing species formed in both, but the addition of JNJ-A07 in the polyprotein context did not result in a loss of NS3 co-precipitation (Figure 29a). Integration of the P1'Ile cleavage site mutation at the NS4A-2K junction in a pIRO-D construct led to a marked shift in NS4B proportions towards the NS4A-2K-NS4B precursor, but not to an almost complete block of precursor processing as is the case in the *trans*-cleavage system (Figure 29b-c). The literature-reported interaction between NS1 and NS4A-2K-NS4B could be reproduced in the polyprotein system but did not show JNJ-A07 sensitivity, consistent with the *trans*-cleavage system (Figure 29a,d).

An additional experiment was designed to investigate which NS4B species get co-precipitated in the pIRO-D system upon reciprocal NS3-HA pulldown. No NS4B-containing species were co-captured unless the P1'Ile cleavage site mutation was integrated into the polyprotein, which in turn led to impairment of NS4A-2K-NS4B processing (Figure 30a-b). In this case, there was pronounced NS4A-2K-NS4B co-precipitation, but this was not alleviated by either JNJ-A07 or Q134A (Figure 30c). Moreover, NS3-HA pulldown of the viral protease complex resulted in co-capture of NS1, which is surprising since these two proteins do not have a direct contact interface. The extent of interaction correlated with the amount of NS4A-2K-NS4B, suggesting that the viral protease complex NS2B/NS3 in the pIRO system is part of a larger multiprotein complex that also involves NS4A-2K-NS4B and NS1 (Figure 30d).

In summary, these results suggest that additional protein-protein interactions that do not occur in the *trans*-cleavage system may stabilize and thus mask the effects of JNJ-A07 on the association of NS2B/NS3 with the NS4A-2K-NS4B precursor.

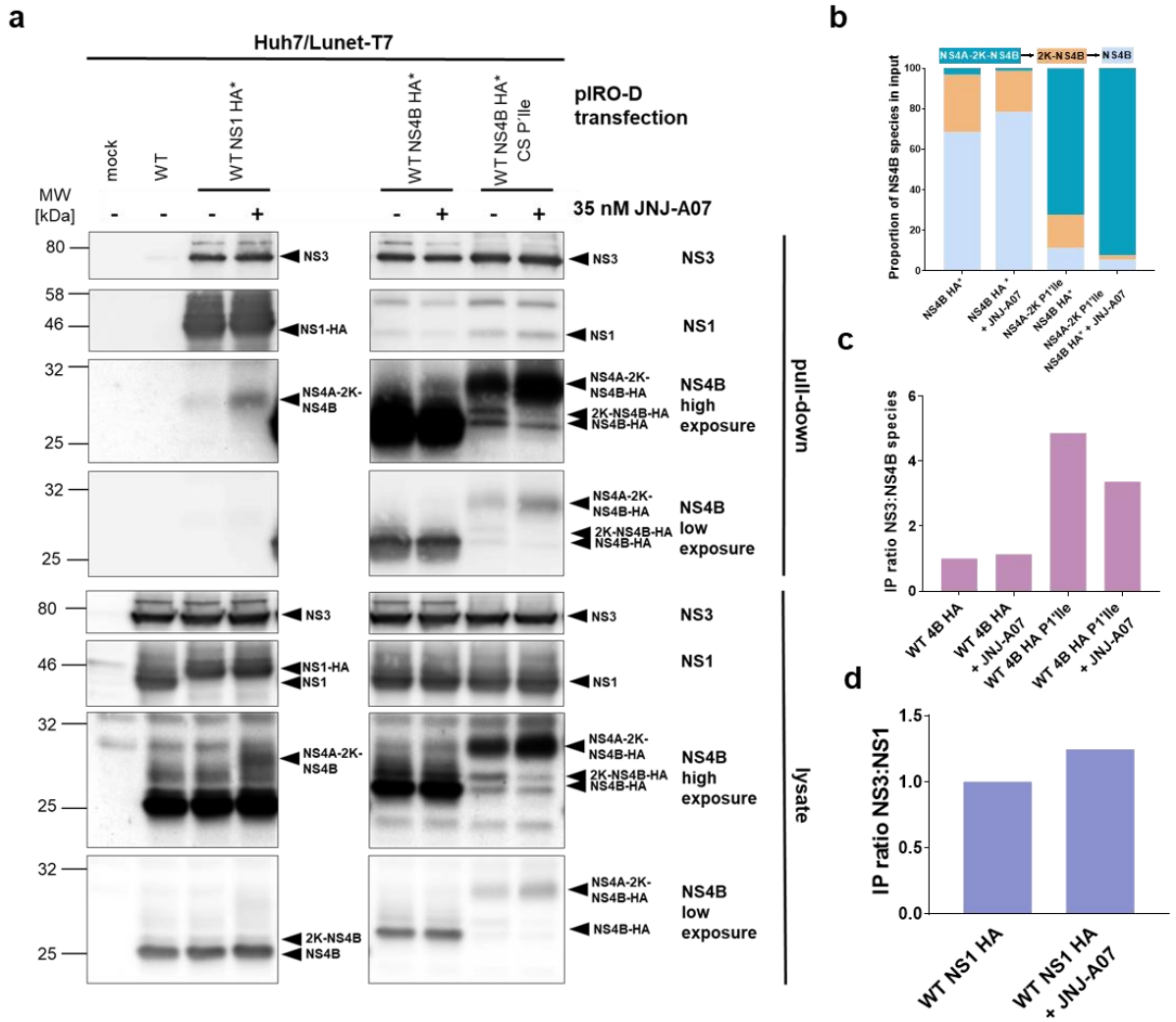

Figure 29. JNJ-A07 and the NS3-nonbinder mutant Q134A display no effect on NS3 co-precipitation in the pIRO-D system.

a, Comparison of NS1-HA and NS4B-HA pulldown in the pIRO-D system. 24 h after seeding, Lunet T7 cells were transfected with indicated constructs (here in a version without delta ribozyme) and treatment with either JNJ-A07 or solvent control was started. Fresh mediun (with or without JNJ-A07) was added after 4 h and 18 post-transfection the cells were harvested. HA-immunoprecipitation was performed according to the standard protocol. Western blot (N=1) shows samples before and after HA-precipitation. **b**, Quantification of NS4B-containing species in the input. For WT polyprotein, the balance of NS4B species is clearly on the side of mature NS4B, while NS4A-2K-NS4B precursor accounts for only a low single-digit percentage. The cleavage site (CS) mutant P1'Ile (mutation between NS4A and 2K) does not cause a complete block of precursor processing as in the trans-cleavage system, but a shift of the equilibrium towards the NS4A-2K-NS4B precursor. In this case, treatment with JNJ-A07 results in a reduction in the proportion of 2K-4B accompanied by an increased proportion of NS4A-2K-NS4B. In the absence of the CS P1'Ile mutation, no clear effect of JNJ-A07 on NS4B composition is observed. **c-d**, The western blot shown in (a) was quantified and IP ratios were calculated between NS4B species and NS3 on the one hand (c), and between NS1-HA and NS3 on the other (d). For none of the conditions analyzed, JNJ-A07 showed an effect on NS3 co-precipitation comparable to the highly significant losses in the *trans*-cleavage system.

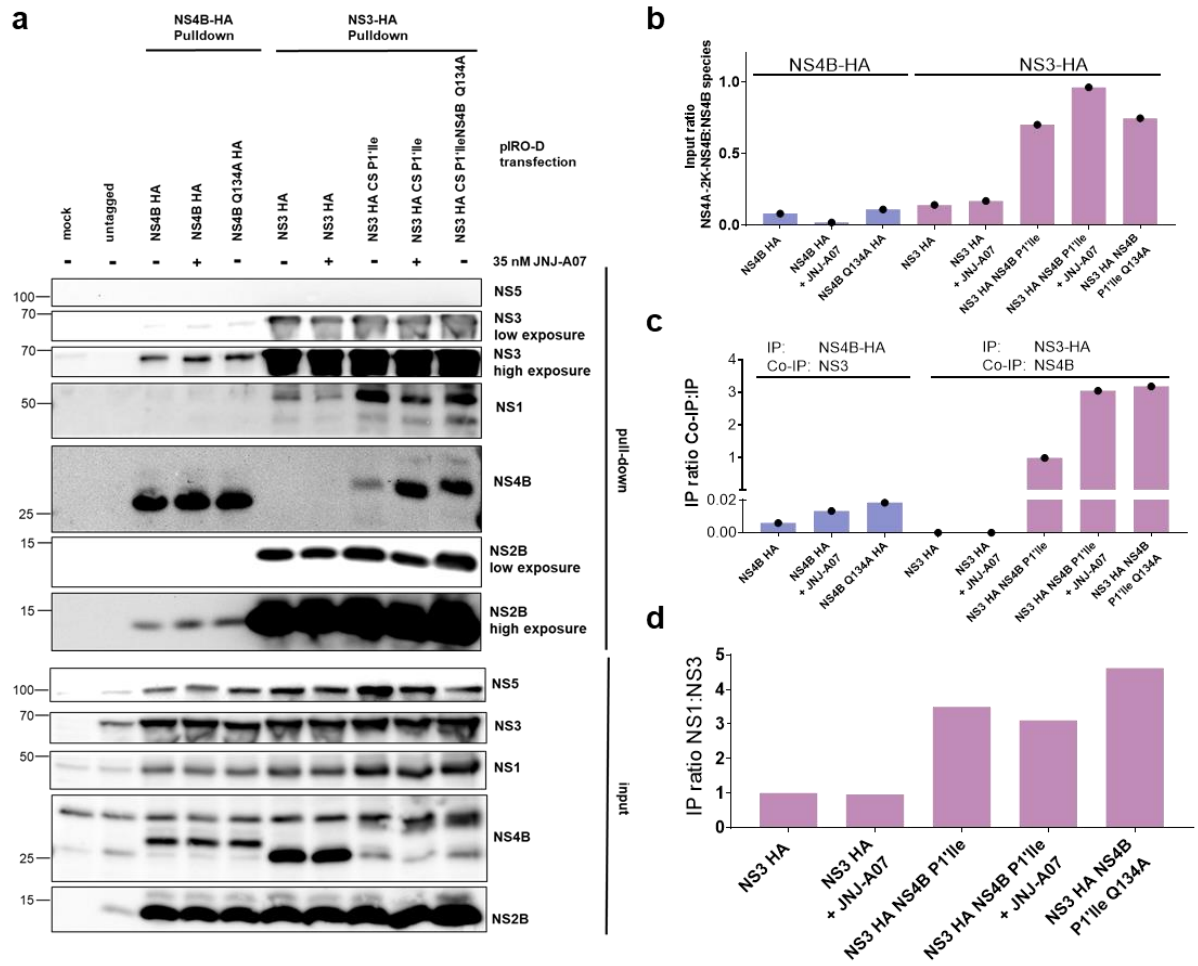

Figure 30. Reciprocal NS3-pulldown co-precipitates NS1 in an NS4A-2K-NS4B dependent manner.
a, Comparison of NS4B-HA pulldown with NS3-HA pulldown in the pIRO-D system. Constructs in this experiment were equipped with a sequence coding for delta ribozyme. Shown is a western blot with samples plotted once before (input) and once after HA-precipitation (N=1). Samples are shown before and after HA-precipitation, with some protein stainings shown with multiple exposure times. The presented western blot served as the basis of various quantifications as depicted in (b), (c) and (d). **b**, Comparison of the fraction of NS4A-2K-NS4B to the total amount of NS4B-containing species in the respective samples. The proportion of NS4A-2K-NS4B precursor in samples without P1'Ile cleavage site mutation is low and becomes strongly dominant by the aforementioned mutation. **c**, NS3-HA pulldown resulted in no measurable NS4B co-precipitation unless the P1'Ile CS mutation was integrated into the polyprotein. In these cases, there was significant co-precipitation of the NS4A-2K-NS4B precursor. The ratio of sample "NS3 HA with P1'Ile cleavage site" was set to 1 and the remaining samples were normalized accordingly. Interestingly, both JNJ-A07 treatment and incorporation of Q134A in the polyprotein tended to increase the interaction, which contrasts with the dramatically decreased co-capturing rate in the *trans*-cleavage system. **d**, For samples subjected to NS3-HA pulldown, the NS1 co-precipitation rate was determined. Please note the correlation of this rate with NS4B co-precipitation on the one hand (c) and with the size of the NS4A-2K-NS4B fraction on the other hand (b).

V.2.6 JNJ-A07-mediated loss of vesicle packets in the pIRO-D system for WT but not for compound resistance mutants

Due to the lack of information about the function of the newly described interaction between the NS4A-2K-NS4B precursor and the viral protease-helicase complex NS2B/NS3, a few known facts about JNJ-A07 and DENV non-structural proteins were used to define a research

direction for the question of how the loss of said interaction leads to a blockade of viral replication. JNJ-A07 blocks DENV RNA replication at a very early stage of the viral replication cycle, i.e. after the release of the RNA genome into the cytoplasm and before virion assembly[376]. Moreover, the two namesake components of the precursor, i.e. NS4A and NS4B were directly or indirectly associated with important roles in ER membrane remodeling [116,165]. Therefore, it was hypothesized that JNJ-A07 might influence the formation of ER-derived DENV replication organelles. This was done again using the pIRO-D system and transfecting Huh7/Lunet-T7 cells with constructs coding for the WT NS1-5 polyprotein or variants thereof harboring JNJ-A07 resistance mutations in NS4B. Cultures were treated with either 35 nM JNJ-A07 or vehicle (Figure 31a) harvested 18 h post-transfection and used to assess transfection efficiency by IF, polyprotein processing by western blot and vesicle packets formation by transmission electron microscopy (TEM). For most constructs, transfection efficiency averaged around 50%, which is adequate for TEM without the need for correlative microscopy (Figure 32a-b). Polyprotein processing was not impacted by either NS4B resistance mutations or JNJ-A07 treatment (Figure 31b). Yet, the cleavage pattern of the NS4B-containing species differed markedly from that obtained in the NS4A-2K-NS4B trans-cleavage system, as virtually exclusively fully processed NS4B was evidenced in the case of the NS1-5 polyprotein (compare Figure 19b and Figure 31b, respectively). Most likely, this is attributable to the high cleavage efficiency in this system, which corroborates the results of the pulse-chase experiments. Irrespective of NS4B mutation and treatment, membrane rearrangements were recorded in all TEM specimens (Figure 31c-d). Among these induced structures are convoluted membranes (CMs) and vesicle packets (VPs), the latter consisting of mostly linear arrays of single membrane vesicles surrounded by a second membrane conforming to the ER. Since the architecture of vesicle packets can only be captured in its entirety by means of tomography, the number of vesicle packet**s** elements (abbreviated in this work as VPEs), i.e., the vesicles that are part of or in proximity to the packets, was counted here to still achieve sufficient throughput in the TEM analysis. From two independent experiments, a cumulative 40 cell profiles were analyzed for the number of detectable VPEs. The values obtained were normalized to the transfection efficiency of each sample to allow comparison between them (Figure 31d). Upon JNJ-A07 treatment, an almost complete loss of VPE formation was observed for the WT polyprotein as well as for a polymorphism with the A137T mutation in NS4B, matching with their sensitivity to the compound in transient replication assays as listed in Figure 14c. Strikingly, 35 nM JNJ-A07 addition did not affect VPE efficiency in any of the NS4B resistance mutants, although this concentration is approximately 45-fold higher than the WT

EC_{50} determined in virus-based replication assays. Moreover, the VPEs of all samples were examined for their morphology (Figure 32c). Whereas JNJ-A07 did not exert a marked effect on vesicle diameter, some of the mutants exhibited statistically significant deviations from the WT, both upward (V91A, T108I) and downward (S85L, L94F). As no correlation was found between the diameter and resistance to the compound, these two features are most likely not related to the mechanism-of-action of JNJ-A07. Nevertheless, this result highlights the involvement of NS4B in the formation of vesicle packets, either as such or as part of the precursor.

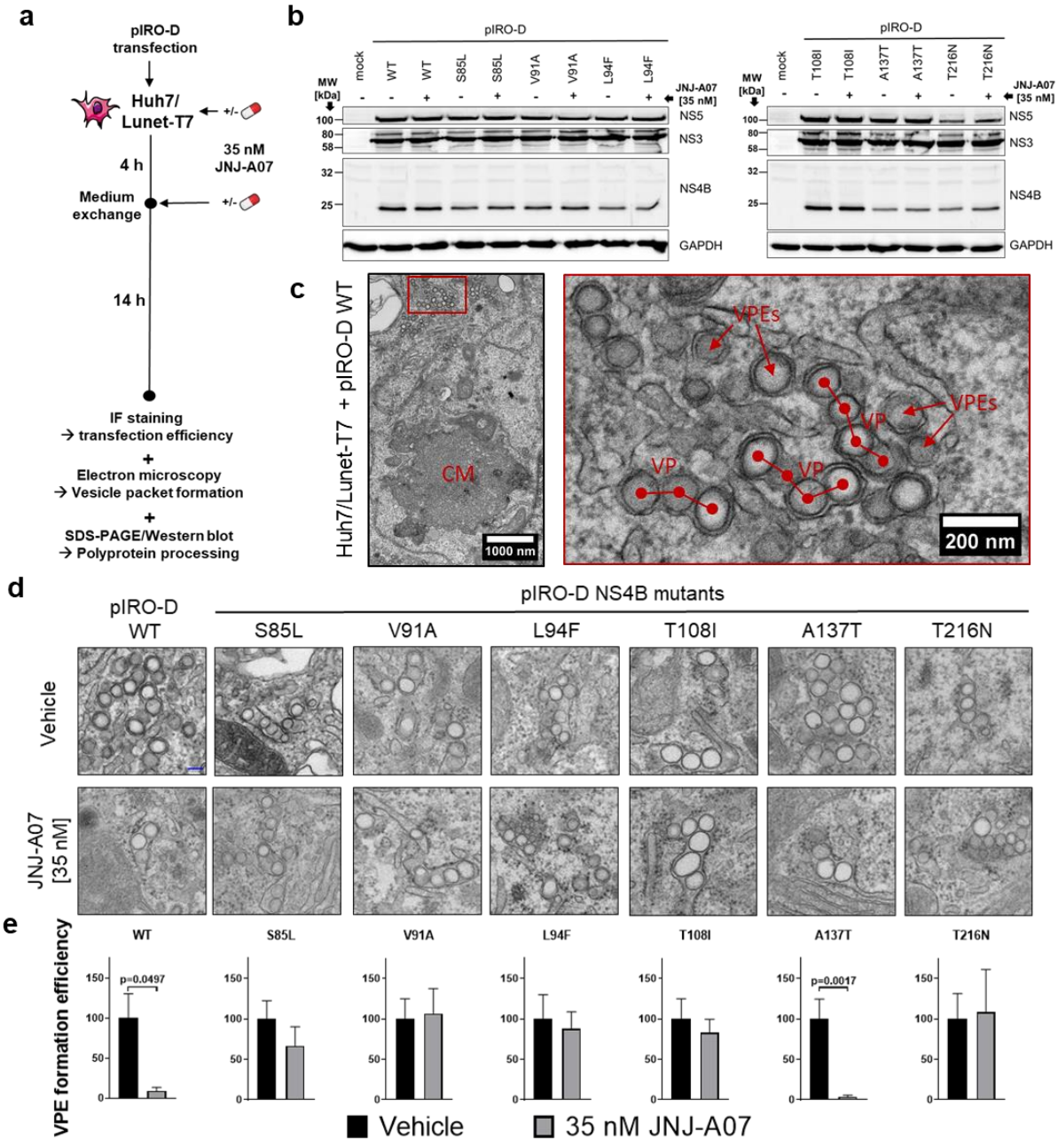

Figure 31. JNJ-A07 induces an almost complete loss of vesicle packets in wild-type cells, but has no marked effect on NS4B mutants resistant to the compound.

a, Experimental procedure. Huh7/Lunet-T7 cells were transfected with pIRO-D plasmids coding for either DENV NS1-NS5 WT or a variant thereof containing a compound resistance mutation in NS4B. Cells were exposed to 35 nM JNJ-A07 or vehicle and 18 h later fixed for immunofluorescence (IF) as well as for transmission electron microscopy (TEM) analysis or lysed to assess protein expression by western blot. **b**, Detection of DENV proteins in transfected cells by western blot. GAPDH was used as a loading control. **c**, TEM analysis of cells transfected with the WT pIRO-D construct. Observed morphological changes include convoluted membranes (CMs) and vesicle packets (VPs), which are string-like arrays of vesicles, here termed vesicle packet elements (VPEs). The panel on the right shows a magnified view of the area framed by the red box in the left panel. **d**, Representational electron micrographs showing VPEs detected in cells upon transfection with the constructs indicated at the top. Blue scale bar = 100 nm. **e**, Quantification of VPEs from 2x 20 cell profiles per transfected cell specimen (n=2), corrected for transfection efficiency as determined by IF (see Supplementary Figure 4a-b). For each construct, the VPE formation efficiency measured with vehicle-treated control cells was adjusted to 100. Results are presented as mean and SEM. Statistically significant effects are highlighted by corresponding p-values as calculated by Dunn's multiple comparison test.

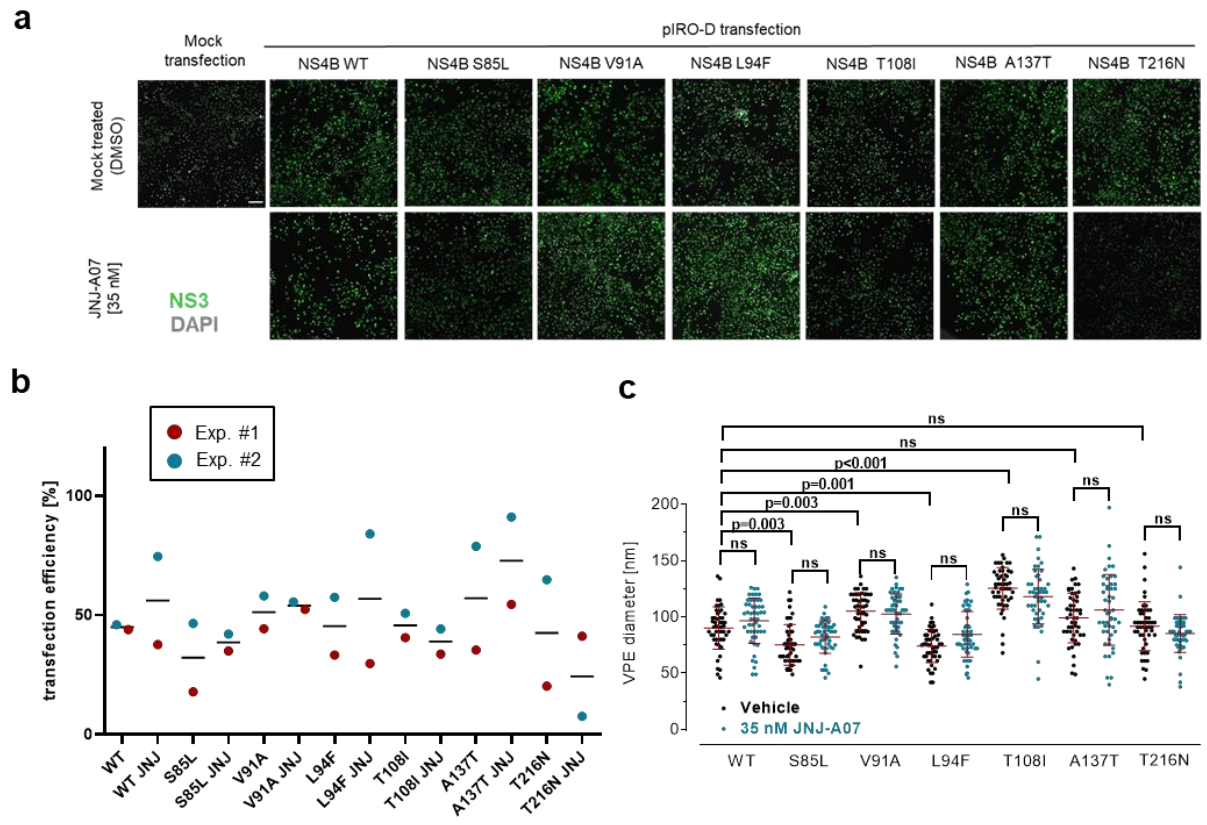

Figure 32. Mutations in NS4B that confer compound resistance can alter the average diameter of vesicle packets elements.
a, To determine the transfection efficiency of pIRO-D WT and mutant constructs, immunofluorescence experiments were conducted with staining against NS3. Sample images from one of the two experimental runs are shown. Scale bar = 500 µm. **b**, Transfection efficiencies of the two sets of experiments. A minimum of 1000 cells were automatically scored for each sample. **c**, For each sample, the diameter of 50 randomly chosen VPEs was assessed. Individual values are shown with mean and standard deviation. Two-way ANOVA followed by Šidák's multiple comparison test was used for statistical analysis.

V.2.7 Interaction between DENV NS2B/NS3 and NS4A-2K-NS4B is functionally linked to replication organelle formation

Previously reported data provided evidence that JNJ-A07 blocks the interaction between NS2B/NS3 and the NS4A-2K-NS4B precursor and prevents the formation of DENV replication organelles, thus raising the question of whether these two phenotypes are functionally linked. Attempting to answer this question, the NS4B mutants Q134A and M142A appeared to be suitable tools. These reside in the cytosolic loop between TMD3 and TMD4 and were known to prevent DENV RNA replication. Furthermore, they were rescued by second-site compensatory mutations. The two primary mutations, not only blocked viral replication, but also drastically reduced the interaction between NS2B/NS3 and NS4A-2K-NS4B, suggesting that the former outcome is a consequence of the latter[117]. As depicted in Figure 33a-b, replication of Q134A was virtually rescued by A69A and A137V, whereas

replication of M142A was at least partially rescued by the JNJ-A07 resistance mutation L94F and by T215A, the latter conveying resistance to NITD-688[371]. The trans-cleavage assay performed here (Figure 33c) confirmed that the Q134A and M142A mutations in NS4B significantly diminished the interaction between NS4A-2K-NS4B and NS2B/NS3 (Figure 33d-e). The finding that the combination of Q134A with its pseudoreversions resulted in an almost complete restoration of this interaction was highly interesting, whereas the M142A mutant in combination with the L94F pseudoreversion resulted in a partial restoration (Figure 33e). This degree of recovery correlated well with the replication competence of the mutants, as reported in the past[117]. A remarkable correlation was noted when these mutants were assayed for their ability to form replication organelles (Figure 34). While VPEs were completely absent for the Q134A mutant, insertion of the two pseudoreversions A69S and A137V re-established VPE formation at WT levels (Figure 34d-e). The NS4B mutation M142A also decreased the efficiency of VPE formation by more than 99%, which was restored to approximately 60% of WT efficiency when the two pseudoreversions were combined with this primary mutation (Figure 34d-e). Interestingly, tubular membrane structures were abundant in this triple mutant, usually accounting for only a few percent in other samples (Figure 35). It is difficult to estimate from a two-dimensional projection whether those VPEs that appeared round were truly spherical or tubular ones recorded in the transverse plane. For this purpose, a tomogram would be useful. Similarly, it remains to be clarified whether RNA replication in this mutant takes place in these tubular structures.

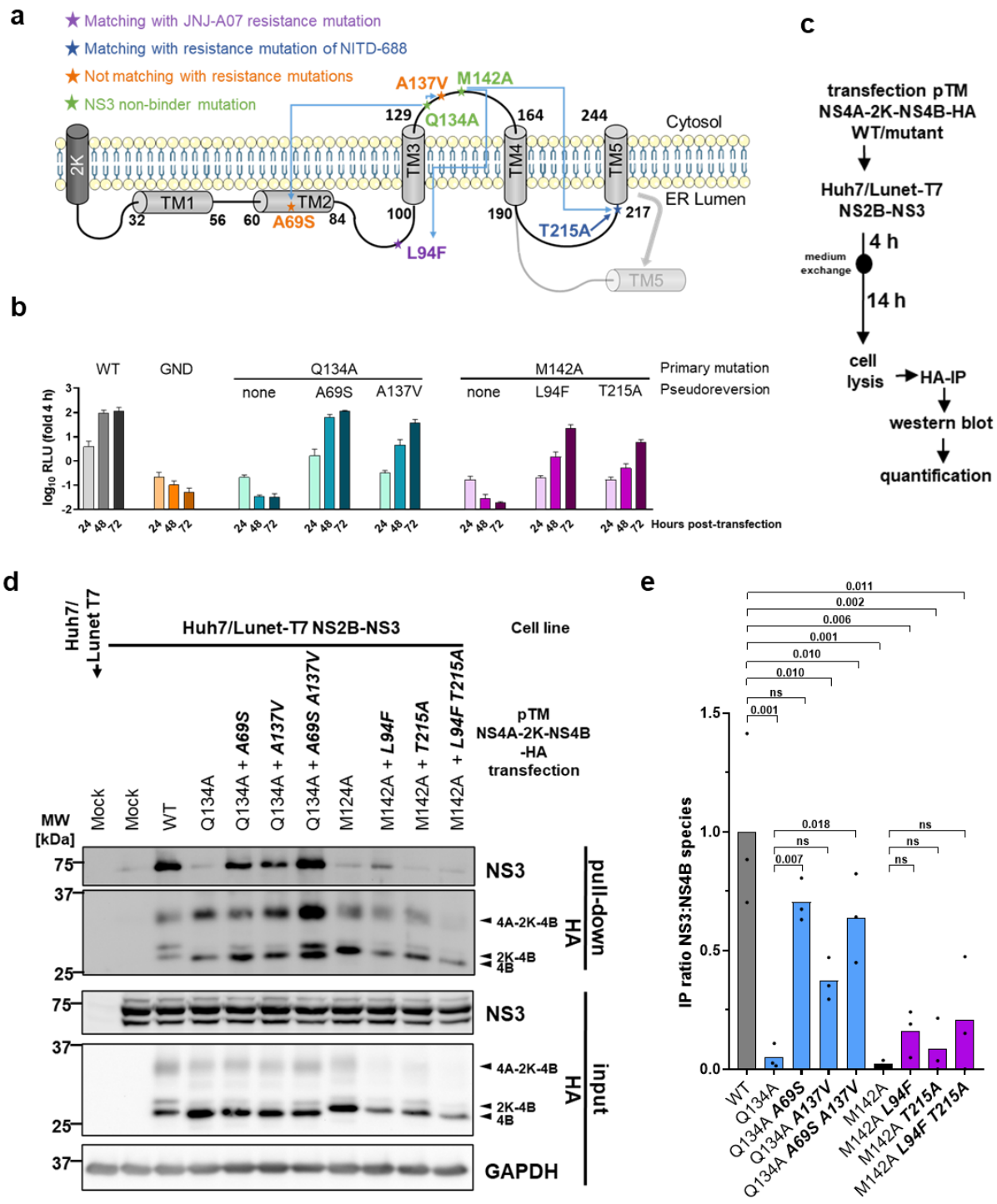

Figure 33. Pseudorevertants of NS3 non-binder mutants NS4B Q134A and M142A rescue the NS3 – NS4B interaction.

a, Membrane topology of NS4B (according to Miller et al. 2006) and location of the NS3 non-binder mutations Q134A and M142A (in green), together with their corresponding pseudoreversions. **b**, Replication kinetics of sgDVs-R2A replicons carrying the NS4B mutations Q134A and M142A, with and without second site pseudoreversions. Modified from Chatel-Chaix et al.[117]. WT and GND mutants were used as positive and negative controls, respectively. Intensity values derived from luciferase measurements were normalized to the 4 h time point, which reflects input RNA. **c**, Experimental setup to study the ability of pseudoreversions to restore the interaction between NS4A-2K-NS4B and NS2B-NS3. **d**, Western blot representative. Protein complexes captured by HA-tag were analyzed together with the corresponding input (20%). GAPDH was used as loading control. Numbers on the left indicate molecular weight (MW) in kDa. d, To obtain the IP ratio of NS3 and NS4B-

containing species, Western blot quantification of three independent experiments was conducted. Repeated measures one-way ANOVA followed by Šidák's multiple comparison test was used for statistical significance analysis. P-values are given; ns = non-significant.

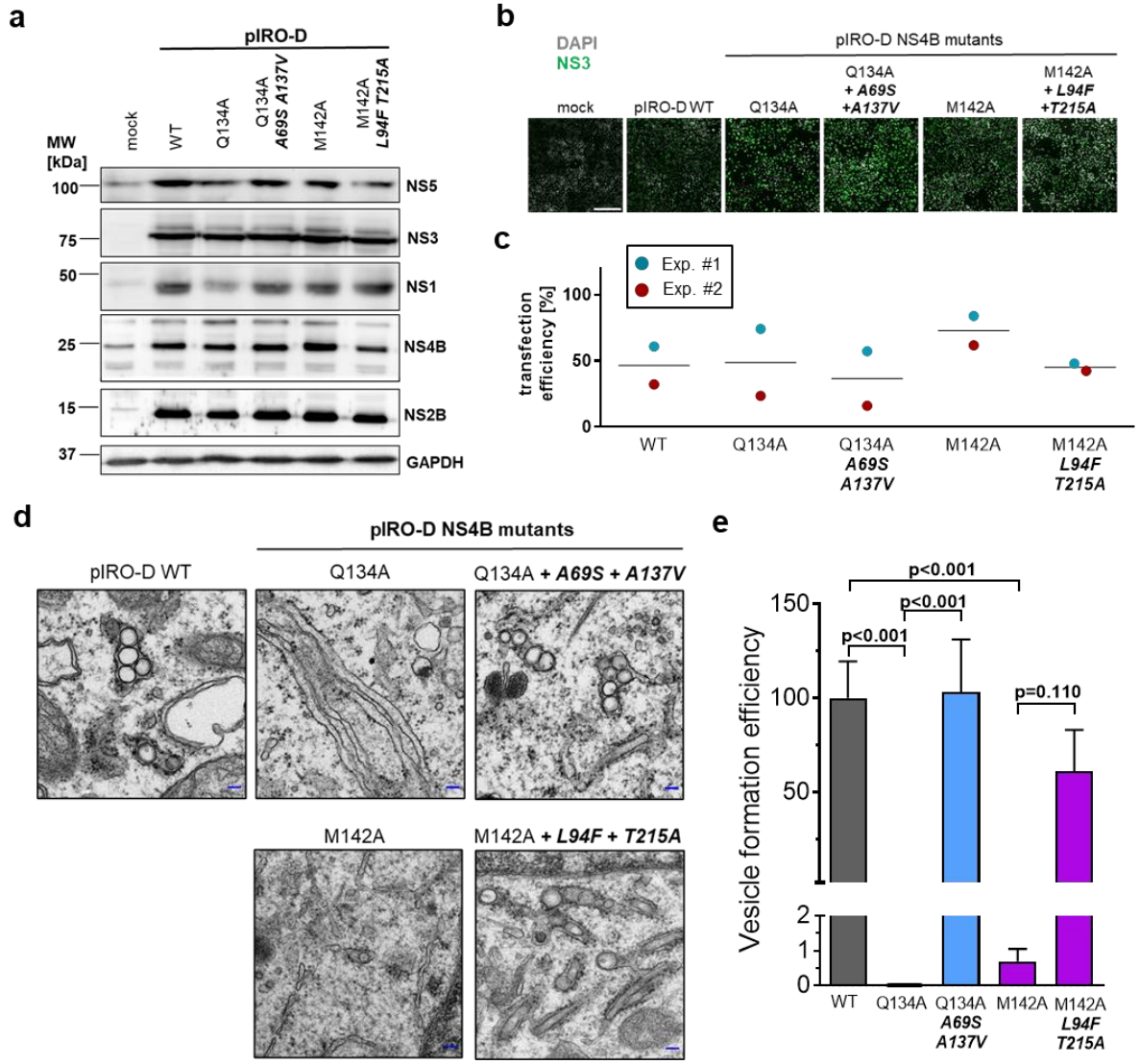

Figure 34. Pseudorevertants of NS3 non-binder mutants NS4B Q134A and M142A also restore the formation of vesicle packets.

a, Cells transfected with pIRO-D (WT or variants harbouring named mutations in NS4B) were examined by western blot to determine protein expression and polyprotein processing. No significant deviations were detected for any of the mutants relative to the WT reference. **b-c** Immunofluorescence was employed to assess the transfection efficiency of the pIRO-D WT and mutant constructs. NS3 was labelled with a monoclonal antibody and probed with a secondary fluorescent antibody. Exemplary images from one of the two experimental runs are depicted in (b). The white scale bar marks 500 µm. A minimum of 1000 cells per condition were evaluated to determine transfection efficiency. The outcomes of both experimental runs are presented in (c). **d-e**, TEM examination of NS3-non-binder mutants and pseudorevertants (emphasized by bold and italic letters). The experimental procedure followed that described in Figure 31a, except that no compound treatment was performed. Typical electron micrographs for each sample condition are depicted in (d). Blue scale bar = 100 nm. To quantify VPEs, twenty cell profiles from each of two independent experiments were analyzed. Values were normalized for transfection efficiency (e).

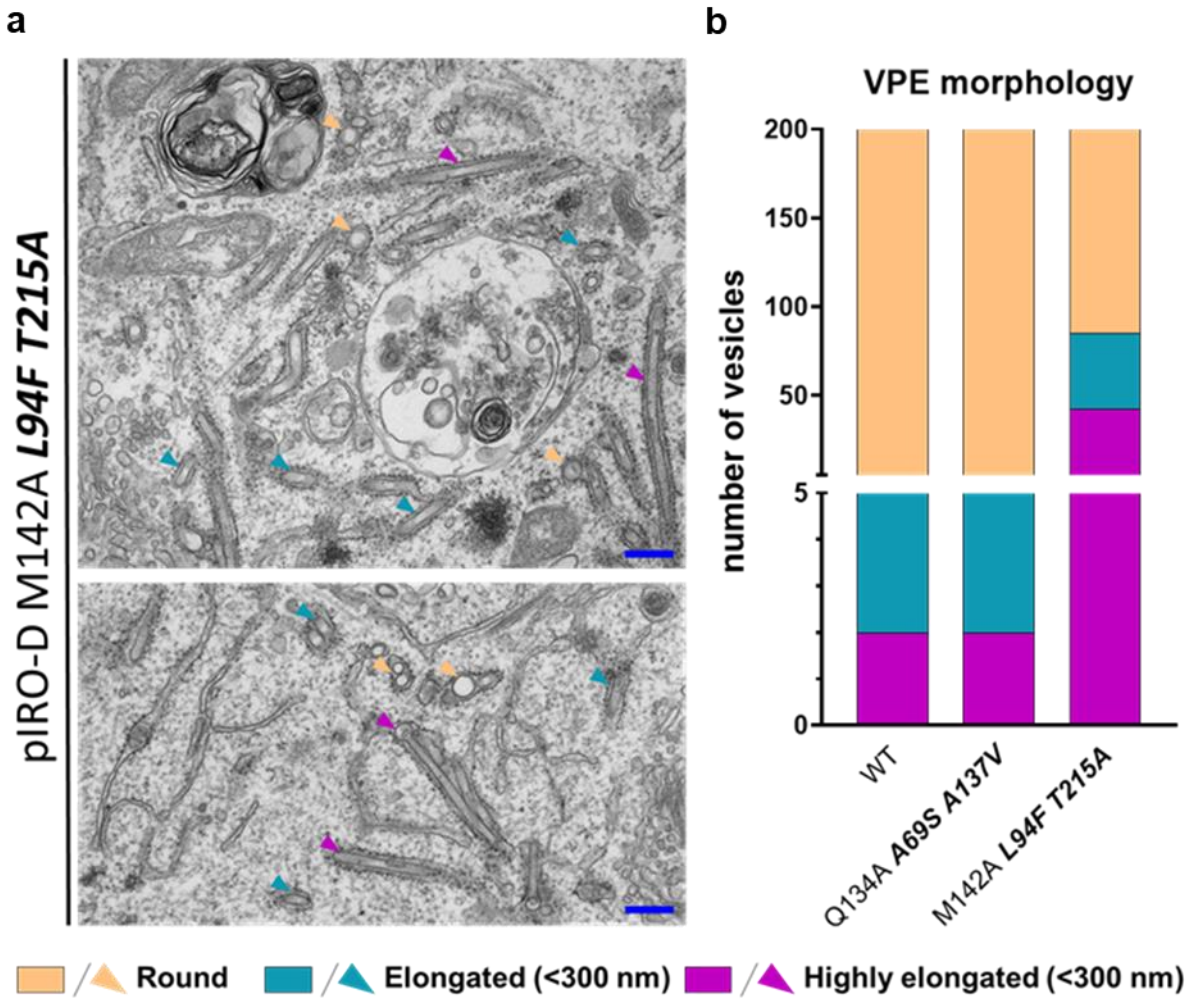

Figure 35. The NS3 non-binder mutant M142A, in combination with the two pseudoreversions L94F and T215A, exhibits a greatly increased proportion of strongly tubular VPEs.
a, Sample images of two independent cell profiles displaying vesicle elongation in cells transfected with pIRO-D NS4B M142A L94F T215A. Colored arrowheads denote representative VPEs of the categories "round" (in yellow), "elongated" (in cyan) and "highly elongated" (in magenta). Scale bar = 300 nm. **b**, Analysis of the triple mutants M142A L94F T215A revealed prominent differences from WT concerning VPE morphology. The fraction of highly elongated VPEs was found to be substantially increased compared to both the WT and the second triple mutant studied, Q134A A69S A137V. Compensatory pseudoreversions are emphasized by bold and italic letters.

V.2.8 JNJ-A07 blocks *de novo* formation of vesicle packets but does not disrupt established ones

As already mentioned in this work, it was known from *in cellulo* experiments that the antiviral effect of JNJ-A07 decreased gradually with the time between infection and the addition of the substance to the cells (Figure 12d). Furthermore, it was found that JNJ-A07 does not disrupt existing NS4A-2K-NS4B and NS2B/NS3 complexes, but rather blocks their *de novo* formation. In addition, a striking correlation between the loss of this interaction and the formation of vesicle packets was found by means of the NS3-nonbinder mutants. Thus, the

question arose whether JNJ-A07 selectively inhibits the *de novo* formation of vesicles instead of disrupting already existing ones.

In a first TEM-based experimental approach, cells transfected with the NS1-5 encoding pIRO-D plasmid were treated with JNJ-A07 4 h or 16 h after transfection (Figure 36a) and in both cases, harvested 20 h after transfection. While in the early treatment the substance was present at a time when vesicle packets were forming, in the cells treated 16 h after transfection these had time to form in large quantity before the substance was added. Under both conditions, polyprotein processing remained unimpaired (Figure 36b). The early treatment induced an almost complete loss of vesicle packets, whereas in cells to which JNJ-A07 was added late after transfection, the efficiency of vesicle formation was reduced to a markedly smaller extent (Figure 36c-f). However, as the treatment period in the latter case was also shorter, it was not feasible to unambiguously deduce whether JNJ-A07 causes active, albeit slow, disruption of existing vesicle packets, or instead suppresses their *de novo* formation. To circumvent this confounding effect, an additional experimental approach was undertaken in which protein synthesis was blocked by cycloheximide (CHX) at a time when vesicle packets had already formed (Figure 37a). In this way, the *de novo* formation of further vesicle packets was restrained, allowing the selective analysis of their natural decay. A CHX mono treatment was compared with a CHX + JNJ-A07 double treatment, the rationale being that the latter would only produce a greater reduction over the former if JNJ-A07 could cause active disruption. An essential prerequisite for this was a complete stop of RNA translation by the level of CHX administered, which was ensured by means of a ribopuromycylation assay (Figure 37b). TEM analysis revealed a similar number of VPEs in cells treated with JNJ-A07 and CHX compared to cells treated with CHX alone, suggesting that JNJ-A07 does not trigger VPE decay (Figure 37c-f).

In combination, these results imply that the interaction between NS2B/NS3 and NS4B-containing proteins is a requirement for the formation of vesicle packets. All evidence points to JNJ-A07 blocking *de novo* biogenesis of vesicle packets but not disrupting ones, concordant with the compound preventing, but not breaking, NS2B/NS3 interaction with NS4A-2K-NS4B.

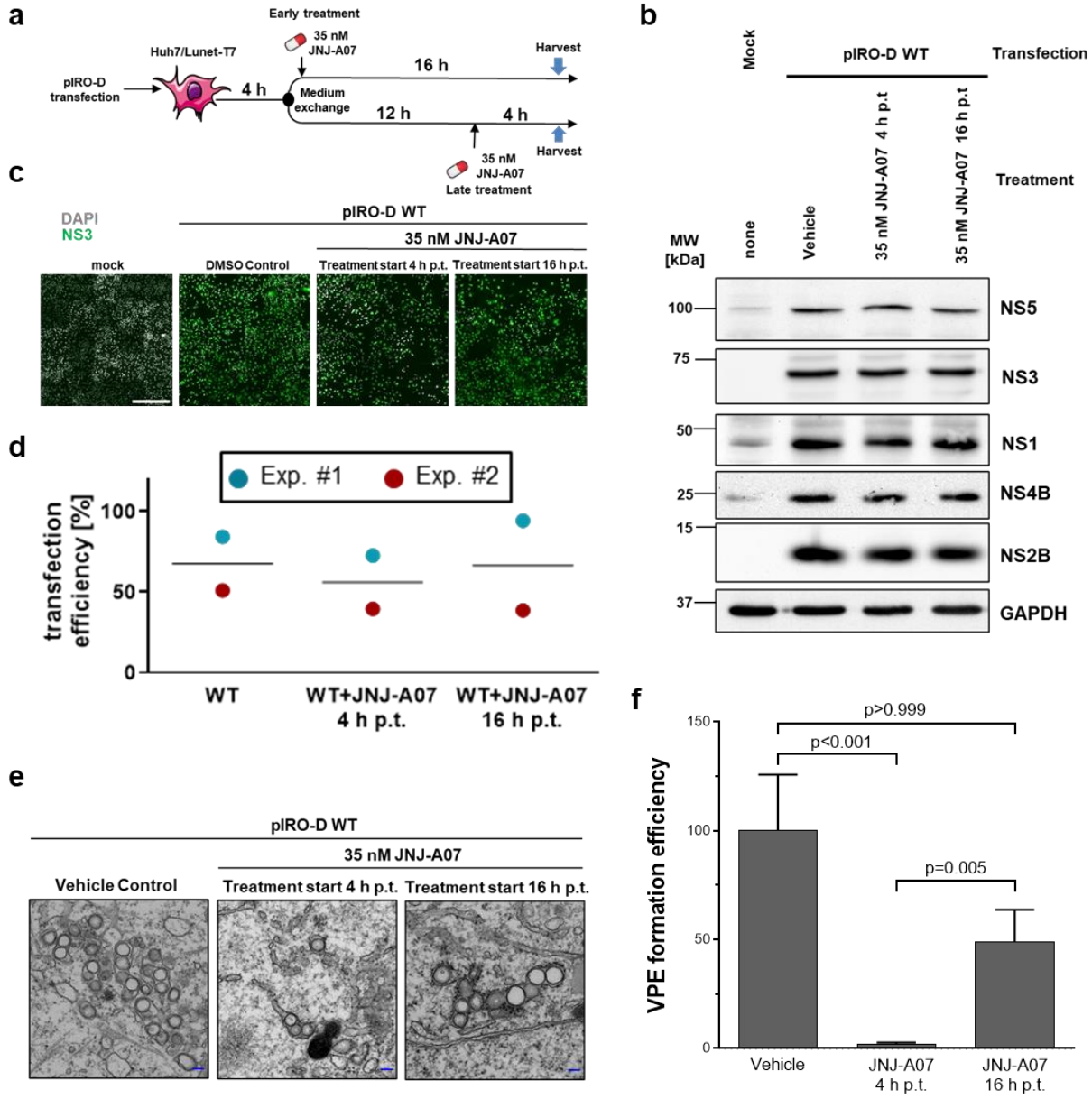

Figure 36. Compared with early JNJ-A07 treatment, the reduction in vesicle packet formation efficiency is smaller in a late treatment scenario.

a, Concept of the experiment. Huh7/Lunet-T7 cells treated at an early and a late time point were collected in parallel and subjected to TEM, WB and IF analysis to assess VPE formation, polyprotein expression and processing, and transfection efficiency. **b**, At 35 nM, JNJ-A07 had no discernible effect on polyprotein processing, regardless of the time of compound addition. One of two western blots is presented. Molecular weight references are given in kDa on the left. **c**, Immunofluorescence NS3 staining to determine transfection efficiency. One of two independent data sets is shown. Scale bar: 500 µm. **d**, Graph displaying the calculated transfection efficiencies from both data sets. **e**, Sample electron micrographs (n=2). Scale bar = 100 nm. **f**, Bar graph plotting VPE formation efficiency with mean and SEM for early and late JNJ-A07 treatment relative to vehicle-treated control cells. VPEs from 20 cell profiles per condition and experiment (n=2) were quantified and normalized to transfection efficiencies as shown in (d). The reported p-values were calculated by Dunn's multiple comparison test performed after a Kruskal-Wallis test.

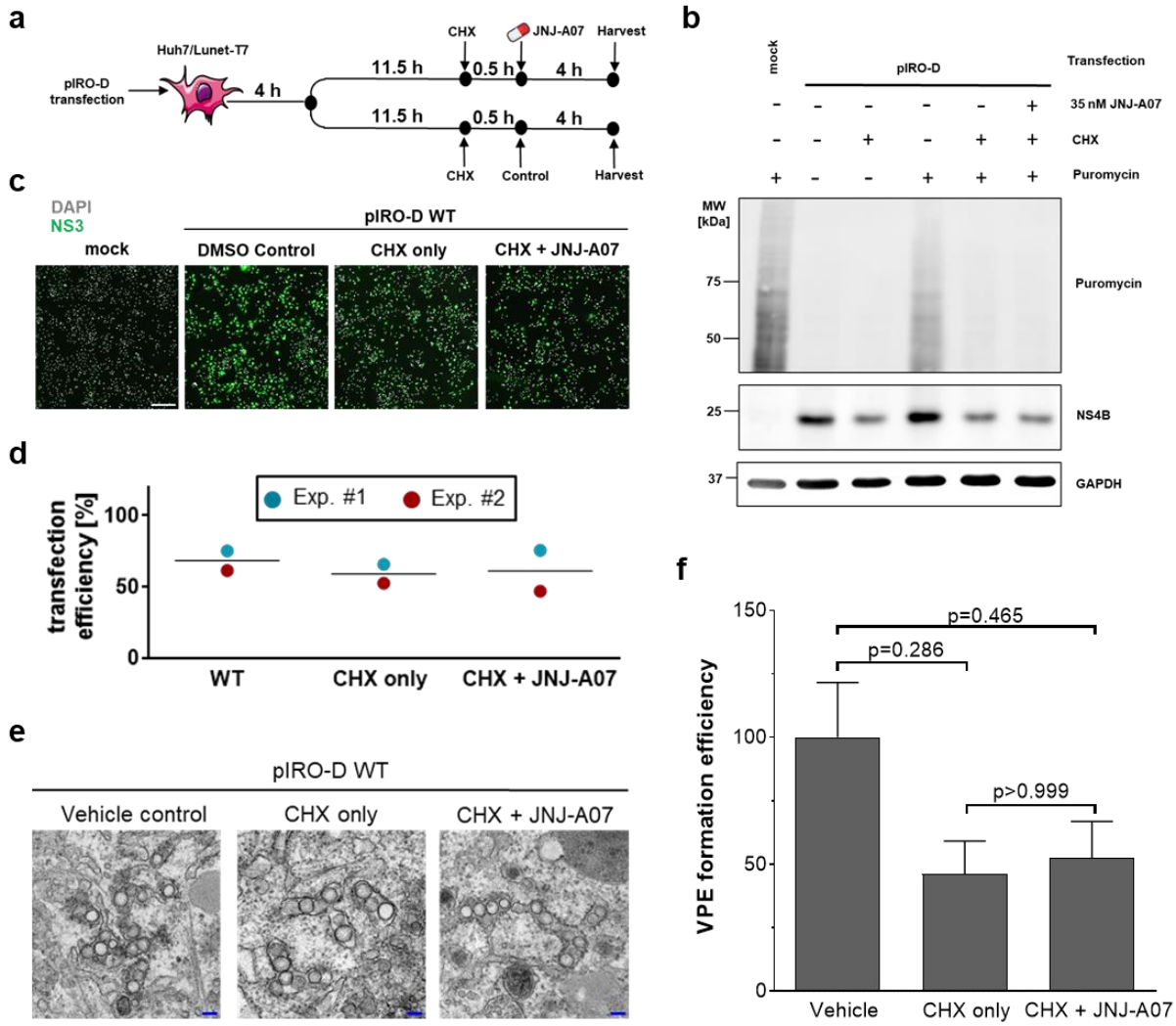

Figure 37. JNJ-A07 prevents the *de novo* formation of vesicle packets but does not affect the integrity of those already formed.
a, Experimental design to distinguish between blockade of *de novo* VPE formation and active VPE disruption. Cells were either pretreated with cycloheximide (CHX; 200 µg/ml) 30 min prior to the addition of JNJ-A07 (35 nM) or treated with CHX exclusively. **b**, Western blot of a ribopuromycylation assay carried out to assure total CHX-mediated block of protein translation. Cells were treated with puromycin (1g/ml) in the last 5 minutes prior to collection. The translation rate is reflected by the amount of puromycin-incorporating polypeptide chains, visualized on WB with a puromycin antibody. **c**, NS3-IF staining for the cycloheximide experiment. Scale bar: 500 µm. **d**, Transfection efficiencies for the cycloheximide experiment were determined by the proportion of NS3-positive cells in the IF analysis. **e**, Example electron micrographs showing vesicle packets in differentially treated cells as outlined in (a). Scale bar = 100 nm. **f**, Efficiency of VPE formation (mean and SEM) derived from the VPE quantification of 20 cell profiles per condition and experiment (n=2). Values were normalized to vehicle-treated cells (vehicle), which were set to 100%. Indicated p-values were calculated by Dunn's multiple comparison test, following a Kruskal-Wallis test.

V.2.9 The mechanism-of-action of the NS4B inhibitor NITD-688 shares features with that of JNJ-A07

Lately, a further DENV inhibitor termed NITD-688 has been reported that targets NS4B while exhibiting a resistance profile that partly overlaps with that of JNJ-A07[371]. Since no detailed

mechanism-of-action has been characterized for this compound to date, an investigation was conducted here to examine whether NITD-688 acts similarly to JNJ-A07. A first step in the comparative study was to review possible effects of NITD-688 on the interaction of NS2B/NS3 with NS4A-2K-NS4B in the *trans*-cleavage system (Figure 38a) by using escalating drug concentrations (from 1 nM to 10,000 nM). Interestingly, the two JNJ-A07-related phenotypes in this system, i.e. loss of NS2B/NS3 co-precipitation with NS4A-2K-NS4B on one side and impaired precursor processing (indicated by the reduction in 2K-NS4B signal) on the other side, could be reproduced for NITD-688 (Figure 38b-c). However, in line with the approximately 900-fold lower antiviral activity of NITD-688 in comparison with JNJ-A07, much higher concentrations of the compound were required to reach a certain effect level (EC_{50} around 3,900 nM and 500 nM, respectively). Strikingly, when analyzing the effect of NITD-688 on DENV vesicle packets formation, just as for JNJ-A07, suppression of *de novo* biogenesis of VPEs was noted, whereas at a later treatment time point, a considerably smaller effect was detected, which is interpreted in the sense that established VPEs could not be resolved by NITD-688 (Figure 38d-h). Taken together, the uncovered findings imply that the DENV inhibitors NITD-688 and JNJ-A07 share a similar mechanism-of-action by blocking the interaction between NS2B/NS3 and NS4A-2K-NS4B thereby compromising the formation of vesicle packets, the putative sites of DENV RNA replication.

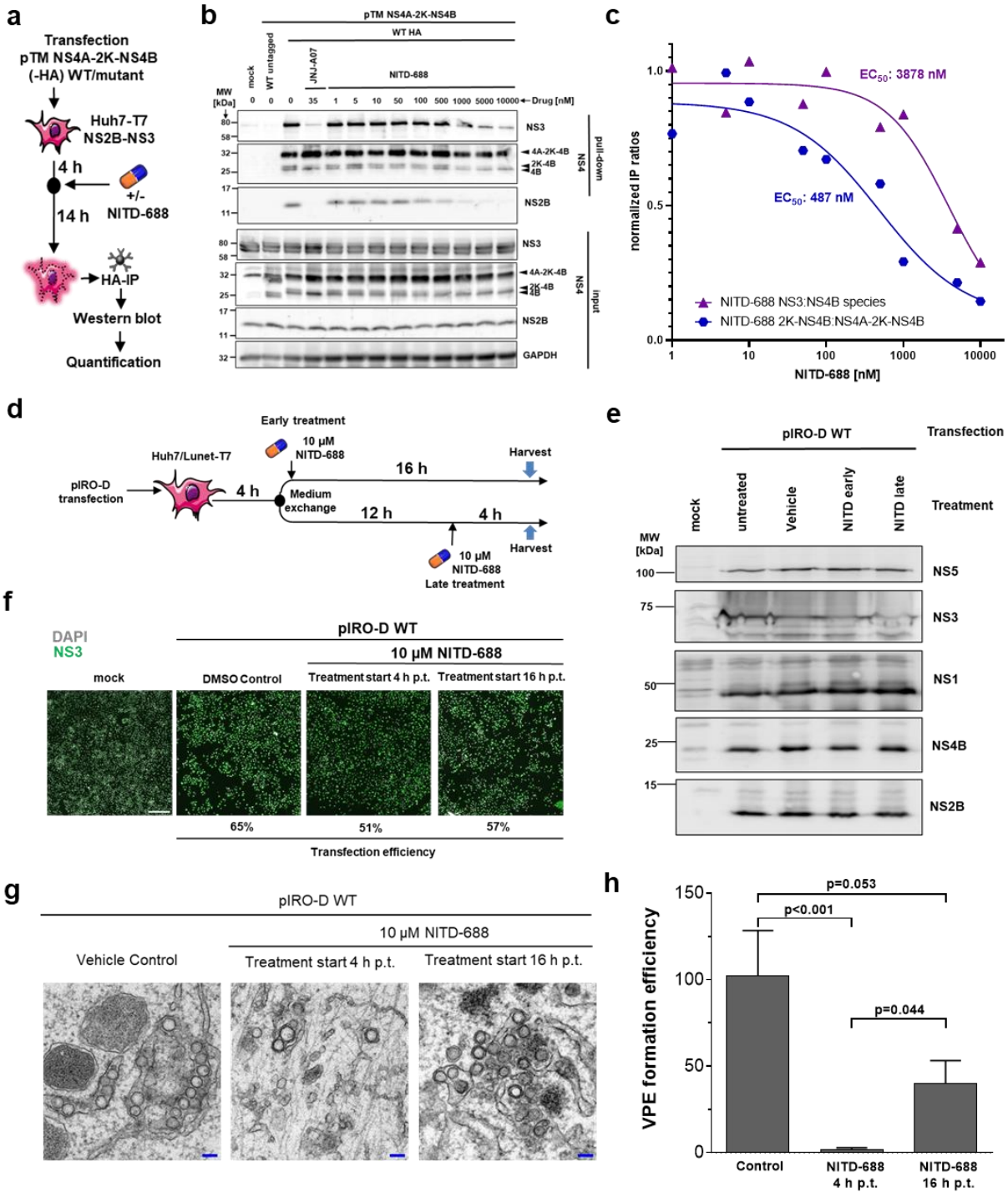

Figure 38. The mechanism-of-action of NITD-688 is similar to the one of JNJ-A07 but requires higher compound concentrations.

a, Experimental design of the dose-response assay: Huh7/Lunet cells that stably express T7 RNA polymerase and DENV NS2B-NS3 were transfected with T7-based expression plasmids encoding NS4A-2K-NS4B(-HA). At 4 h post-transfection, cells were treated with specified concentrations of NITD-688 (or JNJ-A07 as control) and were harvested 14 h later. **b**, Cell lysates were subjected to HA-specific pull-down and were analysed by western blot (N=1). Specimens are shown both as input before HA precipitation and once as eluate after HA precipitation (enrichment factor 4). GAPDH served as loading control. **c**, The western blot shown in (b) was quantified. The ratios of both NS3 and 2K-NS4B to NS4B species were measured after HA precipitation and plotted on an XY graph. Dose-response curves were fitted to the values, based on which EC_{50} values were calculated. **d**, Transmission electron microscopy was employed to investigate whether NITD-688 affects vesicle packets formation and if the timing of treatment is critical. To this end, the experimental design of Figure 31a was adopted

and the JNJ-A07 treatment was replaced by 10 µM NITD-688. **e**, Polyprotein processing control is presented. The numbers on the left indicate the molecular weight in kDa. GAPDH was used as a loading control. **f**, Detection of NS3 by immunofluorescence microscopy to assess transfection efficiency for the indicated samples. Scale bar: 500 µm. **g**, Exemplary image sections from recorded cell profiles showing induced vesicle packets in the samples examined. Scale bar = 100 nm. **h**, Similar to the results with JNJ-A07, NITD-688 (10 µM) showed a highly significant decrease in VPE at early treatment, which was less pronounced at late treatment. For the data shown, 20 cell profiles per sample were evaluated from a single data set. Reported p-values were calculated using Dunn's multiple comparison test, performed after a Kruskal-Wallis test.

V.3 JNJ-1802 prevents complex formation between NS3 and NS4B species

In the chronological course of the overarching development project of novel DENV antiviral compounds, JNJ-A07 was the first candidate to be characterized in preclinical studies comprising various aspects such as *in vivo* potency or mechanism-of-action. JNJ-1802 (whose structure is illustrated in Figure 39a) is from the same chemical series as JNJ-A07 and was reported to exert *in vitro* antiviral activity against the different DENV genotypes[378]. Owing to improved preclinical safety profile, JNJ-1802 was selected for clinical development[378]. JNJ-1802, was shown to be safe and well-tolerated in a Phase 1, first-in-human clinical study and is now being evaluated in Phase 2a clinical studies for the prevention and treatment of DENV infections[398]. In a collective team effort, we recently published a paper on the preclinical development of JNJ-1802, in which we demonstrated, among other things, *in vivo* efficacy against DENV-1 and DENV-2 infections in non-human primates, something that has never been shown before for a DENV antiviral[378]. As part of that work, I examined whether JNJ-1802 also prevents *de novo* complex formation between NS4A-2K-NS4B and the viral protease/helicase complex. I transiently transfected Huh7-T7 NS2B-NS3 cells with a construct encoding NS4A-2K-NS4B, with NS4B being C-terminally tagged with a hemagglutinin affinity tag (HA^{Ct}). In addition, I generated NS4A-2K-NS4B constructs that contained single mutations in the NS4B sequence (V91A, L94F, or T108I, respectively) originating from the profile of JNJ-1802 resistance mutations previously identified by project partners (Figure 39b). Escalating concentrations of JNJ-1802 were added to cell cultures, and cell lysates as well as protein complexes captured via the HA-tag were analyzed by western blot (Figure 39c). A loss of co-precipitated NS3 was evident even at very low concentrations of JNJ-1802, whereas higher concentrations of the compound were required for the three NS4B resistance mutants (Figure 39d-f). Furthermore, an altered cleavage pattern of the NS4A-2K-NS4B precursor was again monitored, which was most evident for the 2K-NS4B intermediate, for which a dose-dependent decrease was observed (Figure 40).

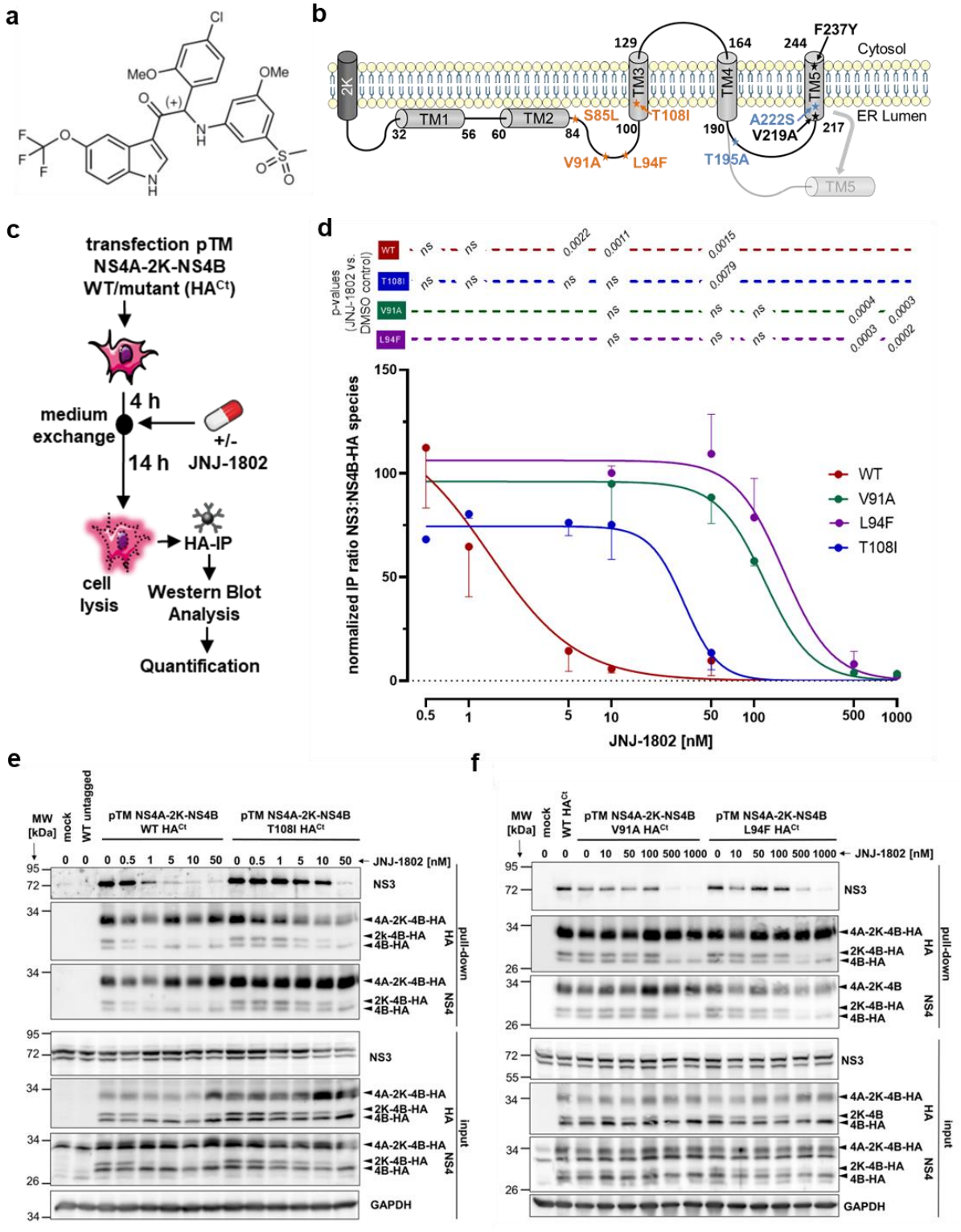

Figure 39. JNJ-1802 prevents the interaction between DENV NS4B and NS3.
a, Molecular structure of JNJ-1802. **b,** Simplified membrane topology of DENV NS4B according to Miller et al.[172]. JNJ-1802-selected resistance mutations colored in orange were present in ≥99% of the quasispecies at the endpoint (passage 42 [sample A]; passage 50 [sample B]) in either of the two independently selected resistant strains. Mutations marked in black were present in <50% of the quasispecies at endpoint; mutations highlighted in blue were transient and had vanished by the end of the experiment. TM, transmembrane. **c,** To determine an effect of JNJ-1802 on NS4A-2K-NS4B precursor-specific interaction with NS2B-NS3, Huh7 cells stably expressing T7 RNA polymerase and DENV-2 NS2B-NS3 were transfected with T7-based expression plasmids

coding for NS4A-2K-NS4B(-HA^{Ct}) (NS4B corresponding to wild-type [WT] or mutant NS4B). At 4 h post-transfection, cells were treated with various concentrations of JNJ-1802 or DMSO, harvested 14 h later and the lysates were used for HA-specific pull-down and subsequent western blot analysis of the captured complexes. **d,** Three independent Co-IP experiments were performed to establish the JNJ-1802 dose-response curves for NS4B interaction with the viral protease complex NS2B/NS3. Ratios of western blot signal intensities of NS3 to the sum of all HA-tagged NS4B-containing species (NS4A-2K-NS4B-HA, 2K-NS4B-HA and NS4B-HA) were determined using NS3- and HA-specific antibodies, respectively, and normalized to the ratio of the corresponding DMSO-treated control. Results are expressed as mean ± standard error of the mean. One-way repeated measures ANOVA followed by Dunnett's multiple comparison test was used to calculate p-values for the comparison of NS3:NS4B-HA ratios between JNJ-1802-treated samples and DMSO control. **e-f,** Shown is a representative set of western blots from the experiment described in (c), containing either WT NS4B and NS4B T108I samples (e) or NS4B mutants V91A and L94F (f). Please note the higher compound concentrations compared to (e).

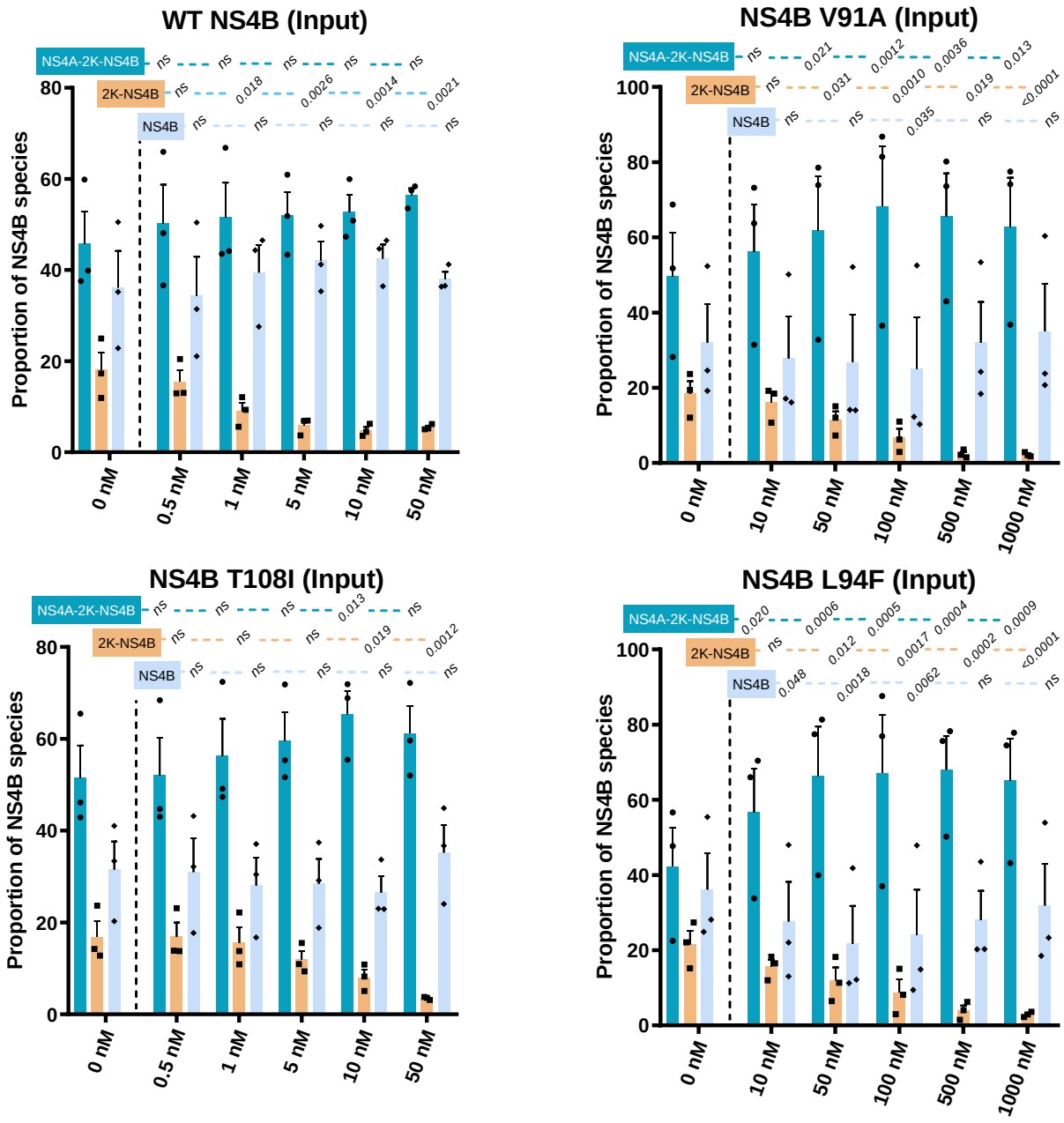

Figure 40. JNJ-1802 alters steady-state proportions of NS4B-containing species in the trans-cleavage system.

For the experiment, whose design is shown in Figure 39c, the western blot intensities of NS4B-containing species were determined individually at the level of the input (total lysates) by means of HA-staining. Column diagrams show the proportional composition of the NS4B-containing species for WT as well as for the three analyzed resistance mutations V91A, L94F and T108I in % for each of the JNJ-1802 concentrations used (sum = 100% in each case). Results are given with mean and SEM. Repeated measures one-way ANOVA with subsequent Dunnett's multiple comparisons test was used to calculate p-values. *ns*, not significant.

A correlation between the loss of interaction between NS3-containing complexes and NS4B species on the one hand and the decrease of the 2K-NS4B intermediate on the other hand was inferred from concordant EC_{50} values. (Table 12).

Next, I addressed the question whether JNJ-1802 blocks the interaction between NS2B/NS3 and NS4A-2K-NS4B or also disrupts existing complexes (Figure 41a). Whereas a significant decline in complexes comprising NS3 and NS4B-containing species was noted in cells treated with the compound 4 h post-transfection, this did not hold when cells were treated with a delay of 20 h (Figure 41b-d). Thus, it can be inferred that JNJ-1802 impedes the *de novo* formation of such complexes, while the compound does not interfere with established ones. Although not yet explicitly shown for JNJ-1802, based on the available results, it can be hypothesized that the inhibition of the formation of NS3- and NS4B-containing protein complexes by the compound is ultimately due to a blocked interaction of the viral protease/helicase complex NS2B/NS3 with the NS4A-2K-NS4B precursor.

Table 12. Comparison of EC_{50} values of JNJ-1802-induced phenotypes for wild-type and resistance mutants.

EC_{50} values (mean ± SEM) for the Co-IP NS3:NS4B species ratio on the one hand and for the change of 2K-NS4B proportion in total lysates on the other hand were obtained by fitting four-parameter dose-response curves to the results of each individual experiment.

NS4B	EC_{50} NS3/NS4B interaction [µM]	EC_{50} 2K-NS4B decrease [µM]
WT	0.0013 ± 0.00030	0.0017 ± 0.0012
V91A	0.13 ± 0.035	0.078 ± 0.028
L94F	0.17 ± 0.082	0.17 ± 0.082
T108I	0.032 ± 0.0098	0.011 ± 0.0048

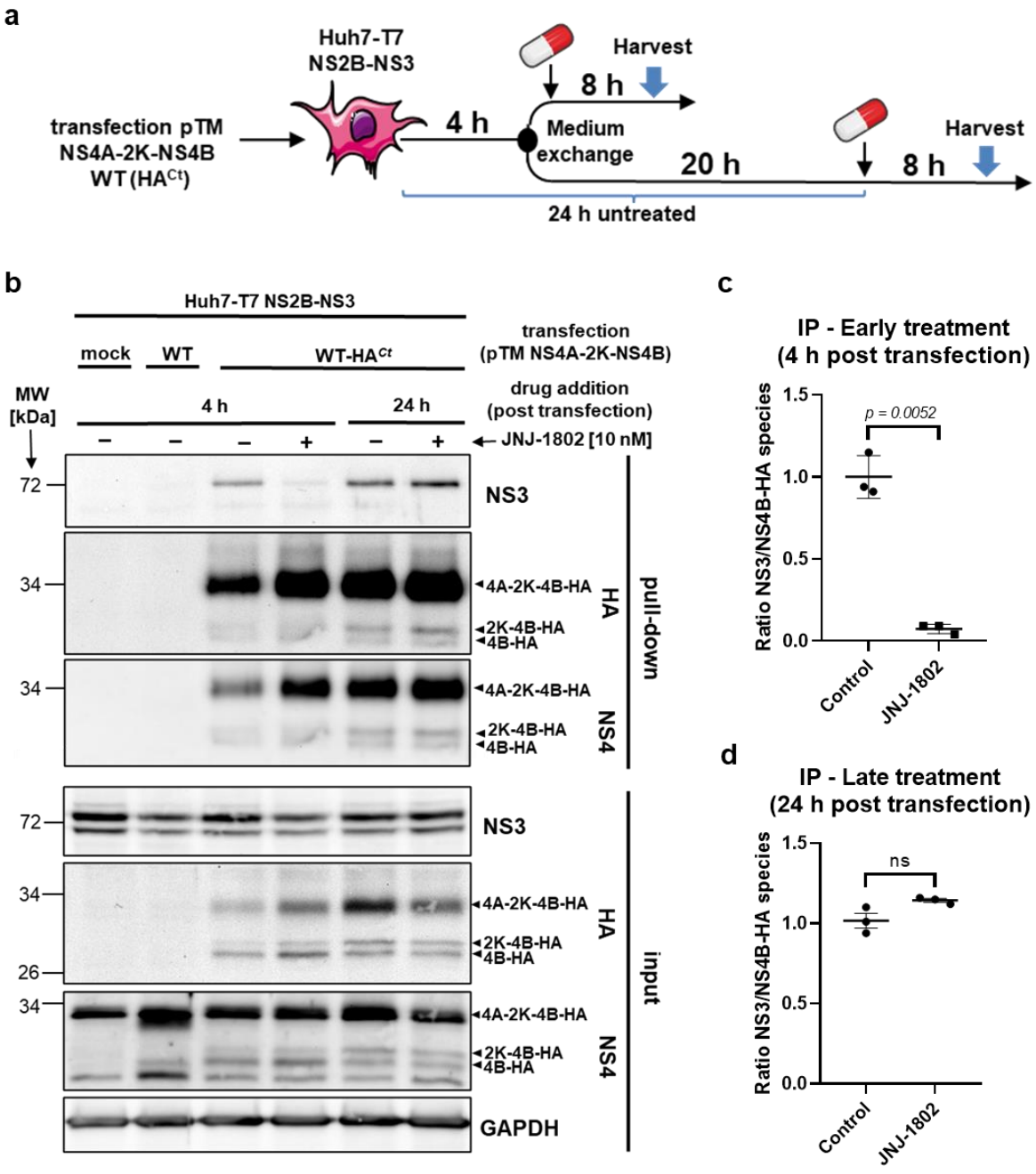

Figure 41. JNJ-1802 prevents *de novo* formation of NS3/NS4B complexes but does not disrupt established ones.

a, Experimental design to investigate the JNJ-1802-induced perturbation of the NS3 – NS4B interaction in relation to the timing of drug application. At designated time points, specimens were treated with 10 nM JNJ-1802 or DMSO control, harvested 8 h thereafter, and cell lysates were subjected to HA-specific pull-down followed by western blot analysis. **b**, A western blot representative of three independent experiments for the assay setup outlined in (a). **c-d**, Comparison of the effect of early and late JNJ-1802-treatment on the NS3/NS4B-HA species ratio in samples after HA pull-down. Results are presented as mean and SEM. Paired two-tailed t-test was used to calculate p-values.

VI. Discussion

VI.1 JNJ-A07 and JNJ-1802 are potent DENV antivirals with outstanding pharmacological properties and a high resistance barrier

Dengue fever poses a growing global health problem, creating a strong need for effective and safe pan-serotype DENV antivirals. As a result, numerous drug development projects have been conducted in the past. However, none of these, which mainly focused on drug repurposing and the development of direct-acting antivirals against enzymatic targets such as NS5 polymerase or NS3 protease, resulted in an approved drug. Instead, many have been discontinued due to in *vivo* inefficacy or toxicity. Therefore, it was consequential to investigate whether a phenotypic screening approach could uncover potent drug candidates with novel or neglected targets. The compounds JNJ-A07 and JNJ-1802 studied in this work are the result of such a process. Their development took into account many lessons learned from previous projects, including the testing of hit compounds against all serotypes and in different cell lines already at an early stage. In addition, extensive mouse experiments were performed to determine the pharmacokinetic and safety profiles. JNJ-A07, the first compound of this series to be studied in preclinical experiments in mice, showed impressive efficacy in this system. Even when the start of treatment was delayed until the peak of the viraemia curve several days after infection, a rapid and significant reduction in viral load was observed. Similar results were obtained for JNJ-1802. It is hypothesized that the latter drug, which is in clinical development, could be beneficial for patients even when they first consult a doctor with already manifested symptoms. In parallel, the low side effect profile also allows testing of prophylactic use (Figure 42).

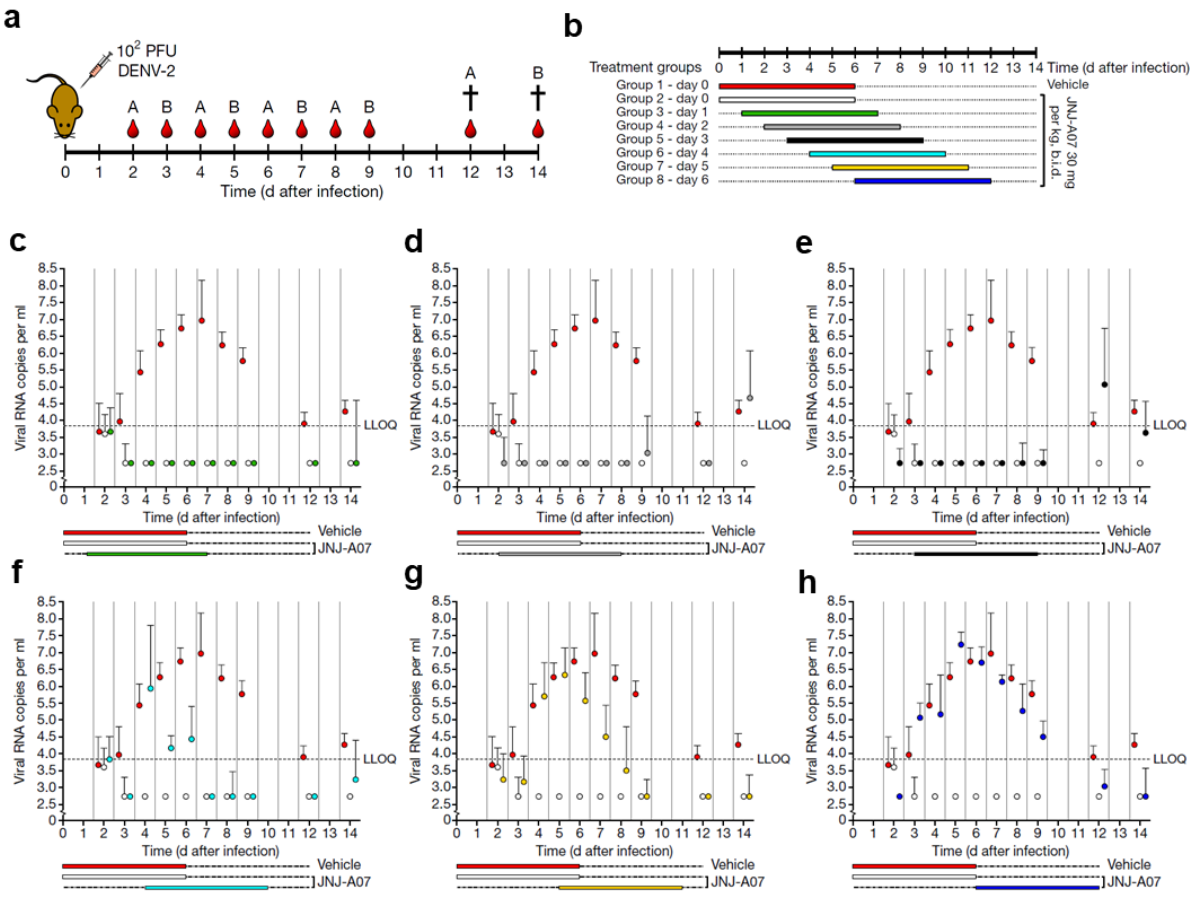

Figure 42. *In vivo* efficacy of JNJ-A07 on DENV replication kinetics in a therapeutic context.
a, Schematic of the *in vivo* kinetic studies in which AG129 were challenged intraperitoneally with 10^2 PFU DENV-2. Each treatment group (n = 8, each) was divided into two subgroups A and B (n = 4, each) for blood collection on alternate days as shown. **b**, Overview of the different treatment groups. Group 1 and 2 represent control groups (vehicle control and quasi-prophylactic JNJ-A07 treatment, respectively). In groups 3-8, JNJ-A07 was administered with a delay of an increasing number of days after infection. **c**, Inhibitory effect of JNJ-A07 on viraemia at different time points post infection in AG129 mice treated with 30 mg/kg JNJ-A07 twice daily for 6 consecutive days. In the delayed treatment groups (groups 3-8), treatment with JNJ-A07 was started on day 1 (green dots/bar), day 2 (grey dots/bar), day 3 (black dots/bar), day 4 (light blue dots/bar), day 5 (yellow dots/bar) or day 6 (dark blue dots/bar) post injection, respectively. In each graph, the results of the vehicle control group (red dots/bar) and the quasi-prophylactic treatment group (white dots/bar) are plotted in addition. Statistical analysis was conducted using the Kruskal-Wallis test. Indeterminate C_t values were imputed at a C_t value of 40 (=limit of detection), corresponding to a viral RNA copy number of 2.6 $\log_{10}$ copies/mL. P-values were adjusted using Holm's correction for multiple comparisons. LLOQ, lowest level of quantification. Adapted from Kaptein et al.[376]

On an individual level, prophylactic treatment should diminish the viral load in such a way that disease symptoms are reduced or, ideally, do not develop at all. Particularly vulnerable parts of a population living in dengue-endemic regions (e.g. those with chronic health conditions) could benefit greatly from such chemoprophylaxis[399]. This is also of interest to travelers who normally live outside dengue risk areas and therefore only need to protect themselves for a limited time[46]. These often exhibit a complete DENV seronegative status, and it is of interest to maintain this even after exposure to the pathogen, in order to avoid creating the basis for a

later heterotypic DENV infection with an increased risk of severe disease. Encouragingly, testing of JNJ-1802 in non-human primates, which have an intact innate immune response similar to that of humans, showed that the development of such immunity can be prevented at sufficiently high doses[378]. Antimalarials like atovaquone and proguanil are examples of the effective use of prophylactic drugs in travel medicine, and it remains to be seen whether JNJ-1802 will one day play a similar role in the fight against dengue[400,401].

Besides, JNJ-1802 could potentially be applied in mass prophylaxis to protect a community in the event of a local outbreak. Mass chemoprophylaxis is particularly necessary and useful for infectious diseases in which transmission chains are difficult to trace, such as vector-borne diseases or those in which a large proportion of infections are asymptomatic[402]. Examples of the successful use of mass chemoprophylaxis include the control of malaria[403], meningococcal disease[402], and filarial infections like lymphatic filariasis and river blindness[404]. It should be noted that mass chemoprophylaxis is always a controversial practice, in part because its effectiveness is difficult to measure over the course of a single outbreak[402]. Chemoprophylaxis is logistically demanding, and the protection is only temporary. The greatest concern, however, is the accelerated development of resistance mutations[403].

Development of resistance to broadly used antiviral drugs is a well-known problem, especially with DAAs[326]. Based on results from this work, it is now known that JNJ-A07 and JNJ-1802 are DAAs that specifically target the interaction between two viral proteins namely NS4A-2K-NS4B and NS3 (the latter always in a stable complex with its cofactor NS2B). Consistent with this, a number of resistance mutations have been identified for both compounds, all of which are in the sequence of NS4B. Some of these, such as L94F, unusually not only conferred resistance but also increased replication fitness in mammalian cells[376]. At first glance, this may indeed seem alarming; on the other hand, it must be mentioned that these resistance mutations were not obtained incidentally, but only through targeted stimulation in a lengthy *in vitro* resistance selection procedure. In addition, a combination of at least three mutations in NS4B was required to achieve high-level resistance. This characteristic makes drug-resistant variants unlikely to arise readily in patients. Moreover, the mutations in NS4B appeared to render the resistant DENV variants incapable of replicating in mosquito cells (Figure 43a-b). This suggests that such mutants, should they evolve, are unlikely to be transmitted from human to human via the insect vector (Figure 43c). Even if the mosquito is not a total barrier to mutants, compound-resistant virus variants should not be able to manifest in the population unless selective pressure is sustained over a long period of time in a large proportion of the population. Assuming the worst-case scenario that this would nevertheless occur, there is still reason to

believe that these variants will be displaced again by the wild-type after the end of an epidemic and cessation of mass chemoprophylaxis.

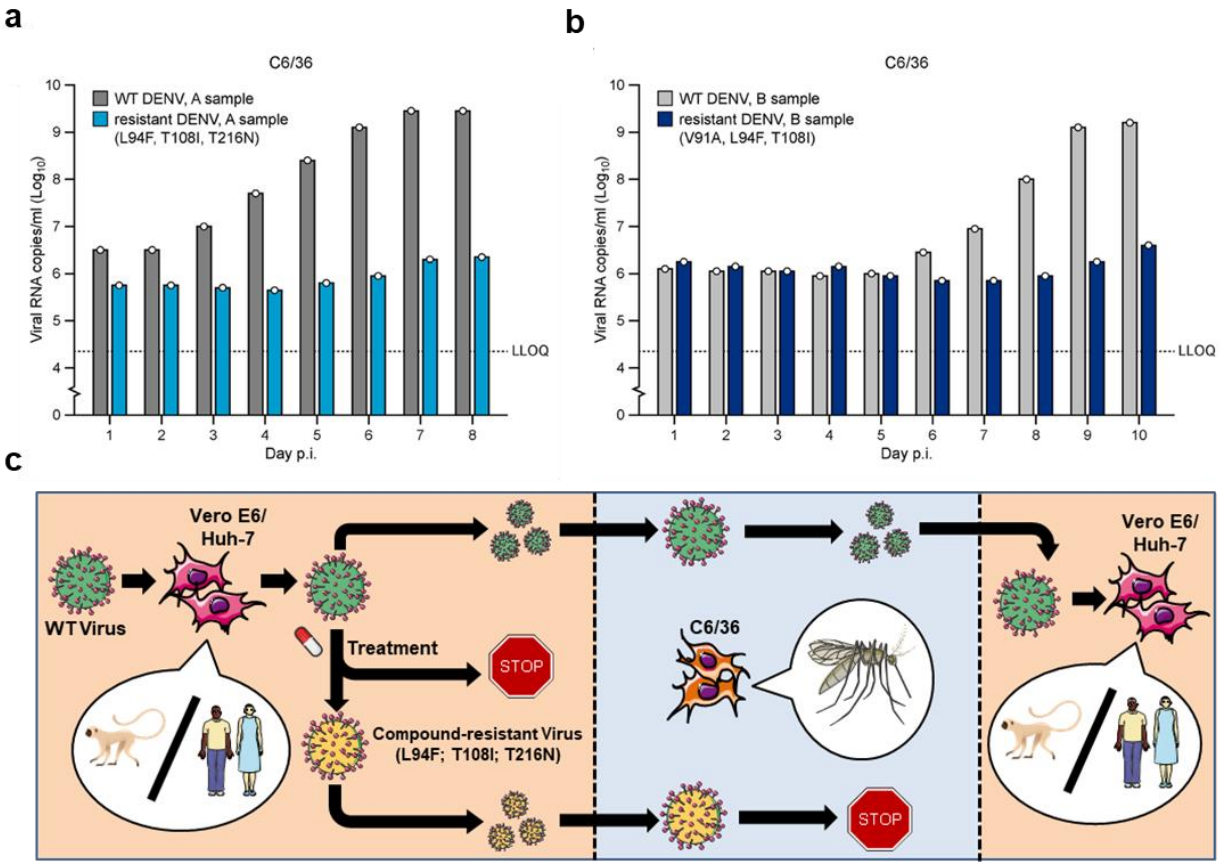

Figure 43. Highly resistant mutant viruses are unable to propagate in mosquito cells.
a, *In vitro* growth kinetics of the selected resistant DENV strain obtained at the endpoint of the *in vitro* resistance selection assay A (compare to Figure 13b; here denoted A sample) in relation to its WT counterpart. The assay was performed on *Aedes albopictus* C6/36 cells. Viral RNA load in the supernatant was assessed by RT-qPCR. **b**, Experiment analogous to (a), but using the JNJ-A07 resistant DENV strain obtained at the endpoint of the *in vitro* resistance selection assay B (compare to Figure 13c; B sample). **c**, Schematic illustration how JNJ-A07 resistance mutations might limit the spread of drug resistant mutants in the human population. Wild-type (WT) virus is transmitted by mosquitoes while NS4B inhibitor treatment suppresses virus replication in humans. Although drug resistant mutants replicate efficiently in humans, some of them without overt loss of fitness, at least highly resistant mutants do not reproduce in mosquito cells, arguing for the inability of these mutants to be transmitted by this insect vector. In addition, emergence of fully resistant mutants in humans takes a long time, exceeding the anticipated treatment duration of infected individuals. Adapted from Kaptein et al.[376]

VI.2 JNJ-A07 and JNJ-1802 target the NS3 – NS4B interaction presumably by binding to a cytosolic loop in NS4B

The main topic of this work was to decipher the mechanism-of-action of JNJ-A07 and JNJ-1802. In this sense, the stimulation of resistance mutations and the consequent observation that these accumulated in NS4B was a fundamental starting point. A second important piece of basic information was that the compounds also showed an antiviral effect in the context of a

subgenomic replicon, so that the primary effect could be confined to steps in the viral life cycle that affect viral replication (e.g. replication organelle formation, translation, polyprotein processing, genome amplification). Since NS4B has no enzymatic activity, it was assumed that the compounds affect one of its protein-protein interactions. In retrospect, it was very useful to perform a literature review and search for NS4B interactions relevant to viral replication, as this quickly brought the one with NS3 into focus. In order to study a compound effect, an expression-based system had to be applied and, in this sense, the *trans*-cleavage system proved to be very suitable, mainly due to its simplicity. Thus, not only were JNJ-A07 and JNJ-1802 shown to suppress the interaction of NS4A-2K-NS4B with NS3, but also mutations mediating compound resistance were found to restore the interaction. Surprisingly, all mutations tested except A137T, which is considered a polymorphism, independently conferred compound resistance, and the Co-IP analysis revealed that for all of them this occurs via the same mechanism, namely the maintenance of the NS3 – NS4B interaction, with additive and synergistic effects, respectively, existing between the individual mutations.

Dose-response experiments were performed for a selection of JNJ-A07 and JNJ-1802 resistance mutations, and since the determined EC_{50} values regarding the NS3 – NS4B interaction correlated impressively well with the EC_{50} values regarding the replication rate, it is currently assumed that compound-induced blockage of the NS3 – NS4B interaction is the primary cause for the antiviral property of the drugs. According to the topology model of Miller et al.[172] and the AlphaFold2 prediction of Wang et al.[171] the mutated amino acids are scattered in NS4B, with most mutations residing in transmembrane regions or luminal loops, which are rather atypical target regions of small molecules. In later experiments, resistance mutations were observed to moderately, but not drastically, decrease DENV-specific accumulation in NS4B-rich cell regions, suggesting that they do not localize directly to the compound binding site but compensatorily alter it so that either compound binding is attenuated or that the interaction can be formed despite compound binding, presumably a combination of both.

The JNJ-A07- and JNJ-1802-mediated inhibition of the NS3 – NS4B interaction along with its rescue by resistance mutations resembled the behavior of known NS3 nonbinding mutants, most notably Q134A and M142A, in that these caused replication deficiency similar to compound addition, but on the other hand, both replication competence and NS3 interaction could be restored by compensatory pseudoreversions dispersed throughout the sequence of NS4B. Of note, the latter partially overlapped with resistance mutations of JNJ-A07 and JNJ-1802. Since the primary NS3 nonbinding mutations accumulated in the cytosolic loop between transmembrane domains 3 and 4, this region on NS4B was previously associated with NS3

interaction[117]. Therefore, and due to the fact that this loop is presumed to be one of the most pharmacologically accessible regions of NS4B, it is hypothesized that this is also the binding region of compounds JNJ-A07 and JNJ-1802.

VI.3 The NS4A-2K-NS4B precursor plays a dominant role in NS3-interaction

Authentic integration of DENV NS4B into biomembranes requires the 2K peptide preceding it N-terminally. In the chronologically earliest publications incorporating parts of this dissertation, NS4B was introduced into the *trans*-cleavage system exclusively via the NS4A-2K-NS4B precursor, as this was described as the most efficient way[117]. In cells that contained the viral protease-helicase complex NS2B/NS3, this is processed via a sequential interplay with the host signal peptidase complex, so that substantial amounts of mature NS4B were eventually present at equilibrium, yet the balance was still on NS4A-2K-NS4B and there were also lower amounts of 2K-NS4B observable. Consequently, a mix of all three species was precipitated via HA-immunoprecipitation and compound-induced effects such as impaired co-precipitation of NS3 could thus not be attributed to a single NS4B species. In publications mentioned above, titles and headings referred to an impaired NS3-NS4B interaction for the sake of simplicity, but it was always specified in the text that NS4B should be understood as a mix NS4B-containing species.

In the detailed analysis of the mechanism-of-action of JNJ-A07, it was observed in the *trans*-cleavage system neither mature NS4A nor mature NS4B formed an interaction with NS3 that was detectable by means of Co-IP. In addition, however, the NS4A-2K-NS4B precursor was found to associate unambiguously with the viral protease-helicase complex NS2B/NS3. Since the known interaction of the NS4A-2K-NS4B precursor with the luminal localized NS1 was not affected by JNJ-A07, it is concluded that JNJ-A07 does not act by affecting the global structure or stability of NS4A-2K-NS4B, but that the compound specifically targets the interface between NS4A-2K-NS4B and NS3 on the cytosolic side.

VI.4 JNJ-A07 does not alter the canonical cleavage sequence of NS4A-2K-NS4B

Compound-induced accumulation of the NS4A-2K-NS4B precursor in the *trans*-cleavage system was first observed for JNJ-A07 and later also for JNJ-1802, accompanied by a decrease

in the fraction of the 2K intermediate, leading to speculation that the compounds slow down the cleavage kinetics of the precursor, for example by binding to the NS4B moiety and altering the folding of the precursor or the accessibility of the cleavage site. Following the publication of these results, an opinion article was released postulating that JNJ-A07 alters the canonical cleavage sequence of NS4A-2K-NS4B via 2K-NS4B to mature NS4B in such a way that the host signal peptidase complex cleaves NS4B directly from NS4A-2K-NS4B, yielding uncleaved NS4A-2K[405]. Further findings subsequently obtained upon detailed elucidation of the mechanism-of-action of JNJ-A07 do not support this conclusion but rather refute it. First, analysis of HA-NS4A-2K-NS4B precursor cleavage by NS2B/NS3 in the presence of JNJ-A07 did not reveal the postulated NS4A-2K protein, but only fully cleaved NS4A. Second, co-expression of the NS4A-2K-NS4B precursor with a catalytically inactive NS2B/NS3 protease in the presence of JNJ-A07 resulted in a dose-dependent loss of the precursor-protease interaction but not in the formation of mature NS4B, which Behnam and Klein[405] suggested should be released independently of the viral protease by the host cell signalase. Third, the same result was found when a modified precursor harboring a P1' substitution at the NS4A-2K cleavage site was used, which according to the claim of Behnam and Klein should phenocopy the blockade mediated by JNJ-A07 at this site.

The trans-cleavage system has proven to be very useful in revealing the impact of the tested compounds on the interaction between NS4A-2K-NS4B and the viral protease-helicase complex NS2B/NS3. On the other hand, it must be stated that due to their independent expression in this system, the molar ratios of NS4A-2K-NS4B to NS2B/NS3 deviate significantly from the 1:1 ratio that naturally results from the processing of the total polyprotein. This and the fact that *cis*-cleavage cannot occur in the *trans*-cleavage system are possible explanations for elevated steady-state amounts of uncleaved precursor.

VI.5 NS3 nonbinding mutants imply a causal relationship between the NS4A-2K-NS4B interaction with NS2B/NS3 and the formation of vesicle packets

The establishment of the pIRO-D system allowed the testing of controversial results obtained with the trans-cleavage system, such as the putative effect of compounds on NS4A-2K-NS4B processing. In fact, cleavage kinetics of the NS4A-2K-NS4B precursor in the polyprotein context (pIRO-D system) were not affected by JNJ-A07 as determined by pulse-chase

experiments, contradicting a central role of JNJ-A07 in altered precursor maturation. Considering that both NS4A and NS4B were already associated with the induction of membrane alterations to build viral replication organelles, it was reasonable to employ the pIRO-D system to study an effect of JNJ-A07 on vesicle packets formation. Analogous to the integrity of the NS4A-2K-NS4B interaction with NS2B/NS3, which was compromised in the trans-cleavage system by JNJ-A07 addition to the WT but not when resistance mutations were present, compound-induced reduction in observed vesicle packets was prevented by resistance mutations, indicating that the interaction plays a critical role in the formation of vesicle packets, the presumed sites of viral RNA replication (Figure 44). Further evidence for a functional link between the interaction of NS2B/NS3 with the NS4A-2K-NS4B precursor on the one hand and ER membrane rearrangements on the other hand emerged from the observation that JNJ-A07 effectively blocked the *de novo* formation of vesicle packets but did not disrupt the integrity of existing ones, consistent with the finding that the drug prevents the interaction of NS2B/NS3 and NS4A-2K-NS4B but does not disrupt the complex once established. Moreover, this can be considered as an explanation for the fact that the drug is active only at early time points after infection, given that this is the stage at which vesicle packets form. Replication of DENV in the absence of vesicle packets is entirely unknown for this virus. Meanwhile, if the compound is employed late, replication continues in the existing vesicle packets and then slowly decreases along with their natural decay. The most pertinent evidence for a causal relationship between the NS4A-2K-NS4B interaction of NS2B/NS3 and the formation of vesicle packets was not obtained by use of JNJ-A07 but by examination of the NS3 nonbinding mutants Q134A and M142A. For these, it can be stated with confidence that all observed phenotypes originate from a structural change in the cytosolic loop between TMD3 and TMD4 of the NS4B protein and that this change is already manifested at the level of the NS4A-2K-NS4B precursor. There, pseudoreversions associated with Q134A and M142A recovered replication competence to varying degrees, and these gradual differences were similarly reflected in the restoring potential of both NS4A-2K-NS4B interaction with NS2B/NS3 and vesicle packets formation efficiency.

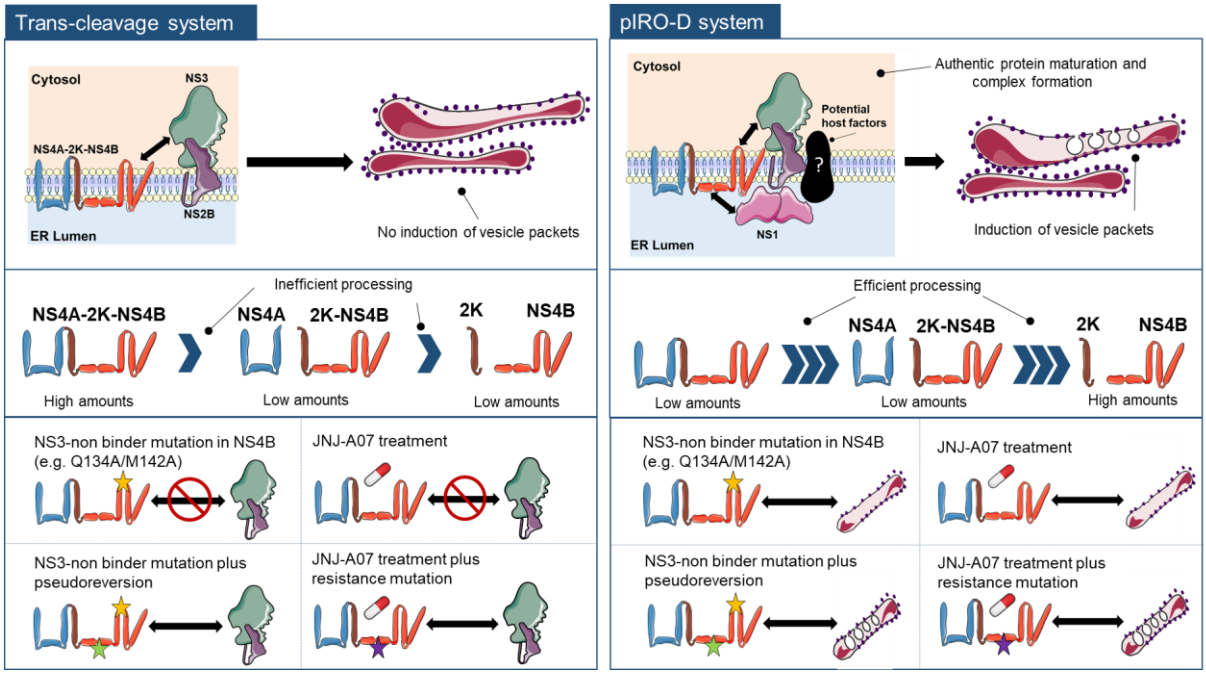

Figure 44. Schematic comparison of observations made with the *trans*-cleavage system and the pIRO-D system.
The *trans*-cleavage system is characterized by a pronounced interaction between NS4A-2K-NS4B precursor and NS2B/NS3 helicase-protease complex, but does not form authentic replication organelles due to the restricted scope of viral proteins, which is the central feature of the pIRO system. In both systems, NS4B is observed together with the precursor species NS4A-2K-NS4B and 2K-NS4B, but the steady state composition is clearly on the NS4A-2K-NS4B precursor in the *trans*-cleavage and strongly on mature NS4B in the pIRO-D system, suggesting more efficient processing in the latter. In the *trans*-cleavage system, both JNJ-A07 treatment and mutations Q134A and M142A, which reside in the cytosolic loop between transmembrane domains 3 and 4, lead to a loss of interaction between NS4A-2K-NS4B and the NS2B/NS3 complex while resistance mutants against JNJ-A07 as well as pseudoreversions of the NS3-non binder mutants can rescue this phenotype. In the pIRO-D system, the effect of JNJ-A07 on this interaction is masked at the Co-IP level, possibly due to a stabilizing effect of NS1. Nevertheless, it seems to be of fundamental importance for the formation of vesicle packet elements, as the effects of JNJ-A07 or of Q134/M142A in ultrastructural analysis correlate perfectly with the Co-IP results in the *trans*-cleavage system.

VI.6 A multiprotein complex containing NS4A-2K-NS4B appears to be of structural relevance to the assembly of vesicle packets

Since pulse-chase experiments did not provide any evidence for JNJ-A07-induced alterations of polyprotein maturation in the pIRO-D system, the effect of the compound on vesicle packets formation does not result from an indirectly delayed release of mature NS4A or NS4B. Instead, a hitherto unknown function of the NS4A-2K-NS4B precursor in the structural assembly of the vesicle packets is hypothesized, which is not mediated by this protein alone, but in conjunction with others. Due to its JNJ-A07- and JNJ-1802-sensitive interaction, the viral protease-helicase complex was identified as an integral partner, but the involvement of other viral as well as host proteins seems possible. The interaction between NS4A-2K-NS4B and NS1 has so far not been associated with vesicle packets formation, but rather with other processes of viral replication,

which is consistent with the lack of JNJ-A07 sensitivity in the data obtained here. Nevertheless, evidence was gained that NS4A-2K-NS4B does not exclusively interact with either NS2B/NS3 or NS1 but that, at least in part, a multimeric complex is formed that encompasses all named proteins and thus extends from the cytosol through the ER membrane and into the ER lumen. It is conceivable that in this way different processes can be coordinated between the inside and the outside of vesicle packets, which could affect both their structure as well as steps in viral replication (Figure 45).

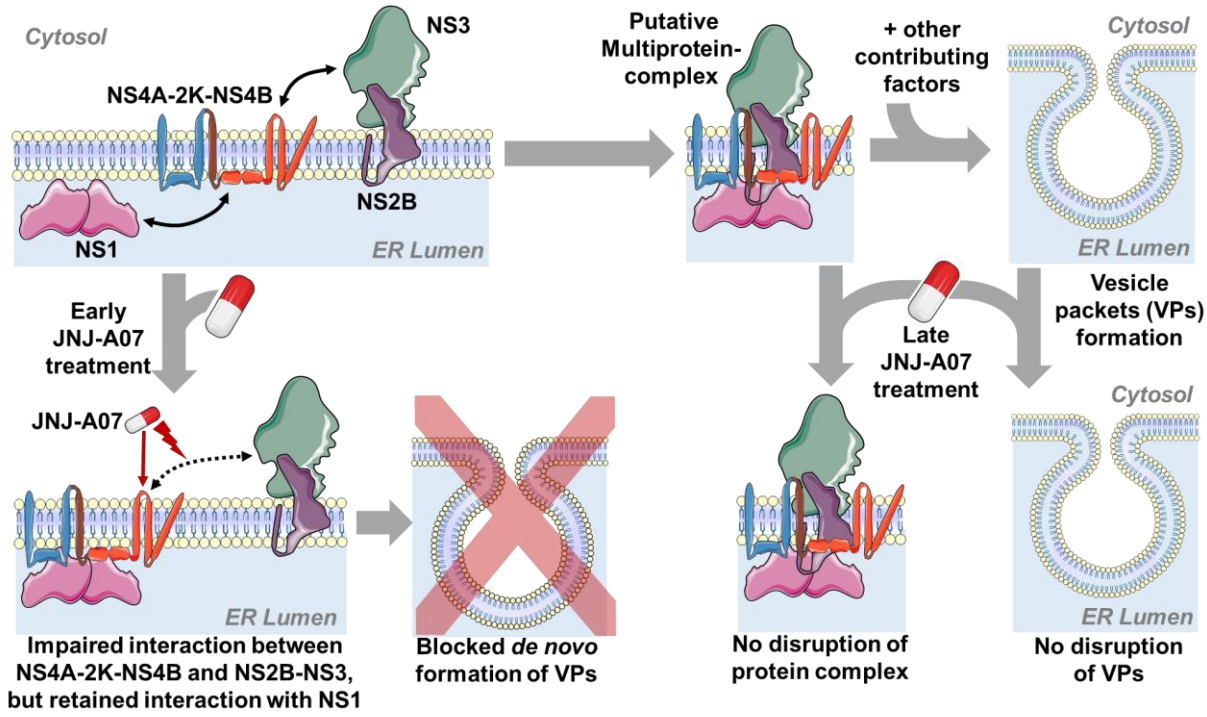

Figure 45. Graphical summary of the mechanism-of-action of JNJ-A07.
Upper panel level: In the course of DENV polyprotein processing, the cleavage intermediate NS4A-2K-NS4B is formed, which engages specific binding with NS1 and the viral protease complex NS2B/NS3. This might result in a larger multiprotein complex that extends from the ER lumen, across the ER membrane, into the cytosol and, together with other factors (e.g. certain NTR regions of the viral genome), initiates *de novo* formation of vesicle packets, the putative organelles of viral replication. Lower panel level: Early application of JNJ-A07 interferes with the functionality of NS4A-2K-NS4B (presumably by targeting the cytosolic loop between NS4B TMD3 and TMD4), so that it can no longer engage the precursor-specific interaction with NS2B/NS3, whereas the binding of NS1 on the luminal side is not affected. This results in the collapse of the *de novo* formation of vesicle packets, which may explain the potent effect of JNJ-A07 on viral replication. If JNJ-A07 is added at a late stage, after vesicle packets have already formed, they remain intact until the end of their life cycle and are not disrupted. This is consistent with our previous observation that JNJ-A07 cannot break established protein complexes between NS4A-2K-NS4B and NS2B/NS3 and is also in line with the known JNJ-A07 property of gradual loss of antiviral activity with increasing time between the onset of viral replication and compound application.

Steady state proportions of NS4B-containing species in the pIRO-D system clearly indicate that the total amount of precursor in this system, like in the context of infection, is low. NS4A-2K-NS4B is a natural substrate of the viral protease NS3 and its efficient processing in the

pIRO-D system is due to the fact that many processing steps are predominantly carried out in *cis*.

A question that cannot be answered at present is whether the formation of a multimeric complex around NS4A-2K-NS4B protects the latter from cleavage, in which case a few molecules per VPE were sufficient for the execution of precursor-specific functions, or whether the detected amounts of NS4A-2K-NS4B are largely attributable to the fraction of VPEs that are currently being established and in which NS4A and NS4B might be released in mature form after full establishment of the organelles to then perform other functions associated with these.

VI.7 The NS4A-2K-NS4B interaction with NS3 is functionally distinct from previously known NS3 – NS4B interactions

Analysis of the mechanism-of-action of JNJ-A07 and JNJ-1802 revealed that the interaction of the DENV NS4A-2K-NS4B precursor with the viral protease-helicase complex NS2B/NS3 is functionally coupled to the formation of vesicle packets. Such an interaction was previously unknown. However, an interaction of the NS3 protease domain with the NS4A-2K junction of the NS4A-2K-NS4B precursor has already been described. This binding is short-lived and serves to proteolytically cleave the substrate at this site (first described for yellow fever virus[118] and later confirmed for other flaviviruses including DENV[116,117]). This interaction is not congruent with the one newly described here because, first, even high concentrations of JNJ-A07 that completely blocked NS3 co-precipitation with the precursor, only reduced, but did not prevent NS4A-2K-NS4B processing. Second, NS4B mutations abrogating NS2B/NS3 interaction with the precursor cluster in the cytosolic loop of NS4B between transmembrane domains 3 and 4, and thus, far away from the NS4A-2K cleavage site.

In addition, another NS3 – NS4B interaction has been described that has a functional effect on the activity of the helicase domain of NS3. In this regard, NS4B presumably acts as a co-factor to coordinate ATP cycles of the helicase and nucleic acid binding in the context of viral genome unwinding[173,183], a process that is not required in the pIRO-D system for the assembly of replication organelles, as demonstrated by the use of a construct with an inactivating mutation in the active site of NS5 polymerase (NS5 GND)[106]. As mentioned earlier, indirect evidence for binding of JNJ-A07 and JNJ-1802 to the cytosolic loop between NS4B transmembrane domains 3 and 4 was found using NS3 non-binding mutants, and since this particular region is considered to be the contact interface with the NS3 helicase domain, it is reasonable to assume that the newly described precursor interaction is also linked to the helicase domain. However,

it is important to emphasize that the helicase domain has several other known functions beyond helicase activity, including rNTPase activity, which is required for the assembly of a type 1 cap[98]. Alternatively, it has long been suggested that the interactions of the NS3 helicase domain with NS5 and NS4B primarily serve to build a highly ordered replicase complex[152]. Evidence that NS4B acts as a cofactor to enhance NS3 helicase activity is entirely derived from biochemical assays using recombinantly expressed (and partially tagged) NS3 and NS4B[182,183]. Critically, it should be noted that first, NS4A-2K-NS4B was not tested in these systems; second, the observations were never extrapolated to more authentic systems; and third, the effect of the interaction on NS3 helicase activity was rather modulatory, so that the dramatic impact of NS3 non-binding mutations such as Q134A and M142A on viral replication could thereby not be explained. The deficiency of these mutants to form vesicle packets, as presented here, provides a plausible explanation for this.

VI.8 Co-IP-based study of NS4A-2K-NS4B interaction with NS3 is limited in the pIRO-D system

While in the trans-cleavage system the Co-IP phenotypes of both the compounds tested and the NS3 non-binding mutants correlated consistently with the EM phenotypes in the pIRO-D system, reproduction of the Co-IP phenotypes in the pIRO-D system proved to be extremely challenging and at times inconsistent. One problem encountered, was that NS4A-2K-NS4B, which has been shown to be a key component in the mechanism-of-action of the compounds tested, is present at low levels in the steady state of the pIRO-D system. Moreover, the co-precipitation of NS4B species in this system was always accompanied by a specific co-precipitation of NS3, which could not be suppressed either by addition of compounds or by the Q134A mutant. Several approaches were tried, including reciprocal pulldowns and different lysis buffer conditions, none of which provided a clearer picture. For the reasons mentioned above, a limitation of the Co-IP approach in the pIRO-D system is currently assumed. One possible explanation follows the consideration that a loss of co-precipitation implies that all direct and indirect interactions to the precipitated entity have been actively disrupted. However, if several independent interactions are present, a single unaffected one may be strong enough to maintain co-precipitation.

It is known that the presence of the viral proteins NS2B, NS3 and NS4A-2K-NS4B as well as the resulting mature proteins NS4A and NS4B, respectively, are not sufficient to induce authentic replication organelles. Conversely, this means that to this end, a more complex

network of protein-protein interactions is required, including components that are present in the polyprotein system but not in the *trans*-cleavage system. Thus, indirect bridging chains of interaction between the NS4A-2K-NS4B precursor and the viral protease complex might form. Furthermore, it should be noted that no interaction between mature NS4B and NS3 was recorded in the trans-cleavage system. If this were to occur in the pIRO-D system, e.g., due to the more authentic kinetics of polyprotein maturation or the assistance of additional components, the precursor-specific interaction would be masked there. In fact, there are several known examples of DENV NS4B interactions that only form in the presence of other viral proteins. For example, the binding of NS4B to STAT2 requires the interplay with NS5[190]. Similarly, NS4B inhibits the activating TBK1 phosphorylation only in concert with NS2A[148]. A more detailed investigation of the complex network of NS3 – NS4B interactions should be the subject of future research.

VI.9 Indirect evidence implies binding of JNJ-A07 and JNJ-1802 to DENV NS4A-2K-NS4B

Detection of compound binding to NS4B (or precursor) proved difficult. The planned method of cross-linking Compound A and Compound B to target structures, followed by click chemistry attachment of a biotin linker allowing streptavidin precipitation of target-compound conjugates, could only be partially established. The conditions of the click reaction required incubation at room temperature for at least 1 h. However, it was found that NS4B or precursor in cell lysates is highly susceptible to aggregation (leading to precipitation), which can only be prevented by continuous cooling. Conversely, when incubated on ice, the click reaction did not proceed. A partial workaround was achieved by chemical fixation of the cells prior to the click reaction. By integrating the click reaction into an immunofluorescence workflow, specific compound accumulation was recorded at intracellular sites enriched for NS4B and its interaction partner, the NS2B/NS3 complex, consistent with the assumption of targeting NS4B (and/or precursor). Previous studies have identified very similar looking structures as convoluted membranes[191]. Since NS4B is thought to be involved in the formation of vesicle packets, it is likely that the drug additionally accumulates in these structures. However, the vesicles are too small to be visualized by light microscopy and suitable labelling methods for correlative imaging that also preserve membrane integrity have yet to be developed. Nonetheless, the high degree of co-localization between the drug and NS4B suggests that the DENV inhibitors studied bind either directly to NS4B (or its precursor) or to an interaction

partner known to be DENV-specific, as no corresponding enrichment of the drug with ZIKV proteins has been recorded.

Using NMR, a method not available for this work, the compound NITD-688 was proven to bind to NS4B in another study[371]. As this thesis has shown by Co-IP and EM that the mechanism-of-action of this compound appears to be the same as that of JNJ-A07 and JNJ-1802, it is hypothesized that the latter ones also bind to NS4B and NS4A-2K-NS4B respectively, although direct evidence is still pending.

VI.10 Compounds targeting DENV and YFV NS4B seem to share a common mechanism

JNJ-1802 and NITD-688 represent the only known DENV NS4B-associated antivirals in advanced stage of development. These compounds, as well as the inhibitor JNJ-A07, appear to be specific for DENV, which raises the question of whether the mechanism is fundamentally DENV exclusive, or whether adapted molecular structures could act in a similar way as antivirals against other flaviviruses. To this end, it is useful to compare the results obtained here with those reported for a YFV compound called BDAA. BDAA is YFV specific and resistance mutations have been localized exclusively in the NS4B sequence[406]. The YFV NS4B P219 mutation site is located on the ER lumen side of the fifth putative transmembrane domain of NS4B, and remarkably, JNJ-A07 and NITD-688 also induced multiple resistance mutations at the corresponding site of DENV NS4B (NITD688: T215A/S; JNJ-A07: T216N/P) as depicted in Figure 46. Besides, BDAA treatment of mammalian cells induced a significant reduction in the number of observed vesicle packets[407]. However, in these studies the effect was measured in infected cells, so it is not yet fully understood whether the decrease is mainly an indirect phenotype resulting from suppressed viral replication or attributable to direct inhibition of vesicle packet biogenesis and/or accelerated degradation. Consistent with the latter, cells treated with BDAA have been reported to elicit an innate cytokine response through cellular pattern recognition receptors recognizing double-stranded viral RNA that may have entered the cytosol as a consequence of structural impairment of vesicle packets[407]. Taken together, the available data on BDAA and NITD-688, in conjunction with the work presented here, lead to the hypothesis that JNJ-A07, JNJ-1802, NITD-688 and BDAA all target specific NS4B-containing species and affect the formation or integrity of flaviviral replication organelles.

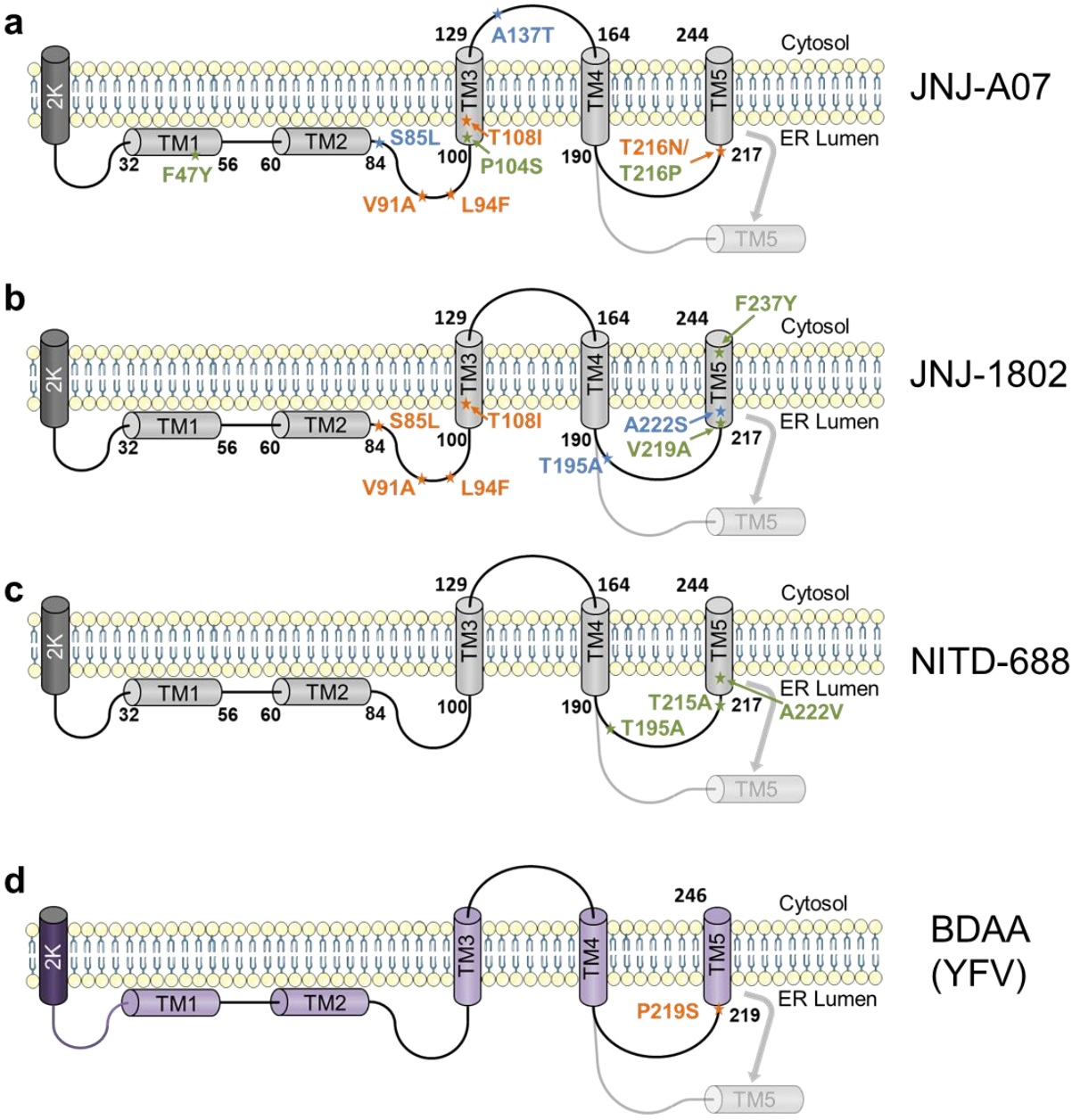

Figure 46. Resistance mutant profiles in different NS4B-targeting compounds.

Panels (a) to (c) show the simplified membrane topology of DENV NS4B according to Miller et al.[172] together with identified resistance mutations against the DENV-specific compounds JNJ-A07[376], JNJ-1802[378] and NITD-688[371]. Panel (d) depicts the positioning of the BDAA resistance mutation P219S in YFV NS4B[406], which is assumed to have a similar membrane topology as that of DENV. Resistance mutations highlighted in orange were present in ≥99% of the quasispecies at endpoint, mutations marked in black were present in less than 99% of the quasispecies at endpoint, and mutations coloured in blue were transient and had disappeared by the end of the experiment. Please note that different protocols were used to obtain resistance mutations for individual compounds.

VI.11 Outlook

The characterization of the mechanism-of-action of JNJ-A07 presented in this dissertation is the most comprehensive of its kind for any flavivirus NS4B-associated compound to date. JNJ-A07 targets an interaction between the NS4A-2K-NS4B precursor and NS2B/NS3, disrupting the *de novo* formation of vesicle packets. Since these organelles are essential for viral replication as the sites of genome amplification, this fully explains the antiviral effect of the compound. Besides, the clinical candidate JNJ-1802 was also shown in this work to block the interaction between the NS4A-2K-NS4B precursor and NS2B/NS3.

The findings presented in this thesis will contribute to a better understanding of the mechanisms-of-action of other known or entirely new NS4B-targeting compounds. The greater our knowledge of NS4B-associated antiviral compounds, the greater the likelihood that pan-flaviviral combination therapies or even pan-flaviviral inhibitors can be developed in the future. There is already some indication supporting the hypothesis that the underlying mechanism, a disturbed NS4A-2K-NS4B interaction with NS3 affecting vesicle packets formation, may also apply to other flaviviruses. In addition to the YFV inhibitor BDAA mentioned in the previous chapter, which is thought to affect vesicle packets integrity, there is one more YFV inhibitor termed CCG-4088 that might be NS4B-targeting, since with NS4B K128R one of two compound revertants occurred in that protein[408]. Interestingly, a ZIKV-specific inhibitor that blocks vesicle packets formation has recently been described. This compound, named SBI-0090799, induced single point mutations in the N-terminal region of NS4A, which is different from the NS4B-targeting compounds against DENV and YFV, but does not rule out an involvement of the NS4A-2K-NS4B precursor[409]. Along these lines, in the work presented here, I have demonstrated that the introduction of an alanine substitution at position Q136 in ZIKV NS4B, which is the direct equivalent to the Q134A mutation in DENV NS4B, similarly prevents interaction to ZIKV NS3, which is thought to cause a defect in viral replication. Last but not least, it was previously observed for WNV that large membrane clusters induced by expression of NS4A-2K-NS4B were arranged more densely when NS2B/NS3 was simultaneously expressed, suggesting an interaction relevant to replication organelle formation[116].

A holistic view of the mechanism of action of JNJ-A07 and JNJ-1802 reveals striking parallels with hepatitis C virus inhibitors that target the non-structural protein 5A (NS5A), such as daclatasvir[410]. Like DENV NS4B (or the NS4A-2K-NS4B precursor), HCV NS5A is an

atypical target protein as it has no defined enzymatic activity and is released by regulated cleavage of an NS4B-NS5A precursor[411]. NS5A binds several viral and host cell factors and exerts diverse functions depending on the interaction partner. Using an expression-based system, it was previously shown that a daclatasvir analogue disrupts the formation of the membranous web, a generic term for HCV replication organelles, which was not the case for a drug-resistant NS5A mutant[412]. Today, NS5A inhibitors constitute a cornerstone of the antiviral treatment regimen for chronic hepatitis C patients[413]. While it is difficult to predict whether the same will hold true for DENV NS4B inhibitors in the future, the results described here provide important insights into this promising class of agents with unprecedented antiviral activity against DENV. Finally, as with HCV NS5A, the results of this thesis underscore that non-enzymatic viral proteins that function as key organizers of viral replication represent highly attractive drug targets.

VII. References

1 Guzman, M. G. *et al.* Dengue: a continuing global threat. *Nature reviews microbiology* **8**, S7-S16 (2010).

2 Simmons, C. P., Farrar, J. J., van Vinh Chau, N. & Wills, B. Dengue. *New England Journal of Medicine* **366**, 1423-1432 (2012).

3 Pepper, O. P. A note on David Bylon and dengue. *Annals of medical history* **3**, 363 (1941).

4 Christie, J. On epidemics of dengue fever: their diffusion and etiology. *Glasgow Medical Journal* **16**, 161 (1881).

5 Rush, B. An account of the bilious remitting fever: as it appeared in philadelphia, in the summer and autumn of the year 1780. *The American Journal of Medicine* **11**, 546-550 (1951).

6 Heilman, J. M., De Wolff, J., Beards, G. M. & Basden, B. J. Dengue fever: a Wikipedia clinical review. *Open medicine* **8**, e105 (2014).

7 Smart, W. R. On dengue or dandy fever. *British medical journal* **1**, 382 (1877).

8 Gupta, N., Srivastava, S., Jain, A. & Chaturvedi, U. C. Dengue in india. *The Indian journal of medical research* **136**, 373 (2012).

9 Ashburn, P. M. & Caraig, C. F. Experimental investigations regarding the etiology of dengue fever. *The Journal of infectious diseases*, 440-475 (1907).

10 Simmons, J. S., St John, J. H. & Reynolds, F. H. Experimental studies of dengue. *Philippine Journal of Science* **44** (1931).

11 Bancroft, T. L. On the aetiology of dengue fever. *Austral. Med. Gaz.* **25**, 17-18 (1906).

12 Hotta, S. Experimental Studies on Dengue: I. Isolation, Identification and Modification of the Virus. *The Journal of Infectious Diseases* **90**, 1-9 (1952).

13 Sabin, A. B. & Schlesinger, R. W. Production of immunity to dengue with virus modified by propagation in mice. *Science* **101**, 640-642 (1945).

14 Hammon, W. M., Rundnick, A. & Sather, G. Viruses associated with epidemic hemorrhagic fevers of the Philippines and Thailand. *Science* **131**, 1102-1103 (1960).

15 Messer, W. B., Gubler, D. J., Harris, E., Sivananthan, K. & De Silva, A. M. Emergence and global spread of a dengue serotype 3, subtype III virus. *Emerging infectious diseases* **9**, 800 (2003).

16 Messina, J. P. *et al.* Global spread of dengue virus types: mapping the 70 year history. *Trends in microbiology* **22**, 138-146 (2014).

17 Westaway, E. G. *et al.* Flaviviridae. *Intervirology* **24**, 183-192 (1985).

18 Blitvich, B. J. & Firth, A. E. A review of flaviviruses that have no known arthropod vector. *Viruses* **9**, 154 (2017).

19 WHO. Arthropod-borne and rodent-borne viral diseases: report of a WHO scientific group [meeting held in Geneva from 28 February to 4 March 1983]. Report No. 9241207191, (World Health Organization, 1985).

20 Lambrechts, L., Scott, T. W. & Gubler, D. J. Consequences of the expanding global distribution of Aedes albopictus for dengue virus transmission. *PLoS neglected tropical diseases* **4**, e646 (2010).

21 Mammen Jr, M. P. *et al.* Spatial and temporal clustering of dengue virus transmission in Thai villages. *PLoS medicine* **5**, e205 (2008).

22 Weaver, S. C. & Vasilakis, N. Molecular evolution of dengue viruses: contributions of phylogenetics to understanding the history and epidemiology of the preeminent arboviral disease. *Infection, genetics and evolution* **9**, 523-540 (2009).

23 Rudnick, A. Ecology of dengue virus. *Asian J Infect Dis* **2**, 156-160 (1978).

24 Gubler, D. J. Perspectives on the prevention and control of dengue hemorrhagic fever. *Gaoxiong yi xue ke xue za zhi= The Kaohsiung Journal of Medical Sciences* **10**, S15-18 (1994).

25 Fagbami, A., Monath, T. & Fabiyi, A. Dengue virus infections in Nigeria: a survey for antibodies in monkeys and humans. *Transactions of the Royal Society of Tropical Medicine and Hygiene* **71**, 60-65 (1977).

26 Carey, D., Causey, O., Reddy, S. & Cooke, A. Dengue viruses from febrile patients in Nigeria, 1964-68. *The Lancet* **297**, 105-106 (1971).

27 Saluzzo, J., Cornet, M., Castagnet, P., Rey, C. & Digoutte, J. Isolation of dengue 2 and dengue 4 viruses from patients in Senegal. *Transactions of the Royal Society of Tropical Medicine and Hygiene* **80**, 5-5 (1986).

28 Gubler, D. J. Dengue and dengue hemorrhagic fever: its history and resurgence as a global public health problem. *Dengue and dengue hemorrhagic fever* (1997).

29 Diallo, M. *et al.* Amplification of the sylvatic cycle of dengue virus type 2, Senegal, 1999–2000: entomologic findings and epidemiologic considerations. *Emerging infectious diseases* **9**, 362 (2003).

30 Diallo, M. *et al.* Potential role of sylvatic and domestic African mosquito species in dengue emergence. *The American journal of tropical medicine and hygiene* **73**, 445-449 (2005).

31 Vasilakis, N., Cardosa, J., Hanley, K. A., Holmes, E. C. & Weaver, S. C. Fever from the forest: prospects for the continued emergence of sylvatic dengue virus and its impact on public health. *Nature Reviews Microbiology* **9**, 532-541 (2011).

32 Vasilakis, N., Tesh, R. B. & Weaver, S. C. Sylvatic dengue virus type 2 activity in humans, Nigeria, 1966. *Emerging infectious diseases* **14**, 502 (2008).

33 Wang, E. *et al.* Evolutionary relationships of endemic/epidemic and sylvatic dengue viruses. *Journal of virology* **74**, 3227-3234 (2000).

34 Rudnick, A. in *Proceedings of the International Conference on Dengue/DHF. University of Malaysia Press, Kuala Lumpur, Malaysia.* 7.

35 Holmes, E. C. & Twiddy, S. S. The origin, emergence and evolutionary genetics of dengue virus. *Infection, genetics and evolution* **3**, 19-28 (2003).

36 Twiddy, S. S., Holmes, E. C. & Rambaut, A. Inferring the rate and time-scale of dengue virus evolution. *Molecular biology and evolution* **20**, 122-129 (2003).

37 Vasilakis, N. *et al.* Evolutionary processes among sylvatic dengue type 2 viruses. *Journal of virology* **81**, 9591-9595 (2007).

38 Rosen, L., Roseboom, L. E., Gubler, D. J., Lien, J. C. & Chaniotis, B. N. Comparative susceptibility of mosquito species and strains to oral and parenteral infection with dengue and Japanese encephalitis viruses. *The American journal of tropical medicine and hygiene* **34**, 603-615 (1985).

39 Reiter, P. Aedes albopictus and the world trade in used tires, 1988-1995: the shape of things to come? *Journal of the American Mosquito Control Association* **14**, 83-94 (1998).

40 Leichtenstern, O. M. L. *Influenza und dengue*. (Wien: Alfred Hölder, 1896).

41 Jansen, C. C. & Beebe, N. W. The dengue vector Aedes aegypti: what comes next. *Microbes and infection* **12**, 272-279 (2010).

42 Roser, M., Ritchie, H. & Ortiz-Ospina, E. World population growth. *Our world in data* (2013).

43 Coale, A. J. & Hoover, E. M. *Population growth and economic development*. Vol. 2319 (Princeton University Press, 2015).

44 Vlahov, D. & Galea, S. Urbanization, urbanicity, and health. *Journal of Urban Health* **79**, S1-S12 (2002).

45 Mousson, L. *et al.* Phylogeography of Aedes (Stegomyia) aegypti (L.) and Aedes (Stegomyia) albopictus (Skuse)(Diptera: Culicidae) based on mitochondrial DNA variations. *Genetics Research* **86**, 1-11 (2005).

46 Wilder-Smith, A. Dengue infections in travellers. *Paediatrics and international child health* **32**, 28-32 (2012).

47 Colón-González, F. J., Fezzi, C., Lake, I. R. & Hunter, P. R. The effects of weather and climate change on dengue. *PLoS neglected tropical diseases* **7**, e2503 (2013).

48 Ebi, K. L. & Nealon, J. Dengue in a changing climate. *Environmental Research* **151**, 115-123 (2016).

49 Messina, J. P. *et al.* The current and future global distribution and population at risk of dengue. *Nature Microbiology* **4**, 1508-1515 (2019).

50 Bhatt, S. *et al.* The global distribution and burden of dengue. *Nature* **496**, 504-507 (2013).

51 Sharp, T. M. *et al.* Knowledge gaps in the epidemiology of severe dengue impede vaccine evaluation. *The Lancet Infectious Diseases* (2021).

52 Puntasecca, C. J., King, C. H. & LaBeaud, A. D. Measuring the global burden of chikungunya and Zika viruses: A systematic review. *PLoS neglected tropical diseases* **15**, e0009055 (2021).

53 Pierson, T. C. & Diamond, M. S. The continued threat of emerging flaviviruses. *Nature microbiology* **5**, 796-812 (2020).

54 Zeng, W., Halasa-Rappel, Y. A., Durand, L., Coudeville, L. & Shepard, D. S. Impact of a nonfatal dengue episode on disability-adjusted life years: a systematic analysis. *The American journal of tropical medicine and hygiene* **99**, 1458 (2018).

55 Gibbons, R. V. *et al.* Analysis of repeat hospital admissions for dengue to estimate the frequency of third or fourth dengue infections resulting in admissions and dengue hemorrhagic fever, and serotype sequences. *The American journal of tropical medicine and hygiene* **77**, 910-913 (2007).

56 Reich, N. G. *et al.* Interactions between serotypes of dengue highlight epidemiological impact of cross-immunity. *Journal of The Royal Society Interface* **10**, 20130414 (2013).

57 Ribeiro, G. S. *et al.* Influence of herd immunity in the cyclical nature of arboviruses. *Current opinion in virology* **40**, 1-10 (2020).

58 Rothman, A. L. Immunity to dengue virus: a tale of original antigenic sin and tropical cytokine storms. *Nature Reviews Immunology* **11**, 532-543 (2011).

59 St John, A. L. & Rathore, A. P. Adaptive immune responses to primary and secondary dengue virus infections. *Nature Reviews Immunology* **19**, 218-230 (2019).

60 Rosenberger, K. D. *et al.* Vascular leakage in dengue–clinical spectrum and influence of parenteral fluid therapy. *Tropical medicine & international health* **21**, 445-453 (2016).

61 Lam, P. K. *et al.* Clinical characteristics of dengue shock syndrome in Vietnamese children: a 10-year prospective study in a single hospital. *Clinical Infectious Diseases* **57**, 1577-1586 (2013).

62 Halstead, S. B. Pathogenesis of dengue: dawn of a new era. *F1000Research* **4** (2015).

63 Murray, N. E. A., Quam, M. B. & Wilder-Smith, A. Epidemiology of dengue: past, present and future prospects. *Clinical epidemiology* **5**, 299 (2013).

64 Guzman, M. G., Alvarez, M. & Halstead, S. B. Secondary infection as a risk factor for dengue hemorrhagic fever/dengue shock syndrome: an historical perspective and role

of antibody-dependent enhancement of infection. *Archives of virology* **158**, 1445-1459 (2013).

65 Calisher, C. H. *et al.* Antigenic Relationships between Flaviviruses as Determined by Cross-neutralization Tests with Polyclonal Antisera. *Journal of General Virology* **70**, 37-43 (1989).

66 Halstead, S. B. Observations related to pathogensis of dengue hemorrhagic fever. VI. Hypotheses and discussion. *Yale J Biol Med* **42**, 350-362 (1970).

67 Katzelnick, L. C. *et al.* Antibody-dependent enhancement of severe dengue disease in humans. *Science* **358**, 929-932 (2017).

68 Halstead, S. & O'rourke, E. Dengue viruses and mononuclear phagocytes. I. Infection enhancement by non-neutralizing antibody. *The Journal of experimental medicine* **146**, 201-217 (1977).

69 Wrammert, J. *et al.* Rapid and massive virus-specific plasmablast responses during acute dengue virus infection in humans. *Journal of virology* **86**, 2911-2918 (2012).

70 Chan, C. Y. *et al.* Antibody-Dependent dengue virus entry modulates cell intrinsic responses for enhanced infection. *Msphere* **4**, e00528-00519 (2019).

71 St John, A. L., Rathore, A. P., Raghavan, B., Ng, M.-L. & Abraham, S. N. Contributions of mast cells and vasoactive products, leukotrienes and chymase, to dengue virus-induced vascular leakage. *elife* **2**, e00481 (2013).

72 Syenina, A., Jagaraj, C. J., Aman, S. A., Sridharan, A. & St John, A. L. Dengue vascular leakage is augmented by mast cell degranulation mediated by immunoglobulin Fcγ receptors. *elife* **4**, e05291 (2015).

73 Kurane, I., Hebblewaite, D., Brandt, W. E. & Ennis, F. A. Lysis of dengue virus-infected cells by natural cell-mediated cytotoxicity and antibody-dependent cell-mediated cytotoxicity. *Journal of virology* **52**, 223-230 (1984).

74 Dung, N. T. P. *et al.* Timing of CD8+ T cell responses in relation to commencement of capillary leakage in children with dengue. *The Journal of Immunology* **184**, 7281-7287 (2010).

75 Weiskopf, D. *et al.* Comprehensive analysis of dengue virus-specific responses supports an HLA-linked protective role for CD8+ T cells. *Proceedings of the National Academy of Sciences* **110**, E2046-E2053 (2013).

76 Culshaw, A. *et al.* Germline bias dictates cross-serotype reactivity in a common dengue-virus-specific CD8+ T cell response. *Nature immunology* **18**, 1228-1237 (2017).

77 Mongkolsapaya, J. *et al.* Original antigenic sin and apoptosis in the pathogenesis of dengue hemorrhagic fever. *Nature medicine* **9**, 921-927 (2003).

78 Dong, D., Xie, W. & Liu, M. Alteration of cell junctions during viral infection. *Thoracic Cancer* **11**, 519-525 (2020).

79 Muller, D. A. & Young, P. R. The flavivirus NS1 protein: molecular and structural biology, immunology, role in pathogenesis and application as a diagnostic biomarker. *Antiviral research* **98**, 192-208 (2013).

80 Puerta-Guardo, H., Glasner, D. R. & Harris, E. Dengue virus NS1 disrupts the endothelial glycocalyx, leading to hyperpermeability. *PLoS pathogens* **12**, e1005738 (2016).

81 Puerta-Guardo, H. *et al.* Flavivirus NS1 Triggers Tissue-Specific Disassembly of Intercellular Junctions Leading to Barrier Dysfunction and Vascular Leak in a GSK-3β-Dependent Manner. *Pathogens* **11**, 615 (2022).

82 Nascimento, E. J. *et al.* Alternative complement pathway deregulation is correlated with dengue severity. *PloS one* **4**, e6782 (2009).

83 Avirutnan, P. *et al.* Vascular leakage in severe dengue virus infections: a potential role for the nonstructural viral protein NS1 and complement. *The Journal of infectious diseases* **193**, 1078-1088 (2006).

84 Chang, H.-H. *et al.* Facilitation of cell adhesion by immobilized dengue viral nonstructural protein 1 (NS1): arginine-glycine-aspartic acid structural mimicry within the dengue viral NS1 antigen. *The Journal of infectious diseases* **186**, 743-751 (2002).

85 Falconar, A. The dengue virus nonstructural-1 protein (NS1) generatesantibodies to common epitopes on human blood clotting, integrin/adhesin proteins and binds to humanendothelial cells: potential implications in haemorrhagic fever pathogenesis. *Archives of virology* **142**, 897-916 (1997).

86 Sun, D. S. *et al.* Antiplatelet autoantibodies elicited by dengue virus non-structural protein 1 cause thrombocytopenia and mortality in mice. *Journal of Thrombosis and Haemostasis* **5**, 2291-2299 (2007).

87 Leitmeyer, K. C. *et al.* Dengue virus structural differences that correlate with pathogenesis. *Journal of virology* **73**, 4738-4747 (1999).

88 Rico-Hesse, R. Microevolution and virulence of dengue viruses. *Advances in virus research* **59**, 315-341 (2003).

89 Rico-Hesse, R. *et al.* Origins of dengue type 2 viruses associated with increased pathogenicity in the Americas. *Virology* **230**, 244-251 (1997).

90 Cologna, R., Armstrong, P. M. & Rico-Hesse, R. Selection for virulent dengue viruses occurs in humans and mosquitoes. *Journal of virology* **79**, 853-859 (2005).

91 Suppiah, J. *et al.* Clinical manifestations of dengue in relation to dengue serotype and genotype in Malaysia: A retrospective observational study. *PLoS neglected tropical diseases* **12**, e0006817 (2018).

92 Kalayanarooj, S. & Nimmannitya, S. Clinical and laboratory presentations of dengue patients with different serotypes. (2000).

93 Chan, K.-S. *et al.* Effect of serotypes on clinical manifestations of dengue fever in adults. *J Microbiol Immunol Infect* **42**, 471-478 (2009).

94 Halsey, E. S. *et al.* Correlation of serotype-specific dengue virus infection with clinical manifestations. *PLoS neglected tropical diseases* **6**, e1638 (2012).

95 Gebhard, L. G., Filomatori, C. V. & Gamarnik, A. V. Functional RNA elements in the dengue virus genome. *Viruses* **3**, 1739-1756 (2011).

96 Bradrick, S. S. Causes and consequences of flavivirus RNA methylation. *Frontiers in microbiology* **8**, 2374 (2017).

97 Wengler, G. & Wengler, G. The NS 3 nonstructural protein of flaviviruses contains an RNA triphosphatase activity. *Virology* **197**, 265-273 (1993).

98 Bartelma, G. & Padmanabhan, R. Expression, purification, and characterization of the RNA 5′-triphosphatase activity of dengue virus type 2 nonstructural protein 3. *Virology* **299**, 122-132 (2002).

99 Ray, D. *et al.* West Nile virus 5′-cap structure is formed by sequential guanine N-7 and ribose 2′-O methylations by nonstructural protein 5. *Journal of virology* **80**, 8362-8370 (2006).

100 Chang, D. C. *et al.* Evasion of early innate immune response by 2′-O-methylation of dengue genomic RNA. *Virology* **499**, 259-266 (2016).

101 Hsu, C. L. & Stevens, A. Yeast cells lacking 5'--> 3'exoribonuclease 1 contain mRNA species that are poly (A) deficient and partially lack the 5'cap structure. *Molecular and cellular biology* **13**, 4826-4835 (1993).

102 Zhou, Y. *et al.* Structure and function of flavivirus NS5 methyltransferase. *Journal of virology* **81**, 3891-3903 (2007).

103 Dong, H. *et al.* Biochemical and genetic characterization of dengue virus methyltransferase. *Virology* **405**, 568-578 (2010).

104 Barrows, N. J. *et al.* Biochemistry and molecular biology of flaviviruses. *Chemical reviews* **118**, 4448-4482 (2018).

105 Wang, A., Thurmond, S., Islas, L., Hui, K. & Hai, R. Zika virus genome biology and molecular pathogenesis. *Emerging microbes & infections* **6**, 1-6 (2017).

106 Cerikan, B. *et al.* A non-replicative role of the 3′ terminal sequence of the dengue virus genome in membranous replication organelle formation. *Cell reports* **32**, 107859 (2020).

107 Berzal-Herranz, A., Berzal-Herranz, B., Ramos-Lorente, S. E. & Romero-López, C. The Genomic 3′ UTR of Flaviviruses Is a Translation Initiation Enhancer. *International Journal of Molecular Sciences* **23**, 8604 (2022).

108 Filomatori, C. V. *et al.* A 5′ RNA element promotes dengue virus RNA synthesis on a circular genome. *Genes & development* **20**, 2238-2249 (2006).

109 Liu, Z.-Y. *et al.* Novel cis-acting element within the capsid-coding region enhances flavivirus viral-RNA replication by regulating genome cyclization. *Journal of virology* **87**, 6804-6818 (2013).

110 Diamond, M. S. & Pierson, T. C. Molecular Insight into Dengue Virus Pathogenesis and Its Implications for Disease Control. *Cell* **162**, 488-492 (2015).

111 Cahour, A., Falgout, B. & Lai, C. Cleavage of the dengue virus polyprotein at the NS3/NS4A and NS4B/NS5 junctions is mediated by viral protease NS2B-NS3, whereas NS4A/NS4B may be processed by a cellular protease. *Journal of virology* **66**, 1535-1542 (1992).

112 Stocks, C. & Lobigs, M. Signal peptidase cleavage at the flavivirus C-prM junction: dependence on the viral NS2B-3 protease for efficient processing requires determinants in C, the signal peptide, and prM. *Journal of virology* **72**, 2141-2149 (1998).

113 Lobigs, M. & Lee, E. Inefficient signalase cleavage promotes efficient nucleocapsid incorporation into budding flavivirus membranes. *Journal of virology* **78**, 178-186 (2004).

114 Lee, E., Stocks, C. E., Amberg, S. M., Rice, C. M. & Lobigs, M. Mutagenesis of the signal sequence of yellow fever virus prM protein: enhancement of signalase cleavage in vitro is lethal for virus production. *Journal of virology* **74**, 24-32 (2000).

115 Amberg, S. M. & Rice, C. M. Mutagenesis of the NS2B-NS3-mediated cleavage site in the flavivirus capsid protein demonstrates a requirement for coordinated processing. *Journal of virology* **73**, 8083-8094 (1999).

116 Roosendaal, J., Westaway, E. G., Khromykh, A. & Mackenzie, J. M. Regulated cleavages at the West Nile virus NS4A-2K-NS4B junctions play a major role in rearranging cytoplasmic membranes and Golgi trafficking of the NS4A protein. *Journal of virology* **80**, 4623-4632 (2006).

117 Chatel-Chaix, L. *et al.* A combined genetic-proteomic approach identifies residues within Dengue virus NS4B critical for interaction with NS3 and viral replication. *Journal of virology* **89**, 7170-7186 (2015).

118 Lin, C., Amberg, S. M., Chambers, T. J. & Rice, C. M. Cleavage at a novel site in the NS4A region by the yellow fever virus NS2B-3 proteinase is a prerequisite for processing at the downstream 4A/4B signalase site. *Journal of virology* **67**, 2327-2335 (1993).

119 Neufeldt, C. J., Cortese, M., Acosta, E. G. & Bartenschlager, R. Rewiring cellular networks by members of the Flaviviridae family. *Nature Reviews Microbiology* **16**, 125-142 (2018).

120 Jones, C. T. *et al.* Flavivirus capsid is a dimeric alpha-helical protein. *Journal of virology* **77**, 7143-7149 (2003).

121 Byk, L. A. & Gamarnik, A. V. Properties and functions of the dengue virus capsid protein. *Annual review of virology* **3**, 263 (2016).

122 Pong, W.-L., Huang, Z.-S., Teoh, P.-G., Wang, C.-C. & Wu, H.-N. RNA binding property and RNA chaperone activity of dengue virus core protein and other viral RNA-interacting proteins. *FEBS letters* **585**, 2575-2581 (2011).

123 Colpitts, T. M., Barthel, S., Wang, P. & Fikrig, E. Dengue virus capsid protein binds core histones and inhibits nucleosome formation in human liver cells. *PloS one* **6**, e24365 (2011).

124 Netsawang, J. *et al.* Nuclear localization of dengue virus capsid protein is required for DAXX interaction and apoptosis. *Virus research* **147**, 275-283 (2010).

125 Li, L. *et al.* The flavivirus precursor membrane-envelope protein complex: structure and maturation. *Science* **319**, 1830-1834 (2008).

126 Nasar, S., Rashid, N. & Iftikhar, S. Dengue proteins with their role in pathogenesis, and strategies for developing an effective anti-dengue treatment: A review. *Journal of medical virology* **92**, 941-955 (2020).

127 Zhang, Y. *et al.* Structures of immature flavivirus particles. *The EMBO journal* **22**, 2604-2613 (2003).

128 Yu, I.-M. *et al.* Structure of the immature dengue virus at low pH primes proteolytic maturation. *Science* **319**, 1834-1837 (2008).

129 Yu, I.-M. *et al.* Association of the pr peptides with dengue virus at acidic pH blocks membrane fusion. *Journal of virology* **83**, 12101-12107 (2009).

130 Zhang, X. *et al.* Dengue structure differs at the temperatures of its human and mosquito hosts. *Proceedings of the National Academy of Sciences* **110**, 6795-6799 (2013).

131 Winkler, G., Heinz, F. X. & Kunz, C. Studies on the glycosylation of flavivirus E proteins and the role of carbohydrate in antigenic structure. *Virology* **159**, 237-243 (1987).

132 Allison, S. L., Schalich, J., Stiasny, K., Mandl, C. W. & Heinz, F. X. Mutational evidence for an internal fusion peptide in flavivirus envelope protein E. *Journal of virology* **75**, 4268-4275 (2001).

133 Erb, S. M. *et al.* Domain-III FG loop of the dengue virus type 2 envelope protein is important for infection of mammalian cells and Aedes aegypti mosquitoes. *Virology* **406**, 328-335 (2010).

134 Modis, Y., Ogata, S., Clements, D. & Harrison, S. C. Structure of the dengue virus envelope protein after membrane fusion. *Nature* **427**, 313-319 (2004).

135 Zhang, Y. *et al.* Conformational changes of the flavivirus E glycoprotein. *Structure* **12**, 1607-1618 (2004).

136 Nowak, T., Färber, P. M., Wengler, G. & Wengler, G. Analyses of the terminal sequences of West Nile virus structural proteins and of the in vitro translation of these proteins allow the proposal of a complete scheme of the proteolytic cleavages involved in their synthesis. *Virology* **169**, 365-376 (1989).

137 Falgout, B. & Markoff, L. Evidence that flavivirus NS1-NS2A cleavage is mediated by a membrane-bound host protease in the endoplasmic reticulum. *Journal of virology* **69**, 7232-7243 (1995).

138 Winkler, G., Maxwell, S. E., Ruemmler, C. & Stollar, V. Newly synthesized dengue-2 virus nonstructural protein NS1 is a soluble protein but becomes partially hydrophobic and membrane-associated after dimerization. *Virology* **171**, 302-305 (1989).

139 Mackenzie, J. M., Jones, M. K. & Young, P. R. Immunolocalization of the dengue virus nonstructural glycoprotein NS1 suggests a role in viral RNA replication. *Virology* **220**, 232-240 (1996).

140 Płaszczyca, A. *et al.* A novel interaction between dengue virus nonstructural protein 1 and the NS4A-2K-4B precursor is required for viral RNA replication but not for formation of the membranous replication organelle. *PLoS Pathogens* **15**, e1007736 (2019).

141 Flamand, M. *et al.* Dengue virus type 1 nonstructural glycoprotein NS1 is secreted from mammalian cells as a soluble hexamer in a glycosylation-dependent fashion. *Journal of virology* **73**, 6104-6110 (1999).

142 Glasner, D. R., Puerta-Guardo, H., Beatty, P. R. & Harris, E. The good, the bad, and the shocking: the multiple roles of dengue virus nonstructural protein 1 in protection and pathogenesis. *Annual review of virology* **5**, 227 (2018).

143 Shu, P. Y. *et al.* Dengue NS1-specific antibody responses: Isotype distribution and serotyping in patients with dengue fever and dengue hemorrhagic fever. *Journal of medical virology* **62**, 224-232 (2000).

144 Xie, X., Gayen, S., Kang, C., Yuan, Z. & Shi, P.-Y. Membrane topology and function of dengue virus NS2A protein. *Journal of virology* **87**, 4609-4622 (2013).

145 Xie, X., Zou, J., Puttikhunt, C., Yuan, Z. & Shi, P.-Y. Two distinct sets of NS2A molecules are responsible for dengue virus RNA synthesis and virion assembly. *Journal of virology* **89**, 1298-1313 (2015).

146 Wu, R.-H. *et al.* Mutagenesis of dengue virus protein NS2A revealed a novel domain responsible for virus-induced cytopathic effect and interactions between NS2A and NS2B transmembrane segments. *Journal of virology* **91**, e01836-01816 (2017).

147 Xie, X. *et al.* Dengue NS2A protein orchestrates virus assembly. *Cell host & microbe* **26**, 606-622. e608 (2019).

148 Dalrymple, N. A., Cimica, V. & Mackow, E. R. Dengue virus NS proteins inhibit RIG-I/MAVS signaling by blocking TBK1/IRF3 phosphorylation: dengue virus serotype 1 NS4A is a unique interferon-regulating virulence determinant. *MBio* **6**, e00553-00515 (2015).

149 Falgout, B., Pethel, M., Zhang, Y.-M. & Lai, C. Both nonstructural proteins NS2B and NS3 are required for the proteolytic processing of dengue virus nonstructural proteins. *Journal of virology* **65**, 2467-2475 (1991).

150 Chappell, K. J., Stoermer, M. J., Fairlie, D. P. & Young, P. R. Mutagenesis of the West Nile virus NS2B cofactor domain reveals two regions essential for protease activity. *Journal of general virology* **89**, 1010-1014 (2008).

151 Aguirre, S. *et al.* Dengue virus NS2B protein targets cGAS for degradation and prevents mitochondrial DNA sensing during infection. *Nature microbiology* **2**, 1-11 (2017).

152 Luo, D., Vasudevan, S. G. & Lescar, J. The flavivirus NS2B–NS3 protease–helicase as a target for antiviral drug development. *Antiviral research* **118**, 148-158 (2015).

153 Luo, D. *et al.* Crystal structure of the NS3 protease-helicase from dengue virus. *Journal of virology* **82**, 173-183 (2008).

154 Phong, W. Y. *et al.* Dengue protease activity: the structural integrity and interaction of NS2B with NS3 protease and its potential as a drug target. *Bioscience reports* **31**, 399-409 (2011).

155 Reddy, S. B. G., Chin, W.-X. & Shivananju, N. S. Dengue virus NS2 and NS4: Minor proteins, mammoth roles. *Biochemical pharmacology* **154**, 54-63 (2018).

156 Li, J. *et al.* Functional profiling of recombinant NS3 proteases from all four serotypes of dengue virus using tetrapeptide and octapeptide substrate libraries. *Journal of Biological Chemistry* **280**, 28766-28774 (2005).

157 Story, R. M. & Steitz, T. A. Structure of the recA protein–ADP complex. *Nature* **355**, 374-376 (1992).

158 Lescar, J. *et al.* Towards the design of antiviral inhibitors against flaviviruses: the case for the multifunctional NS3 protein from Dengue virus as a target. *Antiviral research* **80**, 94-101 (2008).

159 Le Breton, M. *et al.* Flavivirus NS3 and NS5 proteins interaction network: a high-throughput yeast two-hybrid screen. *BMC microbiology* **11**, 1-11 (2011).

160 Heaton, N. S. *et al.* Dengue virus nonstructural protein 3 redistributes fatty acid synthase to sites of viral replication and increases cellular fatty acid synthesis. *Proceedings of the National Academy of Sciences* **107**, 17345-17350 (2010).

161 Tang, W.-C., Lin, R.-J., Liao, C.-L. & Lin, Y.-L. Rab18 facilitates dengue virus infection by targeting fatty acid synthase to sites of viral replication. *Journal of virology* **88**, 6793-6804 (2014).

162 Gebhard, L. G. *et al.* A proline-rich N-terminal region of the dengue virus NS3 is crucial for infectious particle production. *Journal of virology* **90**, 5451-5461 (2016).

163 Hung, Y.-F. *et al.* Amino terminal region of dengue virus NS4A cytosolic domain binds to highly curved liposomes. *Viruses* **7**, 4119-4130 (2015).

164 Miller, S., Kastner, S., Krijnse-Locker, J., Bühler, S. & Bartenschlager, R. The non-structural protein 4A of dengue virus is an integral membrane protein inducing membrane alterations in a 2K-regulated manner. *Journal of Biological Chemistry* **282**, 8873-8882 (2007).

165 Lee, C. M. *et al.* Determinants of dengue virus NS4A protein oligomerization. *Journal of virology* **89**, 6171-6183 (2015).

166 Zou, J. *et al.* Characterization of dengue virus NS4A and NS4B protein interaction. *Journal of virology* **89**, 3455-3470 (2015).

167 Teo, C. S. H. & Chu, J. J. H. Cellular vimentin regulates construction of dengue virus replication complexes through interaction with NS4A protein. *Journal of virology* **88**, 1897-1913 (2014).

168 Jiang, L., Yao, H., Duan, X., Lu, X. & Liu, Y. Polypyrimidine tract-binding protein influences negative strand RNA synthesis of dengue virus. *Biochemical and biophysical research communications* **385**, 187-192 (2009).

169 McLean, J. E., Wudzinska, A., Datan, E., Quaglino, D. & Zakeri, Z. Flavivirus NS4A-induced autophagy protects cells against death and enhances virus replication. *Journal of Biological Chemistry* **286**, 22147-22159 (2011).

170 Zhang, J. *et al.* Flaviviruses exploit the lipid droplet protein AUP1 to trigger lipophagy and drive virus production. *Cell host & microbe* **23**, 819-831. e815 (2018).

171 Wang, Y., Xie, X. & Shi, P.-Y. Flavivirus NS4B protein: Structure, function, and antiviral discovery. *Antiviral Research*, 105423 (2022).

172 Miller, S., Sparacio, S. & Bartenschlager, R. Subcellular localization and membrane topology of the dengue virus type 2 non-structural protein 4B. *Journal of Biological Chemistry* **281**, 8854-8863 (2006).

173 Zou, J. *et al.* Mapping the interactions between the NS4B and NS3 proteins of dengue virus. *Journal of virology* **89**, 3471-3483 (2015).

174 Li, Y. *et al.* Secondary structure and membrane topology of dengue virus NS4B N-terminal 125 amino acids. *Biochimica et Biophysica Acta (BBA)-Biomembranes* **1848**, 3150-3157 (2015).

175 Shurtleff, M. J. *et al.* The ER membrane protein complex interacts cotranslationally to enable biogenesis of multipass membrane proteins. *Elife* **7**, e37018 (2018).

176 Lin, D. L. *et al.* The ER membrane protein complex promotes biogenesis of dengue and Zika virus non-structural multi-pass transmembrane proteins to support infection. *Cell reports* **27**, 1666-1674. e1664 (2019).

177 Ngo, A. M. *et al.* The ER membrane protein complex is required to ensure correct topology and stable expression of flavivirus polyproteins. *Elife* **8**, e48469 (2019).

178 Naik, N. G. & Wu, H.-N. Mutation of putative N-glycosylation sites on dengue virus NS4B decreases RNA replication. *Journal of Virology* **89**, 6746-6760 (2015).

179 Hafirassou, M. L. *et al.* A global interactome map of the dengue virus NS1 identifies virus restriction and dependency host factors. *Cell reports* **21**, 3900-3913 (2017).

180 Zou, J. *et al.* Dimerization of flavivirus NS4B protein. *Journal of virology* **88**, 3379-3391 (2014).

181 Zmurko, J., Neyts, J. & Dallmeier, K. J. R. i. m. v. Flaviviral NS4b, chameleon and jack-in-the-box roles in viral replication and pathogenesis, and a molecular target for antiviral intervention. **25**, 205-223 (2015).

182 Umareddy, I., Chao, A., Sampath, A., Gu, F. & Vasudevan, S. G. Dengue virus NS4B interacts with NS3 and dissociates it from single-stranded RNA. *Journal of general virology* **87**, 2605-2614 (2006).

183 Lu, H. *et al.* Novel insights into the function of an N-terminal region of DENV2 NS4B for the optimal helicase activity of NS3. *Virus Research* **295**, 198318 (2021).

184 Takeuchi, O. & Akira, S. MDA5/RIG-I and virus recognition. *Current opinion in immunology* **20**, 17-22 (2008).

185 Tsai, Y. T., Chang, S. Y., Lee, C. N. & Kao, C. L. Human TLR3 recognizes dengue virus and modulates viral replication in vitro. *Cellular microbiology* **11**, 604-615 (2009).

186 Schneider, W. M., Chevillotte, M. D. & Rice, C. M. Interferon-stimulated genes: a complex web of host defenses. *Annual review of immunology* **32**, 513 (2014).

187 Schoggins, J. W. *et al.* A diverse range of gene products are effectors of the type I interferon antiviral response. *Nature* **472**, 481-485 (2011).

188 Munoz-Jordán, J. L. *et al.* Inhibition of alpha/beta interferon signaling by the NS4B protein of flaviviruses. *Journal of virology* **79**, 8004-8013 (2005).

189 Muñoz-Jordán, J. L. Subversion of interferon by dengue virus. *Dengue Virus*, 35-44 (2010).

190 Ashour, J., Laurent-Rolle, M., Shi, P.-Y. & García-Sastre, A. NS5 of dengue virus mediates STAT2 binding and degradation. *Journal of virology* **83**, 5408-5418 (2009).

191 Chatel-Chaix, L. *et al.* Dengue virus perturbs mitochondrial morphodynamics to dampen innate immune responses. *Cell host & microbe* **20**, 342-356 (2016).

192 Aguirre, S. *et al.* DENV inhibits type I IFN production in infected cells by cleaving human STING. (2012).

193 Kakumani, P. K. *et al.* Role of RNA interference (RNAi) in dengue virus replication and identification of NS4B as an RNAi suppressor. *Journal of virology* **87**, 8870-8883 (2013).

194 Arakawa, M. *et al.* Flavivirus recruits the valosin-containing protein–NPL4 complex to induce stress granule disassembly for efficient viral genome replication. *Journal of Biological Chemistry* **298** (2022).

195 Yu, C.-Y., Hsu, Y.-W., Liao, C.-L. & Lin, Y.-L. Flavivirus infection activates the XBP1 pathway of the unfolded protein response to cope with endoplasmic reticulum stress. *Journal of virology* **80**, 11868-11880 (2006).

196 Pryor, M. J. *et al.* Nuclear localization of dengue virus nonstructural protein 5 Through Its Importin α/β–recognized nuclear localization sequences is integral to viral infection. *Traffic* **8**, 795-807 (2007).

197 Lim, S. P., Noble, C. G. & Shi, P.-Y. The dengue virus NS5 protein as a target for drug discovery. *Antiviral research* **119**, 57-67 (2015).

198 Koonin, E. V. The phylogeny of RNA-dependent RNA polymerases of positive-strand RNA viruses. *Journal of General Virology* **72**, 2197-2206 (1991).

199 Selisko, B., Wang, C., Harris, E. & Canard, B. Regulation of Flavivirus RNA synthesis and replication. *Current opinion in virology* **9**, 74-83 (2014).

200 Selisko, B. *et al.* Molecular basis for nucleotide conservation at the ends of the dengue virus genome. (2012).

201 El Sahili, A. & Lescar, J. Dengue virus non-structural protein 5. *Viruses* **9**, 91 (2017).

202 Johansson, M., Brooks, A. J., Jans, D. A. & Vasudevan, S. G. A small region of the dengue virus-encoded RNA-dependent RNA polymerase, NS5, confers interaction with both the nuclear transport receptor importin-β and the viral helicase, NS3. *Journal of General Virology* **82**, 735-745 (2001).

203 Issur, M. *et al.* The flavivirus NS5 protein is a true RNA guanylyltransferase that catalyzes a two-step reaction to form the RNA cap structure. *Rna* **15**, 2340-2350 (2009).

204 Zhao, Y. *et al.* Molecular basis for specific viral RNA recognition and 2′-O-ribose methylation by the dengue virus nonstructural protein 5 (NS5). *Proceedings of the National Academy of Sciences* **112**, 14834-14839 (2015).

205 Decroly, E., Ferron, F., Lescar, J. & Canard, B. Conventional and unconventional mechanisms for capping viral mRNA. *Nature Reviews Microbiology* **10**, 51-65 (2012).

206 Kumar, A. *et al.* Nuclear localization of dengue virus nonstructural protein 5 does not strictly correlate with efficient viral RNA replication and inhibition of type I interferon signaling. *Journal of virology* **87**, 4545-4557 (2013).

207 Chambers, T. J., McCourt, D. W. & Rice, C. M. Production of yellow fever virus proteins in infected cells: identification of discrete polyprotein species and analysis of cleavage kinetics using region-specific polyclonal antisera. *Virology* **177**, 159-174 (1990).

208 Svitkin, Y. V., Lyapustin, V. N., Lashkevich, V. A. & Agol, V. I. Differences between translation products of tick-borne encephalitis virus RNA in cell-free systems from Krebs-2 cells and rabbit reticulocytes: involvement of membranes in the processing of nascent precursors of flavivirus structural proteins. *Virology* **135**, 536-541 (1984).

209 Zhang, L., Mohan, P. M. & Padmanabhan, R. Processing and localization of Dengue virus type 2 polyprotein precursor NS3-NS4A-NS4B-NS5. *Journal of virology* **66**, 7549-7554 (1992).

210 Mukhopadhyay, S., Kuhn, R. J. & Rossmann, M. G. A structural perspective of the flavivirus life cycle. *Nature Reviews Microbiology* **3**, 13-22 (2005).

211 Kuhn, R. J. *et al.* Structure of dengue virus: implications for flavivirus organization, maturation, and fusion. *Cell* **108**, 717-725 (2002).

212 Zhang, W. *et al.* Visualization of membrane protein domains by cryo-electron microscopy of dengue virus. *Nature Structural & Molecular Biology* **10**, 907-912 (2003).

213 Kuhn, R. J., Dowd, K. A., Post, C. B. & Pierson, T. C. Shake, rattle, and roll: Impact of the dynamics of flavivirus particles on their interactions with the host. *Virology* **479**, 508-517 (2015).

214 Zhang, Y., Kostyuchenko, V. A. & Rossmann, M. G. Structural analysis of viral nucleocapsids by subtraction of partial projections. *Journal of structural biology* **157**, 356-364 (2007).

215 Cerny, D. *et al.* Selective susceptibility of human skin antigen presenting cells to productive dengue virus infection. *PLoS pathogens* **10**, e1004548 (2014).

216 Schaeffer, E. *et al.* Dermal CD14+ dendritic cell and macrophage infection by dengue virus is stimulated by interleukin-4. *Journal of Investigative Dermatology* **135**, 1743-1751 (2015).

217 Troupin, A. *et al.* A role for human skin mast cells in dengue virus infection and systemic spread. *The Journal of Immunology* **197**, 4382-4391 (2016).

218 Wu, S.-J. L. *et al.* Human skin Langerhans cells are targets of dengue virus infection. *Nature medicine* **6**, 816-820 (2000).

219 Prestwood, T. R. *et al.* Trafficking and replication patterns reveal splenic macrophages as major targets of dengue virus in mice. *Journal of virology* **86**, 12138-12147 (2012).

220 Martina, B. E., Koraka, P. & Osterhaus, A. D. Dengue virus pathogenesis: an integrated view. *Clinical microbiology reviews* **22**, 564-581 (2009).

221 Walid, S., Sanusi, S., Zawawi, M. M. & Ali, R. A. A comparison of the pattern of liver involvement in dengue hemorrhagic fever with classic dengue fever. *Southeast Asian Journal of Tropical Medicine and Public Health* **31**, 259-263 (2000).

222 Pancharoen, C., Rungsarannont, A. & Thisyakorn, U. Hepatic dysfunction in dengue patients with various severity. *Journal of the Medical Association of Thailand= Chotmaihet Thangphaet* **85**, S298-301 (2002).

223 Itha, S. *et al.* Profile of liver involvement in dengue virus infection. *National Medical Journal of India* **18**, 127 (2005).

224 Bielefeldt-Ohmann, H., Meyer, M., Fitzpatrick, D. R. & Mackenzie, J. S. Dengue virus binding to human leukocyte cell lines: receptor usage differs between cell types and virus strains. *Virus Research* **73**, 81-89 (2001).

225 Sun, P. *et al.* Functional characterization of ex vivo blood myeloid and plasmacytoid dendritic cells after infection with dengue virus. *Virology* **383**, 207-215 (2009).

226 Povoa, T. F. *et al.* The pathology of severe dengue in multiple organs of human fatal cases: histopathology, ultrastructure and virus replication. *PloS one* **9**, e83386 (2014).

227 Salgado, D. M. *et al.* Heart and skeletal muscle are targets of dengue virus infection. *The Pediatric infectious disease journal* **29**, 238 (2010).

228 Ramos, C. *et al.* Dengue virus in the brain of a fatal case of hemorrhagic dengue fever: case report. *Journal of neurovirology* **4**, 465-468 (1998).

229 Bhoopat, L. *et al.* Immunohistochemical characterization of a new monoclonal antibody reactive with dengue virus-infected cells in frozen tissue using immunoperoxidase technique. *Asian Pacific Journal of Allergy and Immunology* **14**, 107 (1996).

230 de Araújo, J. M. G. *et al.* A retrospective survey of dengue virus infection in fatal cases from an epidemic in Brazil. *Journal of virological methods* **155**, 34-38 (2009).

231 Begum, F., Das, S., Mukherjee, D., Mal, S. & Ray, U. Insight into the tropism of dengue virus in humans. *Viruses* **11**, 1136 (2019).

232 Noisakran, S. *et al.* Cells in dengue virus infection in vivo. *Advances in virology* **2010** (2010).

233 Mendoza, M. Y., Salas-Benito, J. S., Lanz-Mendoza, H., Hernández-Martínez, S. & del Angel, R. M. A putative receptor for dengue virus in mosquito tissues: Location of a 45 kDa glycoprotein. (2002).

234 Hidari, K. I. & Suzuki, T. Dengue virus receptor. *Tropical medicine and health* **39**, S37-S43 (2011).

235 Lee, E., Wright, P. J., Davidson, A. & Lobigs, M. Virulence attenuation of Dengue virus due to augmented glycosaminoglycan-binding affinity and restriction in extraneural dissemination. *Journal of general virology* **87**, 2791-2801 (2006).

236 Artpradit, C. *et al.* Recognition of heparan sulfate by clinical strains of dengue virus serotype 1 using recombinant subviral particles. *Virus research* **176**, 69-77 (2013).

237 Wichit, S. *et al.* Dengue virus type 2 recognizes the carbohydrate moiety of neutral glycosphingolipids in mammalian and mosquito cells. *Microbiology and immunology* **55**, 135-140 (2011).

238 Aoki, C. *et al.* Identification and characterization of carbohydrate molecules in mammalian cells recognized by Dengue Virus Type 2. *Journal of Biochemistry* **139**, 607-614 (2006).

239 Miller, J. L. *et al.* The mannose receptor mediates dengue virus infection of macrophages. *PLoS pathogens* **4**, e17 (2008).

240 Tassaneetrithep, B. *et al.* DC-SIGN (CD209) mediates dengue virus infection of human dendritic cells. *The Journal of experimental medicine* **197**, 823-829 (2003).

241 Pokidysheva, E. *et al.* Cryo-EM reconstruction of dengue virus in complex with the carbohydrate recognition domain of DC-SIGN. *Cell* **124**, 485-493 (2006).

242 Dejnirattisai, W. *et al.* Lectin switching during dengue virus infection. *Journal of Infectious Diseases* **203**, 1775-1783 (2011).

243 Jindadamrongwech, S., Thepparit, C. & Smith, D. Identification of GRP 78 (BiP) as a liver cell expressed receptor element for dengue virus serotype 2. *Archives of virology* **149**, 915-927 (2004).

244 Reyes-del Valle, J., Chávez-Salinas, S., Medina, F. & Del Angel, R. M. Heat shock protein 90 and heat shock protein 70 are components of dengue virus receptor complex in human cells. *Journal of virology* **79**, 4557-4567 (2005).

245 Meertens, L. *et al.* The TIM and TAM families of phosphatidylserine receptors mediate dengue virus entry. *Cell host & microbe* **12**, 544-557 (2012).

246 Kuadkitkan, A., Wikan, N., Fongsaran, C. & Smith, D. R. Identification and characterization of prohibitin as a receptor protein mediating DENV-2 entry into insect cells. *Virology* **406**, 149-161 (2010).

247 Cruz-Oliveira, C. *et al.* Receptors and routes of dengue virus entry into the host cells. *FEMS microbiology reviews* **39**, 155-170 (2015).

248 Vaughan, K., Greenbaum, J., Blythe, M., Peters, B. & Sette, A. Meta-analysis of all immune epitope data in the Flavivirus genus: inventory of current immune epitope data status in the context of virus immunity and immunopathology. *Viral immunology* **23**, 259-284 (2010).

249 Luo, Y.-Y. *et al.* Identification of a novel infection-enhancing epitope on dengue prM using a dengue cross-reacting monoclonal antibody. *BMC microbiology* **13**, 1-16 (2013).

250 Acosta, E. G., Castilla, V. & Damonte, E. B. Functional entry of dengue virus into Aedes albopictus mosquito cells is dependent on clathrin-mediated endocytosis. *Journal of General Virology* **89**, 474-484 (2008).

251 Acosta, E. G., Castilla, V. & Damonte, E. B. Alternative infectious entry pathways for dengue virus serotypes into mammalian cells. *Cellular microbiology* **11**, 1533-1549 (2009).

252 Acosta, E. G., Castilla, V. & Damonte, E. B. Differential requirements in endocytic trafficking for penetration of dengue virus. (2012).

253 Pierson, T. C. & Kielian, M. Flaviviruses: braking the entering. *Current opinion in virology* **3**, 3-12 (2013).

254 Klein, D. E., Choi, J. L. & Harrison, S. C. Structure of a dengue virus envelope protein late-stage fusion intermediate. *Journal of virology* **87**, 2287-2293 (2013).

255 Freire, J. M. *et al.* Intracellular nucleic acid delivery by the supercharged dengue virus capsid protein. *PloS one* **8**, e81450 (2013).

256 Chiu, W.-W., Kinney, R. M. & Dreher, T. W. Control of translation by the 5′-and 3′-terminal regions of the dengue virus genome. *Journal of virology* **79**, 8303-8315 (2005).

257 Paranjape, S. M. & Harris, E. Control of dengue virus translation and replication. *Dengue virus*, 15-34 (2010).

258 Polacek, C., Friebe, P. & Harris, E. Poly (A)-binding protein binds to the non-polyadenylated 3′ untranslated region of dengue virus and modulates translation efficiency. *Journal of General Virology* **90**, 687-692 (2009).

259 Edgil, D., Polacek, C. & Harris, E. Dengue virus utilizes a novel strategy for translation initiation when cap-dependent translation is inhibited. *Journal of virology* **80**, 2976-2986 (2006).

260 Song, Y., Mugavero, J., Stauft, C. B. & Wimmer, E. Dengue and Zika virus 5′ untranslated regions harbor internal ribosomal entry site functions. *MBio* **10**, e00459-00419 (2019).

261 Fernández-García, L. *et al.* The internal ribosome entry site of dengue virus mRNA is Active when cap-dependent translation initiation is inhibited. *Journal of virology* **95**, e01998-01920 (2021).

262 Clyde, K. & Harris, E. RNA secondary structure in the coding region of dengue virus type 2 directs translation start codon selection and is required for viral replication. *Journal of virology* **80**, 2170-2182 (2006).

263 Chambers, T. J., Hahn, C. S., Galler, R. & Rice, C. M. Flavivirus genome organization, expression, and replication. *Annual review of microbiology* **44**, 649-688 (1990).

264 Welsch, S. *et al.* Composition and three-dimensional architecture of the dengue virus replication and assembly sites. *Cell host & microbe* **5**, 365-375 (2009).

265 Cortese, M. *et al.* Ultrastructural characterization of Zika virus replication factories. *Cell reports* **18**, 2113-2123 (2017).

266 Junjhon, J. *et al.* Ultrastructural characterization and three-dimensional architecture of replication sites in dengue virus-infected mosquito cells. *Journal of virology* **88**, 4687-4697 (2014).

267 Paul, D. & Bartenschlager, R. Flaviviridae replication organelles: oh, what a tangled web we weave. *Annu Rev Virol* **2**, 289-310 (2015).

268 Westaway, E. G., Mackenzie, J. M., Kenney, M. T., Jones, M. K. & Khromykh, A. A. Ultrastructure of Kunjin virus-infected cells: colocalization of NS1 and NS3 with double-stranded RNA, and of NS2B with NS3, in virus-induced membrane structures. *Journal of virology* **71**, 6650-6661 (1997).

269 Cortese, M. *et al.* Determinants in Nonstructural Protein 4A of Dengue Virus Required for RNA Replication and Replication Organelle Biogenesis. *Journal of Virology* **95**, e01310-01321 (2021).

270 Akey, D. L. *et al.* Flavivirus NS1 structures reveal surfaces for associations with membranes and the immune system. *Science* **343**, 881-885 (2014).

271 Heaton, N. S. & Randall, G. Dengue virus-induced autophagy regulates lipid metabolism. *Cell host & microbe* **8**, 422-432 (2010).

272 Garcia-Blanco, M. A., Vasudevan, S. G., Bradrick, S. S. & Nicchitta, C. Flavivirus RNA transactions from viral entry to genome replication. *Antiviral research* **134**, 244-249 (2016).

273 Villordo, S. M. & Gamarnik, A. V. Genome cyclization as strategy for flavivirus RNA replication. *Virus research* **139**, 230-239 (2009).

274 Barnard, T. R., Abram, Q. H., Lin, Q. F., Wang, A. B. & Sagan, S. M. Molecular determinants of flavivirus virion assembly. *Trends in biochemical sciences* **46**, 378-390 (2021).

275 Pierson, T. C. & Diamond, M. S. Degrees of maturity: the complex structure and biology of flaviviruses. *Current opinion in virology* **2**, 168-175 (2012).

276 Stadler, K., Allison, S. L., Schalich, J. & Heinz, F. X. Proteolytic activation of tick-borne encephalitis virus by furin. *Journal of virology* **71**, 8475-8481 (1997).

277 Oliveira, E. R., de Alencastro, R. B. & Horta, B. A. New insights into flavivirus biology: the influence of pH over interactions between prM and E proteins. *Journal of Computer-Aided Molecular Design* **31**, 1009-1019 (2017).

278 Junjhon, J. *et al.* Influence of pr-M cleavage on the heterogeneity of extracellular dengue virus particles. *Journal of virology* **84**, 8353-8358 (2010).

279 Dejnirattisai, W. *et al.* Cross-reacting antibodies enhance dengue virus infection in humans. *Science* **328**, 745-748 (2010).

280 Rodenhuis-Zybert, I. A. *et al.* Immature dengue virus: a veiled pathogen? *PLoS pathogens* **6**, e1000718 (2010).

281 Heinz, F. X. & Stiasny, K. Flaviviruses and flavivirus vaccines. *Vaccine* **30**, 4301-4306 (2012).

282 Thomas, S. J. & Yoon, I.-K. A review of Dengvaxia®: development to deployment. *Human vaccines & immunotherapeutics* **15**, 2295-2314 (2019).

283 Sridhar, S. *et al.* Effect of dengue serostatus on dengue vaccine safety and efficacy. *New England Journal of Medicine* **379**, 327-340 (2018).

284 Hadinegoro, S. R. *et al.* Efficacy and long-term safety of a dengue vaccine in regions of endemic disease. *New England Journal of Medicine* **373**, 1195-1206 (2015).

285 Sariol, C. A. & White, L. J. Utility, limitations, and future of non-human primates for dengue research and vaccine development. *Frontiers in immunology* **5**, 452 (2014).

286 Beatty, P. R. *et al.* Dengue virus NS1 triggers endothelial permeability and vascular leak that is prevented by NS1 vaccination. *Science translational medicine* **7**, 304ra141-304ra141 (2015).

287 Deng, S.-Q. *et al.* A review on dengue vaccine development. *Vaccines* **8**, 63 (2020).

288 Wilder-Smith, A. Serostatus-dependent performance of the first licensed dengue vaccine: implications for travellers. *Journal of travel medicine* **25**, tay057 (2018).

289 Wilder-Smith, A. *et al.* Deliberations of the Strategic Advisory Group of Experts on Immunization on the use of CYD-TDV dengue vaccine. *The Lancet Infectious Diseases* **19**, e31-e38 (2019).

290 Mallapaty, S. Dengue vaccine poised for roll-out but safety concerns linger. *Nature* (2022).

291 Bhamarapravati, N. & Sutee, Y. Live attenuated tetravalent dengue vaccine. *Vaccine* **18**, 44-47 (2000).

292 Brewoo, J. N. *et al.* Immunogenicity and efficacy of chimeric dengue vaccine (DENVax) formulations in interferon-deficient AG129 mice. *Vaccine* **30**, 1513-1520 (2012).

293 Whitehead, S. S. Development of TV003/TV005, a single dose, highly immunogenic live attenuated dengue vaccine; what makes this vaccine different from the Sanofi-Pasteur CYD™ vaccine? *Expert review of vaccines* **15**, 509-517 (2016).

294 Achee, N. L. *et al.* A critical assessment of vector control for dengue prevention. *PLoS neglected tropical diseases* **9**, e0003655 (2015).

295 WHO *et al. Dengue: guidelines for diagnosis, treatment, prevention and control*. (WHO, 2009).

296 Bowman, L. R., Donegan, S. & McCall, P. J. Is dengue vector control deficient in effectiveness or evidence?: Systematic review and meta-analysis. *PLoS neglected tropical diseases* **10**, e0004551 (2016).

297 Murray-Smith, S., Weinstein, P. & Skelly, C. Field epidemiology of an outbreak of dengue fever in Charters Towers, Queensland: are insect screens protective? *Australian and New Zealand Journal of Public Health* **20**, 545-547 (1996).

298 Ko, Y.-C., Chen, M.-J. & Yeh, S.-M. The predisposing and protective factors against dengue virus transmission by mosquito vector. *American Journal of Epidemiology* **136**, 214-220 (1992).

299 McBride, W. J. H., Mullner, H., Muller, R., Labrooy, J. & Wronski, I. Determinants of dengue 2 infection among residents of Charters Towers, Queensland, Australia. *American journal of epidemiology* **148**, 1111-1116 (1998).

300 Perich, M., Davila, G., Turner, A., Garcia, A. & Nelson, M. Behavior of resting Aedes aegypti (Culicidae: Diptera) and its relation to ultra-low volume adulticide efficacy in Panama City, Panama. *Journal of medical entomology* **37**, 541-546 (2000).

301 Toledo, M. E. *et al.* Evidence on impact of community-based environmental management on dengue transmission in Santiago de Cuba. *Tropical Medicine & International Health* **16**, 744-747 (2011).

302 Ranson, H., Burhani, J., Lumjuan, N. & Black IV, W. C. Insecticide resistance in dengue vectors. *TropIKA. net* **1** (2010).

303 Kamgang, B. *et al.* Insecticide susceptibility of Aedes aegypti and Aedes albopictus in Central Africa. *Parasites & vectors* **4**, 1-8 (2011).

304 Grisales, N. *et al.* Temephos resistance in Aedes aegypti in Colombia compromises dengue vector control. *PLoS neglected tropical diseases* **7**, e2438 (2013).

305 Lambrechts, L. *et al.* Assessing the epidemiological effect of Wolbachia for dengue control. *The Lancet Infectious Diseases* **15**, 862-866 (2015).

306 Werren, J. H., Baldo, L. & Clark, M. E. Wolbachia: master manipulators of invertebrate biology. *Nature Reviews Microbiology* **6**, 741-751 (2008).

307 Tram, U. & Sullivan, W. Role of delayed nuclear envelope breakdown and mitosis in Wolbachia-induced cytoplasmic incompatibility. *Science* **296**, 1124-1126 (2002).

308 Xi, Z., Khoo, C. C. & Dobson, S. L. Wolbachia establishment and invasion in an Aedes aegypti laboratory population. *Science* **310**, 326-328 (2005).

309 Bourtzis, K. *et al.* Harnessing mosquito–Wolbachia symbiosis for vector and disease control. *Acta tropica* **132**, S150-S163 (2014).

310 Moreira, L. A. *et al.* A Wolbachia symbiont in Aedes aegypti limits infection with dengue, Chikungunya, and Plasmodium. *Cell* **139**, 1268-1278 (2009).

311 Carrington, L. B. *et al.* Field-and clinically derived estimates of Wolbachia-mediated blocking of dengue virus transmission potential in Aedes aegypti mosquitoes. *Proceedings of the National Academy of Sciences* **115**, 361-366 (2018).

312 Flores, H. A. *et al.* Multiple Wolbachia strains provide comparative levels of protection against dengue virus infection in Aedes aegypti. *PLoS pathogens* **16**, e1008433 (2020).

313 Dobson, S., Rattanadechakul, W. & Marsland, E. Fitness advantage and cytoplasmic incompatibility in Wolbachia single-and superinfected Aedes albopictus. *Heredity* **93**, 135-142 (2004).

314 Edenborough, K. M., Flores, H. A., Simmons, C. P. & Fraser, J. E. Using Wolbachia to eliminate dengue: Will the virus fight back? *Journal of virology* **95**, e02203-02220 (2021).

315 Manokaran, G. *et al.* Modulation of acyl-carnitines, the broad mechanism behind Wolbachia-mediated inhibition of medically important flaviviruses in Aedes aegypti. *Proceedings of the National Academy of Sciences* **117**, 24475-24483 (2020).

316 Fattouh, N., Cazevieille, C. & Landmann, F. Wolbachia endosymbionts subvert the endoplasmic reticulum to acquire host membranes without triggering ER stress. *PLoS neglected tropical diseases* **13**, e0007218 (2019).

317 Kellstein, D. & Fernandes, L. Symptomatic treatment of dengue: should the NSAID contraindication be reconsidered? *Postgraduate Medicine* **131**, 109-116 (2019).

318 Gan, V. C. Dengue: moving from current standard of care to state-of-the-art treatment. *Current Treatment Options in Infectious Diseases* **6**, 208-226 (2014).

319 Martins, I. C., Ricardo, R. C. & Santos, N. C. Dengue, West Nile, and Zika Viruses: Potential Novel Antiviral Biologics Drugs Currently at Discovery and Preclinical Development Stages. *Pharmaceutics* **14**, 2535 (2022).

320 Watanabe, S., Low, J. G.-H. & Vasudevan, S. G. Preclinical antiviral testing for dengue virus infection in mouse models and its association with clinical studies. *ACS Infectious Diseases* **4**, 1048-1057 (2018).

321 Libraty, D. H. *et al.* Differing influences of virus burden and immune activation on disease severity in secondary dengue-3 virus infections. *The Journal of infectious diseases* **185**, 1213-1221 (2002).

322 Lim, S. P. Dengue drug discovery: Progress, challenges and outlook. *Antiviral research* **163**, 156-178 (2019).

323 Hernandez-Morales, I. & Van Loock, M. An industry perspective on dengue drug discovery and development. *Dengue and Zika: Control and Antiviral Treatment Strategies*, 333-353 (2018).

324 Troost, B. & Smit, J. M. Recent advances in antiviral drug development towards dengue virus. *Current opinion in virology* **43**, 9-21 (2020).

325 Zompi, S. & Harris, E. Animal models of dengue virus infection. *Viruses* **4**, 62-82 (2012).

326 Pérez-Pérez, M.-J. s., Saiz, J.-C., Priego, E.-M. & Martín-Acebes, M. A. Antivirals against (Re) emerging Flaviviruses: Should We Target the Virus or the Host? *ACS Medicinal Chemistry Letters* **13**, 5-10 (2021).

327 Acosta, E. G. & Bartenschlager, R. The quest for host targets to combat dengue virus infections. *Current opinion in virology* **20**, 47-54 (2016).

328 Behnam, M. A., Nitsche, C., Boldescu, V. & Klein, C. D. The medicinal chemistry of dengue virus. *Journal of medicinal chemistry* **59**, 5622-5649 (2016).

329 García, C. C., Quintana, V. M., Castilla, V. & Damonte, E. B. Towards host-cell targeting therapies to treat dengue virus infections. *Frontiers in anti-infective drug discovery* **7**, 45-87 (2018).

330 Krishnan, M. N. & Garcia-Blanco, M. A. Targeting host factors to treat West Nile and dengue viral infections. *Viruses* **6**, 683-708 (2014).

331 Sayce, A. C., Miller, J. L. & Zitzmann, N. Targeting a host process as an antiviral approach against dengue virus. *Trends in microbiology* **18**, 323-330 (2010).

332 Wu, S.-F. *et al.* Antiviral effects of an iminosugar derivative on flavivirus infections. *Journal of virology* **76**, 3596-3604 (2002).

333 Courageot, M.-P., Frenkiel, M.-P., Duarte Dos Santos, C., Deubel, V. & Desprès, P. α-Glucosidase inhibitors reduce dengue virus production by affecting the initial steps of virion morphogenesis in the endoplasmic reticulum. *Journal of virology* **74**, 564-572 (2000).

334 Rathore, A. P. *et al.* Celgosivir treatment misfolds dengue virus NS1 protein, induces cellular pro-survival genes and protects against lethal challenge mouse model. *Antiviral research* **92**, 453-460 (2011).

335 Low, J. G. *et al.* Efficacy and safety of celgosivir in patients with dengue fever (CELADEN): a phase 1b, randomised, double-blind, placebo-controlled, proof-of-concept trial. *The Lancet infectious diseases* **14**, 706-715 (2014).

336 Watanabe, S. *et al.* Optimizing celgosivir therapy in mouse models of dengue virus infection of serotypes 1 and 2: The search for a window for potential therapeutic efficacy. *Antiviral Research* **127**, 10-19 (2016).

337 van der Schaar, H. M. *et al.* Characterization of the early events in dengue virus cell entry by biochemical assays and single-virus tracking. *Journal of virology* **81**, 12019-12028 (2007).

338 Randolph, V. B., Winkler, G. & Stollar, V. Acidotropic amines inhibit proteolytic processing of flavivirus prM protein. *Virology* **174**, 450-458 (1990).

339 Navarro-Sanchez, E. *et al.* Dendritic-cell-specific ICAM3-grabbing non-integrin is essential for the productive infection of human dendritic cells by mosquito-cell-derived dengue viruses. *EMBO reports* **4**, 723-728 (2003).

340 Farias, K. J. S., Machado, P. R. L., Muniz, J. A. P. C., Imbeloni, A. A. & da Fonseca, B. A. L. Antiviral activity of chloroquine against dengue virus type 2 replication in Aotus monkeys. *Viral immunology* **28**, 161-169 (2015).

341 Tricou, V. *et al.* A randomized controlled trial of chloroquine for the treatment of dengue in Vietnamese adults. *PLoS neglected tropical diseases* **4**, e785 (2010).

342 Borges, M. C., Castro, L. A. & Fonseca, B. A. L. d. Chloroquine use improves dengue-related symptoms. *Memórias do Instituto Oswaldo Cruz* **108**, 596-599 (2013).

343 Shu, Q. & Nair, V. Inosine monophosphate dehydrogenase (IMPDH) as a target in drug discovery. *Medicinal research reviews* **28**, 219-232 (2008).

344 Leyssen, P., Balzarini, J., De Clercq, E. & Neyts, J. The predominant mechanism by which ribavirin exerts its antiviral activity in vitro against flaviviruses and

paramyxoviruses is mediated by inhibition of IMP dehydrogenase. *Journal of virology* **79**, 1943-1947 (2005).

345 Wachsman, M., Hamzeh, F., Assadi, N. & Lietman, P. Antiviral activity of inhibitors of pyrimidine de-novo biosynthesis. *Antiviral Chemistry and Chemotherapy* **7**, 7-13 (1996).

346 Qing, M. *et al.* Characterization of dengue virus resistance to brequinar in cell culture. *Antimicrobial agents and chemotherapy* **54**, 3686-3695 (2010).

347 Wang, Q.-Y. *et al.* Inhibition of dengue virus through suppression of host pyrimidine biosynthesis. *Journal of virology* **85**, 6548-6556 (2011).

348 Schul, W., Yip, A. & Shi, P.-Y. in *Antiviral Methods and Protocols* 269-281 (Springer, 2013).

349 Scaturro, P. *et al.* Characterization of the mode of action of a potent dengue virus capsid inhibitor. *Journal of virology* **88**, 11540-11555 (2014).

350 Noble, C. G., Seh, C. C., Chao, A. T. & Shi, P. Y. Ligand-bound structures of the dengue virus protease reveal the active conformation. *Journal of virology* **86**, 438-446 (2012).

351 Xu, T. *et al.* Structure of the Dengue virus helicase/nucleoside triphosphatase catalytic domain at a resolution of 2.4 A. *Journal of virology* **79**, 10278-10288 (2005).

352 Boldescu, V., Behnam, M. A., Vasilakis, N. & Klein, C. D. Broad-spectrum agents for flaviviral infections: dengue, Zika and beyond. *Nature Reviews Drug Discovery* **16**, 565-586 (2017).

353 Saravolatz, L. D., Depcinski, S. & Sharma, M. Molnupiravir and Nirmatrelvir-Ritonavir: Oral Coronavirus Disease 2019 Antiviral Drugs. *Clinical Infectious Diseases* **76**, 165-171 (2023).

354 De Clercq, E. & Li, G. Approved antiviral drugs over the past 50 years. *Clinical microbiology reviews* **29**, 695-747 (2016).

355 Gustafsson, D. *et al.* The direct thrombin inhibitor melagatran and its oral prodrug H 376/95: intestinal absorption properties, biochemical and pharmacodynamic effects. *Thrombosis research* **101**, 171-181 (2001).

356 Steuer, C., Heinonen, K. H., Kattner, L. & Klein, C. D. Optimization of assay conditions fo r dengue virus protease: effect of various polyols and nonionic detergents. *Journal of biomolecular screening* **14**, 1102-1108 (2009).

357 Adamek, R. N., Maniquis, R. V., Khakoo, S., Bridges, M. D. & Salzameda, N. T. A FRET-based assay for the discovery of West Nile Virus NS2B-NS3 protease inhibitors. *Bioorganic & medicinal chemistry letters* **23**, 4848-4850 (2013).

358 Nitsche, C., Holloway, S., Schirmeister, T. & Klein, C. D. Biochemistry and medicinal chemistry of the dengue virus protease. *Chemical reviews* **114**, 11348-11381 (2014).

359 Nitsche, C. *et al.* Peptide–boronic acid inhibitors of flaviviral proteases: medicinal chemistry and structural biology. *Journal of medicinal chemistry* **60**, 511-516 (2017).

360 Chung, K. Y. *et al.* Higher catalytic efficiency of N-7-methylation is responsible for processive N-7 and 2′-O methyltransferase activity in dengue virus. *Virology* **402**, 52-60 (2010).

361 Malet, H. *et al.* The flavivirus polymerase as a target for drug discovery. *Antiviral research* **80**, 23-35 (2008).

362 Lim, S. P. *et al.* Potent allosteric dengue virus NS5 polymerase inhibitors: mechanism of action and resistance profiling. *PLoS pathogens* **12**, e1005737 (2016).

363 Yeo, K. L. *et al.* Synergistic suppression of dengue virus replication using a combination of nucleoside analogs and nucleoside synthesis inhibitors. *Antimicrobial agents and chemotherapy* **59**, 2086-2093 (2015).

364 Yin, Z. *et al.* An adenosine nucleoside inhibitor of dengue virus. *Proceedings of the National Academy of Sciences* **106**, 20435-20439 (2009).

365 Julander, J. G. *et al.* BCX4430, a novel nucleoside analog, effectively treats yellow fever in a Hamster model. *Antimicrobial Agents and Chemotherapy* **58**, 6607-6614 (2014).

366 Nguyen, N. M. *et al.* A randomized, double-blind placebo controlled trial of balapiravir, a polymerase inhibitor, in adult dengue patients. *The Journal of infectious diseases* **207**, 1442-1450 (2013).

367 Berke, J. M. *et al.* Antiviral activity and mode of action of TMC647078, a novel nucleoside inhibitor of the hepatitis C virus NS5B polymerase. *Antimicrobial agents and chemotherapy* **55**, 3812-3820 (2011).

368 Golitsina, N. L., Danehy Jr, F. T., Fellows, R., Cretton-Scott, E. & Standring, D. N. Evaluation of the role of three candidate human kinases in the conversion of the hepatitis C virus inhibitor 2′-C-methyl-cytidine to its 5′-monophosphate metabolite. *Antiviral research* **85**, 470-481 (2010).

369 Kohler, J. J. & Lewis, W. A brief overview of mechanisms of mitochondrial toxicity from NRTIs. *Environmental and molecular mutagenesis* **48**, 166-172 (2007).

370 Yokokawa, F. Recent progress on phenotype-based discovery of dengue inhibitors. *RSC Medicinal Chemistry* **11**, 541-551 (2020).

371 Moquin, S. A. *et al.* NITD-688, a pan-serotype inhibitor of the dengue virus NS4B protein, shows favorable pharmacokinetics and efficacy in preclinical animal models. *Science Translational Medicine* **13**, eabb2181 (2021).

372 Xie, X. *et al.* Inhibition of dengue virus by targeting viral NS4B protein. *Journal of virology* **85**, 11183-11195 (2011).

373 van Cleef, K. W. *et al.* Identification of a new dengue virus inhibitor that targets the viral NS4B protein and restricts genomic RNA replication. *Antiviral research* **99**, 165-171 (2013).

374 Wang, Q.-Y. *et al.* Discovery of dengue virus NS4B inhibitors. *Journal of virology* **89**, 8233-8244 (2015).

375 Hernandez-Morales, I. *et al.* Characterization of a dengue NS4B inhibitor originating from an HCV small molecule library. *Antiviral research* **147**, 149-158 (2017).

376 Kaptein, S. J. F. *et al.* A pan-serotype dengue virus inhibitor targeting the NS3–NS4B interaction. *Nature* **598**, 504-509 (2021).

377 Goethals, O. *et al.* A pan-serotype antiviral to prevent and treat dengue: A journey from discovery to clinical development driven by public-private partnerships. *Antiviral Research*, 105495 (2022).

378 Goethals, O. *et al.* Blocking NS3–NS4B interaction inhibits dengue virus in non-human primates. *Nature* **615**, 678-686 (2023).

379 Bardiot, D. *et al.* Discovery of indole derivatives as novel and potent dengue virus inhibitors. *Journal of medicinal chemistry* **61**, 8390-8401 (2018).

380 Nakabayashi, H., Taketa, K., Miyano, K., Yamane, T. & Sato, J. Growth of human hepatoma cell lines with differentiated functions in chemically defined medium. *Cancer research* **42**, 3858-3863 (1982).

381 Friebe, P., Boudet, J., Simorre, J.-P. & Bartenschlager, R. Kissing-loop interaction in the 3′ end of the hepatitis C virus genome essential for RNA replication. *Journal of virology* **79**, 380-392 (2005).

382 Appel, N., Pietschmann, T. & Bartenschlager, R. Mutational analysis of hepatitis C virus nonstructural protein 5A: potential role of differential phosphorylation in RNA replication and identification of a genetically flexible domain. *Journal of virology* **79**, 3187-3194 (2005).

383 Schneider, C. A., Rasband, W. S. & Eliceiri, K. W. NIH Image to ImageJ: 25 years of image analysis. *Nature methods* **9**, 671-675 (2012).

384 Hanahan, D., Jessee, J. & Bloom, F. R. [4] Plasmid transformation of Escherichia coli and other bacteria. *Methods in enzymology* **204**, 63-113 (1991).

385 Asif, A., Mohsin, H., Tanvir, R. & Rehman, Y. Revisiting the Mechanisms Involved in Calcium Chloride Induced Bacterial Transformation. *Frontiers in Microbiology* **8** (2017).

386 Saiki, R. K. *et al.* Primer-Directed Enzymatic Amplification of DNA with a Thermostable DNA Polymerase. *Science* **239**, 487-491 (1988).

387 Roberts, R. J. & Murray, K. Restriction Endonuclease. *CRC Critical Reviews in Biochemistry* **4**, 123-164 (1976).

388 Fischl, W. & Bartenschlager, R. High-throughput screening using dengue virus reporter genomes. *Methods in molecular biology (Clifton, N.J.)* **1030**, 205-219 (2013).

389 Orwick-Rydmark, M., Arnold, T. & Linke, D. The Use of Detergents to Purify Membrane Proteins. *Current Protocols in Protein Science* **84**, 4.8.1-4.8.35 (2016).

390 Bradford, M. M. A rapid and sensitive method for the quantitation of microgram quantities of protein utilizing the principle of protein-dye binding. *Analytical Biochemistry* **72**, 248-254 (1976).

391 Laemmli, U. K. Cleavage of structural proteins during the assembly of the head of bacteriophage T4. *nature* **227**, 680-685 (1970).

392 Goellner, S. *et al.* Replication-Independent Generation and Morphological Analysis of Flavivirus Replication Organelles. *STAR protocols* **1**, 100173 (2020).

393 David, A. *et al.* Nuclear translation visualized by ribosome-bound nascent chain puromycylation. *Journal of Cell Biology* **197**, 45-57 (2012).

394 Gardner, M. J. & Altman, D. G. Confidence intervals rather than P values: estimation rather than hypothesis testing. *Br Med J (Clin Res Ed)* **292**, 746-750 (1986).

395 Kocienski, P. Synthesis of Dengue Virus Inhibitor JNJ-A07. *Synfacts* **18**, 0006 (2021).

396 Touret, F. *et al.* Phylogenetically based establishment of a dengue virus panel, representing all available genotypes, as a tool in dengue drug discovery. *Antiviral Research* **168**, 109-113 (2019).

397 Illingworth, C. J. & Mustonen, V. Distinguishing driver and passenger mutations in an evolutionary history categorized by interference. *Genetics* **189**, 989-1000 (2011).

398 Ackaert, O. *et al.* Safety, tolerability and pharmacokinetics of JNJ-1802, a pan-serotype dengue direct antiviral small molecule, in a Phase 1, double-blind, randomized, dose-escalation study in healthy volunteers. *Clinical Infectious Diseases* (2023).

399 Whitehorn, J. *et al.* Dengue therapeutics, chemoprophylaxis, and allied tools: state of the art and future directions. *PLoS neglected tropical diseases* **8**, e3025 (2014).

400 Agudelo Higuita, N. I., White, B. P., Franco-Paredes, C. & McGhee, M. A. An update on prevention of malaria in travelers. *Therapeutic Advances in Infectious Disease* **8**, 20499361211040690 (2021).

401 Nakato, H., Vivancos, R. & Hunter, P. R. A systematic review and meta-analysis of the effectiveness and safety of atovaquone–proguanil (Malarone) for chemoprophylaxis against malaria. *Journal of Antimicrobial Chemotherapy* **60**, 929-936 (2007).

402 McNamara, L. A., MacNeil, J. R., Cohn, A. C. & Stephens, D. S. Mass chemoprophylaxis for control of outbreaks of meningococcal disease. *The Lancet. Infectious diseases* **18**, e272-e281 (2018).

403 Newby, G. *et al.* Review of Mass Drug Administration for Malaria and Its Operational Challenges. *The American Society of Tropical Medicine and Hygiene* **93**, 125-134 (2015).

404 Molyneux, D. H., Bradley, M., Hoerauf, A., Kyelem, D. & Taylor, M. J. Mass drug treatment for lymphatic filariasis and onchocerciasis. *Trends in Parasitology* **19**, 516-522 (2003).

405 Behnam, M. A. & Klein, C. D. Corona versus Dengue: Distinct Mechanisms for Inhibition of Polyprotein Processing by Antiviral Drugs. *ACS Pharmacology & Translational Science* **5**, 508-511 (2022).

406 Guo, F. *et al.* A novel benzodiazepine compound inhibits yellow fever virus infection by specifically targeting NS4B protein. *Journal of Virology* **90**, 10774-10788 (2016).

407 Gao, Z. *et al.* A yellow fever virus NS4B inhibitor not only suppresses viral replication, but also enhances the virus activation of RIG-I-like receptor-mediated innate immune response. *PLoS Pathogens* **18**, e1010271 (2022).

408 Patkar, C. G., Larsen, M., Owston, M., Smith, J. L. & Kuhn, R. J. Identification of inhibitors of yellow fever virus replication using a replicon-based high-throughput assay. *Antimicrob Agents Chemother* **53**, 4103-4114 (2009).

409 Riva, L. *et al.* The Compound SBI-0090799 Inhibits Zika Virus Infection by Blocking De Novo Formation of the Membranous Replication Compartment. *Journal of Virology* **95**, e00996-00921 (2021).

410 Gao, M. *et al.* Chemical genetics strategy identifies an HCV NS5A inhibitor with a potent clinical effect. *Nature* **465**, 96-100 (2010).

411 Bartenschlager, R., Ahlborn-Laake, L., Mous, J. & Jacobsen, H. Kinetic and structural analyses of hepatitis C virus polyprotein processing. *Journal of virology* **68**, 5045-5055 (1994).

412 Berger, C. *et al.* Daclatasvir-like inhibitors of NS5A block early biogenesis of hepatitis C virus–induced membranous replication factories, independent of RNA replication. *Gastroenterology* **147**, 1094-1105. e1025 (2014).

413 Gitto, S., Gamal, N. & Andreone, P. NS 5A inhibitors for the treatment of hepatitis C infection. *Journal of Viral Hepatitis* **24**, 180-186 (2017).

414 IUPAC. in *Biochemistry* Vol. 7 2703-2705 (American Chemical Society, 1968).

415 Lide, D. R. *Handbook of Chemistry and Physics, ed*. (CRC Press, Boca Raton, Florida, United States of America, 1999).

VIII. Appendix

VIII.1 Plasmids

Supplementary Table 1. List of plasmids used and generated in this study.
This table lists all plasmids that were used in this study. The column titled "Cloned" indicates whether plasmids were generated as part of this doctoral thesis. If "no" is stated, the respective plasmid was available from previous work. Otherwise, the abbreviation of the method used to generate the plasmids in this thesis is listed. SC = subcloning; SDM = site-directed mutagenesis; O-PCR = overlap PCR; OE-PCR = overlap extension PCR. An example of each of these cloning methods can be found in Chapter IV.1.8. The following two columns indicate the plasmids that were used as templates for vector (T_{Vector}) and insert (T_{Insert}), respectively. The numbers refer to the index value of plasmids to the left of the name. The column "Enzymes" shows the pair of restriction enzymes used to digest both vector and insert. If PCR techniques were used for cloning, the last column lists the applied primers. Here, the numbers refer to the index values of the oligonucleotides in Supplementary Table 2.

Nr	Name	Cloned	T_{Vector}	T_{Insert}	Enzymes	Primer
1	pTM_DV2_ 2K-NS4B_WT	no	–	–	–	–
2	pTM_DV2_ 2K-NS4B_WT-HA^{Ct}	no	–	–	–	–
3	pTM_DV2_ 2K-NS4B_Q134A-HA^{Ct}	no	–	–	–	–
4	pTM_DV2_ HA^{Nt}-NS4A_WT	no	–	–	–	–
5	pTM_DV2_ HA^{Nt}-NS4A-2K-NS4B_WT	SC	20	4	KpnI&NheI	–
6	pTM_DV2_NS4A-2K-NS4B_A137T-HA^{Ct}	SDM	20	21	NcoI&SpeI	2,3,23,43
7	pTM_DV2_NS4A-2K-NS4B_L94F-HA^{Ct}	no	–	–	–	–
8	pTM_DV2_NS4A-2K-NS4B_M142A_L94F_T215A-HA^{Ct}	SDM	20	9	NcoI&SpeI	27,28,23,43
9	pTM_DV2_NS4A-2K-NS4B_M142A_L94F-HA^{Ct}	SDM	20	11	NcoI&SpeI	6,7,21,43
10	pTM_DV2_NS4A-2K-NS4B_M142A_T215A-HA^{Ct}	SDM	20	11	NcoI&SpeI	27,28,23,43
11	pTM_DV2_NS4A-2K-NS4B_M142A-HA^{Ct}	no	–	–	–	–
12	pTM_DV2_NS4A-2K-NS4B_Q134A_A137V-HA^{Ct}	no	–	–	–	–
13	pTM_DV2_NS4A-2K-NS4B_Q134A_A69S_A137V-HA^{Ct}	SDM	12	12	NcoI&SpeI	4,5,23,43
14	pTM_DV2_NS4A-2K-NS4B_Q134A_A69S-HA^{Ct}	no	–	–	–	–
15	pTM_DV2_NS4A-2K-NS4B_Q134A-HA^{Ct}	no	–	–	–	–
16	pTM_DV2_NS4A-2K-NS4B_S85L-HA^{Ct}	SDM	20	21	NcoI&SpeI	12,13,23,43
17	pTM_DV2_NS4A-2K-NS4B_T108I-HA^{Ct}	no	–	–	–	–
18	pTM_DV2_NS4A-2K-NS4B_T216N-HA^{Ct}	SDM	20	21	NcoI&SpeI	16,17,23,43
19	pTM_DV2_NS4A-2K-NS4B_V91A-HA^{Ct}	no	–	–	–	–
20	pTM_DV2_NS4A-2K-NS4B_WT	no	–	–	–	–
21	pTM_DV2_NS4A-2K-NS4B_WT-HA^{Ct}	no	–	–	–	–
22	pTM_DV2_NS4A-2K-NS4B-HA^{Ct}_CS-P1´Ile	no	–	–	–	–
23	pTM_ ZIKV_HPF2013_ NS4A-2K-NS4B_WT	no	–	–	–	–
24	pTM_ ZIKV_HPF2013_ NS4A-2K-NS4B_ WT-HA^{Ct}	no	–	–	–	–
25	pTM_ ZIKV_HPF2013_ NS4A-2K-NS4B_ Q136A-HA^{Ct}	no	–	–	–	–

Nr	Name	Cloned	T_{Vector}	T_{Insert}	Enzymes	Primer
26	pTM_ ZIKV_HPF2013_ NS4A-2K-NS4B_ Y87S-HA^{Ct}	SDM	24	24	BglII&SpeI	35,37,29,30
27	pTM_ ZIKV_HPF2013_ NS4A-2K-NS4B_ I110T-HA^{Ct}	SDM	24	24	BglII&SpeI	35,37,31,32
28	pTM_ ZIKV_HPF2013_ NS4A-2K-NS4B_ S218T-HA^{Ct}	SDM	24	24	BglII&SpeI	35,37,33,34
29	pIRO-D_ NS1-HA*	No	–	–	–	–
30	pIRO-D_ NS4B-HA*	No	–	–	–	–
31	pIRO-D_Rib_NS3-HA*	SC	42	52	MluI&XhoI	–
32	pIRO-D_Rib_NS3-HA*_NS4A-2K_CS-P1´Ile	SC	31	72	XhoI&BsrGI	–
33	pIRO-D_Rib_NS3-HA*_NS4A-2K_CS-P1´Ile_NS4B_Q134A	O-PCR	31	72,44	XhoI&BsrGI	25,26,45,46
34	pIRO-D_Rib_NS4B_A137T	SDM	42	42	XhoI&BsrGI	2,3,61,69
35	pIRO-D_Rib_NS4B_L94F	SC	42	79	XhoI&BsrGI	–
36	pIRO-D_Rib_NS4B_S85L	SDM	42	42	XhoI&BsrGI	12,13,61,69
37	pIRO-D_Rib_NS4B_T108I	SDM	42	42	XhoI&BsrGI	14,15,61,69
38	pIRO-D_Rib_NS4B_T216N	SDM	42	42	XhoI&BsrGI	16,17,61,69
39	pIRO-D_Rib_NS4B_V91A	SDM	42	42	XhoI&BsrGI	18,19,61,69
40	pIRO-D_Rib_NS4B-HA*	SC	42	30	NheI& BsrGI	–
41	pIRO-D_Rib_NS4B-HA*_Q134A	SC	42	78	NheI& BsrGI	–
42	pIRO-D_Rib_WT	no	–	–	–	–
43	pIRO-D_WT	no	–	–	–	–
44	pIRO-D_Rib_NS4B_Q134A	SC	42	73	NheI& BsrGI	
45	pIRO-D_Rib_NS4B_Q134A_A69S	O-PCR	42	75	XhoI& BsrGI	25,26,61,69
46	pIRO-D_Rib_NS4B_Q134A_A137V	O-PCR	42	76	XhoI& BsrGI	25,26,61,69
47	pIRO-D_Rib_NS4B_Q134A_A69S_A137V	SDM	50	46	NheI& BsrGI	4,5, 45,62
48	pIRO-D_Rib_NS4B_M142A	SC	42	74	NheI& BsrGI	–
49	pIRO-D_Rib_NS4B_M142A_T215A	SDM	42	48	NheI& BsrGI	27,28, 61,69
50	pIRO-D_Rib_NS4B_M142A_L94F	SDM	42	48	NheI& BsrGI	6,7,61,69
51	pIRO-D_Rib_NS4B_M142A_L94F_T215A	SDM	50	50	NheI& BsrGI	27,28,45,62
52	pFK_DV2_sgR2A_NS3-HA-1 cl1	no	–	–	–	–
53	pFK_DV2_sgR2A_WT	no	–	–	–	–
54	pFK_DV2_sgR2A_GND	no	–	–	–	–
55	pFK_DV2_sgR2A_JNJ_WT	no	–	–	–	–
56	pFK_DV2_sgR2A_JNJ_F47Y	no	–	–	–	–
57	pFK_DV2_sgR2A_JNJ_S85L	no	–	–	–	–
58	pFK_DV2_sgR2A_JNJ_V91A	no	–	–	–	–
59	pFK_DV2_sgR2A_JNJ_L94F	no	–	–	–	–
60	pFK_DV2_sgR2A_JNJ_P104S	no	–	–	–	–
61	pFK_DV2_sgR2A_JNJ_T108I	no	–	–	–	–
62	pFK_DV2_sgR2A_JNJ_A137T	no	–	–	–	–
63	pFK_DV2_sgR2A_JNJ_T216N	no	–	–	–	–
64	pFK_DV2_sgR2A_JNJ_T216P	no	–	–	–	–
65	pFK_sgR2A_ZIKV_HPF2013_T7_WT	no	–	–	–	–
66	pFK_sgR2A_ZIKV_HPF2013_T7_GAA	no	–	–	–	–
67	pFK_sgR2A_ZIKV_HPF2013_T7_Y87S	SDM	65	65	KasI&EcoRI	36,37,29,30
68	pFK_sgR2A_ZIKV_HPF2013_T7_I110T	SDM	65	65	KasI&EcoRI	36,37,31,32
69	pFK_sgR2A_ZIKV_HPF2013_T7_S218T	SDM	65	65	KasI&EcoRI	36,37,33,34
70	pTM_empty	no	–	–	–	–

Nr	Name	Cloned	T_{Vector}	T_{Insert}	Enzymes	Primer
71	pTM_DV2_NS4A-2K-NS4B_2A_eGFP-NLS	OE-PCR	20	20,77	NcoI&SpeI	38,39,40,41,42, 43
72	pSM1_ NS4A-2K_CS-P1´Ile	no	–	–	–	–
73	pSM1_ NS4B_Q134A	no	–	–	–	–
74	pSM1_ NS4B_M142A	no	–	–	–	–
75	pSM1_ NS4B-HA*_Q134A_A69S	no	–	–	–	–
76	pSM1_ NS4B-HA*_Q134A_A137T	no	–	–	–	–
77	pWPI_Puro_RCsec61-NLS_opt_DENVC1	no	–	–	–	–
78	pSM1_ NS4B-HA*_Q134A	no	–	–	–	–
79	pSM1_ NS4B_L94F	no	–	–	–	–

VIII.2 Oligonucleotides

Supplementary Table 2. Primers and oligonucleotides used in this study.
Oligonucleotides used in this work are labeled with a name and are shown in 5'-3' orientation. When the index number is listed in the "Primer" column of Supplementary Table 1, they were used for cloning purposes. In the other case, primers were used for sequencing.

Nr	Name	Sequence (5'-3')
1	EMCV_IRES_Fw	CTTGGAATAAGGCCGGTGTG
2	NS4B_A137T_Fw	GCTCAGAAAAGAACAGCGGCG
3	NS4B_A137T_Rv	CGCCGCTGTTCTTTTCTGAGC
4	NS4B_A69S_Fw	CAGCTATATCCAACCAAGCC
5	NS4B_A69S_Rv	GGCTTGGTTGGATATAGCTG
6	NS4B_L94F_Fw	GTTCCCCTTTTCGCCATTGG
7	NS4B_L94F_Rv	CCAATGGCGAAAAGGGGAAC
8	NS4B_M142A_Fw	CAGCGGCGGGCATCGCCAAAAACCCAACTG
9	NS4B_M142A_Rv	CAGTTGGGTTTTTGGCGATGCCCGCCGCTG
10	NS4B_Q134A_Fw	GCAACCAGAGAAGCTGCCAAAAGAGCAGCGG
11	NS4B_Q134A_Rv	CCGCTGCTCTTTTGGCAGCTTCTCTGGTTGC
12	NS4B_S85L_Fw	GCCATTGTTAAAGATGGACATCG
13	NS4B_S85L_Rv	CGATGTCCATCTTTAACAATGGC
14	NS4B_T108I_Fw	CTCTCATCGCAGCTCTTTTCTTATTGGTAGC
15	NS4B_T108I_Rv	GCTGCGATGAGAGTTATGGGGTTGACTTGTG
16	NS4B_T216N_Fw	GGAACACTAACATTGCGGTGTC
17	NS4B_T216N_Rv	GACACCGCAATGTTAGTGTTCC
18	NS4B_V91A_Fw	TCGGAGCACCCCTTCTCGCCATTGGATGCTA
19	NS4B_V91A_Rv	AGGGGTGCTCCGATGTCCATCTTTGACAATGG
20	pTM_FwLeftInner	GTGAGGCAGCTGGGATTTTT
21	pTM_FwLeftOuter	TCTTGGCCCCCACTAGAGTT
22	pTM_RvRightInner	AAAACCCCTCAAGACCCGTT
23	pTM_RvRightOuter	TCGGTTTCCTCACCCAATCG

Nr	Name	Sequence (5'-3')
24	T7_Fw	TAATACGACTCACTATAGGG
25	NS4B_removeHA*_Fw	CAGCAACCCGAGAGCAACATCC
26	NS4B_removeHA*_Rv	GGATGTTGCTCTCGGGTTGCTG
27	NS4B_T215A_Fw	GTTTTGGAACGCTACCATTGC
28	NS4B_T215A_Rv	GCAATGGTAGCGTTCCAAAAC
29	Z_NS4B_Y87S_Fw	GCCATTCAGTGCATGGGACTTTGG
30	Z_NS4B_Y87S_Rv	CCAAAGTCCCATGCACTGAATGGC
31	Z_NS4B_I110T_Fw	GACCCTAACGGTGGCCATCATTTTGC
32	Z_NS4B_ I110T _Rv	GCAAAATGATGGCCACCGTTAGGGTC
33	Z_NS4B_S218T_Fw	GGAACTCCACGACAGCCACTTCACTG
34	Z_NS4B_S218T_Rv	CAGTGAAGTGGCTGTCGTGGAGTTCC
35	Z_pTM_SpeI_Rv	GCTTTGTTAGCAGCCGGATCGTCG
36	Z_pFK_EcoRI_Rv	TTGCCACACCGTCCTTGAG
37	Z_pFK_KasI_pTM_BglI	AGAGTGGGACTTTGTCGTGA
38	NS4B_3´_RV	CCTTCTTGTGTTGGTTGTG
39	NS4A-2APeptide-eGFP	CACAACCAACACAAGAAGGAGAGCCGAGGGCAGGGGAAGTCTTCT AACATGCGGGGACGTGGAGGAAAATCCCGGGCCCATGGTGAGCAA GGGCGAG
40	eGFP_5´_Rv	CTCGCCCTTGCTCACCAT
41	eGFP_5´_Fw	ATGGTGAGCAAGGGCGAG
42	NLS-SpeI_Rv	GGGATCCACTAGTTTACACTTTGCGCTTTTTCTTC
43	TKI Fw_1	TCTCTTAACGATGTTCTTCGCAC
44	TKI Fw_2	GCGATCAATAAATGGATCACAAC
45	NS3_XhoI_Fw	ATCTCAACTCGAGTGGAGAT
46	NS5_Rv	GGATCCACTAGTCCACAGAACTCCTGCTTCTTCC
47	Seq7	GTTATGAGACTCTGTAGAGAG
48	Seq8	CGCAGTCCTCAGTCACTACCACTG
49	Seq9	CTATGTCATCCGTCATAGTGGCG
50	Seq10	GATCGTCAATGCTAATGGTATC
51	Seq11	CACAGGTACCATGCTGCTGCCG
52	Seq12	CAGCACCTATTGTTCCGGCGTTGG
53	Seq13	GTGTGCTCAGCTCTGATGGCTG
54	Seq14	CTCAGAATCAAAGGTCTTCCTAC
55	Seq15	CACTCTGTAGGCCAACCAGACTG
56	Seq16	CCGTGACTGTAGCCAGAAGTGTC
57	Seq17	TCCCGAGACCCATTAACACTGTG
58	Seq18	GACACCGCAATGGTAGTGTTC
59	Seq19	CAGTACATCTCATGTGTGGAG
60	Seq20	GTTCTTGGGTTCTCGTGTCCAC
61	Seq21	GAACCAGTGATCTTCATTTAAG
62	Seq22	CAATCATCTCCACTGATGGCC

Nr	Name	Sequence (5'-3')
63	Seq31	TGGAATCCGCTCAGTAACAAG
64	Seq32	GCACTCAATGACACATGGAAG
65	Seq33	GTCAACTCCTTGGTCACAGCTG
66	Seq34	CGTTAGCCTTAGGCATGATGGTC
67	Seq35	GACCAGGCAGAGATATCAGG
68	Seq36	CAATGTGGCATGTCACACGT
69	Seq37	ATCATGGACCTCCACCCAGGAG
70	Seq38	GACCCATTTCCTCAGAGCAATG
71	Seq39	GAGAATGACCAGTACATATACATG
72	Seq40	GAAGAAAGTCTCTGACCCTGAAC
73	Seq41	CGCAACCATGGCAAACGAGATG
74	Seq42	ACAGTGATTGACCTAGATCCAATAC
75	Seq43	ACTGAGATGGTTCGTTGAGAG
76	Seq44	GAGTCATCACCAAATCCCACA
77	Seq45	AGAGCATGAAACATCATGGCAC
78	Seq46	GATAGTAGGTTTTGGGAGCTG
79	Seq47	CCAAGAGGCACAGTAATGG
80	Seq48	CGGGAGACGGCCTGTTTG
81	Seq49	CCCGTCCAAGGACGTTAAAAG

VIII.3 Amino acid code and properties

Supplementary Table 3. Code and properties of standard amino acids.
This table lists the standard amino acids with their 1-letter abbreviation code as well as their mass and isoelectric point. Information is according to IUPAC guidelines and taken from Lide [415].

Name	1-letter code	Molecular weight [kDa]	Isoelectric point [pH]
Alanine	A	89.10	6.00
Arginine	R	174.20	10.76
Asparagine	N	132.12	5.41
Aspartic acid	D	133.11	2.77
Cysteine	C	121.16	5.07
Glutamic acid	E	147.13	3.22
Glutamine	Q	146.15	5.65
Glycine	G	75.07	5.97
Histidine	H	155.16	7.59
Isoleucine	I	131.18	6.02
Leucine	L	131.18	5.98
Lysine	K	146.19	9.74
Methionine	M	149.21	5.74
Phenylalanine	F	165.19	5.48
Proline	P	115.13	6.30
Serine	S	105.09	5.68

Threonine	T	119.12	5.60
Tryptophan	W	204.23	5.89
Tyrosine	Y	181.19	5.66
Valine	V	117.15	5.96
Any	X		

VIII.4 Antiviral activity of JNJ-A07

Results presented were generated by collaborators and are part of a publication by Kaptein et. al.[376].

Supplementary Table 4. Antiviral activity of JNJ-A07 against DENV-2 in various cell types.

Cell type	DENV-2 strain	Antiviral activity		Toxicity	SI*
		EC_{50} (µM)	EC_{90} (µM)	CC_{50} (µM)	
Vero	16681	0.0001 ± 0.00007	0.0005 ± 0.0004	13 ± 1.1	130,000
Huh7	16681	0.0008 ± 0.0002	0.002 ± 0.001	>25	>31,000
THP-1/DC-SIGN	16681	0.0007 ± 0.0002	0.001 ± 0.0005	>0.5	>714
ImDCs	16681	0.002 ± 0.001	0.009 ± 0.005	140 ± 62	70,000
C6/36	RL	0.003 ± 0.0006	0.007 ± 0.004	18 ± 4.5	6,000
Vero	RL	0.0002 ± 0.00004	0.0005 ± 0.00003	14 ± 0.3	70,000

*Selectivity index (SI) was calculated by dividing the mean CC50 value by the mean EC_{50} value.
Data represent average values ± s.d. from two (for Vero cells infected with DENV-2 RL, and for ImDCs infected with DENV-2/16681), three (for C6/36 cells infected with DENV-2 RL, and for THP-1/DC-SIGN cells infected with DENV-2/16681), or at least five (for Vero and Huh-7 cells infected with DENV-2/16681) independent experiments. CC_{50}, 50% cytotoxic concentration; EC_{50}, 50% effective concentration; EC_{90}, 90% effective concentration; ImDCs, immature dendritic cells.

Supplementary Table 5. In vitro antiviral activity of JNJ-A07 against different DENV genotypes.

Serotype	Genotype	Strain	EC_{50} (µM)	EC_{90} (µM)
DENV-1	G1	Djibouti	<0.00006 ± 0.00004	<0.0001 ± 0.0001
DENV-1	G3	Malaysia*,†	0.0003 ± 0.00007	0.0007 ± 0.0001
DENV-1	G4	Indonesia	<0.00008 ± 0.00005	<0.0002 ± 0.0002
DENV-1	G5	France - Toulon	<0.00003 ± 0.00001	<0.0002 ± 0.0002
DENV-2	Asian America	Martinique†	0.004 ± 0.005	0.005 ± 0.005
DENV-2	American	Trinidad	<0.00003 ± 0.000009	<0.00007 ± 0.00007
DENV-2	Cosmopolitan	France - Toulon	<0.00007 ± 0.00005	<0.0002 ± 0.0002
DENV-2	Asian I	Thailand†	0.001 ± 0.0002	0.001 ± 0.000002
DENV-2	Asian II	Papua New Guinea*	<0.00004 ± 0	<0.00007 ± 0.00004
DENV-2	Sylvatic	Malaysia*	<0.00006 ± 0.00003	0.0002 ± 0.00008
DENV-3	G1	Malaysia	0.0005 ± 0.0002	0.001 ± 0.0003
DENV-3	G2	Thailand	0.001 ± 0.0007	0.002 ± 0.0002
DENV-3	G3	Bolivia	0.0004 ± 0.0003	0.002 ± 0.0009
DENV-3	G5	H87†	0.001 ± 0.0005	0.002 ± 0.0007
DENV-3	G5	Brazil*,‡	0.0002 ± 0.0002	0.0006 ± 0.0005
DENV-4	G1	India	<0.00004 ± 0	<0.0001 ± 0.0001
DENV-4	G2a	Malaysia	0.003 ± 0.003	0.004 ± 0.004
DENV-4	G2b	Martinique	<0.0001 ± 0.0001	0.001 ± 0.0003
DENV-4	G2b	Brazil	<0.0002 ± 0.0001	0.0006 ± 0.0001
DENV-4	G3	Thailand*	0.006 ± 0.006	0.01 ± 0.002
DENV-4	Sylvatic	Malaysia*	0.0003 ± 0.00002	0.0009 ± 0.0004

*DENV strain that was generated using infectious subgenomic amplicons (ISA).
†DENV strain that carries the T108I mutation in NS4B.
‡DENV strain that contains the T108A mutation in NS4B.
Panel was selected as reported by Touret and colleagues[18]. Antiviral assays were carried out on Vero E6 cells. Data represent average values ± s.d. from at least two independently performed experiments (n = 2 to 6). EC_{50}, 50% effective concentration; EC_{90}, 90% effective concentration.

Supplementary Table 6. Antiviral activity of JNJ-A07 against various RNA and DNA viruses.

Virus	Strain	Cells	Antiviral EC_{50} (µM)	Toxicity CC_{50} (µM)	SI*
CHIKV	S27	Huh-7	23	>25	>1
HAdV	C, type 5	HeLa	NA†	6.8	/
HBV	Genotype D	HepG2.117	>22‡	22	<1
HCV	Genotype 1b	Huh-7-CMV-Luc	65	>100	>2

HIV	IIIB	MAGI-CCR5	5.5	33	6
hRV	A16	HeLa	NA†	13	/
hRV	B14	HeLa	NA†	9.1	/
IVA	Taiwan/1/86 (H1N1)	MDCK	>3.6‡	3.6	<1
IVA	PR8/1934 (H1N1)	MDCK	>3.6‡	3.6	<1
IVB	Singapore	MDCK	>3.6‡	3.6	<1
RSV	rgRSV224	HeLa	19	52	3
rVSV	Indiana	A549	57	>90	>2
VACV	Western reserve 56	Vero E6	35	45	1
JEV	CNS769-Laos	Vero E6	>5.0	ND	/
WNV	USA	Vero E6	>5.0	ND	/
YFV	Bolivia	Vero E6	1.8	ND	/
ZIKV	H/PF/2013	Vero E6	4.8	ND	/

*Selectivity index (SI) was calculated by dividing the average CC_{50} value by the average EC_{50} value. †Not approved because any sign of antiviral activity was associated with toxicity. ‡In case the EC_{50} value was higher than the CC_{50} value, the EC_{50} value was set at $>CC_{50}$. CHIKV, chikungunya virus; HadV, human adenovirus; HBV, hepatitis B virus; HCV, hepatitis C virus; HIV, human immunodeficiency virus; hRV, human rhinovirus; IVA, influenza virus A; IVB, influenza virus B; RSV, respiratory syncytial virus; rVSV, recombinant vescular stomatitis virus; VACV, vaccinia virus; JEV, Japanese encephalitis virus; WNV, West Nile virus; YFV, yellow fever virus; ZIKV, Zika virus. ND, not determined.

IX. Publications and presentations

IX.1 Publications and manuscripts in preparation

- Kaptein, S.J.F., Goethals, O., **Kiemel, D.**, Marchand, A., Kesteleyn, B., Bonfanti, J.-F., Bardiot, D., Stoops, B., Jonckers, T.H.M., Dallmeier, K., Geluykens, P., Thys, K., Crabbe, M., Chatel-Chaix, L., Münster, M., Querat, G., Touret, F., de Lamballerie, X., Raboisson, P., Simmen, K., Chaltin, P., Bartenschlager, R., Van Loock, M., and Neyts, J. (2021). A pan-serotype dengue virus inhibitor targeting the NS3–NS4B interaction. Nature *598*, 504-509.

- Goethals, O., Kaptein, S.J.F., Kesteleyn, B., Bonfanti, J.-F., Van Wesenbeeck, L., Bardiot, D., Verschoor, E.J., Verstrepen, B.E., Fagrouch, Z., Putnak, J.R., **Kiemel, D.**, Ackaert, O., Straetemans, R., Lachau-Durand, S., Geluykens, P., Crabbe, M., Thys, K., Stoops, B., Lenz, O., Tambuyzer, L., De Meyer, S., Dallmeier, K., McCracken, M.K., Gromowski, G.D., Rutvisuttinunt, W., Jarman, R.G., Karasavvas, N., Touret, F., Querat, G., de Lamballerie, X., Chatel-Chaix, L., Milligan, G.N., Beasley, D.W.C., Bourne, N., Barrett, A.D.T., Marchand, A., Jonckers, T.H.M., Raboisson, P., Simmen, K., Chaltin, P., Bartenschlager, R., Bogers, W.M., Neyts, J., and Van Loock, M. (2023). Blocking NS3–NS4B interaction inhibits dengue virus in non-human primates. Nature *615*, 678-686.

- **Kiemel, D.**, Kroell, A.-S., Denolly, S., Haselmann, U., Bonfanti, J.-F., Andres J.I., Ghosh, B., Kaptein, S.J.F., Neyts, J., Van Loock, M., Goethals, O., Bartenschlager, R. (2023). Pan-serotype dengue virus inhibitor JNJ-A07 targets NS4A-2K-NS4B interaction with NS3 and blocks replication organelle formation. In preparation (Under review).

IX.2 Presentations and conference contributions

Presenting authors are indicated by underscoring.

- 68th American Society of Tropical Medicine and Hygiene (ASTMH) Annual Meeting, November 20–24, 2019, National Harbor, Maryland, USA

  Kaptein, S.J.F., Goethals, O., **Kiemel, D.**, Marchand, A., Jonckers, T.H.M., Bonfanti, J.-F., Bardiot, D., Kesteleyn, B., Stoops, B., Dallmeier, K., Chatel-Chaix, L., Münster, M., Querat, G., Touret, F., Raboisson, P., Simmen, K., Chaltin, P., de Lamballerie, X., Bartenschlager, R., Van Loock, M., and Neyts, J. Discovery and characterization of a novel potent pan-serotype dengue virus inhibitor exhibiting unprecedented in vivo potency by blocking the NS3/NS4B interaction. Poster presentation

- 34th International Conference on Antiviral Research (ICAR 21), March 22-26, 2021, Virtual Meeting

  Kaptein, S.J.F., Olivia G. M. Goethals, **Kiemel, D.**, Marchand, A., Kesteleyn, B., Bonfanti, J.-F., Bardiot, D., Stoops, B., Jonckers, T.H.M., Dallmeier, K., Chatel-Chaix, L., Münster, M., Querat, G., Touret, F., de Lamballerie, X., Raboisson, P., Simmen, K., Chaltin, P., Bartenschlager, R., Van Loock, M., and Neyts, J. Pan-serotype dengue virus inhibitor that blocks the NS3-NS4B interaction and exhibits unprecedented in vivo potency. Oral presentation.

- 70th American Society of Tropical Medicine & Hygiene (ASTMH) Annual Meeting, November 17-21, 2021, Virtual Meeting

  Goethals, O., Kaptein, S.J., Kesteleyn, B., Bonfanti, J.-F., Jonckers, T.H.M., Marchand, A., Verschoor, E., Verstrepen, B., Van Wesenbeeck, L., Ackaert, O., Straetemans, R., Lachau-Durand, S., Geluykens, P., Crabbe, M., Thys, K., Bardiot, D., Stoops, B., Dallmeier, K., Putnak, R.J., McCracken, M.K., Gromowski, G.D., Rutvisuttinunt, W., Jarman, R.G., Karasavvas, N., Touret, F., Querat, G., de Lamballerie, X., **Kiemel**, **D.**, Chatel-Chaix, L., Münster, M., Milligan, G., Beasley, D., Bourne, N., Barrett, A.D.T., Raboisson, P., Simmen, K., Chaltin, P., Bartenschlager, R., Bogers, W., Neyts, J. and Van Loock, M. Unprecedented Preclinical Efficacy of JNJ-1802, a Novel Pan-Serotype Dengue Antiviral Small Molecule, against Dengue Virus in Non-human Primates and Murine Models. Oral presentation

- 5th Asia Dengue Summit, June 13-15, 2021, Singapore

  Goethals, O., **Kiemel**, **D.**, Kaptein, S.J.F., Geluykens, P., Van Wesenbeeck, L., Neyts, J, Bartenschlager, R., and Van Loock, M. First-in-class, potent, pan-serotype dengue antiviral inhibitor JNJ-1802 targets the nonstructural protein 3-4B interaction. Poster presentation

- 36th International Conference on Antiviral Research (ICAR 23), March 13-17, 2023, Lyon, France

  Kiemel, D., Kroell, A.-S., Denolly, S., Haselmann, U., Bonfanti, J.-F., Andres J.I., Ghosh, B., Van Loock, M., Goethals, O., Bartenschlager, R. JNJ-A07 targets the dengue virus NS4A-2K-NS4B interaction with NS3 and blocks de novo formation of vesicle packets. Oral presentation